FUNCTIONS AND MECHANISMS OF CHLOROPLAST LIPID REMODELING IN PLANTS

By

Kun Wang

A DISSERTATION

Submitted to
Michigan State University
in partial fulfillment of the requirements
for the degree of

Biochemistry and Molecular Biology – Doctor of Philosophy

2017

ABSTRACT

FUNCTIONS AND MECHANISMS OF CHLOROPLAST LIPID REMODELING IN PLANTS

By

Kun Wang

Chloroplasts in plants and algae are organelles that carry out a number of important functions including photosynthesis, fatty acid biosynthesis and oxylipin mediated plant immune responses. Chloroplast membranes with a unique lipid composition are crucial for the functions of chloroplasts. Chloroplast membranes are composed of a specialized glycerolipid matrix with predominately galactolipids, mono- and digalactosyldiacylglycerol (MGDG and DGDG, respectively), and two anionic lipids, phosphatidylglycerol (PG) and sulfoquinovosyldiacylglycerol. The lipid composition of the chloroplast membranes is finely tuned in response to stresses or during various developmental stages to maintain plant fitness.

SENSITIVE TO FREEZING 2 (SFR2) is a galactolipid : galactolipid galactosyltransferase that is highly conserved in land plants. In response to freezing, SFR2 is activated in freezing tolerant plants like Arabidopsis and remodels MGDG to form a class of oligogalactolipids that stabilize the bilayer structures. Phylogenetically, SFR2 is highly conserved in land plants including those that are freezing sensitive. Therefore, I hypothesized that SFR2 in freezing sensitive plants may be involved in plant resilience to other abiotic stresses, like salt or drought stresses because similar to freezing, salt and drought stress cause cell dehydration. In Chapter 2, freezing sensitive tomato was used as a model to test this hypothesis. I generated the *SlSFR2* RNAi lines and observed their hypersensitivity to salt and drought responses. Decreased tolerance was correlated with compromised production of oligogalactolipids in the *SlSFR2* RNAi lines, suggesting SFR2 plays a role in salt and drought tolerance in freezing sensitive plants.

Maintenance of the chloroplast membranes requires a finely tuned lipid anabolic and catabolic machinery. Contrary to the chloroplast lipid biosynthetic enzymes, a large number of the predicted lipid-degrading enzymes in the chloroplasts have unknown functions. In Chapter 3, I identified over 50 chloroplast localized lipases in silico. Using a reverse genetic approach, I first focused on the characterization of an Arabidopsis thylakoid membrane-associated lipase, PLASTID LIPASE1 (PLIP1). PLIP1 is a phospholipase A_1. In vivo, PLIP1 hydrolyzes polyunsaturated acyl groups from a unique chloroplast-specific PG that contains $16:1^{\Delta 3trans}$ at the *sn-2* glyceryl position. *PLIP1* is predominately expressed in seeds, and the *plip1* mutant seeds contain less oil while the *PLIP1* overexpression seeds contain more compared to the wild type. Pulse-chase labeling assays suggest that the acyl groups released by PLIP1 are exported from the chloroplasts, reincorporated into phosphatidylcholine before ultimately entering seed triacylglycerol. Therefore, $16:1^{\Delta 3trans}$ uniquely labels a biochemical active PG pool in developing Arabidopsis embryos, which is subject to PLIP1 mediated acyl export and seed oil biosynthesis.

The Arabidopsis genome encodes two putative PLIP1 paralogs which are designated PLIP2 and 3. PLIP2 and PLIP3 are also localized in the chloroplasts, but with different subplastid locations. PLIP2 possesses similar biochemical properties in vitro to PLIP1, but in vivo studies suggest that PLIP2 prefers MGDG as substrate, while PLIP3 prefers PG. Overexpression of *PLIP2* or *PLIP3* severely stunts plant growth and leads to accumulation of oxylipins. Genetically blocking jasmonate signaling restored the growth of the overexpression plants. The expression of *PLIP2* and *PLIP3*, but not *PLIP1* is induced by abscisic acid (ABA), and *plip1,2,3* triple mutants exhibit compromised jasmonate biosynthesis in response to ABA. Therefore, in Chapter 4, I am proposing that PLIP2 and PLIP3 are involved in linking ABA responses with jasmonate production.

ACKNOWLEDGEMENTS

First and foremost, I would like to thank my advisor and mentor Christoph Benning. He has been supportive since the day I joined the lab. I appreciate all his contribution of time, ideas and funding to make my Ph.D. experience productive and stimulating. He has taught me, consciously and unconsciously, what a great scientist should be. He is a very patient mentor. Despite my lack of experience in plant biology and biochemistry training when I joined the lab, he saw my potential and accepted me. I still remember vividly that he took time to teach me plant physiology himself every Friday afternoon in my third year to prepare me for my tomato project. After I was a bit mature, he allowed me more freedom to pursue the directions that I am interested in and trusted me to independently design projects. He always encouraged me to get out of my comfort zone, and to challenge and improve myself, an attitude surely will benefit me for my whole life.

I would also like to thank the members of my guidance committee, Dr. Sheng Yang He, Dr. Thomas Sharkey, Dr. Dean DellaPenna and Dr. R. Michael Garavito for their thought-provoking discussions, insightful suggestions as well as valuable career advices. They have been part of my inspiration in many ways. My Ph.D. experience would not be so profitable without their expertise, encouragement and support. Several other professors have also helped me kindly on experimental equipment and materials. Dr. Gregg A. Howe generally provided suggestions on my projects and jasmonates related materials. Dr. Shin-Han Shiu kindly spent time teaching me the bioinformatic knowledge for my projects. Dr. Giovanni Stefano and Dr. Melinda Frame gave helpful advice on confocal microscopy.

I also want to thank all the Benning lab members, past and present, for their companionship. All of them have been very nice to me and provided enormous help and precious suggestions on my research. I thank Yang Yang, Wei Ma, Chia-Hong Tsai and Xiaobo Li for their helpful discussions and entertainment; Dr. Barb Sears, Anna Hurlock and Anastasiya Lavell for critically reading my manuscripts and giving constructive feedbacks among many other things. Special mention goes to Dr. Rebecca Roston for patiently teaching me the fundamental bench skills during the first three years of my Ph.D. and Hope Hersh for her assistantship in experiments for the past four years.

I was initially recruited by the Biochemistry and Molecular Biology Department and joined the DOE-Plant Research Laboratory program in 2015. I would like to acknowledge the BMB secretary Jessica Lawrence, PRL staff Eunice Hoeve, Igor Houwat for their help and support through the years, which made my Ph.D. life smooth. I am also hugely appreciative to Jim Klug and Cody Keilen for organizing and maintaining the plant chambers and greenhouses.

More broadly, I thank MSU for providing the wonderful academic and life environment. Besides the world-class scientific facility and faculty, I am also entertained tremendously by the college sports. The Spartan Will spirit will be certainly carried on wherever I go.

Finally, my gratitude goes to friends and family. My time at MSU was made enjoyable and enriched in a large part due to the time spent with many friends. I am grateful to my parents and my wife for may years of love, support and understanding. My wife and I have been having a long-term relationship for over six years. I owe her many thanks to her unconditional love, understanding and support regardless the decision I made in my career and life.

TABLE OF CONTENTS

LIST OF TABLES

LIST OF FIGURES

KEY TO ABBREVIATIONS

ABA – abscisic acid

ABI – ABA INSENSITIVE

ACP – Acyl Carrier Protein

AOC – ALLENE OXIDE CYCLASE

AOS – ALLENE OXIDE SYNTHASE

COI1 – CORONATIN INSENSITIVE 1

DAG – diacylglycerol

DGAT – DAG-acyltransferases

DAD1 – DEFECTIVE IN ANTHER DEHISCENCE1

DGD1 – DGDG Synthase

DGDG – digalactosyldiacylglycerol

ER – endoplasmic reticulum

FA – fatty acid

FAD4 – FATTY ACID DESATURASE4

FAP – FATTY ACID BINDING PROTEINS

FAX1 – FATTY ACID EXPORT1

JA – jasmonic acid

JA-Ile – JA- isoleucine

JAR1 – JASMONATE RESISTENT 1

JAZ – JA ZIM-domain transcriptional repressors

LHCb1 – Light Harvesting Complex b1

LOX – lipoxygenase

MGD1 – MGDG Synthase

MGDG – monoalactosyldiacylglycerol

OPDA – 12-oxo phytodienoic acid

PA – phosphatidic acid

PC – phosphatidylcholine

PDAT – phospholipid: DAG acyltransferases

PE – phosphatidylethanolamine

PG – phosphatidylglycerol

PGD1 – Plastid Galactolipid Degradation1

PI – phosphatidylinositol

PLA_1 – phospholipase A_1

PLA_2 – phospholipase A_2

PLC – phospholipase C

PLD – phospholipase D

PLIP1 – PLASTID LIPASE1

SDP1 – SUGAR DEPENDENT1

SFR2 – SENSITIVE TO FREEZING 2

SQDG – sulfoquinovosyldiacylglycerol

TAG – triacylglycerol

TGD1 – TRIGALACTOSYLDIACYLGLYCEROL1

TGDG – trigalactosyldiacylglycerol

TLC – thin-layer chromatography

CHAPTER 1

Introduction

In plants and algae, chloroplasts are organelles that carry out a number of crucial functions, including photosynthesis, fatty acid biosynthesis and plant immune responses. Chloroplast membranes with a unique lipid composition are essential for the proper functions of chloroplasts. In Arabidopsis, chloroplasts lipids are synthesized by two pathways (Benning, 2009; Hurlock et al., 2014). De novo synthesized fatty acids (FAs) can either directly enter the plastid pathway or are exported to the endoplasmic reticulum (ER) and assembled into lipids there. Lipid precursors synthesized in the ER can also return to the plastid and contribute to chloroplast lipid biosynthesis (Wang and Benning, 2012; Hurlock et al., 2014). To date, many of the genes and the respective enzymes needed for chloroplast lipid biosynthesis have been characterized in Arabidopsis. Certain chloroplast lipid biosynthetic genes are induced, or the corresponding enzymes are activated only in response to specific stresses. They function to remodel the chloroplast membrane composition affecting its biophysical properties to cope with unfavorable conditions.

Besides lipid biosynthesis, maintenance of the chloroplast membranes also requires a finely tuned lipid catabolic machinery. A number of lipid degrading enzymes are predicted to be localized in the chloroplast with unknown physiological functions. It has been proposed that lipases are crucial for various aspects of chloroplast physiology, e.g., membrane turnover, lipid recycling and signaling (Wang, 2002, 2004; Scherer et al., 2010; Richmond and Smith, 2011).

Galactolipid Synthesis and Remodeling in Response to Stress

The galactolipids monogalactosyldiacylglycerol (MGDG) and digalactosyldiacylglycerol (DGDG) are the most abundant lipids in plant leaf tissues and they comprise up to ~50% and ~25% of total chloroplast lipids, respectively (Block et al., 1983). During normal growth and development, MGDG and DGDG are exclusively restricted to the chloroplasts. However, DGDG

was also found in the extraplastidic membranes following phosphate deprivation (Härtel et al., 2000).

Under normal conditions, MGDG synthesis is catalyzed by MGDG synthase (MGD1) with UDP-Gal and diacylglycerol (DAG) as substrates (Awai et al., 2001), while DGDG is synthesized by DGDG synthase (DGD1) using UDP-Gal as the head group donor to further galactosylate MGDG (Dörmann et al., 1995; Dörmann et al., 1999). Phosphate is essential for the synthesis of biological macromolecules including DNA and phospholipids. Highly regulated transcriptional and post-transcriptional mechanisms are evolved in plants in response to phosphate limiting conditions (Rubio et al., 2001; Aung et al., 2006; Chiou et al., 2006). Phosphate liberation from phospholipids and replacement of phospholipids by galactolipids is one of the mechanisms that enables plants to cope with phosphate deficiency (Dörmann and Benning, 2002). Two genes encoding paralogs of MGD1 (*MGD2* and *MGD3*) and a single gene encoding a DGD1 paralog (*DGD2*) are transcriptionally induced during phosphate deprivation (Awai et al., 2001; Kelly and Dörmann, 2002). Presence of the *MGD1* and *DGD1* paralogs enables the maintenance of galactolipid levels under phosphate deprivation and allows the export of DGDG to the extraplastidic membranes, even though the export mechanisms remain enigmatic thus far (Moellering and Benning, 2011).

Another pathway for galactolipid biosynthesis and remodeling is the SFR2 catalyzed oligogalactolipid biosynthesis during freezing. The *sfr2* mutant was discovered in 1996 by Gareth Warren and his colleagues by screening of freezing sensitive mutants in *Arabidopsis thaliana*. As one of the seven identified sensitive to freezing mutants, *sfr2* distinguishes itself by displaying a strong and severe phenotype on the whole plant but maintaining an intact plasma membrane under freezing conditions (Warren et al., 1996). Later, transmission electron microscopy showed that the

chloroplast membranes rather than the plasma membrane of the *sfr2* mutant are disrupted. The chloroplast membranes are fused with other organelle membranes after freezing treatment, which leads to cell disruption upon rewarming (Fourrier et al., 2008). By mapping, *SFR2* was identified as At3g06510, which encodes a beta glycosidase classified as a family I glycosyl hydrolase belonging to a distinct lineage (Thorlby et al., 2004; Xu et al., 2004). Despite the conserved catalytic site suggesting it to be a glycosyl hydrolases, SFR2 possesses no hydrolase activity, but functions as a transferase (Roston et al., 2014). Structural modeling and site-directed mutagenesis of SFR2 revealed three unique regions that might evolutionally separate SFR2 from hydrolases: a loop insertion, the C-terminal peptide, and a hydrophobic patch adjacent to the catalytic site (Roston et al., 2014). The transcript level of *SFR2* and the level of the encoded protein remain constant under all conditions examined including freezing. Instead, SFR2 activity is directly turned on by decreased cytosolic pH and increased cytosolic Mg^{2+} concentration changes concomitant to the freezing (Roston et al., 2014; Barnes et al., 2016). As shown in Figure 1.1, when activated by freezing, this outer-envelope membrane bound enzyme processively transfers the galactosyl residues from MGDG to a second galactolipid acceptor, which gives rise to the formation of oligogalactolipid and DAG (Moellering et al., 2010; Roston et al., 2014). Depending on the galactosyl acceptor, the galactolipid product can be DGDG or higher order oligogalactolipids like trigalactosyldiacylglycerol (TGDG) or tetragalactosyldiacylglycerol (TeDG). However, distinct from the DGDG produced by the UDP-Gal-dependent DGD1/DGD2 lipid galactosyltransferases, which is in βα conformation with respect to the glycosidic linkage (Dörmann et al., 1999; Kelly and Dörmann, 2002), the DGDG produced by SFR2 is in all-β conformation (ββDGDG) (Xu et al., 2003). The other product of SFR2 activity, DAG is converted to triacylglycerol (TAG) and sequestered into lipid droplets. Based on these observations, it is proposed that conversion of

MGDG into oligogalactolipids and DAG replaces non-bilayer forming lipids with bilayer stabilizing ones. This process also adjusts chloroplast envelope membranes as the chloroplast shrinks in response to cellular dehydration accompanying ice formation in the apoplast during freezing. Presence of the oligogalactosyl residues as the head group also increases the hydration of the chloroplast envelope membranes. As a result, the chloroplast membranes are stabilized and do not fuse with other membranes during freezing conditions.

SFR2-like genes are present in the plant kingdom over a wide phylogenic distribution based on the observation of sequenced genomes and expressed tag sequences (EST), including species both resistant and sensitive to freezing (Fourrier et al., 2008). Introduction of SFR2 cDNAs from freezing intolerant plant species, such as soy bean (*Glycine max*) and rice (*Oryza sativa*) can also rescue the freezing phenotype in the Arabidopsis *sfr2* mutant. Therefore, it is likely that SFR2 activity has other physiological roles in plants besides avoiding freezing damage. Freezing-triggered dehydration and cell shrinkage is shared with some other stresses, primarily drought and high salinity. In fact, oligogalactolipid accumulation was observed in desiccated leaves of Arabidopsis under room temperature and recently, lipid analysis of the resurrection plant *Craterostigma plantagineum* revealed that MGDG is converted to DGDG and DAG during the desiccation stage (Gasulla et al., 2013). Even though the responsible enzyme was not confirmed to be SFR2, it implies that MGDG conversion to oligogalactolipids might be a common strategy for plants to deal with dehydration.

Lipases in Lipid Catabolism

Lipases are enzymes that belong to a subclass of the esterases and catalyze the hydrolysis of lipids. They are the key enzymes for lipid turnover and play important roles in a wide range of

biological processes in most, if not all, living organisms (Wang, 2004; Scherer et al., 2010; Richmond and Smith, 2011). Due to their distinct catalytic properties even in organic solvents, lipases also constitute an important group of biocatalysts for biotechnological applications (Jaeger and Eggert, 2002). Based on their substrate preference, lipases from plants are broadly classified into TAG lipases, phospholipases, glycolipases, sulfolipases and monoacylglycerol lipases. They are more commonly classified based on the preference on the glyceryl positions at which the hydrolysis reaction happens. For example, phospholipases can be classified into four major types based on the cleavage sites, phospholipase D (PLD), phospholipase C (PLC), phospholipase A_1 (PLA_1), and phospholipase A_2 (PLA_2) (Figure 1.2). PLD releases the polar head group and produces phosphatidic acid while PLC cleaves the phosphodiester bond at the glyceryl *sn-3* position and produces the phosphorylated head group and DAG. PLAs release acyl groups from the glyceryl moiety at the *sn-1* or *sn-2* positions (Wang et al., 2012).

The Arabidopsis genome encodes about 300 proteins that are annotated as lipases, but most of them have not been biochemically verified and have unknown physiological functions (Li-Beisson et al., 2013; Troncoso-Ponce et al., 2013; Kelly and Feussner, 2016). A group of well characterized lipases named patatin-related PLAs are encoded by 10 genes in Arabidopsis. These lipases are structurally related to patatins, which are potato tuber proteins with acyl-hydrolyzing activities (Scherer et al., 2010). Members of this groups use diverse polar lipids as substrates and are involved in an array of physiological functions, including responses to auxin, pathogens and abiotic stresses (Scherer et al., 2010). One of the members named SUGAR DEPENDENT1 (SDP1) is a lipase that is capable of releasing acyl groups from both TAG and DAG. During seedling development, SDP1 is required for degrading seed storage oil to provide carbon skeletons and energy for the post-germinative growth (Eastmond, 2006). Another recently identified and

characterized lipase is Plastid Galactolipid Degradation1 (PGD1) in *Chlamydomonas reinhardtii* (Li et al., 2012). Expression of PGD1 is induced under nitrogen deprivation and the protein functions as an MGDG lipase. It almost exclusively hydrolyzes newly synthesized acyl groups that have not yet been desaturated from MGDG, and the acyl chains are later exported to the ER and incorporated into TAG. The PGD1 deficient mutant exhibits reduced TAG accumulation, decreased cell viability and altered MGDG and TAG fatty acid (FA) composition following nitrogen depletion.

A number of lipases are predicted to be located in the chloroplast, but most of them have not been characterized so far and have unknown physiological functions. Conceivably, these lipases are required for the membrane maintenance, turnover and oxylipin biosynthesis in the chloroplasts. One of the characterized plastid lipases is DEFECTIVE IN ANTHER DEHISCENCE1 (DAD1) which is a PLA_1 that is primarily present in the reproductive tissues, where it initiates JA biosynthesis critical for pollen maturation, anther dehiscence and flower opening in Arabidopsis (Ishiguro et al., 2001). In leaf tissues, *DONGLE* encodes a DAD1-homologous lipase contributing to wounding-induced JA production (Hyun et al., 2008).

Oxylipin Biosynthesis and Signaling

Lipids are frequently subject to oxidation through enzymatic and non-enzymatic processes (Mosblech et al., 2009). Oxylipins comprise a diverse class of lipophilic metabolites derived from the oxidation of polyunsaturated FAs, including FA hydroperoxides, hydroxy-, oxo-, or keto-FAs (Grechkin, 1998). Oxylipins are constitutively present at low levels in seed plants and their levels increase in response to a variety of responses (Mueller, 2004). The enzymatic process is primarily mediated by lipoxygenases (LOX) and some of their oxylipin products, e.g., jasmonate, are

essential for plant defense and reproduction (Porta and Rocha-Sosa, 2002). In parallel, oxidative stress and the formation of reactive oxygen species can also lead to chemically mediated lipid oxidation independent of lipoxygenases. Even though non-enzymatic lipid oxidation is generally regarded as deleterious, lipid peroxidation derived reactive electrophile species (RES) have emerged as signaling molecules that are capable of reprogramming plant transcriptomes through class II TGA transcription factors (Farmer and Mueller, 2013).

The enzymatic lipid oxidation process is initiated by the LOXs to produce lipid hydroperoxide using polyunsaturated FAs as substrates. The most common substrates in plants are linolenic (18:3; carbon number : double bonds number) and linoleic acids (18:2) (Grechkin, 1998), expects the debate that FAs esterified to the glycerol backbone could also be used as substrates (Feussner et al., 2001; Stelmach et al., 2001). Their products, 9- and 13-hydroperoxy FAs, can then enter an array of pathways leading to various products (Mosblech et al., 2009). One of the best characterized pathway is the ALLENE OXIDE SYNTHASE pathway which leads to the synthesis of oxylipins, including 12-oxo phytodienoic acid (OPDA), jasmonic acid (JA) and JA derivatives, *e.g.*, the bioactive JA-isoleucine (JA-Ile) (Turner et al., 2002; Wasternack and Hause, 2013).

JA production and signaling are primarily induced by wounding damage caused by herbivorous insects or necrotrophic microbes (Creelman et al., 1992; Howe and Schilmiller, 2002; Trusov et al., 2006). ~80% of wounding and insect attach related genes are under the control of JA in Arabidopsis leaves (Reymond et al., 2004). During plant growth and development, JA is essential for stamen development, sizes of petioles and petals, as well as lignin biosynthesis (Feys et al., 1994; McConn and Browse, 1996; Ellis et al., 2002; Buseman et al., 2006; Denness et al., 2011). Upon wounding damage or herbivory attack, JA production and activation of the JA

signaling represses plant growth by changing the plant transcriptome and interfering with the gibberellin signaling cascade (Yang et al., 2012). This was generally explained by the concept of growth-defense tradeoff (Huot et al., 2014; Zust et al., 2015). Recently, JA signaling mediated growth-defense tradeoff was genetically uncoupled in the *jazQ phyB* mutant which is deficient in five JA ZIM-domain transcriptional repressors (JAZs) and the photoreceptor phyB (Campos et al., 2016). In addition, synergetic or antagonistic interactions between JA and other phytohormones have also emerged. Classically, salicylic acid signaling antagonizes JA signaling for resistance against biotrophic and necrotrophic pathogens, respectively, while ethylene works synergistically with JA in activating the defense against the necrotrophic pathogens (Glazebrook, 2005). JA biosynthesis is also stimulated by applied ABA or during ABA-inducing abiotic stress conditions (Creelman and Mullet, 1995; Adie et al., 2007; Avramova, 2017), but the underlying mechanisms are not well understood. During abiotic stress, rising ABA levels induce JA synthesis, which synergistically optimizes the plant's abiotic defense by altering the plant transcriptome, facilitating stomata closure, inhibiting cell division, as well as epigenetically modifying defense genes during dehydration responses (Murata et al., 2015; Riemann et al., 2015; Liu et al., 2016; Valenzuela et al., 2016). A basic-helix-loop-helix transcription factor MYC2 plays roles in both JA perception and ABA signaling, and has been proposed as one of the factors linking ABA and JA signaling (Kazan and Manners, 2013).

As shown in Figure 1.3, JA biosynthesis starts in the plastids. Released poly-unsaturated FAs are oxidized by LOXs and ALLENE OXIDE SYNTHASE (AOS). The unstable allene oxides are subsequently cyclized by ALLENE OXIDE CYCLASE (AOC), leading to the production of 12-oxo phytodienoic acid (OPDA) and dinor-OPDA (Wasternack and Hause, 2013; Heitz et al., 2016). OPDA and dinor-OPDA are exported from the chloroplasts through unknown mechanisms,

and subsequently enter peroxisomes where they are subject to reduction and β-oxidation before the completion of JA synthesis (Wasternack and Hause, 2013; Heitz et al., 2016). Among many of the possible subsequent JA modifications, the conjugate JA-Ile produced by JASMONATE RESISTENT 1 (JAR1) is the active hormone molecule for JA signaling (Staswick and Tiryaki, 2004; Fonseca et al., 2009).

JA perception and signaling happens in the nucleus. Similar to other phytohormones, JA perception and signaling also fit the 'relief of repression model' (Santner and Estelle, 2009). In the absence of JA-Ile, key mediators including MYC transcription factors are repressed by JAZs in the resting state (Zhang et al., 2015). In the presence of JA-Ile, the F-box subunit of an SCF-type ubiquitin E3 ligase, CORONATIN INSENSITIVE 1 (COI1), forms the JA receptor complex together with JA-Ile and JAZs (Katsir et al., 2008). This subsequently leads to the ubiquitination mediated degradation of JAZs, liberating MYCs from the transcriptional repression and initiating the downstream signaling (Thines et al., 2007; Zhang et al., 2015).

Overview

Many aspects of the function and mechanisms of chloroplast lipid remodeling remain to be determined. The results in Chapter 2 expands the physiological functions of SFR2 to freezing sensitive plants. Chapter 3 explores chloroplast lipid catabolism and describes a novel lipase, PLASTID LIPASE 1 (PLIP1), that connects lipid catabolism with seed oil biosynthesis. In Chapter 4, the focus is on two paralogs of PLIP1, PLIP2 and PLIP3, that release FAs which are subsequently converted to oxylipins. A new hypothesis is provided suggesting that these lipases link ABA signaling with oxylipin biosynthesis. In Chapter 5, future perspectives are discussed and possible experiments are proposed for each chapter.

APPENDIX

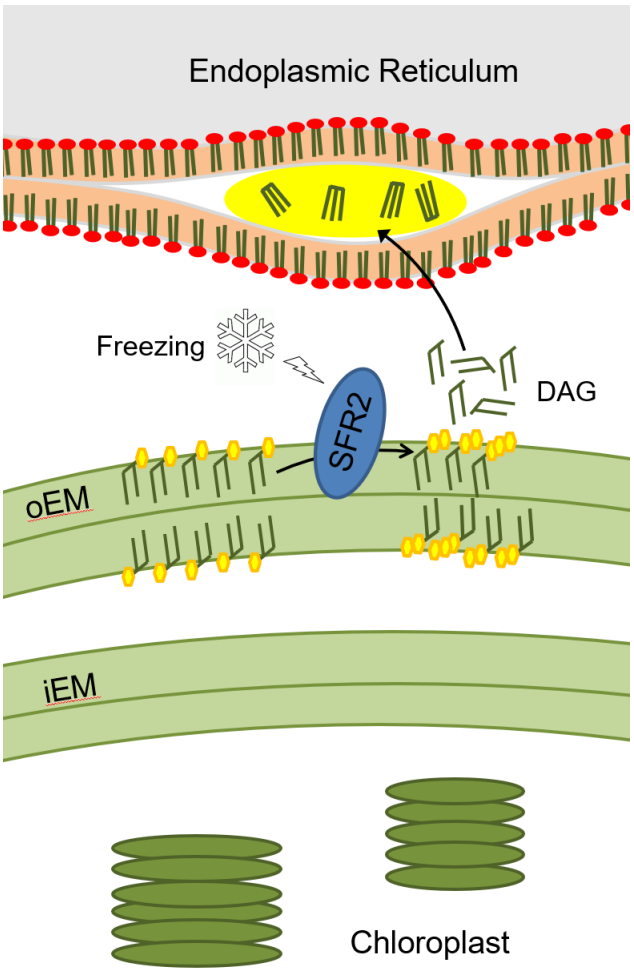

Figure 1. 1. Proposed model of SFR2-dependent galactolipid remodeling during Freezing. SFR2 is activated in the wild-type Arabidopsis plant during freezing. It removes the MGDG head group and transfers it to another MGDG (or DGDG) for the production of DGDG (or TGDG). The other product, DAG, is converted to TAG. This transgalactosylation activity stabilizes the membrane bilayer. Acyl chains and glycerol bonds are represented as green sticks, while galactosyl head groups are represented as yellow circles. DAG, diacylglycerol; DGDG, digalactosyldiacylglcyerol; MGDG, monogalactosyldiacylglycerol; TAG, triacylglycerol; TGDG, trigalactosyldiacylglycerol. oEM, outer envelope membrane; iEM, inner envelop membrane.

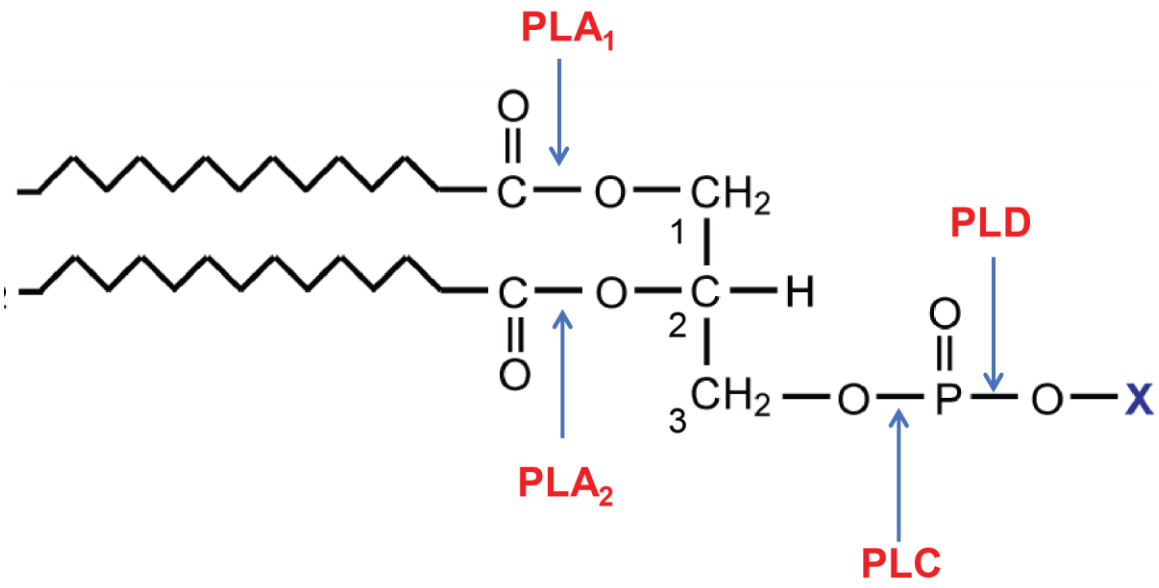

Figure 1. 2. Ester bond specificity of the phospholipases.
Phospholipase A1 (PLA1) and phospholipase A2 (PLA2) hydrolyze the ester bond from the sn-1 (1) and sn-2 (2) glyceryl positions, respectively. Phospholipase C (PLC) and phospholipase D (PLD) catalyze the hydrolysis of the phosphodiester bond adjacent or distal to the sn-3 glyceryl bond, respectively. X represents the derivatives for the phosphoryl-head group, such as choline, glycerol, ethanolamine, etc.

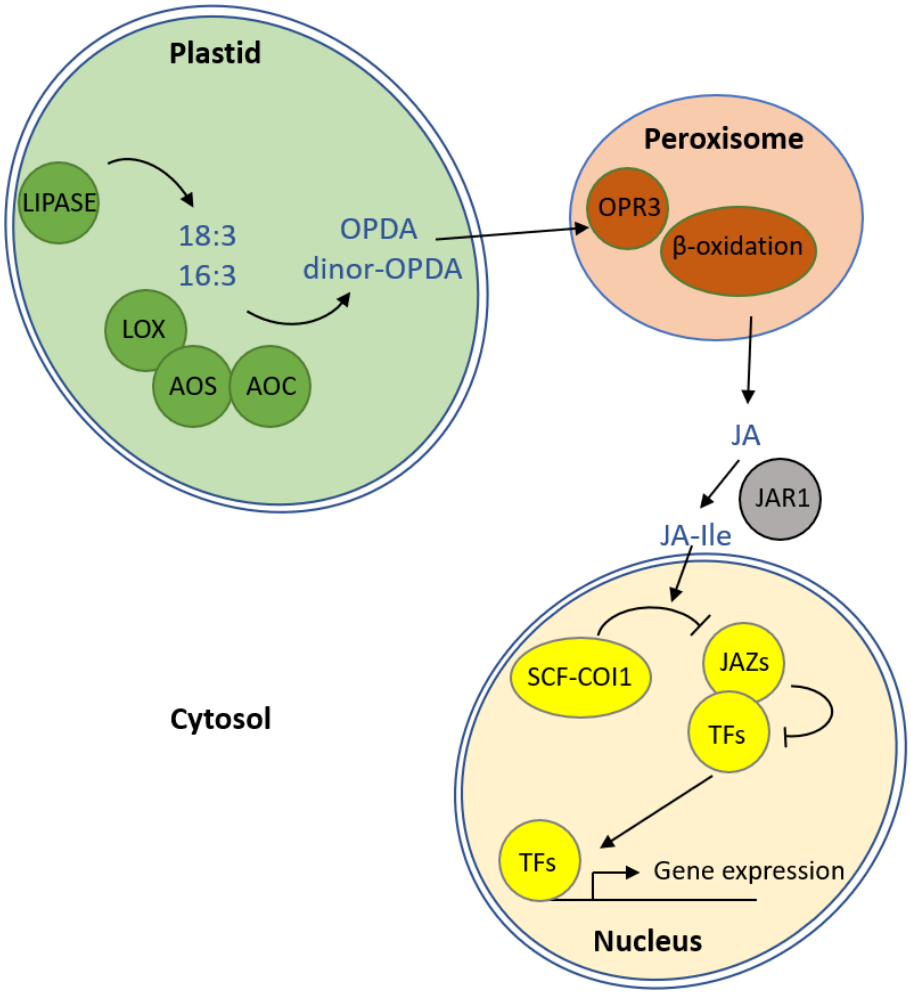

Figure 1. 3. Jasmonic acid biosynthesis and signaling in the context of cellular compartments. Jasmonic acid (JA) biosynthesis starts in the plastids, where the OPDA and dinor-OPDA are synthesized and exported from the plastids to peroxisomes before the completion of JA synthesis. JA is converted to the bioactive form, JA-Ile, in the cytosol. JA-Ile triggers the degradation of the JAZ proteins together with COI1, and the released TFs initiate gene expression in the nucleus. Enzymes are shown with black text in colored circles, while the metabolites are shown in blue text. AOC, ALLENE OXIDE CYCLASE; AOS, ALLENE OXIDE SYNTHASE; JAZ, Jasmonate ZIM domain (JAZ) transcriptional repressors; JAR, JASMONATE RESISTENT1; LOX, lipoxygenases; OPDA, 12-oxo Phytodienoic Acid OPR3; OPR3, OXOPHYTODIENOIC ACID REDUCTAXSE3; SCF-COI1, SKP1-CUL1-F-box (SCF)- CORONATINE INSENSITIVE1(COI1); TFs, transcription factors.

REFERENCES

REFERENCES

Adie, B.A., Perez-Perez, J., Perez-Perez, M.M., Godoy, M., Sanchez-Serrano, J.J., Schmelz, E.A., and Solano, R. (2007). ABA is an essential signal for plant resistance to pathogens affecting JA biosynthesis and the activation of defenses in Arabidopsis. Plant Cell **19,** 1665-1681.

Aung, K., Lin, S.I., Wu, C.C., Huang, Y.T., Su, C.L., and Chiou, T.J. (2006). pho2, a phosphate overaccumulator, is caused by a nonsense mutation in a microRNA399 target gene. Plant Physiol **141,** 1000-1011.

Avramova, Z. (2017). The jasmonic acid-signalling and abscisic acid-signalling pathways cross talk during one, but not repeated, dehydration stress: a non-specific 'panicky' or a meaningful response? Plant Cell Environ **40,** 1704-1710.

Awai, K., Marechal, E., Block, M.A., Brun, D., Masuda, T., Shimada, H., Takamiya, K., Ohta, H., and Joyard, J. (2001). Two types of MGDG synthase genes, found widely in both 16:3 and 18:3 plants, differentially mediate galactolipid syntheses in photosynthetic and nonphotosynthetic tissues in *Arabidopsis thaliana*. Proc Natl Acad Sci U S A **98,** 10960-10965.

Barnes, A.C., Benning, C., and Roston, R. (2016). Chloroplast membrane remodeling during freezing stress is accompanied by cytoplasmic acidification activating SENSITIVE TO FREEZING 2. Plant Physiol **171,** 2140-2149.

Benning, C. (2009). Mechanisms of lipid transport involved in organelle biogenesis in plant cells. Annu Rev Cell Dev Biol **25,** 71-91.

Block, M.A., Dorne, A.J., Joyard, J., and Douce, R. (1983). Preparation and characterization of membrane fractions enriched in outer and inner envelope membranes from spinach chloroplasts. II. Biochemical characterization. J Biol Chem **258,** 13281-13286.

Buseman, C.M., Tamura, P., Sparks, A.A., Baughman, E.J., Maatta, S., Zhao, J., Roth, M.R., Esch, S.W., Shah, J., Williams, T.D., and Welti, R. (2006). Wounding stimulates the accumulation of glycerolipids containing oxophytodienoic acid and dinor-oxophytodienoic acid in Arabidopsis leaves. Plant Physiol **142,** 28-39.

Campos, M.L., Yoshida, Y., Major, I.T., de Oliveira Ferreira, D., Weraduwage, S.M., Froehlich, J.E., Johnson, B.F., Kramer, D.M., Jander, G., Sharkey, T.D., and Howe, G.A. (2016). Rewiring of jasmonate and phytochrome B signalling uncouples plant growth-defense tradeoffs. Nat Commun **7,** 12570.

Chiou, T.J., Aung, K., Lin, S.I., Wu, C.C., Chiang, S.F., and Su, C.L. (2006). Regulation of phosphate homeostasis by MicroRNA in Arabidopsis. Plant Cell **18,** 412-421.

Creelman, R.A., and Mullet, J.E. (1995). Jasmonic acid distribution and action in plants: regulation during development and response to biotic and abiotic stress. Proc Natl Acad Sci U S A **92,** 4114-4119.

Creelman, R.A., Tierney, M.L., and Mullet, J.E. (1992). Jasmonic acid/methyl jasmonate accumulate in wounded soybean hypocotyls and modulate wound gene expression. Proc Natl Acad Sci U S A **89,** 4938-4941.

Denness, L., McKenna, J.F., Segonzac, C., Wormit, A., Madhou, P., Bennett, M., Mansfield, J., Zipfel, C., and Hamann, T. (2011). Cell wall damage-induced lignin biosynthesis is regulated by a reactive oxygen species- and jasmonic acid-dependent process in Arabidopsis. Plant Physiol **156,** 1364-1374.

Dörmann, P., and Benning, C. (2002). Galactolipids rule in seed plants. Trends Plant Sci **7,** 112-118.

Dörmann, P., Balbo, I., and Benning, C. (1999). Arabidopsis galactolipid biosynthesis and lipid trafficking mediated by DGD1. Science **284,** 2181-2184.

Dörmann, P., Hoffmann-Benning, S., Balbo, I., and Benning, C. (1995). Isolation and characterization of an Arabidopsis mutant deficient in the thylakoid lipid digalactosyl diacylglycerol. Plant Cell **7,** 1801-1810.

Eastmond, P.J. (2006). SUGAR-DEPENDENT1 encodes a patatin domain triacylglycerol lipase that initiates storage oil breakdown in germinating Arabidopsis seeds. Plant Cell **18,** 665-675.

Ellis, C., Karafyllidis, I., Wasternack, C., and Turner, J.G. (2002). The Arabidopsis mutant cev1 links cell wall signaling to jasmonate and ethylene responses. Plant Cell **14,** 1557-1566.

Farmer, E.E., and Mueller, M.J. (2013). ROS-mediated lipid peroxidation and RES-activated signaling. Annu Rev Plant Biol **64,** 429-450.

Feussner, I., Kuhn, H., and Wasternack, C. (2001). Lipoxygenase-dependent degradation of storage lipids. Trends Plant Sci **6,** 268-273.

Feys, B., Benedetti, C.E., Penfold, C.N., and Turner, J.G. (1994). Arabidopsis mutants selected for resistance to the phytotoxin coronatine are male sterile, insensitive to methyl jasmonate, and resistant to a bacterial pathogen. Plant Cell **6,** 751-759.

Fonseca, S., Chini, A., Hamberg, M., Adie, B., Porzel, A., Kramell, R., Miersch, O., Wasternack, C., and Solano, R. (2009). (+)-7-iso-Jasmonoyl-L-isoleucine is the endogenous bioactive jasmonate. Nat Chem Biol **5,** 344-350.

Fourrier, N., Bedard, J., Lopez-Juez, E., Barbrook, A., Bowyer, J., Jarvis, P., Warren, G., and Thorlby, G. (2008). A role for SENSITIVE TO FREEZING2 in protecting chloroplasts against freeze-induced damage in Arabidopsis. Plant J **55,** 734-745.

Gasulla, F., Vom Dorp, K., Dombrink, I., Zahringer, U., Gisch, N., Dörmann, P., and Bartels, D. (2013). The role of lipid metabolism in the acquisition of desiccation tolerance in Craterostigma plantagineum: a comparative approach. Plant J **75,** 726-741.

Glazebrook, J. (2005). Contrasting mechanisms of defense against biotrophic and necrotrophic pathogens. Annu Rev Phytopathol **43,** 205-227.

Grechkin, A. (1998). Recent developments in biochemistry of the plant lipoxygenase pathway. Prog Lipid Res **37,** 317-352.

Härtel, H., Dörmann, P., and Benning, C. (2000). DGD1-independent biosynthesis of extraplastidic galactolipids after phosphate deprivation in Arabidopsis. Proc Natl Acad Sci U S A **97,** 10649-10654.

Heitz, T., Smirnova, E., Widemann, E., Aubert, Y., Pinot, F., and Menard, R. (2016). The rise and fall of jasmonate biological activities. Subcell Biochem **86,** 405-426.

Howe, G.A., and Schilmiller, A.L. (2002). Oxylipin metabolism in response to stress. Curr Opin Plant Biol **5,** 230-236.

Huot, B., Yao, J., Montgomery, B.L., and He, S.Y. (2014). Growth-defense tradeoffs in plants: a balancing act to optimize fitness. Molecular plant **7,** 1267-1287.

Hurlock, A.K., Roston, R.L., Wang, K., and Benning, C. (2014). Lipid trafficking in plant cells. Traffic **15,** 915-932.

Hyun, Y., Choi, S., Hwang, H.J., Yu, J., Nam, S.J., Ko, J., Park, J.Y., Seo, Y.S., Kim, E.Y., Ryu, S.B., Kim, W.T., Lee, Y.H., Kang, H., and Lee, I. (2008). Cooperation and functional diversification of two closely related galactolipase genes for jasmonate biosynthesis. Dev Cell **14,** 183-192.

Ishiguro, S., Kawai-Oda, A., Ueda, J., Nishida, I., and Okada, K. (2001). The DEFECTIVE IN ANTHER DEHISCIENCE gene encodes a novel phospholipase A1 catalyzing the initial step of jasmonic acid biosynthesis, which synchronizes pollen maturation, anther dehiscence, and flower opening in Arabidopsis. Plant Cell **13,** 2191-2209.

Jaeger, K.E., and Eggert, T. (2002). Lipases for biotechnology. Curr Opin Biotechnol **13,** 390-397.

Katsir, L., Schilmiller, A.L., Staswick, P.E., He, S.Y., and Howe, G.A. (2008). COI1 is a critical component of a receptor for jasmonate and the bacterial virulence factor coronatine. Proc Natl Acad Sci U S A **105,** 7100-7105.

Kazan, K., and Manners, J.M. (2013). MYC2: the master in action. Molecular plant **6,** 686-703.

Kelly, A.A., and Dörmann, P. (2002). DGD2, an arabidopsis gene encoding a UDP-galactose-dependent digalactosyldiacylglycerol synthase is expressed during growth under phosphate-limiting conditions. J Biol Chem **277,** 1166-1173.

Kelly, A.A., and Feussner, I. (2016). Oil is on the agenda: Lipid turnover in higher plants. Biochim Biophys Acta **1861,** 1253-1268.

Li-Beisson, Y., Shorrosh, B., Beisson, F., Andersson, M.X., Arondel, V., Bates, P.D., Baud, S., Bird, D., Debono, A., Durrett, T.P., Franke, R.B., Graham, I.A., Katayama, K., Kelly, A.A., Larson, T., Markham, J.E., Miquel, M., Molina, I., Nishida, I., Rowland, O., Samuels, L., Schmid, K.M., Wada, H., Welti, R., Xu, C., Zallot, R., and Ohlrogge, J. (2013). Acyl-lipid metabolism. Arabidopsis Book **11,** e0161.

Li, X., Moellering, E.R., Liu, B., Johnny, C., Fedewa, M., Sears, B.B., Kuo, M.H., and Benning, C. (2012). A Galactoglycerolipid Lipase Is Required for Triacylglycerol Accumulation and Survival Following Nitrogen Deprivation in *Chlamydomonas reinhardtii*. Plant Cell **11,** 4670-4686.

Liu, N., Staswick, P.E., and Avramova, Z. (2016). Memory responses of jasmonic acid-associated Arabidopsis genes to a repeated dehydration stress. Plant Cell Environ **39,** 2515-2529.

McConn, M., and Browse, J. (1996). The critical requirement for linolenic acid is pollen development, not photosynthesis, in an arabidopsis mutant. Plant Cell **8,** 403-416.

Moellering, E.R., and Benning, C. (2011). Galactoglycerolipid metabolism under stress: a time for remodeling. Trends Plant Sci **16,** 98-107.

Moellering, E.R., Muthan, B., and Benning, C. (2010). Freezing tolerance in plants requires lipid remodeling at the outer chloroplast membrane. Science **330,** 226-228.

Mosblech, A., Feussner, I., and Heilmann, I. (2009). Oxylipins: structurally diverse metabolites from fatty acid oxidation. Plant Physiol Biochem **47,** 511-517.

Mueller, M.J. (2004). Archetype signals in plants: the phytoprostanes. Curr Opin Plant Biol **7,** 441-448.

Murata, Y., Mori, I.C., and Munemasa, S. (2015). Diverse stomatal signaling and the signal integration mechanism. Annu Rev Plant Biol **66,** 369-392.

Porta, H., and Rocha-Sosa, M. (2002). Plant lipoxygenases. physiological and molecular features. Plant Physiol **130,** 15-21.

Reymond, P., Bodenhausen, N., Van Poecke, R.M., Krishnamurthy, V., Dicke, M., and Farmer, E.E. (2004). A conserved transcript pattern in response to a specialist and a generalist herbivore. Plant Cell **16,** 3132-3147.

Richmond, G.S., and Smith, T.K. (2011). Phospholipases A_1. Int J Mol Sci **12,** 588-612.

Riemann, M., Dhakarey, R., Hazman, M., Miro, B., Kohli, A., and Nick, P. (2015). Exploring jasmonates in the hormonal network of drought and salinity responses. Front Plant Sci **6,** 1077.

Roston, R.L., Wang, K., Kuhn, L.A., and Benning, C. (2014). Structural determinants allowing transferase activity in SENSITIVE TO FREEZING 2, classified as a family I glycosyl hydrolase. J Biol Chem **289,** 26089-26106.

Rubio, V., Linhares, F., Solano, R., Martin, A.C., Iglesias, J., Leyva, A., and Paz-Ares, J. (2001). A conserved MYB transcription factor involved in phosphate starvation signaling both in vascular plants and in unicellular algae. Genes Dev **15,** 2122-2133.

Santner, A., and Estelle, M. (2009). Recent advances and emerging trends in plant hormone signalling. Nature **459,** 1071-1078.

Scherer, G.F., Ryu, S.B., Wang, X., Matos, A.R., and Heitz, T. (2010). Patatin-related phospholipase A: nomenclature, subfamilies and functions in plants. Trends Plant Sci **15,** 693-700.

Staswick, P.E., and Tiryaki, I. (2004). The oxylipin signal jasmonic acid is activated by an enzyme that conjugates it to isoleucine in Arabidopsis. Plant Cell **16,** 2117-2127.

Stelmach, B.A., Muller, A., Hennig, P., Gebhardt, S., Schubert-Zsilavecz, M., and Weiler, E.W. (2001). A novel class of oxylipins, sn1-O-(12-oxophytodienoyl)-sn2-O-(hexadecatrienoyl)-monogalactosyl Diglyceride, from Arabidopsis thaliana. J Biol Chem **276,** 12832-12838.

Thines, B., Katsir, L., Melotto, M., Niu, Y., Mandaokar, A., Liu, G., Nomura, K., He, S.Y., Howe, G.A., and Browse, J. (2007). JAZ repressor proteins are targets of the SCF(COI1) complex during jasmonate signalling. Nature **448,** 661-665.

Thorlby, G., Fourrier, N., and Warren, G. (2004). The SENSITIVE TO FREEZING2 gene , required for freezing tolerance in *Arabidopsis thaliana* , encodes a β-glucosidase **16,** 2192-2203.

Troncoso-Ponce, M.A., Cao, X., Yang, Z., and Ohlrogge, J.B. (2013). Lipid turnover during senescence. Plant Sci **205-206,** 13-19.

Trusov, Y., Rookes, J.E., Chakravorty, D., Armour, D., Schenk, P.M., and Botella, J.R. (2006). Heterotrimeric G proteins facilitate Arabidopsis resistance to necrotrophic pathogens and are involved in jasmonate signaling. Plant Physiol **140,** 210-220.

Turner, J.G., Ellis, C., and Devoto, A. (2002). The jasmonate signal pathway. Plant Cell **14 Suppl,** S153-164.

Valenzuela, C.E., Acevedo-Acevedo, O., Miranda, G.S., Vergara-Barros, P., Holuigue, L., Figueroa, C.R., and Figueroa, P.M. (2016). Salt stress response triggers activation of the jasmonate signaling pathway leading to inhibition of cell elongation in Arabidopsis primary root. J Exp Bot **67,** 4209-4220.

Wang, G., Ryu, S., and Wang, X. (2012). Plant phospholipases: an overview. Methods Mol Biol **861,** 123-137.

Wang, X. (2002). Phospholipase D in hormonal and stress signaling. Curr Opin Plant Biol **5,** 408-414.

Wang, X. (2004). Lipid signaling. Curr Opin Plant Biol **7,** 329-336.

Wang, Z., and Benning, C. (2012). Chloroplast lipid synthesis and lipid trafficking through ER-plastid membrane contact sites. Biochem Soc Trans **40,** 457-463.

Warren, G., McKown, R., Marin, a.L., and Teutonico, R. (1996). Isolation of mutations affecting the development of freezing tolerance in *Arabidopsis thaliana* (L.) Heynh. Plant Physiol **111,** 1011-1019.

Wasternack, C., and Hause, B. (2013). Jasmonates: biosynthesis, perception, signal transduction and action in plant stress response, growth and development. An update to the 2007 review in Annals of Botany. Ann Bot **111,** 1021-1058.

Xu, C., Fan, J., Riekhof, W., Froehlich, J.E., and Benning, C. (2003). A permease-like protein involved in ER to thylakoid lipid transfer in Arabidopsis. EMBO J **22,** 2370-2379.

Xu, Z., Escamilla-Trevino, L., Zeng, L., Lalgondar, M., Bevan, D., Winkel, B., Mohamed, A., Cheng, C.L., Shih, M.C., Poulton, J., and Esen, A. (2004). Functional genomic analysis of *Arabidopsis thaliana* glycoside hydrolase family 1. Plant Mol Biol **55,** 343-367.

Yang, D.L., Yao, J., Mei, C.S., Tong, X.H., Zeng, L.J., Li, Q., Xiao, L.T., Sun, T.P., Li, J., Deng, X.W., Lee, C.M., Thomashow, M.F., Yang, Y., He, Z., and He, S.Y. (2012). Plant hormone jasmonate prioritizes defense over growth by interfering with gibberellin signaling cascade. Proc Natl Acad Sci U S A **109,** E1192-1200.

Zhang, F., Yao, J., Ke, J., Zhang, L., Lam, V.Q., Xin, X.F., Zhou, X.E., Chen, J., Brunzelle, J., Griffin, P.R., Zhou, M., Xu, H.E., Melcher, K., and He, S.Y. (2015). Structural basis of JAZ repression of MYC transcription factors in jasmonate signalling. Nature **525,** 269-273.

Zust, T., Rasmann, S., and Agrawal, A.A. (2015). Growth-defense tradeoffs for two major anti-herbivore traits of the common milkweed *Asclepias syriaca*. Oikos **124,** 1404-1415.

CHAPTER 2

SENSITIVE TO FREEZING2 Aids in Resilience to Salt and Drought in Freezing-Sensitive Tomato

The work presented in this chapter has been published in Plant Physiology (www.plantphysiol.org) with the copyright belonging to American Society of Plant Biologists:

Wang, K., Hersh, H.L., and Benning, C. (2016). SENSITIVE TO FREEZING2 Aids in Resilience to Salt and Drought in Freezing-Sensitive Tomato. Plant Physiology **172,** 1432-1442.

ABSTRACT

SENSITIVE TO FREEZING2 (SFR2) is crucial for protecting chloroplast membranes following freezing in Arabidopsis (*Arabidopsis thaliana*). It has been shown that SFR2 homologs are present in all land plants, including freezing-sensitive species, raising the question of SFR2 function beyond freezing tolerance. Similar to freezing, salt and drought can cause dehydration. Thus, it is hypothesized that in freezing-sensitive plants SFR2 may play roles in their resilience to salt or drought. To test this hypothesis, *SlSFR2* RNAi lines were generated in the cold / freezing-sensitive species tomato (*Solanum lycopersicum* [M82 *cv*]). Hypersensitivity to salt and drought of *SlSFR2*-RNAi lines was observed. Higher tolerance of wild-type tomatoes was correlated with the production of trigalactosyldiacylglycerol, a product of SFR2 activity. Tomato SFR2 in vitro activity is Mg2+-dependent and its optimal pH is 7.5, similar to that of Arabidopsis SFR2, but the specific activity of tomato SFR2 in vitro is almost double that of Arabidopsis SFR2. When salt and drought stress were applied to Arabidopsis, no conditions could be identified at which SFR2 was induced prior to irreversibly impacting plant growth, suggesting that SFR2 protects Arabidopsis primarily against freezing. Discovery of tomato SFR2 function in drought and salt resilience provides further insights into general membrane lipid remodeling-based stress tolerance mechanisms and together with protection against freezing in freezing-resistant plants such as Arabidopsis, it adds lipid remodeling as a possible target for the engineering of abiotic stress-resilient crops.

INTRODUCTION

As one of the major environmental plant stresses, freezing greatly afflicts the production of crops and limits the geographic distribution of naturally occur- ring plants (Pearce, 2001). Adaptations to freezing have been studied at the physiological, metabolic, molecular, and genetic levels (Andrews, 1996; Browse and Xin, 2001; Griffith and Yaish, 2004). The Arabidopsis (*Arabidopsis thaliana*) mutant *sensitive to freezing2* (*sfr2*) was discovered as a freezing-sensitive plant during a forward genetic mutant screen (Warren et al., 1996). The SFR2 protein is associated with the outer envelope membrane of chloroplasts and is crucial for maintaining chloroplast membrane integrity after exposure to freezing temperatures (Fourrier et al., 2008; Roston et al., 2014). Despite the fact that this protein was originally classified as a family I glycosyl-hydrolase and originally described as glucosidase (Thorlby et al., 2004), SFR2 has galactosyltransferase activity (Moellering et al., 2010; Roston et al., 2014). Once activated under freezing conditions, SFR2 processively transfers galactosyl residues from the most abundant chloroplast membrane lipid monogalactosyldiacylglycerol (MGDG) to a second galactolipid acceptor, forming oligogalactolipids and diacylglycerol (DAG). The DAG is then converted to triacylglycerol (Moellering et al., 2010). This mechanism of remodeling chloroplast membrane lipids upon freezing helps adjusting envelope membranes by removing extra polar lipids as the organelle shrinks due to apoplastic ice formation and cellular dehydration. Membranes are stabilized by increasing the ratio of bilayer-forming to nonbilayer-forming lipids. In addition, through increased abundance of polar oligo- galactolipid head groups, the hydration of the envelope membrane is increased during freezing-related dehydration (Moellering et al., 2010).

Phylogenetic analysis shows that *SFR2* orthologs are ubiquitous in the genomes of land plants, including freezing-sensitive species. Ectopic expression of *SFR2* orthologs from freezing-

sensitive soybean (*Glycine max*) and rice (*Oryza sativa*) has been shown to revert the *sfr2* phenotype in Arabidopsis (Fourrier et al., 2008). This finding suggests that SFR2 orthologs are functionally interchangeable regardless of their origin from freezing-tolerant or -sensitive species. Therefore, we hypothesized that SFR2 must play physiological roles beyond freezing resilience in plants that never encounter freezing temperatures in their natural habitats. Given the sessile nature of all plants, encountering unfavorable growth conditions even in lush tropical environments is at times inevitable. Unfavorable conditions might include periods of high temperature and drought, or increased salt concentrations in soils following coastal flooding. Salt and drought stress are conceptually closely related to freezing, as all are accompanied by severe dehydration of plant cells (Andrews, 1996; Verslues et al., 2006). Drought stress directly decreases the water potential in the apoplast and causes water deficiency within the symplast. Increased salt exposure can change the cellular ion and solute homeostasis, which directly limits water availability for other cellular processes such as biochemical reactions or membrane hydration. Upon freezing, cellular dehydration is caused by extracellular ice formation, which acts as a nucleation site for water drawn out of the cell (Andrews, 1996). Cellular dehydration in plants usually is accompanied by the shrinkage of the symplast and organelles, bringing different cellular membranes into close proximity, which can lead to the fusion of membranes along with membrane bilayer structure disruption. To alleviate cellular dehydration, plants have evolved common signaling pathways, transcriptional responses, and metabolic adjustments shared in response to freezing, salt, and drought exposure (Zhu, 2002; Mahajan and Tuteja, 2005; Krasensky and Jonak, 2012), further suggesting that these abiotic stresses elicit similar protective mechanisms in plants.

As outlined above, SFR2-mediated remodeling of membrane lipids was shown to protect chloroplast membrane structure during dehydration caused by freezing. The same may be true for

cellular dehydration as the result of salt or drought stress. In fact, in the resurrection plant *Craterostigma plantagineum* MGDG is increasingly converted to digalactosyldiacylglycerol (DGDG) and DAG during desiccation (Gasulla et al., 2013). Even though the responsible enzyme has not yet been identified, this observation suggests that MGDG conversion to higher order galactolipids might be a general strategy for plants coping with dehydration. Recently, SFR2 was shown to interact in guard cells with Open Stomata1, an SnRK2-type protein kinase involved in mediating ABA responses in Arabidopsis (Waadt et al., 2015). It remains to be shown whether this interaction is physiologically relevant or whether SFR2 may be involved in remodeling of chloroplast membranes in guard cells in response to dehydration. Here, tomato (*Solanum lycopersicum*) was chosen as a representative cold-sensitive plant to explore possible roles of SFR2 in the protection of plants against dehydration-inducing abiotic stresses other than freezing. In addition, we tested whether SFR2 could protect Arabidopsis against other abiotic stresses than freezing.

MATERIALS AND METHODS

Plant Materials and Growth Conditions

Tomato cultivar M82 seeds were generously provided by Dr. Cornelius Barry, Michigan State University. Seed were germinated by being plated on a moisturized filter paper for a week, then seedlings were transferred to soil and kept in a growth chamber with the condition set as 200-300 μE $m^{-2}s^{-1}$ with a 16 h light/8 h dark and 24/20°C (day/night). Plants were watered with tomato nutrient formula water, specifically, 12.2 g 15-30-15 (N-P-K, %weight) fertilizer, 0.13 g Fe iron and 0.05 g calcium nitrate in one gallon deionized water.

Arabidopsis (*Arabidopsis thaliana*) Columbia-2 and *sfr2-3* seeds (Moellering et al., 2010a) were sterilized and plated on Murashige and Skoog medium (Murashige and Skoog, 1962) containing 1% (w/v) Sucrose. Plants were grown under 100 μE $m^{-2}s^{-1}$ with a 16-h-light / 8-h-dark cycle and 22°C.

Rnai Plasmid Constructions and Tomato Transformation

Total RNA was extracted from tomato M82 leaves using the Plant RNeasy RNA extraction kit (Qiagen); 600 ng RNA was reverse transcribed using SuperScript® III Reverse Transcriptase (life technology) and oligo(dT)18 following the manufacturer's protocols. The *SlSFR2* RNAi construct was built by first amplifying the 509-bp (121-629bp) cDNA of *SlSFR2* Using primers as shown in Table 2.1. PCR products were purified by QIAquick PCR Purification Kit (Qiagen) and then inserted into the pENRT/D vector according to the pENTR/D-TOPO Cloning kit instruction (Life Technologies). The 509-bp *SlSFR2* fragment was finally recombined into pHELLSGATE12 vector by the LR reaction using Gateway LR Clonase II Enzyme Mix (Life technologies). Tomato transformation was done essentially as described (McCormick, 1991).

Quantitative Real-Time PCR

Total RNA from the 4th leaves of 8-week old tomatoes was isolated and reverse transcribed as described above. qRT-PCR was performed using the SYBR Green PCR Core Reagents mix (Life Technologies) based on the manufacturer's instructions. Table 2.1 lists the primers used. The $2^{-\Delta\Delta Ct}$ calculation was used to determine the relative mRNA levels.

Lipid Analysis

Lipids were extracted from approximately 50 mg 4-week-old tomato 2nd and 4th leaves as previously described (Moellering et al., 2010b). Polar lipids were analyzed on activated ammonium sulfate-impregnated silica gel TLC plates (Si250; Mallinckrodt Baker, Phillipsburg, NJ, USA, which are no longer available, and which were later substituted by DC-Fertigplatten SIL G-25; MACHEREY-NAGEL, Germany) using a solvent system consisting of chloroform: methanol: acetic acid: water (85:20:10:4, v/v/v/v). Lipids were visualized by brief exposure to iodine vapor or staining with α-naphthol to detect glycolipids.

Protein Production

An *SlSFR2* yeast expression construct was built by amplifying the full *Sl*SFR2 coding sequence from a cDNA, which was inserted into the pYES2.1 vector according to the manufacturer's instructions (Invitrogen). The recombinant protein contained a C-terminal 6XHis tag. Arabidopsis *AtSFR2* and cucumber *CsMGD1* constructs are described in (Roston et al., 2014). Protein production was essentially done as described in (Roston et al., 2014). Microsomes were harvested from yeast cells post induction as described in (Dahlqvist et al., 2000) and stored at -80 °C until use. Protein extraction was done according to (Kushnirov, 2000) and protein production

was analyzed by SDS-PAGE and immunoblotting as described in (Roston et al., 2014). SFR2 assays were performed as described in (Roston et al., 2014), except that the $MgCl_2$ concentration was elevated to 8 mM.

Stress Assays

For Arabidopsis, after 7 days of growth in regular medium seedling were transferred to MS plates with extra concentrations of salts for salt treatment, or of PEG-8000 to generate different water potentials for drought treatment. For the drought assay, the detailed recipe for preparing PEG-infused plates is descried in (van der Weele et al., 2000). Plants were grown for 3 weeks before ion leakage or lipid analysis.

Tomato seeds were first germinated on moisturized filter paper for 1 week under standard conditions as described above, and then transferred to soil and grown for 2 weeks before application. For the salt assay, three-week-old plants were acclimated by daily watering with nutrient solution, to which 50 mM NaCl was added, for 5 days and then followed by increasing NaCl to 100 mM for a week and 150 mM for another 2 days. Plant and leaf images were taken at the end of the salt treatment. Plants were watered daily with normal nutrient solution for one week after the end of the salt treatment to ensure they resume normal growth.

For the drought assay, three-week-old tomato plants were not watered for 3 days to acclimate the plants followed by watering with nutrient solution for 4 days. The then the three-week-old plants were not watered for another 9 days, followed by daily watering. Lipids were extracted and analyzed at the end of the drought treatment. Plant and leaf images were taken 2 days after resuming watering.

Water potential and relative water content measurements were conducted before the rewatering phase. Water potential was measured with a pressure chamber (PMS instrument company, Model 600) following the equipment manual. Water content measurement was performed according to (Barrs and Weatherley, 1962).

The electrolyte assays were performed as described (Gilmour et al., 1988). Briefly, 3 to 5 leaf blades were immersed in 3 ml of deionized water and the samples were gently agitated for 3 hours. Conductivity was measured using a conductivity meter (YSI model 35). One hundred percent leakage was defined by placing the leaves in -80°C for 10 hours and then agitating them for 3 hours before conductivity of the solution was measured. Electrolyte leakage was expressed as a percentage of the final conductivity.

Chlorophyll Measurements

Chlorophyll was quantified as described (Lichtenthaler and Wellburn, 1983). In brief, Leaf pigments were extracted in 80% (v/v) acetone from punched discs and measured spectrophotometrically on an Uvikon 930 spectrophotometer (Kontron instruments, Germany). Chlorophyll *a*, chlorophyll *b* and total carotenoids were calculated from leaf absorbance at 663nm and 646nm with the following equations: Chlorophyll *a* (mg/l) = $12.21A_{663} - 2.81A_{646}$; Chlorophyll *b* (mg/l) = $20.13A_{646} - 5.03A_{663}$; Total chlorophyll (mg/l) = chlorophyll *a* + chlorophyll *b*.

Protein Measurement

Leaf disks were ground with liquid nitrogen to which 100 µl extraction buffer (0.1M Tris HCl, pH 6.8; 1% SDS; 15% glycerol; 5% (v/v) β-mercaptoethanol) was added, followed by vigorous mixing. Samples were boiled at 100℃ for 10 minutes followed with centrifugation at

13,000 x *g* for 5 mins and the proteins were quantified using a Bradford assay (BioRad) following the manufacturer's instructions.

RESULTS

Salt and Drought Treatment Similarly Affect Arabidopsis Wild Type and *sfr2-3* Mutant

SFR2 has been shown to be essential for freezing tolerance in Arabidopsis. In principle, if SFR2 provides protection against cellular dehydration in general, one might expect that it also protects Arabidopsis against salt and drought stress. To test this hypothesis, we investigated whether salt or drought tolerance is compromised in the Arabidopsis *sfr2-3* mutant, which carries an *sfr2* loss-of-function allele (Moellering et al., 2010a). For the salt stress assay, wild-type (WT, Col-2) and mutant *sfr2-3* seedlings were grown for one week on regular MS medium prior to the transfer to MS plates containing different concentrations of NaCl (Figure 2.1). Within three weeks of treatment, all plants were increasingly stunted with increasing NaCl concentrations (Figure 2.1). No significant difference in growth was observed between the wild type and *sfr2-3* (Figure 2.1). Ion leakage of the leaf tissues also increased in parallel with NaCl concentrations with no difference observed for the wild type and *sfr2-3* (Figure 2.1). To check whether SFR2 was activated during the treatment, lipids were analyzed by thin-layer chromatography (TLC) (Figure 2.1). To activate SFR2 in vivo, leaves were treated by $MgCl_2$ infiltration (Moellering et al., 2010b) and as a result WT leaves contained TGDG, a specific product of SFR2, while *sfr2-3* did not (Figure 2.1). No TGDG was detected in all salt treated plant leaves, suggesting that SFR2 was not activated under the conditions tested (Figure 2.1). Root bending assays in response to NaCl treatment and direct salt treatment of soil-grown plants showed consistently no differences between the wild type and the *sfr2-3* mutant (Figure 2.2).

For the drought assay, WT and *sfr2-3* plants were grown on control MS plates (Ψ=-2.5 MPa) for a week before transfer to other plates with lower water potentials (Figure 2.1). When grown on MS medium with Ψ as low as -7.5MPa, both wild type and *sfr2-3* were dead after 2

weeks. After three weeks of growth on MS medium with Ψ=-5 MPa, plants were alive but growth was pronouncedly compromised (Figure 2.1). No differences were observed between WT and *sfr2-3* (Figure 2.1). In addition, no TGDG accumulation was observed suggesting that SFR2 was not activated during the drought treatment (Figure 2.1). Similar results were also observed for soil-grown plants as shown in Figure 2.3.

Apparently, for Arabidopsis no condition of salt or drought treatment could be identified that would lead to activation of SFR2 before the plants were irreversibly compromised. One interpretation is that salt and drought stress affect essential cellular processes other than chloroplast membrane stability and if those become compromised in Arabidopsis prior to the membranes, the hypothesis stated above cannot be tested in Arabidopsis. Therefore, we shifted the focus of this study to the freezing-sensitive tomato, in which we were able to study the function of SFR2 in other abiotic stresses than freezing.

Identification of an SFR2 Orthologue of *Solanum lycopersicum*

To identify the SFR2 orthologue of tomato (M82), a BLASTp search of the tomato genome protein database (http://solgenomics.net/) was performed using the Arabidopsis SFR2 sequence (*At*SFR2) as the query (Fernandez-Pozo et al., 2015). Tomato gene Solyc01g058140.2.1 encoded the top scoring protein fragment with a reported E-value of zero and the respective protein was designated *Sl*SFR2. The two aligned protein sequences showed 59% identity overall and 72% similarity (Figure 2.4). To corroborate that *Sl*SFR2 has galactolipid : galactolipid galactosyltransferase activity, the respective cDNA was expressed in a yeast strain that also expresses a *Cucumis sativus* MGDG synthase-encoding cDNA (*CsMGD1*) (Shimojima et al., 1997) ensuring the production of MGDG, which is the substrate for SFR2. Arabidopsis and tomato

SFR2 cDNAs were tested in parallel. SFR2 protein production in yeast was confirmed by immunoblot using an anti-His antibody against a c-terminal 6xHIS-TAG included with both constructs (Figure 2.5) and the lipids were extracted from induced cultures. When *LacZ*, *AtSFR2* or *SlSFR2* were expressed in yeast lacking MGDG, no galactolipids were detected by TLC (Figure 2.5). When *CsMGD1*was expressed alone, only MGDG was present. Co-expression of *SlSFR2* or *AtSFR2* with *CsMGD1* led to the formation of the oligogalactolipids DGDG, tri- (TGDG) and tetragalactosyldiacylglycerol (TeGDG). Therefore, *SlSFR2* encodes an SFR2 protein with galactolipid : galactolipid galactosyl transferase activity.

*Sl*SFR2 Has Higher Specific Activity Than *At*SFR2

It seemed possible that the specific activity and activation of SFR2 orthologs from freezing-insensitive and -sensitive plants differ. The activity of *At*SFR2 is Mg^{2+} and pH-dependent (Moellering et al., 2010b; Roston et al., 2014; Barnes et al., 2016) and we tested whether this was also the case for *Sl*SFR2. To estimate *Sl*SFR2 and *At*SFR2 specific activities, microsomes were prepared from the respective yeast cultures and MGDG-based galactosyl transfer activity was assayed in the presence of 8 mM $MgCl_2$ at pH 7.5 (Moellering et al., 2010b) using approximately equal amounts of SFR2 proteins as estimated by immunoblotting (Figure 2.6). A *LacZ* expressing line was included as a background control. Under these conditions, *Sl*SFR2 activity was nearly twice that of *At*SFR2 (Figure 2.6) and given that approximately equal amounts of protein were used, its specific activity must be higher than that of the Arabidopsis enzyme. Using different concentrations of $MgCl_2$ ranging from 0 to 12 mM (Figure 2.6), both enzymes showed similarly strong Mg^{2+} dependency of their activity. When the pH-dependency of *Sl*SFR2 was tested using a series of buffers with varying pH, it was apparent that the optimal pH for *Sl*SFR2 is approximately

7.5 (Figure 2.6), which agrees with that observed for *At*SFR2 (Roston et al., 2014). Thus, aside from an observed higher specific activity of *Sl*SFR2, both orthologues behaved essentially the same under the conditions tested.

Generation of *SlSFR2 RNAi* Lines in Tomato

To explore physiological functions of *Sl*SFR2 in cold/freezing-sensitive tomato, an *SlSFR2*-RNAi construct was introduced into tomato M82 (Figure 2.7). In total, 23 transgenic lines were generated and the presence of the *SlSFR2*-RNAi construct was confirmed by PCR using genomic DNA (Figure 2.8). To examine the RNAi effect, *SlSFR2* transcript abundance of the transgenic lines was quantified by quantitative real-time PCR (Figure 2.7) and the majority of lines showed an 80% reduction in transcript abundance.

To estimate the maximal in vivo *Sl*SFR2 activity in the RNAi transgenic lines, we incubated detached tomato leaves in a 0.5 M $MgCl_2$ aqueous solution for 6 hours, which fully activates the enzyme, or water only (mock) followed by lipid extraction and TLC of the polar lipids (Fig. 4; Supplemental Fig. S5 for additional lines). Arabidopsis and tomato WT produced TGDG in the $MgCl_2$-treated leaves only. However, most of the 13 lines with low *SlSFR2* RNA abundance showed a decreased ability to produce TGDG following $MgCl_2$ treatment (Figure 2.7; Figure 2.7). Based on the extent of *SlSFR2* transcript levels, TGDG reduction and number of seeds recovered from individual transgenic plants, the two transgenic lines 2 and 29 (L2 and L29) were selected for further study. As shown in Figure 2.7, L2 and L29 produced very little TGDG or TeGDG in response to $MgCl_2$ treatment showing the effect of RNAi suppression of *SlSFR2*.

SlSFR2 RNAi Transgenic Lines Show Increased Salt and Drought Sensitivity

When grown under normal conditions, *SlSFR2* RNAi transgenic lines L2 and L29 had no obvious growth defects at all ages tested (Figure 2.10, 2.11 and 2.12). To detect responses to cellular dehydration, *SlSFR2 RNAi* lines and M82 WT plants were subjected to salt and drought stress conditions. To apply salt stress, two- (Figure 2.11) or three-week-old plants (Figure 2.10) were watered over a period of time with an aqueous nutrient solution containing an increasing amount of NaCl to allow slow acclimatization. Plants of two different ages were included in the analysis to observe the robustness of the response during at least two different developmental stages. Precautions were taken that at the end of the treatment both, *SlSFR2* RNAi lines and M82 WT plants, were able to recover and resume normal growth after rewatering with nutrient solution, from which NaCl was omitted. At the end of the treatment with NaCl, *SlSFR2* RNAi lines and M82 WT plants showed a visible reduction in growth compared to nutrient solution only-watered plants (Figure 2.10 and 2.11). Fresh weight measured for the two-week-old L2 and L29 lines was significantly reduced ($p<0.01$; *t*-test*)* compared to the WT plants (Figure 2.11). The three-week-old L2 and L29 plants showed increased chlorosis and decreased size on older leaves, e.g. the second leaf which is the second oldest true leaf (Figure 2.10). On the two-week-old plants the cotyledons were most chlorotic (Figure 2.11). On the three-week-old plants the second and the fourth true leaves were compared as representatives of older and younger leaves, respectively (Figure 2.10). While the fourth leaves were slightly chlorotic on all plants but did not show much difference between WT and *SlSFR2* RNAi transgenic lines (Figure 2.10), the second leaves of L2 and L29 were more chlorotic and had visibly reduced leaf sizes (Figure 2.10). Hence in general, the older leaves on either plant showed the most severe response to salt treatment, which could be described as accelerated senescence.

To apply drought stress, water was withheld from three-week-old plants for 3 days followed by watering for two days to acclimatize the plants to drought. This acclimatization treatment was followed by withholding water for 9 days followed by rewatering for 2 days. Before rewatering, water potential and relative water content of the WT plants were measured as indicated in Figure 2.12. Even though *SlSFR2* RNAi lines were not affected at the level of the whole plant with regard to fresh weight or plant height, the older leaves as represented by the second leaves were smaller and had less fresh weight at the end of the drought period ($p<0.01$; *t*-test) (Figure 2.12). After two days of rewatering, most severe chlorosis of older leaves was observed (Figure 2.10), similar as was seen after salt treatment (Figure 2.10). It should be noted that both, WT and *SlSFR2* RNAi transgenic lines were able to recover from this drought treatment following rewatering.

Chlorophyll and Protein Content of *SlSFR2 RNAi* Transgenic Lines

Leaf protein and chlorophyll content are sensitive markers for abiotic stresses, including salt and drought. Thus, chlorophyll contents were quantified on both, the 4th and 2nd leaves of three-week-old-plants (Figure 2.13) or the cotyledons and 2nd leaves of two-week-old plants (Figure 2.14) undergoing stress treatment to corroborate the visual phenotypes. Consistent with the observed chlorosis of three-week-old plants, a decrease in chlorophyll was only observed for the 2nd leaves during salt (Figure 2.13) and drought stress (Figure 2.13) or the cotyledons of two-week-old plants following salt treatment (Figure 2.14). Similarly, measuring the total leaf protein content of three-week-old-plants (Figure 2.15), the 2nd but not the 4th leaves of the transgenic lines showed a decrease in protein content in response to both stress treatments.

SFR2 is Activated in Older Leaves in Response to Salt and Drought Treatment

To assess a direct correlation of the observed phenotypes of *SlSFR2* RNAi transgenic lines with SFR2 function, lipids were extracted and analyzed for oligogalactolipids as a measure of SFR2 activation. The 2nd and 4th leaves of three-week-old (Figure 2.16), and the cotyledon and 2nd leaf of two-week-old plants (Figure 2.17) of WT and *SlSFR2* RNAi transgenic lines treated as described above were assayed. Unstressed WT and *SlSFR2* RNAi transgenic lines did not produce detectable amounts of TGDG or TeGDG (Figure 2.16 and 2.17). However, following salt treatment TGDG was detected in the 2nd leaves in three-week-old (Figure 2.16), and cotyledons of two-week-old (Figure 2.17) WT plants, but not in the *SlSFR2* RNAi transgenic lines L2 and L29. Younger leaves on both sets of plants did not show an induction of *Sl*SFR2 in WT or transgenic lines (Figure 2.16 and 2.17). It should be noted that similar to *At*SFR2, the *SlSFR2* transcript level did not change during the salt treatment (Figure 2.18), suggesting that the tomato SFR2 protein is present at all times and directly activated.

Lipid analysis following drought stress was done for three-week-old plants (Figure 2.16). Lipids were extracted from the 2nd and 4th leaves directly following the 9 day drought treatment before the recovery phase to avoid the turnover of potential oligogalactolipids during recovery. Similar to the salt treatment, no TGDG was detected in the 2nd leaves of the *SlSFR2* RNAi transgenic lines L2 and L29, but in the 2nd leaves of the WT plants (Figure 2.16). Therefore, the growth and chlorosis phenotypes observed for older leaves of the *SlSFR2* RNAi transgenic lines above coincided with the absence of SFR2 activity following salt and drought treatment.

DISCUSSION

*At*SFR2 and *Sl*SFR2 are Genuine Orthologues

The current study was based on the premise that all plant genomes characterized harbor a presumed *SFR2* orthologue, including plants that do never encounter freezing in their natural environments. Functionality of different predicted orthologues including those from freezing-sensitive plants was indirectly shown by heterologously restoring the freezing tolerance of the Arabidopsis *sfr2* mutant (Fourrier et al., 2008). At that time the biochemical activity of *At*SFR2 was not accurately known, but later shown to be the processive transfer of galactosyl residues from MGDG to a galactolipid acceptor to form oligogalactolipids and DAG (Moellering et al., 2010b; Roston et al., 2014). Here we conclusively determined that the recombinant SFR2 orthologue from tomato, *Sl*SFR2, when produced in a suitable yeast host containing the MGDG substrate has galactolipid : galactolipid galactosyltransferase activity comparable to its Arabidopsis orthologue *At*SFR2 (Figure 2.6). Further biochemical comparison of the two recombinant proteins in yeast-derived microsomal fractions indicated that both enzyme respond qualitatively similarly to changes in pH and $MgCl_2$ concentrations in the buffer (Figure 2.6). Thus, the two enzymes from a freezing-tolerant and a -sensitive species appear to function fundamentally in similar ways at the biochemical level. However, it should be noted that *Sl*SFR2 exhibited about 2 fold higher galactolipid : galactolipid galactosyltransferase activity than *At*SFR2 (Figure 2.6).

*At*SFR2 was shown to contain multiple sequence regions that are important for its galactosyl transferase activity (Roston et al., 2014). The *Sl*SFR2 sequence is only 72% similar to that of *At*SFR2 (Figure 2.4), allowing room for sufficient diversity to explain these subtle differences. Hence, surveying a larger range of *SFR2* orthologues from diverse plants for their specific SFR2 activity might yield enzymes with different activation profiles or extent of activities

that might be better suited for future efforts to engineer tolerance to cellular dehydration based on SFR2 for increasingly stress tolerant crops. For example, overexpression of a cDNA encoding a tightly regulated SFR2 enzyme may not lead to crop protection, while a constitutively activated SFR2 orthologue or one with higher sensitivity to $MgCl_2$ might be more suitable for engineering purposes.

In Arabidopsis, the *AtSFR2* transcript and protein levels are kept constant in the tissues and under all conditions tested (Thorlby et al., 2004). Similarly, we observed a constant abundance of *SlSFR2* transcripts at all instances tested in tomato (Figure 2.18), suggesting that as in Arabidopsis activation of SFR2 occurs post-transcriptional/translational.

Aside from the direct determination of the activity of *Sl*SFR2, reducing the abundance of *SlSFR2* transcripts in *SlSFR2* RNAi lines decreased the formation of the oligogalactolipids TGDG and TeGDG in response to $MgCl_2$ (Figure 2.7), providing further corroboration that *Sl*SFR2 is involved in the formation of these oligogalactolipids in vivo. It should be noted that 0.5 M $MgCl_2$ used in this experiment constitutes a much higher concentration than found under physiological conditions, which is usually 2-10 mM (Shaul, 2002). We used this concentration of $MgCl_2$ here as a simple method to induce the enzyme in vivo and estimate the maximal enzyme activity.

Oligogalactolipid Formation by *Sl*SFR2 Protects Against Salt and Drought Stress

Having established in multiple ways that *Sl*SFR2 is a genuine orthologue of *At*SFR2 with a similar activity profile, we can pursue the question whether *Sl*SFR2 protects tomato, a generally cold/freezing sensitive plant, against other forms of cellular dehydration induced by osmotic stress, either high salt or drought. A set of *SlSFR2* RNAi lines with up to 80% reduction in mRNA abundance was generated and analyzed to answer this question. Exposing different WT and

transgenic plants at different ages to salt and drought stress using generally accepted protocols (Conroy et al., 1988; Shalata and Tal, 1998; Umezawa et al., 2000), we were able to show that older leaves on the *SlSFR2* RNAi plants remain smaller and senesce earlier than corresponding leaves on WT plants (Figure 2.10, 2.11 and 2.12). Most importantly, this phenotype strictly correlated with the inability to generate oligogalacotlipids in those leaves in the transgenic lines (Figure 2.16 and 2.17). Hence we conclude that the ability to produce oligogalcotlipids as a result of induction of *Sl*SFR2 activity under salt and drought stress allows WT tomato plants to continue to produce biomass under these adverse conditions.

The fact that older leaves are most severely affected by different abiotic stress regimes while young leaves stay relatively protected has been previously observed. For example, the drought-tolerant plant *Senecio medley-woodii* responds to drought stresses with a gradual dehydration of leaves progressing from the oldest to the young leaves until the older leaves were eventually shed while the younger leaves were still be able to maintain or even increase transpiration (Donatz and Eller, 1993). In Arabidopsis during drought stress, enzymes protecting against oxidative stress including catalase, peroxidase, superoxide dismutase and glutathione reductase accumulate in mature but not in young leaves, suggesting indirectly that older leaves may be more susceptible to drought-induced oxidative damage (Jung, 2004). Even though the concept that water translocation from older to younger leaves during dehydration stress may still be debatable, it is well known that younger photosynthetically active tissues are preferably protected (Munns and Tester, 2008; Chaves et al., 2009). In rice, young leaves are protected from salt stress as NaCl accumulates preferably in the older leaves (Wang et al., 2012). Similarly, younger leaves are more effective than older in adjusting the osmotic potential by increasing solute concentrations, which helps maintain water status and turgor pressure during dehydration

conditions (Hajlaoui et al., 2010). It is possible that the salt stress phenotype of the older tomato leaves observed in our hands is caused by a combination of NaCl toxicity and cellular dehydration. However, dehydration must be at least partially responsible, because a similar phenotype was observed during drought stress alone.

Lipid Remodeling by SFR2 Protects Against Different Abiotic Stresses in Different Plants

SFR2 has been shown to play a crucial role in freezing tolerance in Arabidopsis, but is not activated during salt or drought stress, at least prior to the occurrence of irreversible damage (Figure 2.1, 2.2 and 2.3). While Arabidopsis is freezing tolerant, it is much more sensitive to salt and drought stress and effects of salt or drought become lethal before the SFR2-based lipid remodeling system is activated. However, in freezing-intolerant tomato, SFR2 is activated during salt and drought stress before the plants are irreversibly damaged and, hence, is able to protect old leaves from stress-induced senescence (Figure 2.10 and 2.16).

What are the common principles by which SFR2 potentially protects against cellular dehydration in different plants? Given that *SFR2* mRNA levels are not regulated in different plants, the enzyme itself must be activated by post-transcriptional mechanisms. We recently showed that SFR2 in Arabidopsis is activated upon freezing by a decrease in cytosolic pH and an increase in the concentration of $MgCl_2$ (Barnes et al., 2016). Typically, chloroplasts contain up to 10 mM $MgCl_2$, a higher concentration than found in the cytosol (Shaul, 2002). The SFR2 protein is likely ubiquitously present in the outer envelope membranes of plant chloroplasts as has been directly shown for Arabidopsis (Fourrier et al., 2008). It should be noted that we tested the available antibody raised against *At*SFR2, but failed to detect cross reactivity with *Sl*SFR2. In addition, we were unable to assay *Sl*SFR2 in isolated tomato chloroplasts, perhaps due to interference with

secondary metabolites present in the tomato extracts. However, as in vivo activation in tomato shows (Figure 2.16 and 2.17), *Sl*SFR2 has access to its substrate MGDG, which is exclusively present in the plastid. Hence we assume that *Sl*SFR2 is likely also present in the outer envelopes of chloroplasts as shown for Arabidopsis. Therefore, a simple hypothesis for the protective function of *Sl*SFR2 during drought and salt stress causing severe cellular dehydration is that *Sl*SFR2 acts as a first line of defense being present at all times in the chloroplast envelopes. It is activated when the chloroplast membranes are directly disrupted during dehydration allowing leakage of $MgCl_2$ from the chloroplast. Alternatively, the $MgCl_2$ concentration increases due to loss of water from the cytosol during dehydration. Once activated by the cytosolic increase in $MgCl_2$, the removal of the non-bilayer forming lipid MGDG and the synthesis of higher order oligogalactolipids stabilize the chloroplast membranes similarly as proposed for *At*SFR2 function during the response to freezing in Arabidopsis (Moellering et al., 2010b; Moellering and Benning, 2011). Therefore, SFR2 constitutes a first line of defense providing a common molecular membrane lipid remodeling mechanism against cellular dehydration accompanying different abiotic stresses such as drought, increased salt, or freezing, thereby explaining its presence in all plants currently tested.

However, other mechanisms than disruption of the chloroplast membrane raising the cytosolic $MgCl_2$ concentration and lowering the pH to activate SFR2 cannot be excluded. It is possible that $MgCl_2$ or protons released from vacuoles are sensed by SFR2 upon salt or drought stress in tomato, and $MgCl_2$ and protons could enter the cytosol through specific channels that may be differently regulated in different plants in response to different abiotic stresses. Therefore, understanding the mechanisms of SFR2 activation in different plants in response to different

abiotic stresses may provide new plant-specific avenues to engineer crops to be more tolerant to specific abiotic stresses.

ACKNOWLEDGEMENT

This work was done with the assistance of Hope Lynn Hersh, who helped with the plant maintenance and contributed Figure 2.18. We thank Dr. Cornelius Barry (Michigan State University) for generously providing tomatoM82 seeds, Ms. Kathleen Imre and Dr. Rob Last (Michigan State University) for the tomato transformation protocol, Dr.Wayne Loescher (Michigan State University) for advice on salt and drought assays and providing the pressure chamber, Dr. Sarah J. Gilmour (Michigan State University) for providing the conductivity meter, and Dr. Rebecca Roston (University of Nebraska) for scientific discussions.

APPENDIX

Primer name	Sequence 5’ – 3’	Purpose
Sl_SFR2 RNAi F	CACCCGCTCTCCCATAGACGACTC	For RNAi constructs
Sl_SFR2 RNAi R	GGCATGATCCTTGACCAATC	For RNAi constructs
Sl_SFR2 F	AGCTCCAAACTGCTGCTAAA	For qPCR
Sl_SFR2 R	CTCATCAAGTCCTCCTGCATAC	For qPCR
Sl_TIP41-like F	GGTTCCTATTGCTGCGTT	qPCR reference gene
Sl_TIP41-like R	CGAAGACAAGGCCTGAAA	qPCR reference gene
Sl_PDF2 F	GCCAATCAAGCACTCCAG	qPCR reference gene
Sl_PDF2 R	ACCTTTCCCCTTTTGCTTCT	qPCR reference gene
pHELLSGATE12-FW	GAAGGAGAAAAACTAGAAATTTACC	For genotyping

Table 2. 1. Primers used in this study.

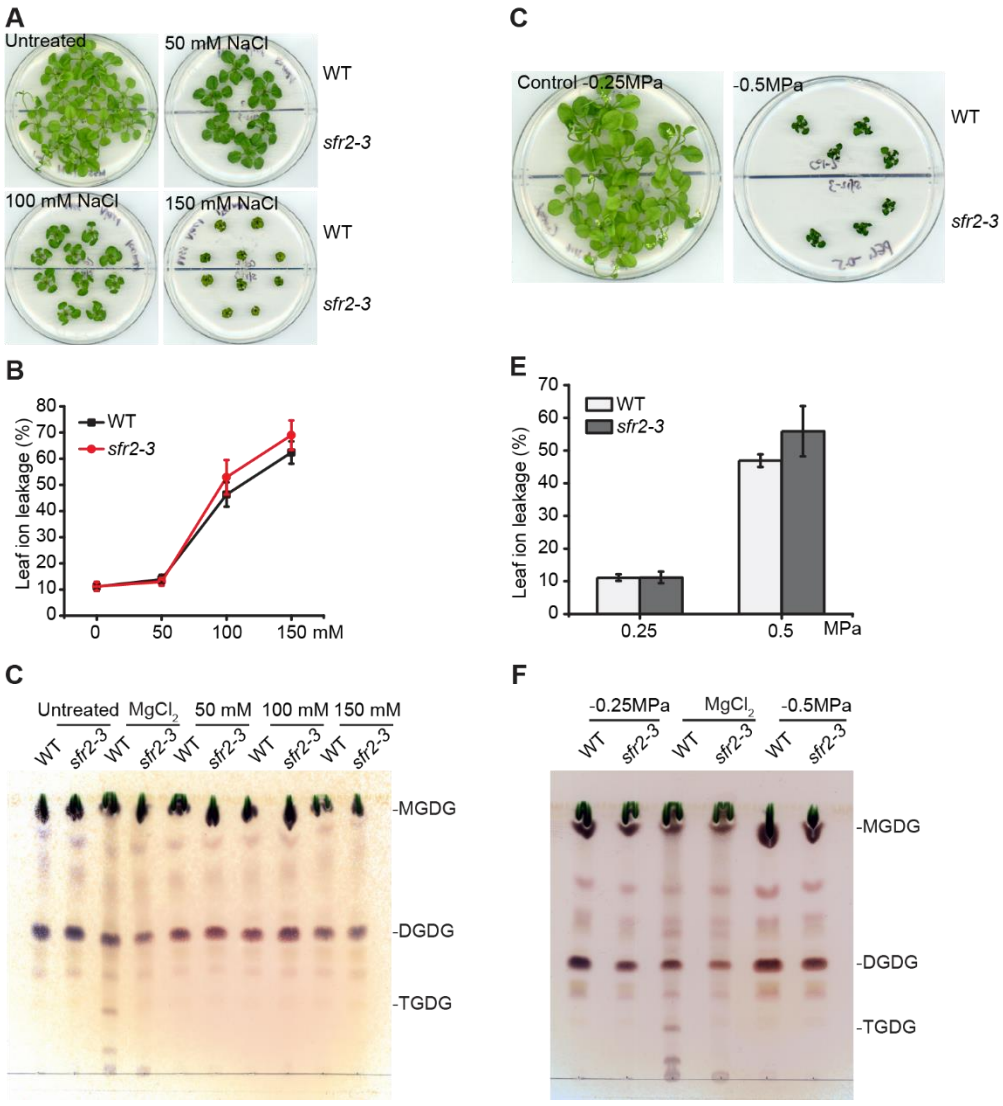

Figure 2. 1. SFR2 is not involved in protection against salt or drought stress in Arabidopsis.
(A) and **(D)** Images of plants grown on MS agar plates with, **(A)**, different concentrations of NaCl or with, **(D)**, different water potentials as indicated. One-week-old normal MS-grown seedlings were transferred to salt or drought mimicking plates and grown for 3 weeks before the pictures were taken.
(B) and **(E)** Ion leakage measurements of the, **(B)**, salt or, **(E)**, drought-treated plant leaves (n=4, ± SD).
(C) and **(F)** Thin-layer chromatography of the lipids from, **(C)**, salt-stressed leaves or, **(D)**, drought-stressed leaves. $MgCl_2$ treated WT samples served as positive controls for SFR2 activation. Lipids were stained for sugar head groups. DGDG, digalactosyldiacylglycerol; MGDG, monogalactosyldiacylglycerol; TGDG, trigalactosyldiacylglycerol.

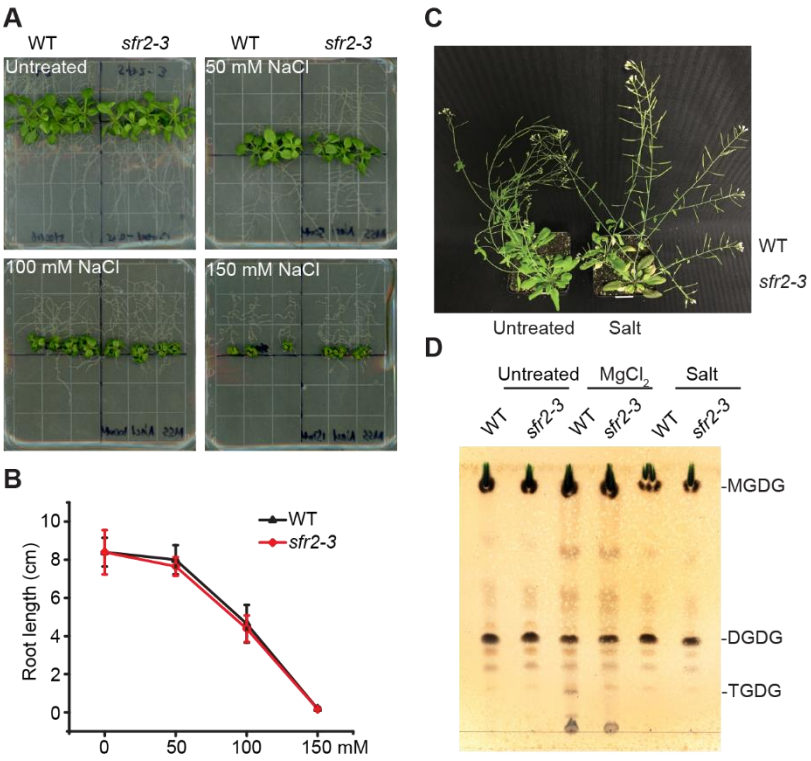

Figure 2. 2. SFR2 is not involved in protection against salt stress in Arabidopsis.
(A) and **(B)** Root bending assay with salt treated plants. 1-week-old vertically grown WT and *sfr2-3* seedlings were transferred to MS agar plates with different concentrations of NaCl and grown on plates 180° inverted for 2 weeks. **(A)**, representative images of the 3-week-old plants. **(B)**, bended roots were isolated and measured (n=6-12, ± SD).
(C) and **(D)** Salt stress assay with soil-grown plants. **(C)**, plant image of untreated and salt treated plants. To avoid possible growth differences for different pots, WT and *sfr2-3* were grown together in the same pots. Two-week old plants were watered with Arabidopsis nutrient solution with extra 50 mM NaCl for one week, 100 mM NaCl for one week, 150 mM NaCl for four days and 200 mM NaCl for five days. Pictures were taken at the end of the treatment. **(D)**, TLC analysis of lipids extracted from leaves of untreated or salt treated plants. $MgCl_2$ treated WT samples served as positive controls for SFR2 activation. Lipids were stained for sugar head groups. DGDG, digalactosyldiacylglycerol; MGDG, monogalactosyldiacylglycerol; TGDG, trigalactosyldiacylglycerol.

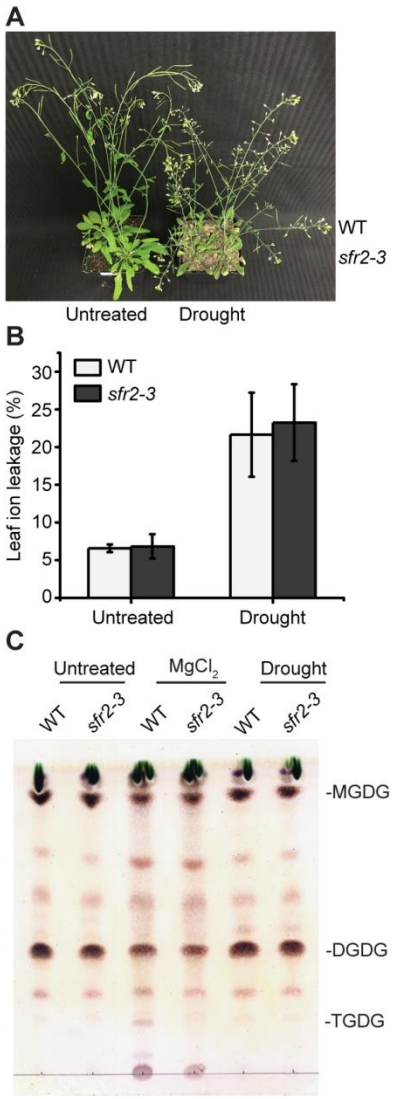

Figure 2. 3. SFR2 is not involved in protection against drought in Arabidopsis.
(A) Plant image of untreated and drought treated soil-grown plants. WT and *sfr2-3* were grown in the same pots. Water was withheld from two-week-old plants and pictures were taken after three weeks of drought treatment.
(B) Ion leakage measurement of the untreated or drought- treated plant leaves (n=5-8, ± SD). C, TLC analysis of lipids extracted from leaves of untreated or drought stressed plants as indicated. $MgCl_2$-treated WT samples served as positive controls for SFR2 activation. Lipids were stained for sugar head groups. For lipid abbreviations, refer to the legend of Supplemental Figure S1.

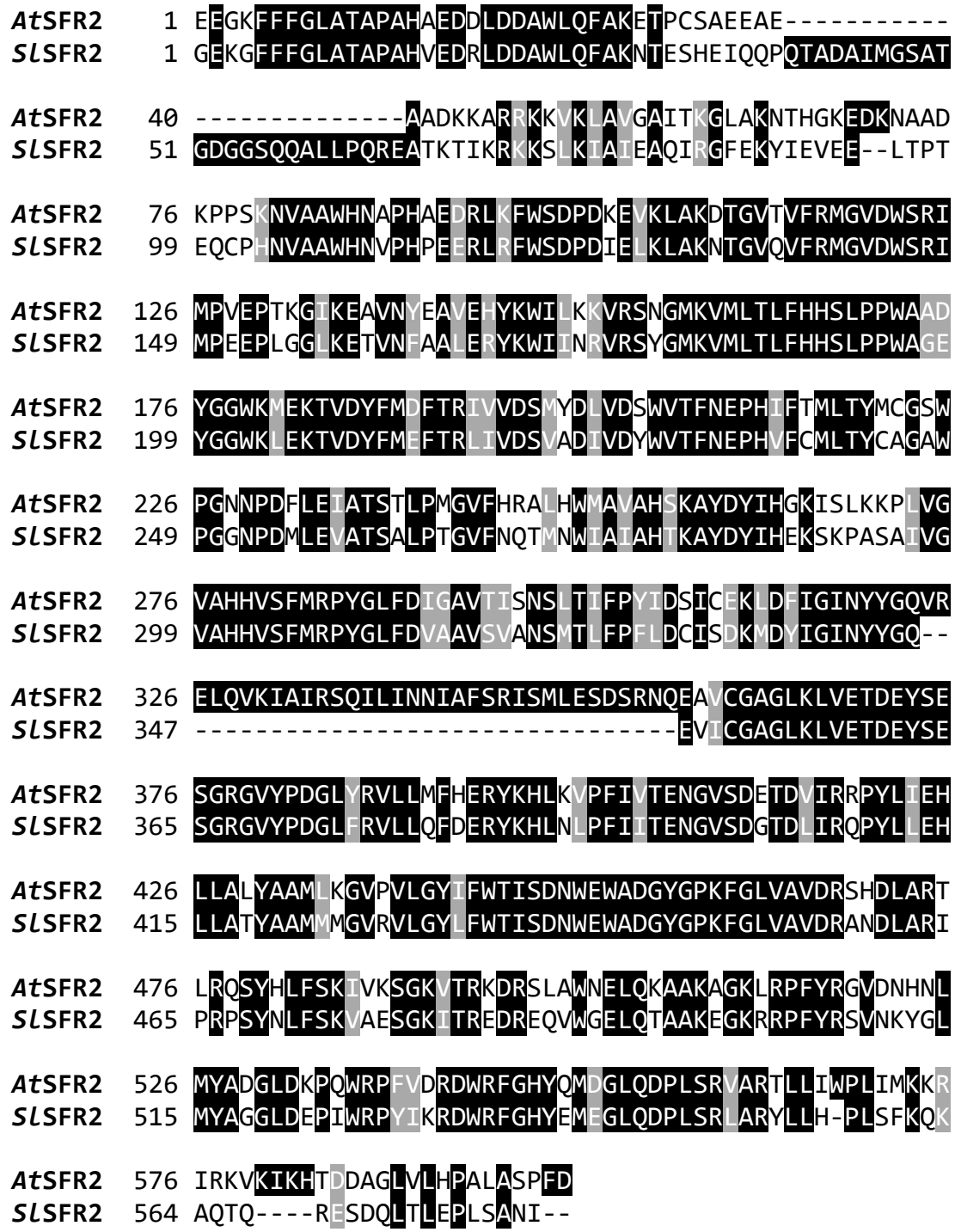

Figure 2. 4. Protein sequence alignment between *At*SFR2 and *Sl*SFR2.
Amino acid sequences were aligned by Clustal Omega (http://www.ebi.ac.uk/Tools/msa/clustalo/) and consensus sequences were highlighted using BOXSHADE 3.21 (http://www.ch.embnet.org/software/BOX_form.html). Identical residues were highlighted black and similar residues were highlighted grey. Identity between two sequences is 59% (407/679); positives are 72% (493/679) and gaps are 9% (67/679).

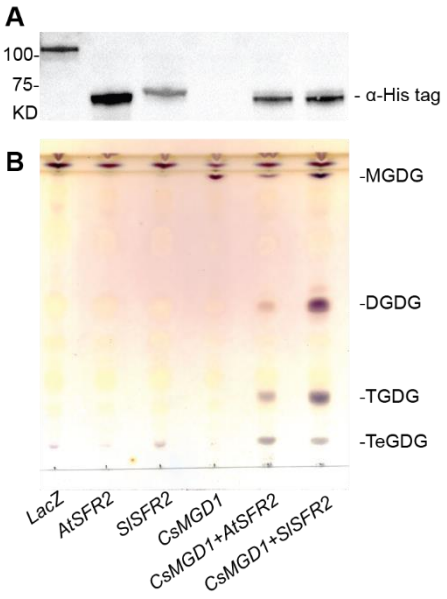

Figure 2. 5. *Sl*SFR2 is a galactolipid : galactolipid galactosyltransferase (GGGT).
(A) Immunoblot of the proteins extracted from yeast that are transformed with constructs as indicated. *LacZ*, *AtSFR2*, and *SlSFR2* constructs incorporate a His-tag at the C-terminus of the protein, but not the *CsMGD1* construct.
(B) Thin-layer chromatography of the lipids extracted from yeast strains as indicated. Galactolipids were selectively stained by α-naphthol. Strains solely producing LacZ, *At*SFR2, or *Sl*SFR2 cannot produce galactolipids (left three lanes). Expression of *CsMGD1* produces MGDG (the fourth lane) and co-expressing *CsMGD1* with *AtSFR2* or *SlSFR2* results in the production of MGDG and DGDG, TGDG and tetragalactosyldiacylglycerol (TeGDG) (fifth and sixth lanes). For lipid abbreviations, refer to the legend of Figure 2.1.

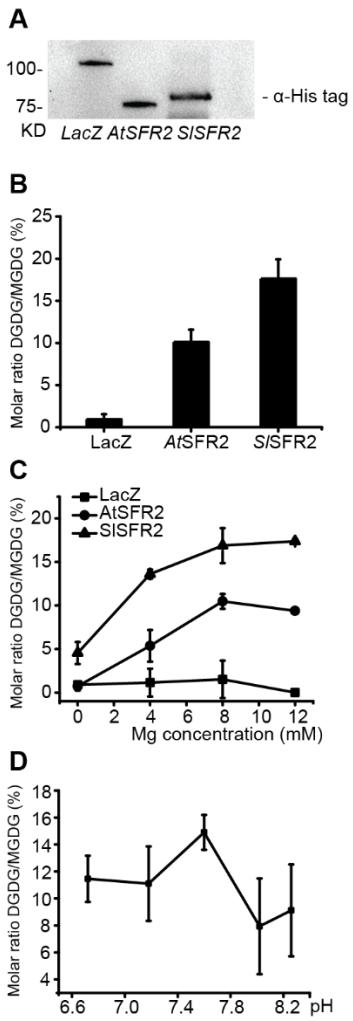

Figure 2. 6. Activity of *Sl*SFR2 in vitro.

(A) Immunoblot of yeast microsomes containing approximately equal amounts of recombinant His-tagged LacZ and SFR2 proteins. *At*SFR2 and *Sl*SFR2 microsomes with these comparable protein amounts were used for the assays.

(B) Activity comparison between *At*SFR2 and *Sl*SFR2 in a buffer with pH 7.5 and 8 mM $MgCl_2$. Activity is shown as the molar ratio between the product DGDG and the substrate MGDG (n=3, ±SD).

(C) Magnesium dependency of SFR2 activity. Assay buffers contained $MgCl_2$ concentrations ranging from 0 to 12 mM (n=3-4, ±SD). D, pH dependency of *Sl*SFR2 activity. Assays buffers had a range of pHs from 6.72 to 8.26 (n=3, ±SD).

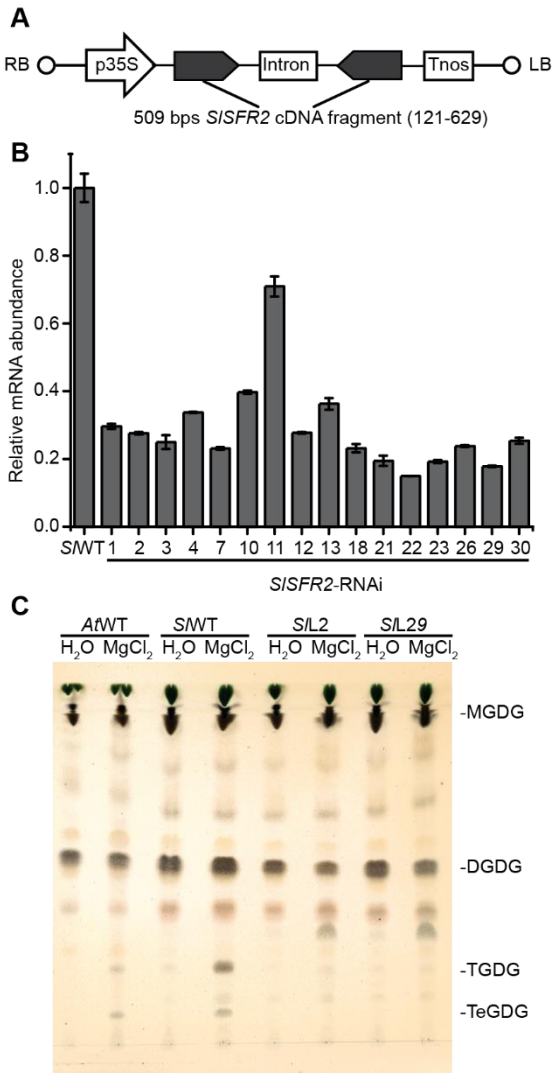

Figure 2. 7. Generation the *SlSFR2*-RNAi lines.
(A) Simplified diagram of the *SlSFR2*-RNAi construct. RB, right border; p35S, Cauliflower mosaic virus (CaMV) 35S promoter; Intron, pyruvate dehydrogenase kinase (PDK) intron; Tnos, NOS-terminator; LB, left border.
(B) Quantitative RT-PCR probing *SlSFR2* mRNA abundance in wild type (*Sl*WT) and *SlSFR2*-RNAi lines. C, thin-layer chromatography of the lipids from Arabidopsis WT plants (*At*WT), tomato WT plants (*Sl*WT) or select transgenic lines (*Sl*L2 and *Sl*L29). The leaves were incubated in either water or 0.5 M $MgCl_2$ aqueous solution for 6 hours before lipid extraction. For lipid abbreviations, refer to the legend of Figure 2.1.

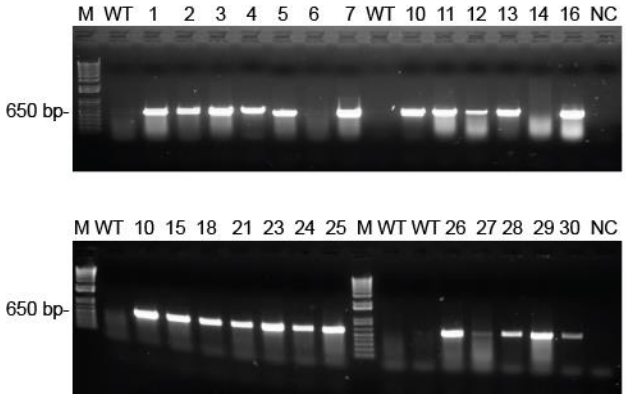

Figure 2. 8. Genotyping of wild type (WT) and *SlSFR2*-RNAi lines.
Genomic DNA was extracted from 8-week old plant leaves and used as template to generate PCR fragments containing parts of the pHELLSGATE12 vector and *SlSFR2* sequences using primers 1 and 9 as shown in Supplemental Table 1. Amplicon size is expected to be 583 bp. M, 1Kb plus DNA ladder (Cat. No. 10787-018, Invitrogen); NC, negative PCR control without genomic DNA.

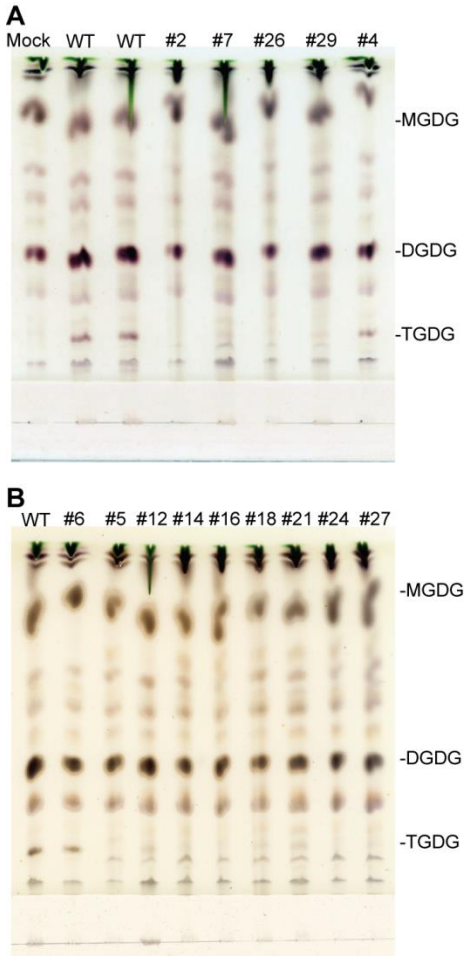

Figure 2. 9. Activation of *Sl*SFR2 in additional *SlSFR2*-RNAi lines.
Detached leaves were incubated in 0.5 M $MgCl_2$ aqueous solution for 6 h. Tomato wild-type leaf was incubated with water (Mock) **(A)** and wild-type samples (WT) incubated in 0.5 M $MgCl_2$ aqueous solution for 6 h **(B)** were included for comparison. Lipids were extracted at the end of the treatment and separated on TLC plates. For lipid abbreviations, refer to the legend of Figure 2.2.

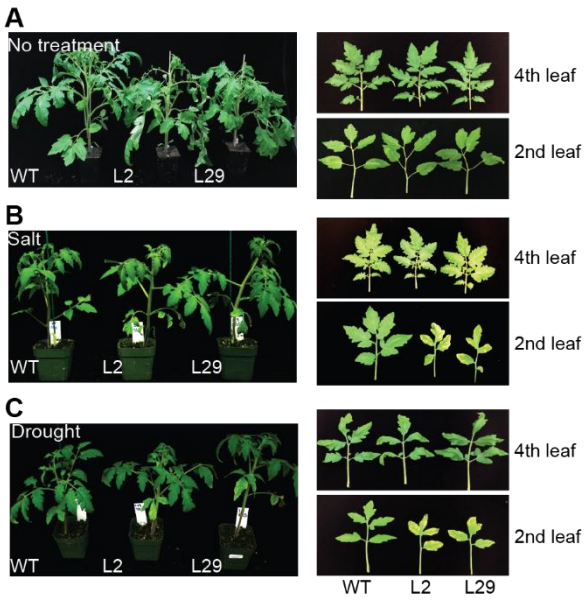

Figure 2. 10. *SlSFR2*-RNAi lines are sensitive to salt and drought.
(A) Whole plant images of wild-type (WT) and *SlSFR2*-RNAi lines L2 and L29 grown under normal condition or **(B)**, with salt treated or **(C)**, drought treated. The plants were three-week-old at the beginning of the treatment and images were taken at five weeks of age. In the panels on the right leaf appearances of the representative fourth (4^{th}) and second (2^{nd}) leaves are shown.

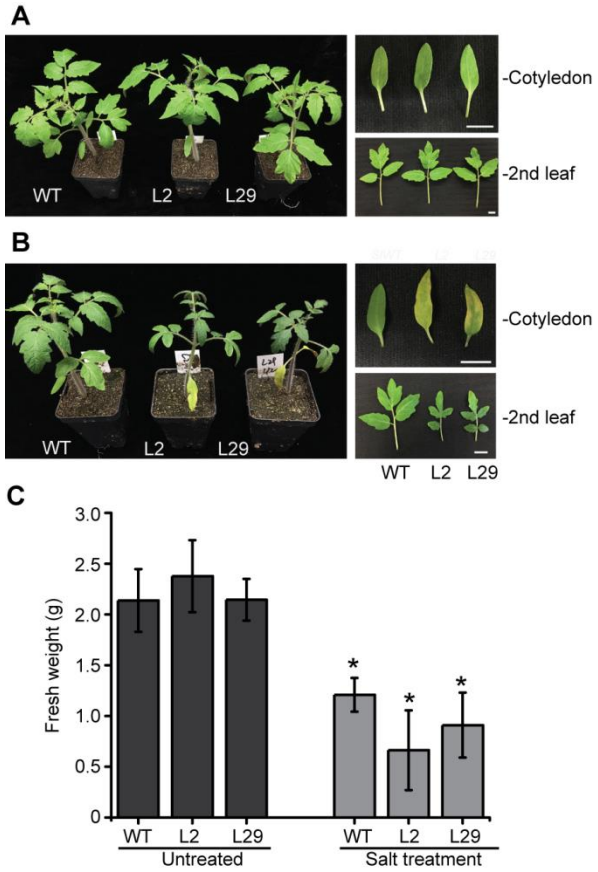

Figure 2. 11. Effects of salt treatment on two-week-old tomato plants.
Wild-type tomato M82 (WT) and 2 *SlSFR2*-RNAi lines L2 and L29 were daily watered with nutrient solution to which 50 mM NaCl was added for 1 day, 100 mM for 2 days for acclimation, followed by watering with 150 mM for 9 days. The plants were two-week-old at the beginning of the treatment and images were taken at 26 days of age.
(A) Plant and leaf phenotype of untreated plants.
(B) Plant and leaf phenotype of salt-treated plants.
(C) Fresh weight quantification of the above ground parts. Statistics: n=4 for untreated controls, ±SD; n=9-12 for salt treated plants, ±SD. * Indicates $p<0.01$, *t*-test. The size bars equal 1 cm.

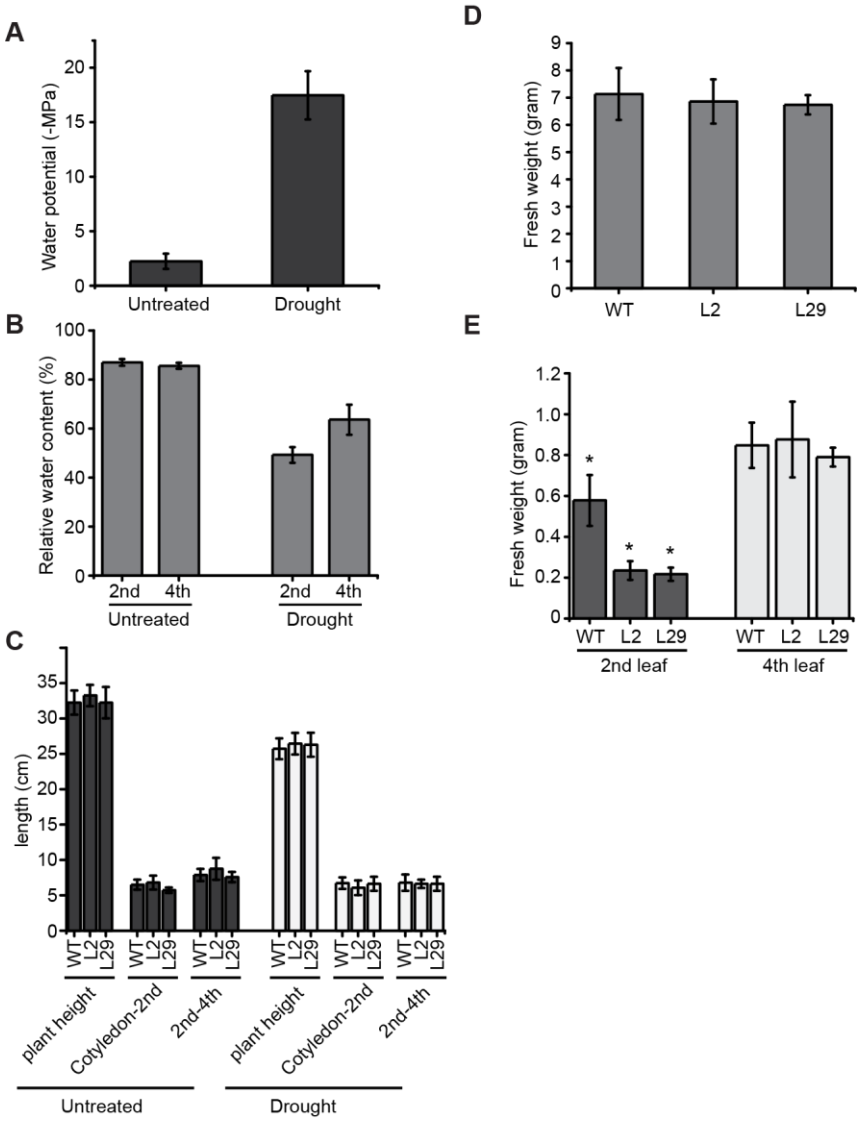

Figure 2. 12. Effect of drought treatment on WT and *SlSFR2*-RNAi plants.
Water was withheld three days from three-week-old plants for acclimation. Watering was resumed for four days, followed by withholding of water for nine days.
(A) Water potential measurement of the untreated control and drought-treated WT plants at the end of the treatment. n=10 for untreated plants; n=8 for drought-treated plants, ± SD.
(B) Relative water content measurement of the 2nd and 4th leaves of the untreated and drought treated WT plants (n=3-5, ± SD).
(C) Measurement of the plant height and internode length of untreated controls and drought treated plants. n=4 for untreated plants; n=7-8 for drought treated plants, ± SD.
(D) Fresh weight measurement of the above ground parts of the whole plant of drought-treated WT and *Sl*SFR2 RNAi lines L2 and L29 (n=8, ± SD).
(E) Fresh weight measurement of the 2nd and 4th leaves of the drought-treated WT or *Sl*SFR2 RNAi lines L2 and L29. Statistics: n=4-5, ± SD. *indicates $p<0.01$, *t*-test.

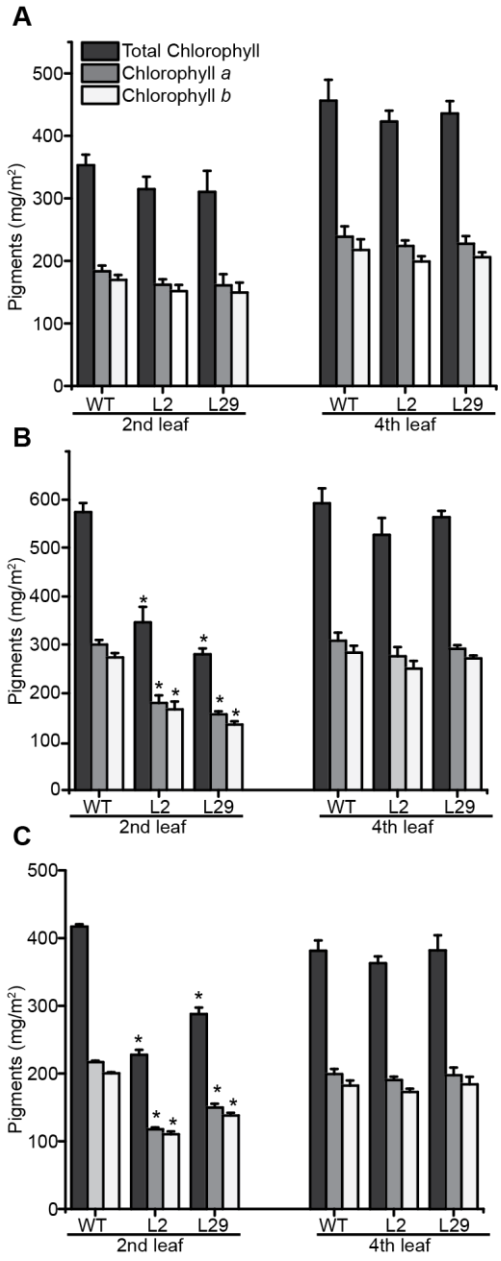

Figure 2. 13. Chlorophyll in the leaves of untreated and stressed three-week-old tomato plants.

(A) Total chlorophyll and chlorophyll *a, b* content in untreated or **(B)** Salt-treated and **(C)**, of drought-treated wild-type (WT) and transgenic L2 and L29 lines plants as shown in Figure 2.10. Statistics: n = 3, ±SD.* indicates $p<0.01$, *t*-test.

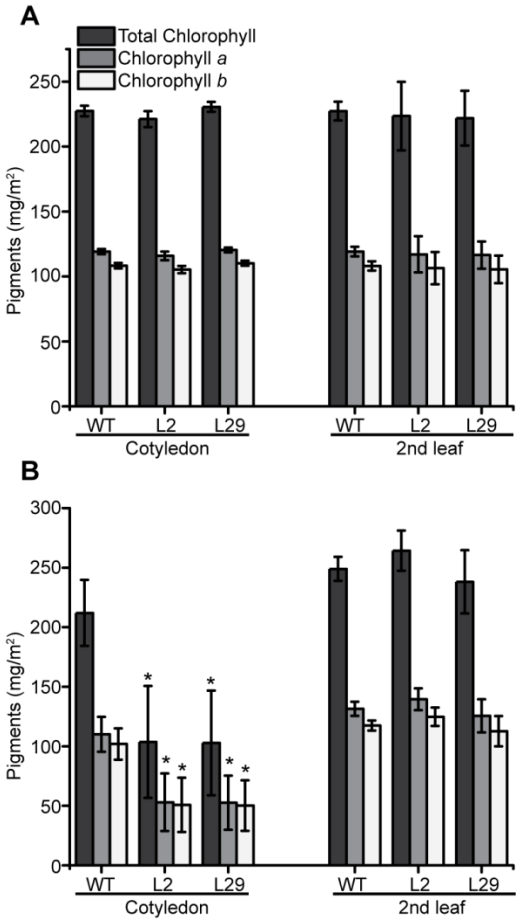

Figure 2. 14. Chlorophyll in the leaves of untreated and salt-treated two-week-old tomato plants.

(A) Total chlorophyll and chlorophyll *a*, *b* content in untreated, and **(B)**, salt-treated wild-type (WT) and transgenic L2 and L29 lines plants as shown in Figure 2.11. Statistics: n = 4, ±SD. * indicates $p<0.01$, *t*-test.

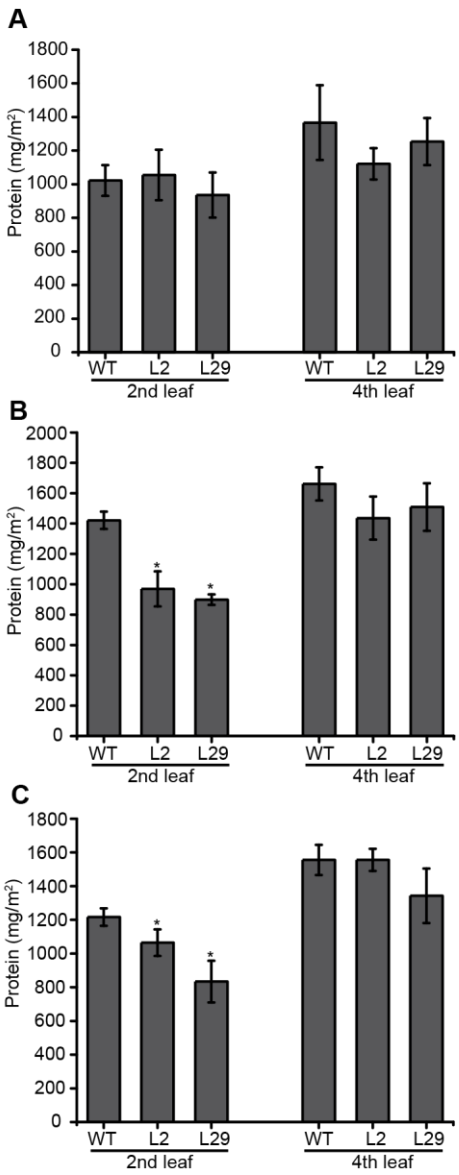

Figure 2. 15. Total protein in leaves from untreated and stress treated three-week-old tomato plants.

(A) Total protein in untreated, **(B)**, salt-treated and **(C)**, of drought-treated wild-type (WT) and transgenic L2 and L29 lines plants as shown in Figure 2.10. Statistics: n = 3-5, ±SD. * indicates $p<0.01$, *t*-test.

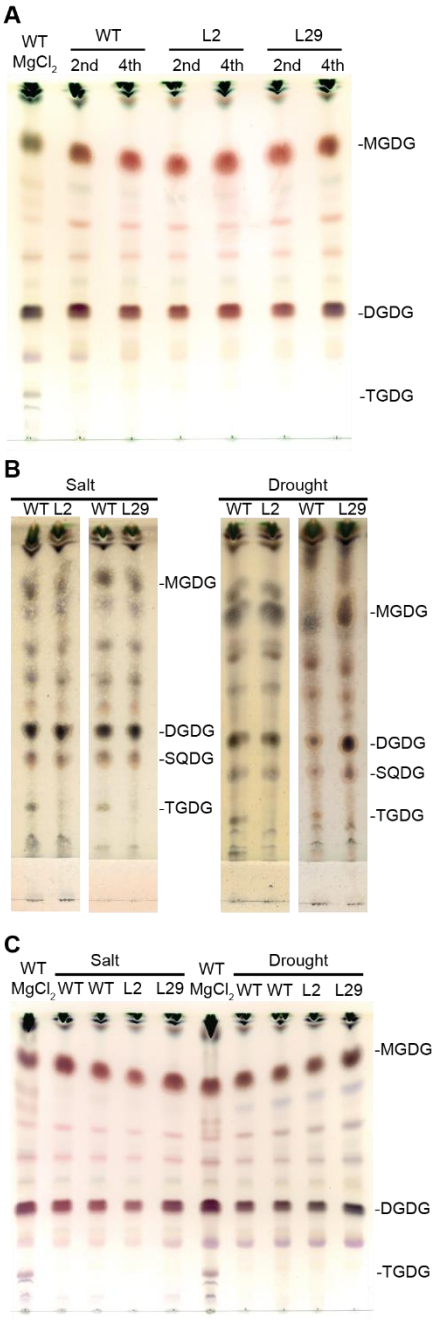

Figure 2. 16. SFR2 activation in three-week-old tomato plants subjected to salt or drought stress.

(A) Lipids were extracted from the 2nd and 4th leaves of untreated wild-type (WT) and *SlSFR2*-RNAiplants (L2, L9) and analyzed by thin-layer chromatography.

(B) Lipids were extracted from the 2nd leaves and **(C)**, from the 4th leaves of salt and drought-treated plants as indicated. Lipids were stained for sugar head groups. Extracts of $MgCl_2$-treated wild-type leaves (WT, $MgCl_2$; SFR2 induced) were included **(A, C)** to detect the diagnostic trigalactosyldiacylglycerol (TGDG) following SFR2 induction. DGDG, digalactosyldiacylglycerol; MGDG, monogalactosyldiacylglycerol; SQDG, sulfoquinovosyldiacylglycerol. A representative result is shown.

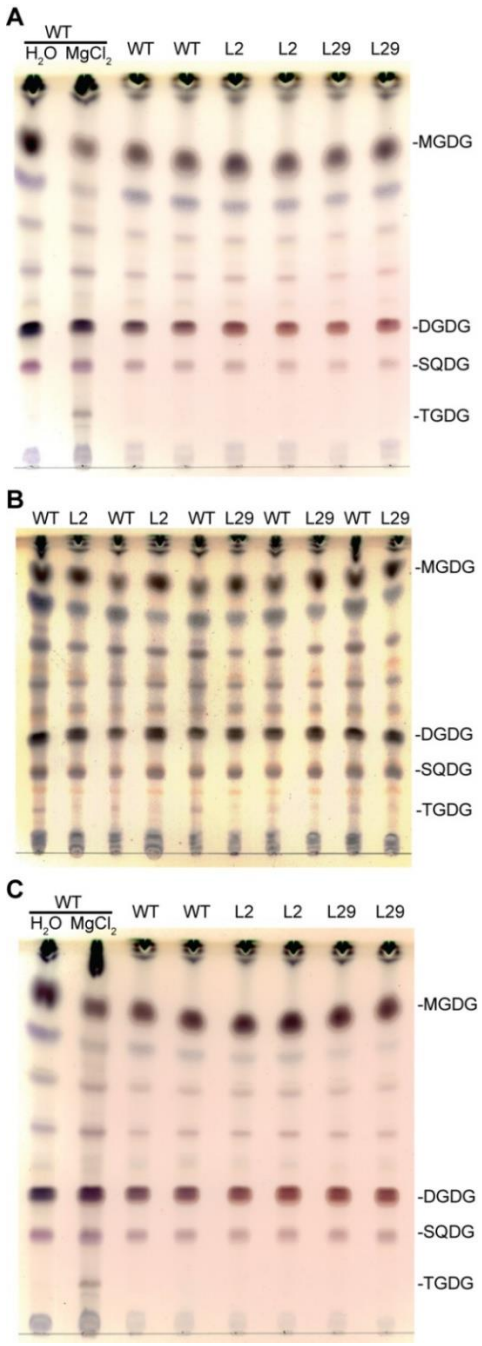

Figure 2. 17. SFR2 activation in two-week-old tomato plants subjected to salt stress.
(A) Lipids were extracted from cotyledons and 2nd leaves of untreated wild-type (WT) and *SlSFR2*-RNAi plants (L2, L9) and analyzed by thin-layer chromatography.
(B) Lipids were extracted from the cotyledons and **(C)**, from the 2nd leaves of salt-treated plants as indicated. Lipids were stained for sugar head groups. Extracts of water-treated (WT, H_2O, mock) or $MgCl_2$-treated wild-type leaves (WT, $MgCl_2$; SFR2 induced) were included **(A, C)** to detect the diagnostic trigalactosyldiacylglycerol (TGDG) following SFR2 induction. DGDG, digalactosyldiacylglycerol; MGDG, monogalactosyldiacylglycerol; SQDG, sulfoquinovosyldiacylglycerol. A representative result is shown.

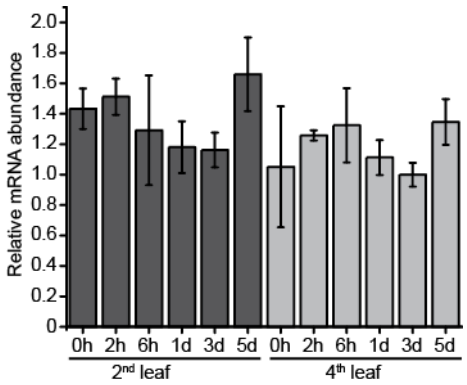

Figure 2. 18. *SlSFR2* transcript levels during salt treatment.
Three-week-old tomato plants were treated with nutrient solution to which 100 mM NaCl was added. RNA was extracted from 2nd and 4th leaves at different time points, 0, 2, 6 hours (h), 1, 3 and 5 days (d). mRNA abundance was normalized to mRNA abundance at 0 hour in the 4th leaf.

REFERENCES

REFERENCES

Barnes, A.C., Benning, C., and Roston, R. (2016). Chloroplast membrane remodeling during freezing stress is accompanied by cytoplasmic acidification activating SENSITIVE TO FREEZING 2. Plant Physiol, **171,** 2140-2149.

Barrs, H.D., and Weatherley, P.E. (1962). A Re-Examination of the Relative Turgidity Technique for Estimating Water Deficits in Leaves. Aust J Biol Sci **15,** 413-428.

Chaves, M.M., Flexas, J., and Pinheiro, C. (2009). Photosynthesis under drought and salt stress: regulation mechanisms from whole plant to cell. Ann Bot **103,** 551-560.

Conroy, J.P., Virgona, J.M., Smillie, R.M., and Barlow, E.W. (1988). Influence of Drought Acclimation and CO(2) Enrichment on Osmotic Adjustment and Chlorophyll a Fluorescence of Sunflower during Drought. Plant Physiol **86,** 1108-1115.

Dahlqvist, A., Stahl, U., Lenman, M., Banas, A., Lee, M., Sandager, L., Ronne, H., and Stymne, S. (2000). Phospholipid:diacylglycerol acyltransferase: an enzyme that catalyzes the acyl-CoA-independent formation of triacylglycerol in yeast and plants. Proc Natl Acad Sci U S A **97,** 6487-6492.

Donatz, M., and Eller, B.M. (1993). Plant water status and water translocation in the drought deciduous CAM-succulent *Senecio-Medley-Woodii*. J Plant Physiol **141,** 750-756.

Fernandez-Pozo, N., Menda, N., Edwards, J.D., Saha, S., Tecle, I.Y., Strickler, S.R., Bombarely, A., Fisher-York, T., Pujar, A., Foerster, H., Yan, A., and Mueller, L.A. (2015). The Sol Genomics Network (SGN)--from genotype to phenotype to breeding. Nucleic Acids Res**43,** D1036-1041.

Fourrier, N., Bedard, J., Lopez-Juez, E., Barbrook, A., Bowyer, J., Jarvis, P., Warren, G., and Thorlby, G. (2008). A role for SENSITIVE TO FREEZING2 in protecting chloroplasts against freeze-induced damage in Arabidopsis. Plant J **55,** 734-745.

Gilmour, S.J., Hajela, R.K., and Thomashow, M.F. (1988). Cold Acclimation in Arabidopsis thaliana. Plant Physiol **87,** 745-750.

Hajlaoui, H., El Ayeb, N., Garrec, J.P., and Denden, M. (2010). Differential effects of salt stress on osmotic adjustment and solutes allocation on the basis of root and leaf tissue senescence of two silage maize (Zea mays L.) varieties. Ind Crop Prod **31,** 122-130.

Jung, S.Y. (2004). Variation in antioxidant metabolism of young and mature leaves of *Arabidopsis thaliana* subjected to drought. Plant Sci **166,** 459-466.

Kushnirov, V.V. (2000). Rapid and reliable protein extraction from yeast. Yeast **16,** 857-860.

Lichtenthaler, H.K., and Wellburn, A.R. (1983). Determinations of total carotenoids and chlorophylls a and b of leaf extracts in different solvents. Biochem Soc Trans **11,** 591-592.

McCormick, S. (1991). Transformation of Tomato with *Agrobacterium tumefaciens*. *In* K Lindsey, ed, *Plant Tissue Culture Manual.* Kluwer Academic, Dordrecht, The Netherlands, pp 1–9

Moellering, E.R., and Benning, C. (2011). Galactoglycerolipid metabolism under stress: a time for remodeling. Trends Plant Sci **16,** 98-107.

Moellering, E.R., Muthan, B., and Benning, C. (2010). Freezing tolerance in plants requires lipid remodeling at the outer chloroplast membrane. Science **330,** 226-228.

Munns, R., and Tester, M. (2008). Mechanisms of salinity tolerance. Annu Rev Plant Biol **59,** 651-681.

Murashige, T., and Skoog, F. (1962). A Revised Medium for Rapid Growth and Bio Assays ith Tobacco Tissue Cultures. Physiol Plant **15,** 473-497.

Roston, R.L., Wang, K., Kuhn, L.A., and Benning, C. (2014). Structural determinants allowing transferase activity in SENSITIVE TO FREEZING 2, classified as a family I glycosyl hydrolase. J Biol Chem **289,** 26089-26106.

Shalata, A., and Tal, M. (1998). The effect of salt stress on lipid peroxidation and antioxidants in the leaf of the cultivated tomato and its wild salt-tolerant relative Lycopersicon pennellii. Physiol Plant **104,** 169-174.

Shaul, O. (2002). Magnesium transport and function in plants: the tip of the iceberg. Biometals **15,** 309-323.

Shimojima, M., Ohta, H., Iwamatsu, A., Masuda, T., Shioi, Y., and Takamiya, K. (1997). Cloning of the gene for monogalactosyldiacylglycerol synthase and its evolutionary origin. Proc Natl Acad Sci USA **94,** 333-337.

Thorlby, G., Fourrier, N., and Warren, G. (2004). The SENSITIVE TO FREEZING2 gene , required for freezing tolerance in *Arabidopsis thaliana* , encodes a beta-glucosidase. Plant Cell **16,** 2192-2203.

Umezawa, T., Shimizu, K., Kato, M., and Ueda, T. (2000). Enhancement of salt tolerance in soybean with NaCl pretreatment. Physiol Plant **110,** 59-63.

van der Weele, C.M., Spollen, W.G., Sharp, R.E., and Baskin, T.I. (2000). Growth of *Arabidopsis thaliana* seedlings under water deficit studied by control of water potential in nutrient-agar media. J Exp Bot **51,** 1555-1562.

Wang, H., Zhang, M., Guo, R., Shi, D., Liu, B., Lin, X., and Yang, C. (2012). Effects of salt stress on ion balance and nitrogen metabolism of old and young leaves in rice (Oryza sativa L.). BMC Plant Biol**12,** 194.

CHAPTER 3

A Plastid Phosphatidylglycerol Lipase Contributes to the Export of Acyl Groups from Plastids for Seed Oil Biosynthesis

The work presented in this chapter has been published in The Plant Cell (www.plantcell.org) with copyright belonging to American Society of Plant Biologists:

Wang, K., Froehlich, J.E., Zienkiewicz, A., Hersh, H.L., and Benning, C. (2017). A Plastid Phosphatidylglycerol Lipase Contributes to the Export of Acyl Groups from Plastids for Seed Oil Biosynthesis. Plant Cell **29,** 1678-1696.

ABSTRACT

The lipid composition of thylakoid membranes inside chloroplasts is conserved from leaves to developing embryos. A finely tuned lipid assembly machinery is required to build these membranes during *Arabidopsis thaliana* development. Contrary to thylakoid lipid biosynthetic enzymes, the functions of most predicted chloroplast lipid-degrading enzymes remain to be elucidated. Here, we explore the biochemistry and physiological function of an Arabidopsis thylakoid membrane-associated lipase, PLASTID LIPASE1 (PLIP1). PLIP1 is a phospholipase A_1. In vivo, PLIP1 hydrolyzes polyunsaturated acyl groups from a unique chloroplast-specific phosphatidylglycerol that contains $16:1^{\Delta 3trans}$ as its second acyl group. Thus far, a specific function of this $16:1^{\Delta 3trans}$-containing phosphatidylglycerol in chloroplasts has remained elusive. The *PLIP1* gene is highly expressed in seeds, and *plip1* mutant seeds contain less oil and exhibit delayed germination compared to wild type. Acyl groups released by PLIP1 are exported from the chloroplast, reincorporated into phosphatidylcholine, and ultimately enter seed triacylglycerol. Thus, $16:1^{\Delta 3trans}$ uniquely labels a small but biochemically active plastid phosphatidylglycerol pool in developing Arabidopsis embryos, which is subject to PLIP1 activity, thereby contributing a small fraction of the polyunsaturated fatty acids present in seed oil. We propose that acyl exchange involving thylakoid lipids functions in acyl export from plastids and seed oil biosynthesis.

INTRODUCTION

Life on the Earth is driven by photosynthesis, which converts light energy into chemical energy and provides us with food and industrial feedstock. Photosynthesis takes place in chloroplast thylakoids, where protein complexes containing chlorophyll, carotenoids and other cofactors are embedded into photosynthetic membranes (Kobayashi et al., 2016). Photosynthetic membranes are composed of a specialized glycerolipid matrix with four major polar lipids (in order of abundance): mono- and digalactosyldiacylglycerol, (MGDG and DGDG, respectively), phosphatidylglycerol (PG) and the sulfolipid sulfoquinovosyldiacylglycerol (SQDG) (Andersson and Dörmann, 2009; Benning, 2010; Boudière et al., 2014). To date, many of the genes and the respective enzymes needed for photosynthetic membrane lipid biosynthesis have been characterized in *Arabidopsis thaliana.* However, we are only beginning to explore the dynamic changes in photosynthetic membranes under various developmental and environmental conditions and the underlying mechanisms of plastid lipid turnover and its regulation.

Lipid turnover requires lipases, which are enzymes that hydrolyze ester bonds of glycerolipids (Troncoso-Ponce et al., 2013; Kelly and Feussner, 2016). Lipases are involved in a large number of cell biological processes, from maintaining lipid homeostasis to lipid signaling (Wang, 2004; Scherer et al., 2010; Richmond and Smith, 2011). Phospholipases can be classified into four major types based on their lipid substrate cleavage sites: phospholipase D (PLD), phospholipase C (PLC), phospholipase A_1 (PLA_1), and phospholipase A_2 (PLA_2). PLD releases the polar head group and produces phosphatidic acid, while PLC cleaves the phosphodiester bond at the glyceryl *sn-3* position and produces the phosphorylated head group and diacylglycerol. PLA_1 and PLA_2 release acyl groups from the glyceryl moiety at the *sn-1* and *sn-2* positions, respectively (Wang et al., 2012). The Arabidopsis genome encodes approximately 300 proteins that are

annotated as lipases, but most of them have not been biochemically verified or have unknown physiological functions (Li-Beisson et al., 2013; Troncoso-Ponce et al., 2013; Kelly and Feussner, 2016). Some of the characterized chloroplast-located lipases have intriguing physiological functions. For example, DEFECTIVE IN ANTHER DEHISCENCE1 (DAD1) (Ishiguro et al., 2001) is a chloroplast-located PLA_1 that catalyzes the initial step of jasmonic acid (JA) production, which is necessary for proper pollen development and biotic stress resistance. Despite their potentially important functions in membrane maintenance and signaling, the bulk of chloroplast-localized lipases remain uncharacterized.

In land plants, fatty acid (FA) biosynthesis occurs in plastids. In Arabidopsis, two pathways are responsible for glycerolipid biosynthesis (Benning, 2009; Hurlock et al., 2014). De novo synthesized FAs either directly enter the prokaryotic pathway in plastids or are exported to the endoplasmic reticulum (ER) to be assembled into glycerolipids by the eukaryotic pathway. In developing embryos, the bulk of synthesized FAs is incorporated into triacylglycerol (TAG), which serves as the primary energy repository to fuel seed germination. Oleic acid (18:1; carbon : double bonds) is the FA predominantly exported from chloroplasts. Exported FAs are activated to acyl-CoAs and initially incorporated into phosphatidylcholine (PC), which is present in the outer envelope membrane of chloroplasts and in the ER, before reentering the cytosolic acyl-CoA pool by a process referred to as acyl-editing (Bates et al., 2007). Acyl-editing allows 18:1 to be further desaturated into polyunsaturated acyl groups attached to PC before reentering the acyl-CoA pool for incorporation of FAs into other lipids, including TAG. In fact, acyl-editing is one of the reported mechanisms for directing polyunsaturated FAs into TAG during embryogenesis through the action of diacylglycerol acyltransferase (Katavic et al., 1995; Routaboul et al., 1999), in parallel with direct head group exchange between PC and diacylglycerol (DAG) (Bates et al., 2012) or

acyl transfer from PC to DAG by phospholipid : diacylglycerol acyl transferase (Dahlqvist et al., 2000). Whether lipids other than PC are subject to acyl exchange remains to be determined.

Here, we report on the function of *PLASTID LIPASE1* (*PLIP1*). This gene encodes a thylakoid-associated PLA_1 that specifically releases polyunsaturated *sn-1* acyl groups from $16:1^{\Delta 3t}$-PG ($16:1^{\Delta 3t}$, 16 carbons with one *trans* double bond following carbon 3 counting from the carboxyl end, which is always at the *sn-2* glyceryl position), a chloroplast-specific lipid. The unusual *trans* double bond is introduced by FA DESATURASE4 (FAD4), which has diverged during evolution from other desaturases introducing *cis* double bonds (Gao et al., 2009). In developing seeds, the polyunsaturated acyl groups released by PLIP1 from $16:1^{\Delta 3t}$-PG in the chloroplast are incorporated into PC before being incorporated into TAG. PLIP1 initiates a mechanism leading to FA export from the chloroplast and the incorporation of FAs derived from the thylakoid membrane lipid pool into seed TAG. In addition, $16:1^{\Delta 3t}$-PG serves as a specific substrate for PLIP1 in vivo, providing insights into the specialized function of this unusual chloroplast lipid.

MATERIALS AND METHODS

Plant Material and Growth Conditions

Experiments were performed with *Arabidopsis thaliana* ecotype Columbia (Col-0). Seeds of T-DNA insertion lines SALK_102149 (*plip1-1*) and SALK_147687 (*plip1-2*) were obtained from the Arabidopsis Biological Resource Center, Ohio State University. Lines overexpressing *PLIP1* (or $PLIP1^{S422A}$) were generated by subcloning the coding sequence of *PLIP1* or $PLIP1^{S422A}$ (see below for their origin) into pEarleyGate 101 (YFP at the C-terminus) (Earley et al., 2006), followed by introducing constructs into Col-0 plants by *Agrobacterium tumefaciens*-mediated floral dip (Clough and Bent, 1998). Transformed seeds were initially screened for resistance to Basta, followed by confirmation by RT-PCR. Primers used for genotyping of T-DNA insertion lines or for RT-PCR analysis of overexpression lines are given in Supplemental Table 1. Arabidopsis seeds were vernalized at 4 °C in the dark for two days before being sown on soil and grown under 100 μmole $m^{-2}s^{-1}$ (Sylvania FO/741/ECO) in a 16 h light (22 °C) and 8 h dark (20 °C) cycle. Alternatively, sterilized and vernalized seeds were sown onto Phytoagar plates containing 1 × Murashige and Skoog (MS) growth medium (Murashige and Skoog, 1962) and 1% sucrose under 100 μmole $m^{-2}s^{-1}$ in the same light/dark cycle at 22 °C (Wang et al., 2016).

Quantitative Reverse-Transcription PCR

Total RNA was isolated from leaves of 4-week-old Arabidopsis plants grown on soil as previously described (Wang et al., 2016) using an RNeasy Plant Mini kit (Qiagen). Total RNA (600 ng) was used to synthesize complementary DNA using SuperScript III Reverse Transcriptase (Invitrogen). qRT-PCR was performed using SYBR Green PCR Core Reagents mix (Life Technologies) based on the manufacturer's instructions. The $2^{-\Delta\Delta Ct}$ calculation was used to

determine the relative mRNA levels. Table 3.1 lists the primers used. Reference primers were as previously described (Robinson and Bolhuis, 2001). For tissue-specific expression analysis, 100 mg dry seeds, five seedlings, roots harvested from five plants, 10 fully opened flowers or 10 siliques harvested nine days after flowering were pooled as one biological repeat.

Confocal Laser Scanning Microscopy

Imaging of YFP fusions was performed on leaves of 4-week-old Arabidopsis grown on soil using an Olympus FluoView 1000 confocal laser scanning microscope (Olympus) with excitation at 514 nm and emissions at 600 nm. Chlorophyll autofluorescence was visualized using excitation at 633 nm and emission at 700 nm. Images were merged and pseudocolored using Olympus FluoView 1000 confocal microscope software (Olympus).

Protein Extraction and Immunoblot Analysis

Intact chloroplasts were isolated from 4-week-old Arabidopsis plants grown on MS medium essentially according to (Aronsson and Jarvis, 2002; Roston et al., 2011), followed by sub-fractionation into stroma and thylakoid according to (Keegstra and Yousif, 1986; Roston et al., 2012) with minor modifications. In brief, isolated intact chloroplasts were pelleted and ruptured by resuspension in hypertonic solution (0.6 M sucrose in TE buffer) and the suspension was homogenized with a Dounce tissue homogenizer. After incubation on ice for 10 min, bulk thylakoid fractions were harvested by three 1500 × *g* 5-min centrifugations at 4 °C. Supernatants were subjected to another 100,000 × *g* 2-h centrifugation at 4 °C to remove envelope membranes, and the final supernatants were harvested as the stroma fraction. Total protein from each fraction was extracted using a Plant Total Protein Extraction Kit (Sigma) according to the manufacturer's

instructions, and protein was quantified using the Bio-Rad Bradford assay. Appropriate amounts of extracted organellar or total cellular protein were separated by SDS-PAGE (4-20% gradient, Bio-Rad), transferred to polyvinylidene fluoride membranes (Bio-Rad) and subjected to immunoblot analysis using primary antisera in 1:1000 to 1:5000 dilutions in TBST buffer (137 mM NaCL; 20 mM Tris base pH 7.5; 0.5% Tween-20). Secondary anti-rabbit or anti-chicken IgG antibodies were diluted 1:10,000. Positive immunoreactions were visualized using the Horseradish Peroxidase reaction with SuperSignal West Dura Extended Duration Substrate (Thermo Scientific), and the chemiluminescent signal was captured using the ChemiDoc^{TM} MP imaging system (Bio-Rad) according to the manufacturer's instructions.

Recombinant Protein and Antiserum Production

The *PLIP1* sequence was amplified from Arabidopsis wild-type cDNA (see above under RT-PCR procedure) and inserted into pGEM-T-EASY plasmid (Promega). It was then subcloned into the pET41a plasmid through BamHI and XhoI restriction sites. The PLIP1^{S422A} point mutation construct was generated with a Q5 Site-Directed Mutagenesis Kit (New England Biolabs). Constructs were confirmed by sequencing. Final pET41a-*PLIP1* and pET41a-*PLIP1*^{S422A} constructs were transformed into BL21 (DE3) *E. coli* strains for protein production. Cultures grown in LB medium (containing 0.1% glucose) were inoculated with fresh *E. coli* colonies and grown to log phase (OD_{260} 0.8) at 37 °C. Protein production was then induced by adding isopropyl-β-D-thiogalactopyranoside (IPTG) to a final concentration of 0.2 mM, and the culture was transferred to 14 °C. Cells were harvested after 3 h of induction. Cultures were harvested and sonicated to lyse cells. Supernatant was collected after centrifugation at 10,000 × *g* for 30 min, and subjected to another 1-h centrifugation at 100,000 × *g* to remove the majority of membrane bound

PLIP1. The supernatant was collected and used to extract and purify PLIP1 recombinant proteins using a Ni-NTA column as described (Lu and Benning, 2009), except with a modified washing buffer (50 mM Tris HCl, pH 7.5; 600 mM NaCl; 40 mM imidazole). Purified protein was concentrated using an Amicon Ultra-15 Centrifugal Filter (Millipore, UFC901024) and recovered with 1 × PBS buffer. The protein was quantified using the Bio-Rad Bradford assay, aliquoted, and stored at -20 °C in 30% glycerol.

Recombinant PLIP1^{S422A} was produced in *E.* coli and purified with a Ni-NTA column as described above. Purified protein was separated by SDS-PAGE and the corresponding band of PLIP1^{S422A} was isolated. Protein was recovered by immersing the gel bands into 1 × PBS buffer at 4 °C overnight with gentle agitation. Recovered proteins were concentrated with an Amicon Ultra-15 Centrifugal Filter to a final purity above 98%. Antisera were raised in rabbits by Cocalico Biologicals, Inc. using their standard protocol.

Chloroplast Import Assay

The N-terminal 6×His tag and TEV cleavage site of pET41a-*PLIP1* were removed using a Q5 Site-Directed Mutagenesis Kit (New England Biolabs) and the construct was confirmed by sequencing prior to use for import assays. The *FtsH8* gene was used as a control. Isolation of pea chloroplasts, import assays and post-import trypsin treatment were done as previously described (Xu et al., 2005).

PLIP1 Lipase Assay

Commercial lipid substrates were purchased from Avanti Polar Lipids Inc.. For each PLIP1 lipase reaction, 60 µg lipids were used. The organic solvent was removed under an N_2 stream, and

the lipids were resuspended in 300 µL reaction buffer (0.1 M PBS, pH 7.4; 4.2 mM Anzergent 3-12 (Anatrace)) and dispersed by sonication for 3 × 10 s on ice (Misonix; Sonicator 3000 with microprobe; power setting 1.5). Then, 0.5 µg protein in 20 µL 1 × PBS with 30% glycerol was added to each reaction. The mixture was sonicated again for 10 s with the same parameters mentioned above and incubated at ambient temperature (~22 °C) for 1.5 h or as indicated for time courses. The linear range of the reaction was determined by plotting the substrate degradation percentage along a time course as indicated in Supplemental Figure 2. The reaction was stopped by lipid extraction, followed by lipid analysis with TLC and gas chromatography as described below.

To prepare tobacco PG substrates, total lipids were isolated from 4-week-old plant leaves and resolved by polar TLC. The PG bands were isolated and lipids were recovered from silica powder by extraction with chloroform-methanol (1:1 by volume).

Lipid Analysis

Lipid extraction, TLC of polar and neutral lipids, transesterification, and gas chromatography were done as described in (Wang and Benning, 2011). Polar lipids were analyzed on activated ammonium sulfate-impregnated silica gel TLC plates (TLC Silica gel 60; EMD Chemical, Germany) using a solvent system consisting of acetone, toluene and water (91:30:7-7.5 by volume). The amount of water was adjusted according to ambient humidity (in general, 7 for summer; 7.5 for winter). This solvent system was also used for separation of lyso-lipids derived from MGDG and PG during in vitro lipase assays. For TAG quantification, lipids were resolved by TLC on DC-Fertigplatten SIL G-2 (MACHEREY-NAGEL, Germany) using a solvent system consisting of petroleum ether, ether and acetic acid (80:20:1 by volume). For total FA analysis of

dry seeds, 3 h transesterification was conducted directly on a number of seeds as specified. Lipids were visualized on TLC plates by brief exposure to iodine vapor. To separate lyso-lipids from PC, PE or PI, a solvent system consisting of chloroform, methanol, glacial acetic acid and water (65:35:8:5 by volume) was used. To separate lyso-PS from PS, the running solvent consisted of chloroform, methanol and ammonium hydroxide (28-30% NH_3 in water) (65:25:5 by volume). To separate lyso-lipids from DGDG and SQDG the running solvent contained chloroform, methanol, glacial acetic acid and water (85:20:10:4 by volume).

Pulse-Chase Labeling

For the leaf labeling experiments, detached leaves from 4-week-old soil-grown plants were incubated in non-radioactive medium (25mM MES-KOH, pH 5.7; 0.01% Triton X-100) in the light (25W incandescent bulb, ~40 μmole $m^{-2}s^{-1}$) at ambient temperature for 1 h. Radiolabeling was initiated by adding sodium [^{14}C]-acetate (specific activity 100 mCi/mmol in ethanol; American Radiolabeled Chemicals, Inc.) to the medium to provide 1 μCi/mL, followed by a 1-h incubation with gentle agitation. The leaves were then washed twice in non-radioactive medium prior to incubation in non-radioactive medium for another 48 h. At various time points after application of the label, samples were harvested and the metabolism was halted by immediate lipid extraction. Lipids were extracted and separated by TLC as described above, and radioactivity in each lipid fraction was analyzed using a scintillation counter (MicroBeta Trilux, Perkin Elmer) with 3 ml of scintillator solution (4a20, Research Products International Corporation) for 1 min per sample, or using phosphorimaging (FBCS 810, Fisher Biotech) with quantification by Quantity One (V 4.6.6).

Embryo labeling experiments were done as described (Bates et al., 2012). Briefly, the

newly opened flowers of 4-week-old soil-grown plants were tagged, and nine days later, siliques were harvested for embryo isolation. For each time point, a 100 µL volume of embryos was collected from approximately 50 siliques and pre-incubated in non-radioactive buffer (5 mM MES, pH 5.8; 0.5% sucrose; 0.5 × MS) in the light (~40 µmole $m^{-2}s^{-1}$) for 20 min with gentle agitation at room temperature. Labeling was initiated by removing the old medium and replacing it with the same medium containing 5 µCi sodium [^{14}C] acetate. Pulse labeling lasted for one hour, followed by washing and replacing with non-radioactive medium to start the chase. Samples were collected at the indicated time points, and the reaction was quenched by immediate lipid extraction as described above.

Observation of Embryo Morphology

Siliques were harvested nine days after flowering and subsequently cleared with a clearing solution (chloral hydrate : glycerol : water = 8 :2 :1) according to (Herr Jr, 1993). Developing embryos were dissected from siliques after clearance and observed under a Nikon C2 microscope.

Hormone Extraction and Arabidopside measurement

Hormone extraction and quantification was done according to (Zeng et al., 2011) with minor modifications. Briefly, hormones were extracted from 100 mg (fresh weight) leaf tissue or 50 mg dry seeds with an extraction buffer composed of methanol:water (80:20 v/v) containing 0.1% formic acid, 0.1 g/L butylated hydroxytoluene (BHT) and 100 nM abscisic acid (ABA)-d6 as an internal standard. Hormones were analyzed by LC/MS/MS as described (Zeng et al., 2011). Standard curve samples were prepared by serial dilution of stock ABA, IAA, SA, JA, JA-Ile, and OPDA to reach final concentrations from 1 nM to 1000 nM of each hormone with a fixed

concentration of ABA-d6 of 100 nM. Peak integration and calibration curve processing was performed using Masslynx software (version 4.1).

Arabidopsides were extracted following the hormone extraction procedure without adding internal standards. Samples were analyzed using a Waters Xevo G2-XS Q-TOF mass spectrometer interfaced with a Waters Acquity binary solvent manager and Waters 2777c autosampler. 10 µl samples were injected onto an Acquity UPLC CSH C18 column (100 x 2.1 mm, Waters Corp) held at 40 ˚C. A gradient of solvent A (acetonitrile/water (60:40) containing 10 mM ammonium formate and 0.1% formic acid) and solvent B (Isoproponal / acetonitrile (90:10) containing 10 mM ammonium formate and 0.1% formic acid) was applied in a 10-minute program with a mobile phase flow rate of 0.3 ml/minute. The elution was performed as follows: hold for 1 min after injection at 95% A / 5% B, followed by a seven-minute linear ramp to 0% A / 100% B, hold for one minute at 100% B, then return to 95% A / 5% B and equilibrate for one minute. LC separated analytes were ionized by negative ion mode electrospray ionization and mass spectra were acquired using an MSe method in continuum mode over m/z 50 to 1500 to provide data under non-fragmenting and fragmenting conditions (collision energy ramp from 15-60 V). Peak areas from extracted ion chromatograms for OPDA/OPDA-MGDG ([M-H]-, m/z 847.5), OPDA/OPDA-DGDG ([M-H]-, m/z 1009.57), OPDA/dnOPDA-MGDG ([M-H]-, m/z 819.5) were obtained using Masslynx (version 4.1) software. Identification was based on accurate mass and OPDA or dnOPDA fragment ions (m/z values are 291.19 and 263.16, respectively). The peaks of the Arabidopsides were normalized to that of 18:3/18:3-DGDG ([M-H]-, m/z 981.61).

Phylogenetic analysis

The presumed orthologues land plant sequences of Arabidopsis PLIP1 and FAD4 were

obtained by BLAST analysis against the NCBI database with default parameters. Only one sequence per plant with the highest alignment score and over 40% sequence similarity with the Arabidopsis sequence was considered a presumed orthologue. The amino acid alignment was created using MUSCLE with default settings in MEGA (version 7.0.21) software. The Maximum Likelihood phylogenetic trees were built using MEGA (version 7.0.21), and the bootstrap percentages were based on 1000 replicates.

The correlation coefficiency score was obtained essentially according to (Pazos et al., 2005). The 18S rRNA sequences were obtained from the SILVA rRNA database (Quast et al., 2013). The tree built with 18S rRNA sequences was subtracted as background from both the FAD4 and PLIP1 trees before calculating the Pearson's correlation coefficient. The accession numbers of the PLIP1, FAD4 orthologous sequences and the 18S rRNA sequences are listed in Supplemental Table 1.

Accession Numbers

Sequence data from this article can be found in the Arabidopsis TAIR database (https://www.arabidopsis.org/) under the following accession numbers: At3g61680 for *PLIP1*, At2g29980 for *FAD3*, At4g27030 for *FAD4*, At5g42020 for *BIP2*, At1g06430 for *FTSH8*.

RESULTS

PLIP1 is a Chloroplast Thylakoid-Associated Protein

The Arabidopsis genome encodes approximately 300 putative lipases (Li-Beisson et al., 2013; Troncoso-Ponce et al., 2013; Kelly and Feussner, 2016), among which 46 were included in the Chloroplast 2010 Project, which was aimed at assigning functions to nearly all plastid-localized proteins (Lu et al., 2008; Ajjawi et al., 2010). We hypothesized that some of these putative chloroplast lipases may play roles in the maintenance of photosynthetic membranes and perhaps have specialized roles in tissues with high demands on lipid metabolism, such as developing seeds that accumulate TAG. We initially focused on one of the predicted chloroplast lipase genes, At3g61680, which encodes a protein with a conserved Lipase 3 domain and a strongly predicted transit peptide, which we subsequently named PLIP1. With its Lipase 3 domain, which is a signature for triacylglycerol lipases, this Arabidopsis protein shares similarities with a bona fide lipase of Chlamydomonas, PLASTID GALACTOGLYCEROLIPID DEGRADATION1 (PGD1), involved in the turnover of chloroplast MGDG, leading to the export of acyl groups and their incorporation into TAG following nutrient deprivation (Li et al., 2012), although the two proteins do not share sequence similarity outside the Lipase 3 domain and are not orthologues.

To experimentally verify the subcellular location of PLIP1, the *PLIP1* coding sequence derived from an Arabidopsis wild-type (Col-0) cDNA was spliced at its 3'-end (creating a C-terminal fusion) to the open reading frame of yellow fluorescent protein (YFP). When the *PLIP1-YFP* construct was stably expressed in the wild type under the control of the cauliflower mosaic virus (CaMV) 35S promoter, the YFP and chlorophyll signals overlapped (Figure 3.1 A). Although transgenic lines used in this experiment had constitutive expression of *PLIP1-YFP*, ubiquitous YFP signals were not detected. Instead, only about 10 to 15% of mesophyll chloroplasts showed

YFP signals, and the cells observed in the *PLIP1-YFP* transgenic plants were slightly smaller than wild type.

To corroborate the suborganellar location of PLIP1, we isolated intact chloroplasts from 4-week-old wild-type seedlings and fractionated them into thylakoid membranes and stroma. Immunoblot analysis of PLIP1 showed increasing signal intensity from whole plant tissue to intact chloroplasts and thylakoids, consistent with an association of PLIP1 with the thylakoids (Figure 3.1B). Fractionation quality was controlled for by including marker proteins for each fraction. The thylakoid protein Light Harvesting Complex b1 (LHCb1) showed a similar intensity pattern to that of PLIP1. To exclude the possibility of contamination with ER-associated proteins, the ER-specific marker BiP2 was also included (Figure 3.1 B). The fractionation of the stroma-specific Rubisco large subunit and the thylakoid-specific light-harvesting chlorophyll a/b-binding protein (LHCP) were visible on a Coomassie Brilliant Blue-stained SDS-PAGE gel (Figure 3.1 C).

The *PLIP1* gene is predicted to encode a 71,735 D protein for which a molecular or biochemical function had not been experimentally determined. Based on the ARAMEMNON database, PLIP1 is not predicted to contain any transmembrane domains (Schwacke et al., 2003). Therefore, it seemed likely that PLIP1 is a peripheral thylakoid membrane protein. To learn more about its suborganellar location and processing en route, we translated *PLIP1* cDNA in vitro in the presence of labeled methionine. During the import of the translation product into isolated pea (*Pisum sativum*) chloroplasts, the PLIP1 precursor was processed into a smaller intermediate protein that was present in both the stroma and chloroplast membrane fractions. In addition, the trypsin-resistance of PLIP1 suggested that it is located inside the chloroplast (Figure 3.1 D). Interestingly, the intermediate PLIP1 form was further processed into a smaller mature protein, which was mainly associated with the stroma fraction. We used thylakoid lumen-localized FtsH8

as a control for proper fractionation and import (Rodrigues et al., 2011), which was processed and imported into the thylakoids with a pattern different from that of PLIP1, suggesting that PLIP1 is probably not imported into the thylakoid lumen but instead attaches to the outside leaflet of thylakoid membranes and can be released into the stroma with additional processing. Summing up all localization data, PLIP1 is likely a thylakoid membrane-associated protein.

PLIP1 is a Phospholipase A_1 With a Preference for Unsaturated Acyl Groups

PLIP1 is annotated as a TAG lipase in TAIR (https://www.arabidopsis.org/). To verify its activity and determine its enzymatic properties, we tried to develop an in vitro lipase assay with recombinant PLIP1 purified from *E. coli*. However, expression of the recombinant *6×His-PLIP1* construct was very low, as detected by immunoblotting against the His tag. Analysis of transgenic *E. coli*-derived lipid extracts by thin-layer chromatography (TLC) showed that, when *PLIP1* was expressed, PG and phosphatidylethanolamine (PE), the two major polar lipids of *E. coli*, were degraded, leading to the accumulation of free FAs (Figure 3.2 A). This observation suggested that PLIP1 is a lipase that releases acyl groups from PG and PE.

Lipases belong to a group of serine esterases with a lipase signature motif, an Asp-His-Ser triad, with some exceptions having only a Ser-Asp dyad, and in all cases Ser serves as the active site residue, participating in the reaction mechanism (Brady et al., 1990; Winkler et al., 1990; Richmond and Smith, 2011; Kelly and Feussner, 2016). Alignment of the PLIP1 protein sequence with those of classic lipases using NCBI's conserved domain database (Marchler-Bauer et al., 2015) identified two potential catalytic residues, Asp^{483} and Ser^{422}, but the conserved His site was not present (Figure 3.3). Replacing these two residues with Ala, respectively, abolished PLIP1 lipase activity, and the respective mutant proteins were abundantly produced in *E. coli*, as PG and

PE were not degraded (Figure 3.2 B). Taken together, these data suggest that PLIP1 is a lipase with Ser^{422} as the catalytic residue. Taking advantage of the enhanced production of nonfunctional $PLIP1^{S422A}$ in *E. coli*, we purified the mutant protein and raised an antibody in rabbits to specifically detect PLIP1.

To develop an in vitro lipase assay, recombinant PLIP1 and $PLIP1^{S422A}$ were produced in *E. coli* and affinity-purified from the soluble fraction (Figure 3.2 C). We chose Anzergent 3-12 as the solubilizing detergent from a series of other reagents, because of its high compatibility with PLIP1 enzyme activity and because it was not co-chromatographing with native plant membrane lipids during subsequent TLC analysis. In the final optimized system (Figure 3.4), in vitro lipase activity of PLIP1 was observed on a wide range of substrates. As an example (shown in Figure 3.2D), PC was provided to PLIP1 and $PLIP1^{S422A}$. At the end of the reaction, lipids were extracted and separated by TLC. Lipase activity based on the production of lyso-PC was only observed with PLIP1, but not with $PLIP1^{S422A}$ (Figure 3.2 D).

PLIP1 in vitro activity with PC and other glycerolipids as substrates always resulted in lyso-lipid products, implying that PLIP1 can only hydrolyze one of the two acyl-glyceryl ester bonds in glycerolipids. To investigate which glyceryl position PLIP1 prefers, two PCs with reversed acyl compositions were offered to PLIP1. At the end of the reaction, lipids were extracted, lyso-PC was isolated by TLC, and FA methyl esters derived from the lyso-lipid were analyzed by gas-liquid chromatography (Figure 3.5A). For PC with a composition of $18:1^{\Delta 9}$/16:0 (*sn-1/sn-2*), $18:1^{\Delta 9}$ was selectively released and 16:0 was retained in the lyso-product. The result was reversed with PC containing 16:0/$18:1^{\Delta 9}$ as the lyso-product contained $18:1^{\Delta 9}$. Therefore, PLIP1 is a lipase that prefers the *sn-1* glyceryl position of the respective glycerolipid. Furthermore, to determine a possible acyl group preference of PLIP1 at the *sn-1* glyceryl position, PLIP1 was offered different

combinations of pure PC molecules carrying the same acyl groups at the *sn-2* but acyl groups with different degrees of saturation at the *sn-1* position (Figure 3.5 B). Comparing 18:0/18:1 with 18:1/18:1, PLIP1 enzyme activity was approximately twice as high for 18:1/18:1-PC, and when comparing 18:0/18:2 with 18:2/18:2, its activity was elevated nearly four-fold for 18:2/18:2-PC. Therefore, PLIP1 is a phospholipase A_1 with a preference for more unsaturated acyl groups.

To survey PLIP1 substrate preference in vitro, we offered the majority of the plant glycerolipids, including galactoglycerolipids, phospholipids, as well as TAG (Figure 3.5 C). High enzyme activity was detected for all tested phospholipids and MGDG. Given the plastid location of PLIP1, possible native substrates were limited to PG and MGDG. The low activities detected for SQDG, DGDG and TAG suggested that these are not likely substrates of PLIP1 (Figure 3.5 C). Based on these results, despite its conserved Lipase 3 domain, PLIP1 is apparently not a TAG lipase.

18:3/16:1$^{\Delta 3t}$-PG is the Preferred Substrate of PLIP1 In Vivo

The in vitro assays in combination with its established chloroplast location narrowed down possible native PLIP1 substrates to MGDG and PG (Figure 3.5 C). However, given the complexity of native plant acyl compositions, this limited survey based on an in vitro lipase assay alone could only provide a first approximation of the likely PLIP1-preferred substrate in vivo. To assess PLIP1 activity in its native biological context, we took advantage of the Arabidopsis transgenic lines used for PLIP1 localization described above. In total, 30 independent *PLIP1-YFP* (*PLIP1*-OX) and 14 *PLIP1*^{S422A}*-YFP* (*PLIP1*^{S422A}-OX) overexpression lines were generated and three *PLIP1*-OX lines were selected as representatives. As shown in Figure 4A, compared to wild type, the *PLIP1*-OX lines had smaller rosettes and fewer leaves, which were slightly pale yellow, whereas *PLIP1*^{S422A}-

OX plants were indistinguishable from wild-type and empty vector control plants. On a fresh weight basis, the total leaf acyl group content of the smaller *PLIP1*-OX plants was not reduced (Table 3.2). A comparison of the relative abundance of polar lipids (Figure 3.6 A) and the acyl group composition of individual polar lipids of EV control plants and two *PLIP1*-OX lines is shown in Figure 3.7B, C and Supplemental Figure 3.5B-E. In *PLIP1*-OX lines, the levels of lipids associated with chloroplasts (MGDG, PG and DGDG) decreased, while the levels of lipids mostly associated with the ER (PC, PE and PI) increased (Figure 3.6 A), suggesting a reduced ratio of plastid-to-extraplastidic membranes in the *PLIP1*-OX lines. Acyl group analysis of individual membrane lipids showed the greatest changes for PG (Figure 3.7 B). Specifically, the ratio of 16:0 to $16{:}1^{\Delta 3t}$ was increased in the *PLIP1*-OX lines. For 18-carbon acyl groups, which are primarily present at the *sn-1* position of plastid PG, polyunsaturated 18:3 levels decreased with a concurrent increase in the relative abundance of 18:1 and 18:2. Based on these changes in the molecular composition of PG, we hypothesize that $18{:}3/16{:}1^{\Delta 3t}$-PG is a preferred substrate of PLIP1 in its native environment.

MGDG, the most abundant lipid in chloroplasts, also showed a subtly reduced ratio of 16:3 to 18:3 in *PLIP1*-OX lines (Figure 3.6 B). For ER lipids, a decrease in 18:2 and an increase in 18:1 were observed for PC (Figure 4.7 C), as well as for PE and PI (Figure 3.6 E). Since PLIP1 is located in the chloroplast and is spatially separated from ER lipids, observation of this ER lipid alteration suggested that turnover of chloroplast lipids can affect the synthesis of ER lipids, assuming that lipid precursors are transported from the chloroplast to the ER. The other two photosynthetic membrane lipids, DGDG and SQDG, showed very minor changes in their molecular compositions in the *PLIP1*-OX lines (Figure 3.6 C and D), which is consistent with the low activity of PLIP1 on DGDG and SQDG in vitro (Figure 3.5 C).

The altered morphology of the *PLIP1*-OX lines raised a concern that the lipid phenotype might be a secondary phenotype due to the plants' abnormal development and growth. Therefore, we investigated whether growth and lipid phenotypes could be separated. Besides stunted growth, the three *PLIP1*-OX lines had shorter leaf petioles than wild type and accumulated anthocyanin under normal growth conditions (Figure 3.7 A), phenotypes reminiscent of plants with activated JA signaling (Yan et al., 2007; Zhang and Turner, 2008; Campos et al., 2016). Given that PLIP1 releases polyunsaturated FAs including 18:3, a precursor of JA and other oxylipins, we hypothesized that the reduced growth of *PLIP1*-OX plants is due to the production of oxylipins and the activation of JA signaling. Quantitative PCR analysis showed that the expression of JA-responsive marker genes was constitutively increased in *PLIP1*-OX lines compared to wild type (Figure 3.8). Targeted hormone analysis of mesophyll tissues showed that the levels of 12-oxo Phytodienoic acid (OPDA) and OPDA-containing glycerolipids called Arabidopsides were strongly elevated in the *PLIP1*-OX mesophyll tissues (Figure 3.9). JA and to some extent OPDA signaling require the coreceptor CORONATINE INSENSITIVE1 (COI1) (Xie et al., 1998; Ribot et al., 2008). To corroborate that the growth phenotype is secondary and caused by the activation of JA signaling pathways, we crossed *PLIP1*-OX lines with a *coi1* mutant to block COI1-dependent OPDA and JA signaling. As a result, the growth phenotype was largely (but not fully) restored in the offspring of this cross as validated by analysis of variance, while the lipid phenotype remained identical to that of the *PLIP1*-OX lines (Figure 3.10). Thus, we were able to at least partially separate the growth and lipid phenotypes, suggesting that the changes in lipid composition observed represent the primary phenotype resulting from PLIP1 overproduction in the PLIP-OX lines and are not the result of abnormal growth.

Overexpression of *PLIP1* Accelerates Recycling of Plastid PG Acyls Groups and Their Transfer to PC

The analysis of the *PLIP1*-OX lines described above depicts the lipid composition at steady-state. However, lipid metabolism is a dynamic process, and pulse-chase labeling is an effective way of probing the dynamics of lipid metabolism and movement of acyl groups through different lipid pools and between organelles (Xu et al., 2008; Li et al., 2012). Therefore, we employed pulse-chase labeling of membrane lipids using [^{14}C]-acetate, which can be readily incorporated into acyl groups in plastids by the FA synthase complex. The pulse phase of the experiment (shown in Figure 3.11 A) indicated that MGDG, PG and PC contained the majority of the label in empty vector (EV) control leaves, with PG accounting for approximately 15% of the label after 1 hour. However, in *PLIP1*-OX1, incorporation of label into PG accounted for nearly 70% of total label at the end of the pulse phase. This result suggests that incorporation of de novo synthesized acyl groups into PG is greatly accelerated in *PLIP1*-OX lines. During the chase phase (Figure 3.11 B), PG rapidly lost most of the label (within a day), and the label concomitantly increased in PC and to a smaller extent in PE in the *PLIP1*-OX1 line. The EV control line showed less drastic changes in labeling during the chase phase. The rapid increase and subsequent loss of PG label in *PLIP1*-OX1 during the pulse and chase phases, respectively, suggested a rapid acyl exchange, preferably on PG, in these lines and supported our hypothesis that PG is the preferred PLIP1 substrate in its native environment.

The most notable acyl group change observed in the *PLIP1*-OX lines was the increased 16:0-to-16:1$^{\Delta 3t}$ ratio in PG (Figure 3.7 B). However, 16-carbon FAs only exist at the *sn-2* position of plastid PG. This implies that acyl groups at the glycerol *sn-2* position affect PLIP1-catalyzed hydrolysis at the glyceryl *sn-1* position of PG. To test this possibility, we provided purified

recombinant PLIP1 with a set of commercial PCs with 16:0 at the glyceryl *sn-1* position, but 18-carbon acyl groups of different saturation levels at the glyceryl *sn-2* position. The highest enzyme activity was observed for PC with 18:2 at the *sn-2* position, followed by 18:1, with the lowest activity observed for 18:0 (Figure 3.11 C), suggesting that unsaturated *sn-2* acyl groups enhance PLIP1 activity. Therefore, it follows that 16:1$^{\Delta 3t}$ should be favored over 16:0 at the *sn-2* position of PG. To test this hypothesis, plant-derived PG composed of species containing 16:0 or 16:1$^{\Delta 3t}$ at the glyceryl *sn-2* position was extracted from tobacco (*Nicotiana benthamiana*) leaves and offered to PLIP1 in vitro. Total PG was degraded, while lyso-PG was produced over time (Supplemental Figure 6A). The fraction of 16:1$^{\Delta 3t}$ in lyso-PG increased over time, while 16:0 decreased (Figure 3.11 D), indicating that 16:1$^{\Delta 3t}$-PG is preferred by PLIP1 under these conditions when native PG substrate is offered. The opposite pattern between 16:0 and 16:1 $^{\Delta 3t}$ was observed in retained PG (Figure 3.12 B). Therefore, we concluded that 18:3/16:1$^{\Delta 3t}$-PG is the preferred native substrate of PLIP1 based on data gathered from the above-described combination of in vitro and in vivo experiments.

Another interesting observation during the chase phase of the labeling experiment was the sequential labeling of PG and PC, which points towards a precursor-product relationship between these two lipids. This observation was also consistent with the decreased plastid-to-extraplastidic lipid ratio observed during steady-state lipid analysis of the *PLIP1*-OX lines (Figure 3.6 A). Therefore, we hypothesized that 18:3 released from 18:3/16:1$^{\Delta 3t}$-PG was exported from the plastid and incorporated into PC. PC is known for its intermediate role in acyl editing involving desaturation of PC-acyl groups (18:1 to 18:2 and 18:3) followed by acyl exchange (Bates et al., 2007). We reasoned that the reduced 18:2 content of PC in the *PLIP1*-OX lines might be due to the increased competition of incorporation of plastid-derived 18:3 into PC via the activity of ER

desaturases FAD2 and FAD3, generating 18:3 from 18:1 and 18:2 bound to PC. To test this hypothesis, we crossed a *PLIP1*-OX1 plant to a *fad3-2* mutant plant (Figure 3.11 E and 3.13), which is deficient in the desaturation of 18:2 to 18:3 on ER lipids (PC, PI and PE). We expected that PLIP1 overexpression might rescue the *fad3-2* defect. As reported (Browse et al., 1993), the *fad3-2* mutant had a reduced 18:3 content in ER lipids. The overexpression of *PLIP1* in the *fad3-2* mutant background partially reversed this phenotype by increasing the 18:3 content in ER lipids PC, PI, and PE (Figure 3.11 E and 3.13 F). These 18:3 acyl groups must have been derived from the chloroplast, where the FAD7/8 desaturases (Li-Beisson et al., 2013) catalyze the lipid-linked desaturation of acyl groups from 18:2 to 18:3. This increase in 18:3 in PC is paralleled by a decrease in 18:3/16:1$^{\Delta 3t}$-PG (Figure 3.13 E). Taken together, these data support our hypothesis that in the *PLIP1*-OX lines, 18:3 increasingly moves from plastid 18:3/16:1$^{\Delta 3t}$-PG to PC, which interferes with the desaturation of acyl groups on PC by ER desaturases FAD2 and 3 and the PC-based acyl editing process.

PLIP1 Contributes a Small Fraction of Precursors for TAG Biosynthesis During Embryogenesis

The analysis of PLIP1, thus far, has focused on its biochemical function in vitro and in vivo using overexpression lines. However, these experiments can shed only limited light on the physiological functions of PLIP1. Querying the native tissue-specific and developmental expression of *PLIP1*, the highest gene expression was detected primarily in seeds and reproductive tissues, including flowers and siliques (Figure 3.14 A). Since *PLIP1* encodes a lipase and is highly expressed in seeds, we postulated that it might play a role in seed lipid metabolism, which is dominated by the biosynthesis of TAG. In fact, towards the end of seed development, over 90%

of total acyl groups are stored in TAG (Li et al., 2006; Li-Beisson et al., 2013). To explore the physiological function of PLIP1 during embryogenesis, two independent T-DNA insertion lines were obtained (Alonso et al., 2003). The T-DNA allele corresponding to SALK_102149 was designated as *plip1-1,* and the second, corresponding to SALK_147687, was designated as *plip1-2*. The T-DNA insertions were in the 3' and 5' UTRs, respectively (Figure 3.15 A). Quantitative RT-PCR analysis indicated that both lines carry leaky alleles (Figure 3.15 B, numbers on panel). Under normal growth conditions, the two *plip1* mutant alleles were physiologically indistinguishable from the wild-type plants (WT) (Figure 3.15 B). Lipid analysis also showed no changes in vegetative tissues (Figure 3.15 C-J). However, in dry seeds, where *PLIP1* mRNA is highly abundant, the insertion lines showed an approximate 10% reduction in total seed acyl group content indicative of a decrease in TAG, while the overexpression lines had a 40-50% increased seed acyl group content (Figure 3.14 B). Seed weight changes were consistent with the changes in seed TAG levels; the *plip1* mutants had smaller seeds than wild type, while the seeds of the overexpression lines were larger (Figure 3.14 C). Compromised germination was also observed for the seeds of the two *plip1* mutants (Figure 3.14 D), a typical phenotype related to the reduction in the major seed carbon reserve, TAG. Surprisingly, seeds from the overexpression lines also had slower germination rates than wild type, despite their elevated TAG content (Figure 3.14 D). To investigate whether this is caused by altered seed development due to altered plant hormone levels, we analyzed the major hormones typically present in dry seeds. As shown in Supplemental Figure 9, the hormone levels of the *plip1* mutant seeds were not significantly different from those of the WT seeds, whereas the *PLIP1*-OX1 seeds had elevated OPDA and JA-Ile levels (Figure 3.16), both of which are effective germination inhibitors (Dave et al., 2011; Dave and Graham, 2012). Arabidopsides were not detected in seeds of any genotypes. It must be noted that mature *PLIP1*-

OX lines had shorter and bushier inflorescences than wild type (Figure 3.17 A), and that seed yield was reduced by approximately 60% for the *PLIP1*-OX lines (Figure 3.17 B). Thus, overall oil yield was not elevated in the *PLIP1*-OX plants. Nevertheless, the phenotype of the *plip1* reduced function mutant suggested that PLIP1 might play a role in TAG biosynthesis during embryogenesis.

To gain more information on how the plastid-located PLIP1 contributes to TAG biosynthesis during embryogenesis, we analyzed TAG acyl groups in dry seeds. In the insertional mutants, especially in the slightly stronger *plip1-2* allele, 18:3 levels increased relative to 18:1 (Figure 3.14 E). For the two *PLIP1*-OX lines, 18:2 levels decreased, while 18:3 and 18:1 levels increased, a pattern that resembled the leaf PC acyl group profile in the *PLIP1*-OX lines (Figure 3.7 C). This suggested that increased TAG may be derived from increased flux of acyl groups through PC in the overexpression lines. Based on the lipid analysis in vegetative tissues of the *PLIP1*-OX lines (Figure 3.7), we hypothesized that PLIP1 in developing embryos contributes to TAG biosynthesis by catalyzing the turnover of PG, increasing the flux of acyl groups into PC and ultimately TAG. To corroborate this hypothesis, we analyzed PG and PC content and composition in developing seeds isolated from siliques seven days after flowering. Total PG content was approximately 1.6% of total lipids in both WT and *plip1-2*, while developing seeds of *PLIP1*-OX1 contained approximately 50% less PG (Figure 3.14 F, inserted panel). With regard to acyl composition, relative levels of $16{:}1^{\Delta 3t}$ and 18:3 decreased in the *PLIP1*-OX1 line, while they increased in *plip1-2*, supporting a role for PG as the substrate of PLIP1 in developing seeds. PC accounts for approximately 10% of the total lipids at this stage of developing seeds (Figure 3.14 G, inserted panel), and the acyl compositions of PC in different genotypes resembled that of TAG

in dry seeds (Figure 3.14 G), implying that the altered TAG acyl compositions in *PLIP1*-OX and *plip1* mutant seeds at least partially reflect the metabolism of PC.

It has been proposed that acyl editing of PC, head group exchange, and PDAT activity represent the mechanisms for directing polyunsaturated FAs from PC into TAG during seed development (Dahlqvist et al., 2000; Bates et al., 2012). In the *fad3-2* mutant, approximately 15% of 18:3 was retained in total seed FAs (Figure 3.18), suggesting that the proposed PLIP1-based mechanism is a relatively small but significant contributor to the incorporation of 18:3 into seed TAG compared to the PC-based FAD2/3 desaturation pathway. In fact, consistent with the observation in leaf tissues (Figure 3.11 E), overexpressing *PLIP1* in the *fad3-2* background restored the 18:3 level to 36% (Figure 3.18).

As discussed above, 16:1$^{\Delta 3t}$-PG is likely the preferred substrate of PLIP1 and 16:1$^{\Delta 3t}$ only exists at the *sn-2* position of plastid PG. FAD4 is the enzyme in Arabidopsis that specifically introduces *trans*-double bonds into the 16:0 acyl chain of PG (Gao et al., 2009). Transcript analysis of *FAD4* during seed development showed that this gene is upregulated during embryogenesis, in a time course that correlates well with oil biosynthesis during embryogenesis (Figure 3.19 A). It should be noted that the transcript levels of *FAD4* are on the same order of magnitude in leaf and seed tissues (Winter et al., 2007) (Figure 3.19 A), but the 16:1$^{\Delta 3t}$-PG level varies drastically between these two tissues.

Our hypothesis that PLIP1 contributes to embryonic TAG biosynthesis predicts that removal of 16:1$^{\Delta 3t}$-PG should result in a similar seed phenotype to that observed for the *plip1* mutants. To test this hypothesis, we characterized two *FAD4* loss-of-function lines, *fad4-2* and *fad4-3* (Gao et al., 2009). As shown in Figure 8B, 16:1$^{\Delta 3t}$ was not detected in PG in either *fad4-2* or *fad4-3* leaf tissues. Similar to the *plip1* mutants, *fad4-2* and *fad4-3* showed a nearly 10%

reduction in total seed acyl group content (Figure 3.19 C), reduced seed weight, but no altered seed yield (Figure 3.19 D). The *fad4-2* and *fad4-3* mutants also had altered seed acyl group profiles, specifically reduced 18:2 and increased 18:3 content (Figure 3.19 E), similar to the changes in *plip1-2* seed acyl group composition (Figure 3.14 E). Taken together, these observations led us to conclude that acyl groups in plastid 16:1$^{\Delta 3t}$-PG contribute to TAG biosynthesis during embryogenesis and that this requires PLIP1 activity.

Alignment of the predicted PLIP1 sequences found in land plants (Table 3.3 for species and accession numbers) followed by phylogenetic analysis shows that PLIP1 proteins are conserved in land plants (Figure 3.20), except for the orchid family, for which genomes of two species are available in NCBI (*Phalenopsis equestris* and *Dendrobium catentum*. Interestingly, presumed FAD4 homologs are also ubiquitous among land plants, except for the two representatives of the orchid family (Figure 3.20). Calculation of the linear correlation coefficient between the PLIP1 and FAD4 phylogenetic trees after extracting the 18S rRNA background from 26 sequenced land plant species (Pazos et al., 2005) resulted in a score of 0.971, suggesting that these two proteins are coevolving. This supports our hypothesis that PLIP1 and FAD4 function in the same pathway.

Overexpression of *PLIP1* Increases PG Recycling and TAG Biosynthesis During Embryogenesis

To determine whether increased turnover of plastid PG is responsible for increased TAG biosynthesis during embryogenesis in the *PLIP1*-OX lines, we harvested siliques at nine days after flowering from WT and *PLIP1*-OX1 plants and isolated the developing seeds. Seeds at this developmental stage have robust lipid metabolism (Le et al., 2010; Bates et al., 2012). However,

siliques of the same age collected from *PLIP1*-OX1 plants were shorter than those from WT (Figure 3.21 A), which raised the concern that embryos from *PLIP1*-OX1 and WT might be at different developmental stages. However, upon closer examination, WT and *PLIP1*-OX1 had nearly mature embryos with fully developed cotyledons and radicals (Figure 3.21 B), indicating they were at a similar developmental stage and likely metabolically comparable. Therefore, we performed [^{14}C]-acetate pulse-chase labeling on the isolated developing seeds. Pulse time points were collected after 20 and 60 minutes and are shown before time 0 of the chase start on the X-axis, followed by three chase time points; a representative example of multiple repeats is shown (Figure 3.21 C). Compared to PC and TAG, plastid lipids PG and MGDG were not highly labeled during embryogenesis, likely due to their small pool size; therefore, an expanded view for PG is shown in the lower graph of Figure 9C. *PLIP1*-OX1 had higher incorporation of label into PG and increased turnover during the chase phase (Figure 3.21 C), as was observed for the equivalent experiment done on leaves. The altered labeling patterns for PG and MGDG resembled those observed in the leaf labeling assays (Figure 3.11 A and B). The most strongly labeled lipids were TAG and PC, reflecting their end-product status (TAG) or large pool size (PC) in developing seeds. However, the much smaller PG pool (mostly in the chloroplast as 16:1$^{\Delta 3t}$-PG) seemed to be more metabolically active in *PLIP1*-OX1 than in WT. Incorporation of label into PG during the pulse under the conditions tested was faster than could be captured by the earliest sampling time points. The rate and extent of incorporation into TAG was increased in the *PLIP1*-OX1 line, consistent with increased total acyl group content in these seeds, while the PC pool was similarly labeled in the WT and overexpression lines.

DISCUSSION

PLIP1 Prefers PG as Natural Substrate

Recombinant lipases are notoriously difficult to produce and to study in vitro. PLIP1 is no exception, as its production in *E. coli* led to membrane degradation, which confirmed its general lipase activity, but made PLIP1 challenging to purify (Figure 3.2). Furthermore, while recombinant PLIP1 was specifically acting on the glyceryl *sn-1* position, it is active on a range of polar lipids found in plants and bacteria in vitro (Figure 3.5 C). Notably, it did not act on TAG and had very little activity on the two glycolipids found in the chloroplast, DGDG and sulfolipid, but showed high activity towards PG and MGDG. Because it was impractical to test the full spectrum of all possible combinations of glycerolipid molecular species occurring in chloroplasts in vitro, we explored the in vivo specificity of PLIP1 by overproducing the protein in chloroplasts, which we determined was the location of PLIP1 in plant cells using multiple independent approaches (Figure 1). This allowed us to test PLIP1 lipase activity in a quasi-native environment with the caveat that PLIP1 is normally not abundant in leaf chloroplasts and is more likely active in the chloroplasts of developing embryos based on the gene's expression profile and the reduced-function phenotype visible in seeds (Figure 3.14). However, leaf chloroplasts are much more readily accessible for assays than embryo chloroplasts, and we assumed that findings on PLIP1 activity would be transferable between the two tissues, which we ultimately confirmed. Based on the in vivo analysis of PLIP1, 18:3/16:1$^{\Delta 3t}$-PG emerged as the most likely in vivo substrate for PLIP1, which was corroborated in vitro using a native, leaf-isolated molecular species mixture of PG (Figure 3.11 D). It should be noted that in the overexpression lines, effects on MGDG and PC were observed in addition to PG (Figure 3.6 B and Figure 3.7 B and C). This could be directly due to the activity of PLIP1 on MGDG or caused by secondary effects related to acyl exchange and acyl transfer in

the case of PC, which is not in the thylakoid membranes and should not be directly accessible to PLIP1.

The Location of PLIP1 Limits the Availability of Likely Substrates In Vivo

To explain the observed substrate preference of PLIP1 in vivo, one might invoke the presence of factors in its native environment that are simply not present in vitro. Another, more likely explanation might be the limited accessibility of certain lipid molecular species to PLIP1 due to its specific membrane location, assuming that specific membrane leaflets or lateral subdomains have a specific lipid composition. We have some clarity now on the location of PLIP1, its likely peripheral association with thylakoid membranes based on fractionation, chloroplast import, and protease protection experiments, and its dual processing (Figure 3.1). Fractionation showed that PLIP1 is associated with thylakoid membranes, while import and protease protection assays were consistent with three possible suborganellar locations for PLIP1: stroma, thylakoid or the stroma leaflet of the inner envelope membrane (Figure 3.1). PLIP1 is not predicted to contain transmembrane domains, but it must be a peripheral membrane protein to gain access to its substrate. Most likely, PLIP1 is a peripheral thylakoid protein, but it also has the ability to be transiently free in the stroma or even has access to the inner envelope membrane. Double processing of PLIP1, as observed, can be interpreted as first generating an intermediate during protein import into the stroma, while the second processing possibly releases the majority of the mature protein from the thylakoid fraction into the soluble stroma fraction. A conserved twin-arginine motif is generally required for importing proteins into thylakoids (Robinson and Bolhuis, 2001; Goosens and van Dijl, 2016), but PLIP1 is missing a canonical motif, although it contains two sets of twin-arginine in its transit peptide usually part of such a motif. Therefore, PLIP1 may

peripherally attach to the thylakoid membrane but is likely prevented from being further imported into the thylakoid lumen.

For the likely substrate of PLIP1, 18:3/16:1$^{\Delta 3t}$-PG, we only know that it is exclusively present in chloroplasts, where the FAD4 desaturase required for its synthesis is located as well (Gao et al., 2009). However, the presence of 18:3/16:1$^{\Delta 3t}$-PG in a specific suborganellar membrane, leaflet, or lateral membrane domain is not known. All we can conclude based on our localization of PLIP1 is that 18:3/16:1$^{\Delta 3t}$-PG must be present in the stroma leaflet of the thylakoid or envelope membranes to be accessible to PLIP1.

PLIP1 Contributes to TAG Biosynthesis in Developing Embryos

PG is required for proper embryo development. The development of embryos in a *pgp1 pgp2* double mutant affected in PG biosynthesis in chloroplasts, mitochondria and the endoplasmic reticulum is delayed, and maturing seeds shrink during desiccation, resulting subsequently in compromised germination (Tanoue et al., 2014). Originally, it was proposed that the chloroplast-specific molecular lipid species, 16:1$^{\Delta 3t}$-PG, is critical for the function of the photosynthetic membrane, but its complete replacement with 16:0-PG in the Arabidopsis *fad4* mutant had only mild effects on leaf photosynthesis (Browse et al., 1985; McCourt et al., 1985). What was possibly neglected before was that the expression level of *FAD4* is on the same order of magnitude in leaf and developing seeds (Figure 3.19 A), but the level of 16:1$^{\Delta 3t}$-PG in developing seeds was much lower than that in leaves. The discovery that PLIP1 preferentially metabolizes 16:1$^{\Delta 3t}$-PG during seed development potentially explains the small 16:1$^{\Delta 3t}$-PG pool, and points towards roles for this lipid in seeds. In fact, decreased *PLIP1* expression in T-DNA insertional lines reduced seed TAG content without affecting growth or seed hormone levels (Figure 3.14 B), corroborating a possible

contribution of PLIP1 to seed TAG biosynthesis. The *plip1* low-TAG seed phenotype is recapitulated in the *fad4* mutant (Figure 3.19 C), and further phylogenetic analysis suggests coevolution of PLIP1 and FAD4 in land plants. These findings support a role for PLIP1 in seed TAG biosynthesis and provide a possible function for this unusual lipid molecular species.

It should be noted that *PLIP1*-OX plants produced seeds with higher TAG content, but 40% fewer seeds, compared to wild type (Figure 3.17). Overall, seed oil production per plant was reduced in line with the reduced growth of the *PLIP1*-OX plants, likely due to the activation of oxylipin-induced defense pathways (Figure 3.9 and 3.10). During the labeling experiment with developing seeds, saturating substrate levels were provided (Figure 3.21 C). Therefore, higher carbon incorporation into TAG in *PLIP1*-OX seeds reflects an increased capacity for TAG biosynthesis in individual embryos, in spite of the reduced plant growth and the decreased overall seed yield of the plants (Figure 3.7 A and Figure 3.17 B).

PLIP1 Enables Channeling of Acyl Groups from Plastid 16:1$^{\Delta 3t}$-PG to TAG at the ER

How can PLIP1, a lipase, be a component of a mechanism directing FAs synthesized in the plastid into TAG lipid droplets in the cytosol during embryogenesis? A large body of evidence suggests that PC is a critical precursor for TAG biosynthesis in developing seeds. As shown in Figure 3.22, several pathways, including acyl exchange (Figure 3.22, reactions 1) and desaturation of acyl groups on PC by FAD2/3 followed by transfer of 18:3 from the acyl-CoA pool to DAG (Figure 10, reaction 4), head group exchange generating DAG with 18:3 acyl groups (Figure 3.22, reaction 3), and transfer of acyl groups from PC to DAG by PDAT (Figure 3.22, reaction 5) contribute to the incorporation of polyunsaturated FAs into TAG during seed development (Dahlqvist et al., 2000; Bates et al., 2012; Li-Beisson et al., 2013). However, even in the *rod1*

lpcat1 lpcat2 triple mutant carrying the strongest known alleles at each locus, which in combination should completely disrupt acyl editing and head group exchange, the capacity of seeds to produce 18:3-containing TAGs is only reduced by half (Bates et al., 2012). Therefore, other compensatory mechanisms likely exist for incorporating polyunsaturated FAs into ER lipids and TAGs that could involve PLIP1 or PDAT. We propose that PLIP1 is part of a chloroplast acyl editing mechanism augmenting the supply of polyunsaturated FAs to the cytosolic acyl-CoA and PC pools, as depicted in Figure 3.22, reaction 2. This is particularly apparent whenever PLIP1 is highly abundant, as the turnover of plastid PG accelerates (Figure 3.11 and Figure 3.21). Acyl group flux is increased from PG to PC in *PLIP1* overexpression lines, and these acyl groups eventually end up in TAGs, which is evident from the pulse-chase labeling experiments (Figure 3.11 and 3.21). Partial restoration of the low 18:3-PC lipid phenotype of the *fad3-2* mutant by overexpression of *PLIP1* in mesophyll tissues and seeds (Figure 3.11 E and 3.18) supports a role for PLIP1 in plastid acyl export. The resemblance of acyl compositions of PC and TAG in seeds is indicative of the precursor-product relationship between these two lipids (Figure 3.14), but the detailed mechanism needs further investigation. In vegetative and seed tissues, overexpression of *PLIP1* results in a marked decrease in 18:2 and increase of 18:1 in PC, a phenotype reminiscent of the *fad2* mutant. This suggests that the elevated 18:3 flux from plastids out competes the incorporation of unsaturated fatty acids by the FAD2/3 pathway. Consistent with this assumption, in the *plip1* mutant, which lacks the PLIP1-dependent plastid acyl export pathway, one would expect that the ER-based FAD2/3 mechanism for the incorporation of unsaturated FAs into PC and TAG to be more active. In fact, the decreased 18:1 and increased 18:3 contents in PC and total acyl groups (reflecting mostly TAG), as observed in the *plip1* mutant seeds (Figure 3.14 E and G), corroborate this prediction. The FAD2/3 desaturation pathway counteracts the reduced 18:3 export

in the *plip1* mutants but does not affect loss of plastid-derived acyl group flux, leading to the observed decrease in seed TAG. The reversibly compensatory activity of the PLIP1-mediated plastid export of 18:3 acyl groups and the ER-based FAD2/3 desaturation pathway explains the seemingly paradoxical observation that 18:3 contents are high in both the *plip1* mutants and the *PLIP1* overexpression lines.

It should be noted that nearly 85% of the seed TAG 18:3 is dependent on FAD3, and the contribution of PLIP1 to seed 18:3 reflects the finding that the PLIP1-mediated pathway contributes about 10% of the acyl groups in TAG in seeds, even though overexpression of *PLIP1* is able to significantly increase 18:3 content in the *fad3-2* seeds (Figure 3.18). This may seem like a minor contribution. However, even the ablation of the presumed key enzyme of TAG biosynthesis, DGAT1, leads to only a 20-40% reduction in seed oil content (Katavic et al., 1995; Routaboul et al., 1999). Furthermore, in a PDAT-loss of function mutant affecting a pathway parallel to DGAT (Figure 3.22, reactions 5 and 4, respectively), seeds show no changes in oil content nor composition (Mhaske et al., 2005), even though a double mutant deficient in these two pathways exhibits up to 80% reduction in seed oil content and a loss in seed viability. These results indicate that other parallel mechanisms exist to account for the remaining small fraction of TAG. The regulatory network governing the different TAG biosynthesis pathways is complex, allowing for redundancy and compensatory mechanisms. The PLIP1-mediated pathway described here could represent one of the alternative mechanisms for TAG biosynthesis. At the present time, the lack of a PLIP1 loss-of-function mutant prevents us from more accurately quantifying the contribution of a PLIP1-dependent pathway of polyunsaturated FA incorporation into TAG under different conditions or in different loss-of-function mutants. Despite repeated attempts, we have not yet succeeded in isolating a homozygous PLIP1 loss-of-function mutant using targeted gene

disruption methods. Thus, we cannot rule out that PLIP1 has additional essential functions in embryo metabolism that still need to be discovered.

PLIP1 Takes Part in Acyl Group Export from Chloroplasts

The hypothesis outlined above (Figure 3.22) also implies that PLIP1 activity leads to acyl export from the plastid. Assuming that PLIP1 acts at the stroma surface of the thylakoids or the inner envelope membrane, additional chloroplast proteins are likely necessary to direct acyl groups from chloroplast PG into TAGs. Recently, chalcone isomerase-like chloroplast proteins were shown to be FATTY ACID BINDING PROTEINS (FAP), which may be associated with chloroplast fatty acid export (Ngaki et al., 2012). The expression pattern of *FAP*s resembles that of *PLIP1*, and all FAPs are located in the stroma of chloroplasts. One FAP, FAP1, shows high proclivity for binding 18:3. Therefore, it seems possible that 18:3 released by PLIP1 from 18:3/16:1$^{\Delta 3t}$-PG is bound by FAP, thereby sequestering it to avoid cytotoxicity of free FAs or to mediate FA transfer to the chloroplast envelope membrane. Another protein possibly involved is FATTY ACID EXPORT1 (FAX1), a likely acyl group or FA transporter of the inner envelope membrane of plastids (Li et al., 2015). In the *fax1* mutant, of the four thylakoid lipids, PG levels are increased the most, especially 18:3/16:1$^{\Delta 3t}$-PG, and the levels of PC are reduced. Also, TAG biosynthesis, especially its polyunsaturated FA content, correlates with the presence of FAX1 in reproductive tissues. Hence, it seems possible that PLIP1, FAP and FAX1 work together to channel a small fraction of plastid synthesized acyl groups through 16:1$^{\Delta 3t}$-PG into PC outside the plastid and ultimately into TAG during seed development.

Movement of de novo synthesized lipid groups through the chloroplast membrane lipid pool has been observed in Chlamydomonas, in which PGD1 is a lipase specific for newly

synthesized 18:1/18:1-MGDG, while 18:3/16:4 MGDG is resistant to its activity (Li et al., 2012). In this case, *PGD1* expression is induced following N-deprivation and participates in the channeling of acyl groups into TAG biosynthesis under these conditions. Although plants synthesize TAG in vegetative tissues under stress (Moellering et al., 2010), they generally produce bulk TAG in developing embryos. PLIP1 is too distantly related to PGD1 to be an orthologue, and Chlamydomonas does not contain PC, while Arabidopsis lacks 18:3/16:4-MGDG. However, both lipases point towards a common theme, the need for channeling of plastid-synthesized acyl groups through the chloroplast lipid pool prior to incorporation into extraplastidic TAGs. The specific substrate selectivity of these two lipases also partially explains the existence of unusual molecular species of chloroplast lipids, 18:3/16:4 MGDG in Chlamydomonas and 18:3/16:1$^{\Delta 3t}$-PG in Arabidopsis and most other plants and algae. It seems likely that unusual acyl groups tag specific molecular species for specific purposes. In the case of 18:3/16:4 MGDG in Chlamydomonas, it is tagged as a structural thylakoid membrane lipid resistant to PGD1, while in the case of 18:3/16:1$^{\Delta 3t}$-PG in Arabidopsis, it is the preferred substrate for PLIP1, leading to 18:3 acyl export, rather than having a specific function related to photosynthetic light capture and conversion as previously assumed. Chlamydomonas also contains 16:1$^{\Delta 3t}$-PG, and genomes of plants and algae encode many more potential plastid-targeted lipases. Therefore, it is likely that acyl hydrolysis catalyzed by specific plastid lipases and their respective native substrates is a common process for maintaining photosynthetic membrane lipid homeostasis while enabling the exchange and export of acyl groups for the synthesis of extraplastidic lipids or as precursors for retrograde signaling molecules, a possibility that still begs to be explored.

ACKNOWLEDGEMENTS

This work was done in collaboration with several colleagues. John E. Froehlich conducted the chloroplast import assay in Figure 3.1. Agnieszka Zienkiewicz assisted with the confocal microscopy experiment in Figure 3.1. I would also like to thank Dr. Danny Schnell, Michigan State University, for providing antibodies against LHCb1, Dr. Gregg Howe for providing the *coi1-30* seeds, Dr. Dan Jones for providing the ABA-d6 internal standard and Dr. Anthony Schilmiller for assisting with plant hormone and Arabidopside measurement. We would also like to thank Dr. Rebecca Roston, University of Nebraska, Lincoln, and Dr. Barb Sears, Michigan State University for their advice on conducting the experiments or critically reading the manuscript. This work was supported by the Division of Chemical Sciences, Geosciences and Biosciences, Office of Basic Energy Sciences of the United States Department of Energy Grants DE-FG02-98ER20305 and DE-FG02-91ER20021, the US Department of Energy-Great Lakes Bioenergy Research Center Cooperative Agreement DE-FC02-07ER64494, and by AgBioResearch, Michigan State University.

APPENDIX

Primer name	Sequence 5' – 3'	Purpose
PEG_PLIP1 F	CACCATGGCGTTTAATACGGCTATG	For pEarlyGate 101/4
PEG101_PLIP1 R	GACACGTGTCATGATCTCCTCGG	For pEarlyGate 101
BamHI_PLIP1 F	TCGGATCCATGGCGTTTAATACGGCTATG	For the pET41a to produce PLIP1
PLIP1_XhoI R	GACTCGAGTTAGACACGTGTCATGATCTCC	
pET41a_His del F	ATGTATATCTCCTTCTAAAGTAAACAAA	pET41a construct for chloroplast import
pET41a_His del R	ATGGCGTTTAATACGGCTATG	
PLIP1_S422A F	AGTCTCTCATTAATAGTGAATTTGATGCTTATC	S422A point mutation
PLIP1_S422A R	GCCTCCAAGAGCATGACCCGTG	
PLIP1_D483A F	GAGCCTTTTCGTGTAATTATCCTGACCA	D483A point mutation
PLIP1_D483A R	GTGGGACGATAGCTCTATGCATCA	
PLIP1_qPCR F	AGTTCTATAATCCCAAGTCCGA	For qPCR analysis of PLIP1 expression
PLIP1_qPCR R	CTCCTTATCTCAAGCAGCCT	
TIP-41_like qPCR F	GTGAAAACTGTTGGAGAGAAGCAA	qPCR reference gene
TIP-41_like qPCR R	TCAACTGGATACCCTTTCGCA	
PDF2 qPCR F	TAACGTGGCCAAAATGATGC	qPCR reference gene
PDF2 qPCR R	GTTCTCCACAACCGCTTGGT	
LBb1.3	ATTTTGCCGATTTCGGAAC	For genotyping of *plip1* mutants
plip1-1 LP	AGATTCTAGCGGAGCTTGGTC	For genotyping of *plip1-1*
plip1-1 RP	GCCTCTTCAAACCAAATCTCC	
plip1-2 LP	TTATTACCGGAGCGACAACAC	For genotyping of *plip1-2*
plip1-2 RP	TCCAATAACGGTTAAGCAACG	
fad3-2 genotype F	GTCACGATGAGAAGTTGCCTTGG	For genotyping of *fad3-2*
fad3-2 genotype R	CAATGTCGTGATGAATGTTGTTAAAGAAT	
VSP1 F	AGAGCTGGAGCTGGTGTTGTTAAG	For qPCR analysis of VSP1 (At5g24780) expression
VSP1 R	GAACACCCATTCCGGTAACACCAT	
LOX2 F	GGGCGTACTGGTCGTGGTTA	For qPCR analysis of LOX2 (At3g45140) expression
LOX2 R	TCCCGAGTTCCAAGAGGTTTT	
VSP2 F	GCAAGTGGTGTACAAGTCAAAGGT	For qPCR analysis of VSP2 (At5g24780) expression
VSP2 R	ATCCTCAACCAAATCAGCCCATTG	

Table 3. 1. Primers used in this study.

Table 3. 1. (cont'd)

JAZ1 F	GCACCGCTAATAGCTTAGCCAAGA	For qPCR analysis of JAZ1 (At1g19180) expression
JAZ1 R	TCTGTCAATGGTGTTGGGGAGGAT	
JAZ10.1-3 F	AGAGCTGGAGCTGGTGTTGTTAAG	For qPCR analysis of JAZ10.1, 10.2 and 10.3 (At5g13220) expression
JAZ10.1-3 R	GAACACCCATTCCGGTAACACCAT	
CYP94C1 F	TCTCACTCTTTCACTTACTCTTCC	For qPCR analysis of CYP94C1 (AT2G27690) expression
CYP94C1 R	CGTTTGATGGATTCGCTGTG	

Genotype	Acyl Groups (μg/mg FW)
Col-0	3.48 ± 0.067
plip1-1	3.51 ± 0.076
plip1-2	3.51 ± 0.063
EV control	3.55 ± 0.055
PLIP1^{S422A}-OX1	3.53 ± 0.055
PLIP1^{S422A}-OX2	3.59 ± 0.049
PLIP1-OX1	3.56 ± 0.062
PLIP1-OX2	3.54 ± 0.063
PLIP1-OX3	3.56 ± 0.067

Table 3. 2. Leaf acyl group contents in different genotypes.
Acyl group contents were determined by measuring total leaf fatty acid methyl esters. Plants were grown on soil for 4 weeks. Four independent samples were averaged, and the SD is indicated. FW, fresh weight.

Organism	PLIP1	FAD4	18S rRNA
Arabidopsis thaliana	NP_191727.2	NP_194433.1	AC004708
Arabidopsis lyrata	XP_002876633.1	XP_002869582.1	ADBK01000671
Eutrema salsugineum	XP_006402456.1	XP_006413113.1	AHIU01024615
Brassica rapa	XP_009138759.1	XP_009109956.1	AENI01003060
Manihot esculenta	OAY49032.1	OAY28524.1	AB233568
Populus trichocarpa	XP_002301404.2	XP_006370685.1	AARH02003126
Cucumis sativus	KGN44530.1	XP_004152938.1	ACHR02000003
Glycine max	XP_014627545.1	XP_003551889.1	ACUP02007833
Citrus sinensis	KDO66297.1	XP_006452281.1	AJPS01002884
Solanum lycopersicum	XP_004231212.1	XP_004244133.1	AB971540
Zea mays	NP_001183891.2	XP_008662704.1	AC150267
Brachypodium distachyon	XP_010233458.2	XP_003571398.1	ADDN02000002
Selaginella moellendorffii	XP_002982750.1	XP_002962129.1	ADFJ01002076
Gossypium raimondii	XP_012437750.1	XP_012460522.1	ALYE01001348
Elaeis guineensis	XP_010913778.1	XP_010908683.1	ASJS01014373
Oryza sativa	XP_015630701.1	XP_015648482.1	AF069218
Ananas comosus	XP_020098248.1	XP_020103087.1	AP014632
Physcomitrella patens	XP_001766893.1	XP_001752601.1	AB251495
Capsella rubella	XP_006292392.1	XP_006285104.1	KR029093
Capsella grandiflora	XP_006292392.1	XP_006285104.1	KR029092

Table 3. 3. Sequences used in the PLIP1 and FAD4 phylogenetic analyses.
For PLIP1 and FAD4 protein sequences, accession numbers in NCBI GenBank are listed for the corresponding organism. For the 18S rRNA sequences, accession numbers in the SILVA rRNA database are listed.

Table 3. 3. (cont'd)

Ricinus communis	EEF39083.1	XP_002522972.1	AASG02002472
Theobroma cacao	XP_017970999.1	EOY12432.1	AF207040
Malus domestica	XP_017185317.1	XP_008385990.1	ACYM01009980
Camelina sativa	XP_010413364.1	XP_010433413.1	GABL01042315
Sorghum bicolor	KXG32911.1	XP_002443967.1	ABXC02001831
Eucalyptus grandis	XP_010053810.1	XP_010060414.1	AUSX01001791

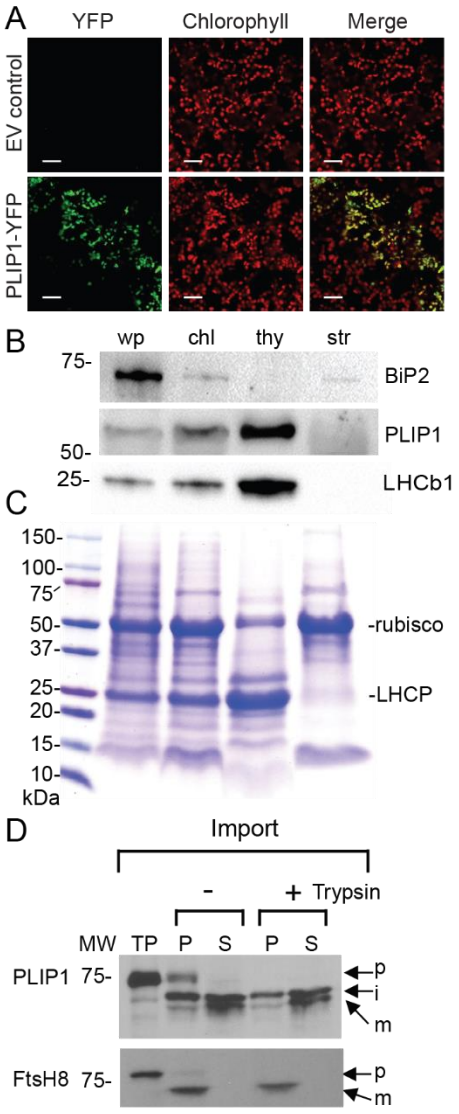

Figure 3. 1. Subcellular localization of PLIP1 in Arabidopsis.
(A) Subcellular localization of PLIP1-YFP in leaf mesophyll cells of 3-week-old Arabidopsis Col-0 transformed with *PLIP1-YFP* driven by the 35S promoter or empty vector (EV) control using confocal laser scanning microscopy. Chlorophyll autofluorescence is shown in red, and YFP fluorescence is shown in green. Overlay of chlorophyll and YFP is shown as well (Merge). Representative images from one experiment are presented. Scale bars: 30 µm.
(B) PLIP1 enrichment in chloroplast fractions analyzed by immunoblotting. Intact and subfractionated chloroplasts were prepared using 4-week-old Arabidopsis (Col-0) plants grown on MS medium. Equal amounts of protein of leaf tissues from the whole plant (wp), intact chloroplasts (chl), thylakoid (thy) and stroma (str) were separated by SDS-PAGE or further subjected to immunoblotting analysis using an antibody against PLIP1^{S422A}, a non-functional mutant of PLIP1. Immunoblotting was used to detect marker proteins BiP2 (endoplasmic reticulum) and LHCb1 (thylakoid). For protein loading, 12 µg per fraction were loaded for PLIP1; 2 µg per fraction for BiP2 and LHCb1.

Figure 3. 1. (cont'd)

(C) SDS-PAGE Coomassie Brilliant Blue staining was used to detect Rubisco large subunit (stroma) and light-harvesting chlorophyll a/b-binding protein (LHCP) (thylakoid), which were used as markers. Numbers indicate protein molecular mass in kDa. For protein loading, 12 µg per fraction were loaded.
(D) Chloroplast import experiments with labeled PLIP1 and control protein FtsH8. Chloroplasts were treated with (+) or without (−) trypsin. Total chloroplast membranes (P) or soluble (S) fractions were analyzed by SDS-PAGE followed by fluorography. TP, translation products; p, precursor; i, intermediate; m, mature form; MW, molecular weight markers.

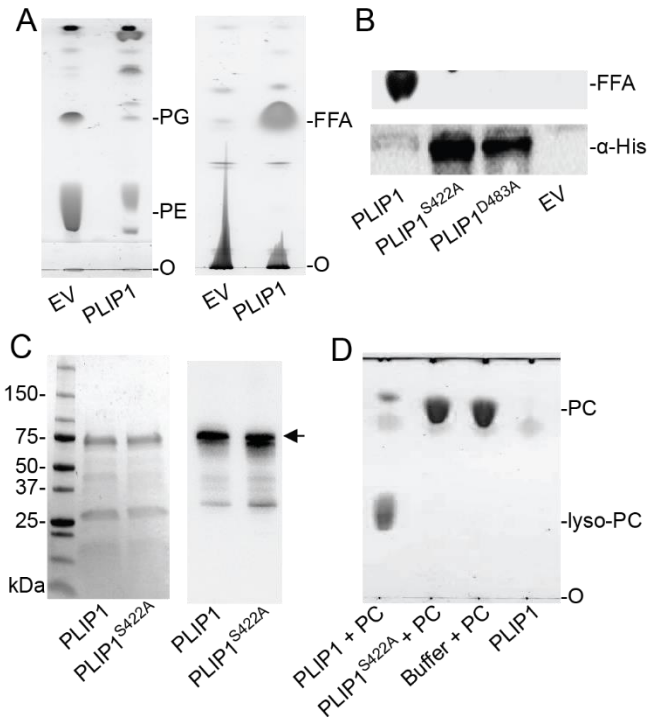

Figure 3. 2. Recombinant PLIP1 has lipase activity.

(A) Thin layer chromatographic analysis of polar (left) and neutral (right) lipids in *E. coli* containing a 6×His-PLIP1 expression construct or empty vector control (EV) at 6 h following induction. FFA, free fatty acid; O, origin of sample loading; PE, phosphatidylethanolamine; PG, phosphatidylglycerol. TLC plates were stained with iodine vapor.

(B) Mutation of the PLIP1 active site motif. Lipid extracts of *E. coli* cultures 6 h after induction expressing *6×His-PLIP1* or two point mutation alleles, *6×His -PLIP1*^{S422A} or *6×His-PLIP1*^{D483A}, or containing an empty vector control (EV) were analyzed by thin layer chromatography to detect FFA products (top panel). Protein extracts were analyzed for protein production using an antibody against the 6×His tag.

(C) SDS-PAGE analysis of purified PLIP1 and PLIP1^{S422A} proteins. Loading was 5 µg per lane for both samples. SDS-PAGE separated proteins were stained by Coomassie Brilliant Blue (left) or detected by immunoblotting with an antibody raised against PLIP1^{S422A}. Numbers indicate protein molecular mass in kDa. 6×His-PLIP1 and 6×His-PLIP1^{S422A} are indicated by the arrow.

(D) Thin-layer chromatogram of products of a representative in vitro lipase reaction using PC with wild type (PLIP1 + PC) and the mutant enzyme (PLIP1^{S422A} + PC). Substrate without enzyme (Buffer + PC) and enzyme without substrate (PLIP1) were included as controls. PC, phosphatidylcholine. O, origin of sample loading. Lipids were visualized by iodine vapor staining.

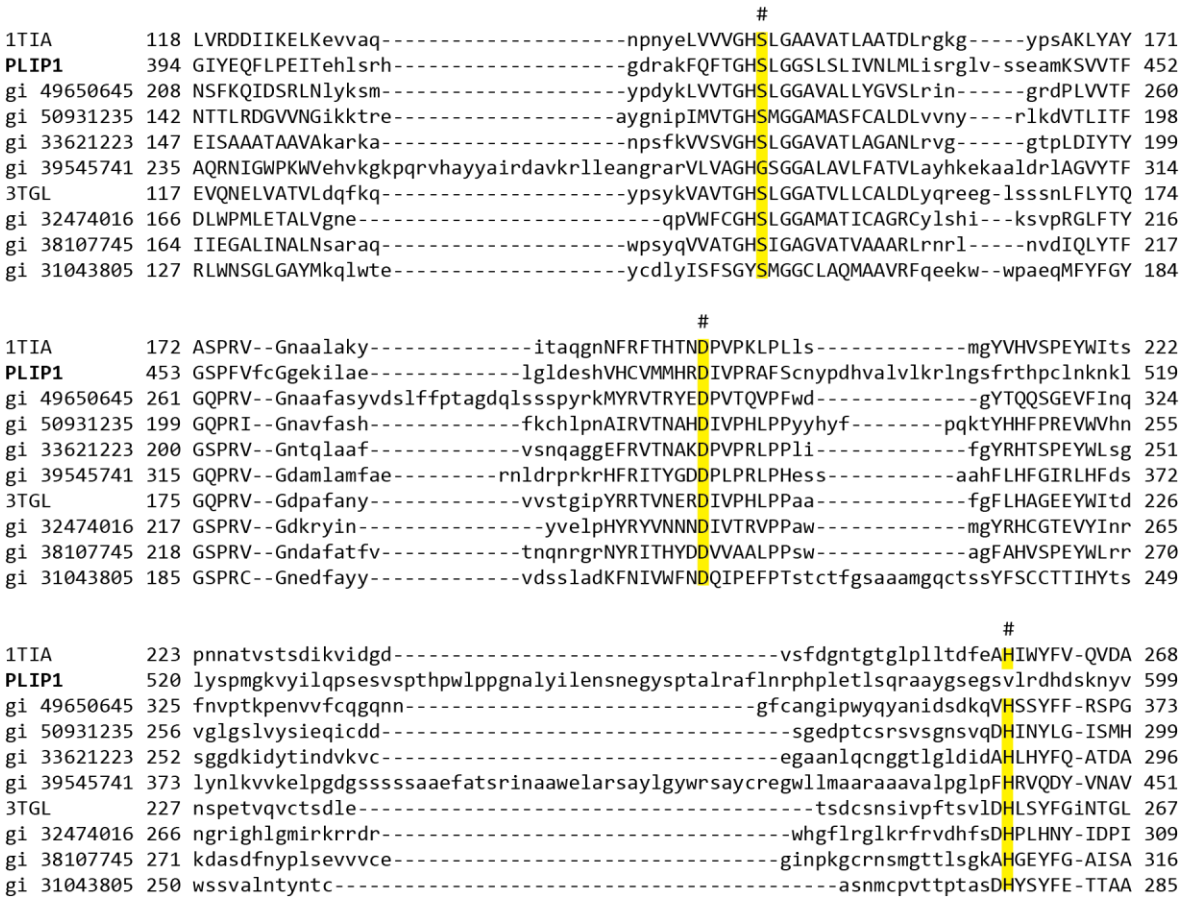

Figure 3. 3. Alignment of PLIP1 with class 3 lipase protein sequences in the NCBI conserved domain database (CDD).

The alignment results were obtained by BLAST analysis of the PLIP1 protein sequence against the CDD database using CD-search (https://www.ncbi.nlm.nih.gov/Structure/cdd/wrpsb.cgi) with default settings. Reference protein names are represented by either Protein Data Bank ID (*e.g.*, 1TIA and 3TGL) or NCBI GI number. The conserved catalytic triads are highlighted in yellow.

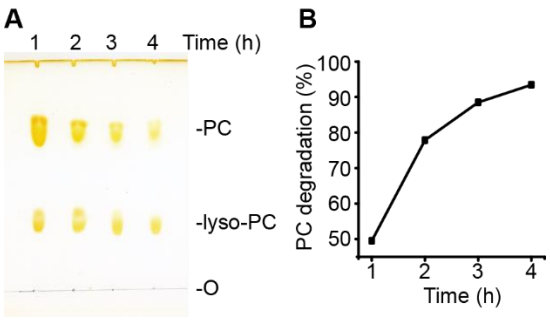

Figure 3. 4. Time course of PLIP1 lipase activity with phosphatidylcholine (PC) as substrate.

(A) Results of thin layer chromatography of substrate PC and lyso-PC product at different time points. O, origin of sample loading. 120 µg substrate 18:1/18:1-PC was provided to 1 µg recombinant PLIP1 and the lipase assay was stopped at the indicated time points. Lipids were subsequently extracted and analyzed by TLC and stained with iodine vapor.

(B) Fraction of PC degradation at different time points, as indicated in **(A)**. Fatty acid methyl esters of acyl groups of both PC and lyso-PC at each time point were analyzed by liquid gas chromatography. The fraction of PC degradation is calculated as 2 (molarity of lyso-PC acyl groups) / (2 (molarity of lyso-PC acyl groups) + (molarity of PC acyl groups)) *100.

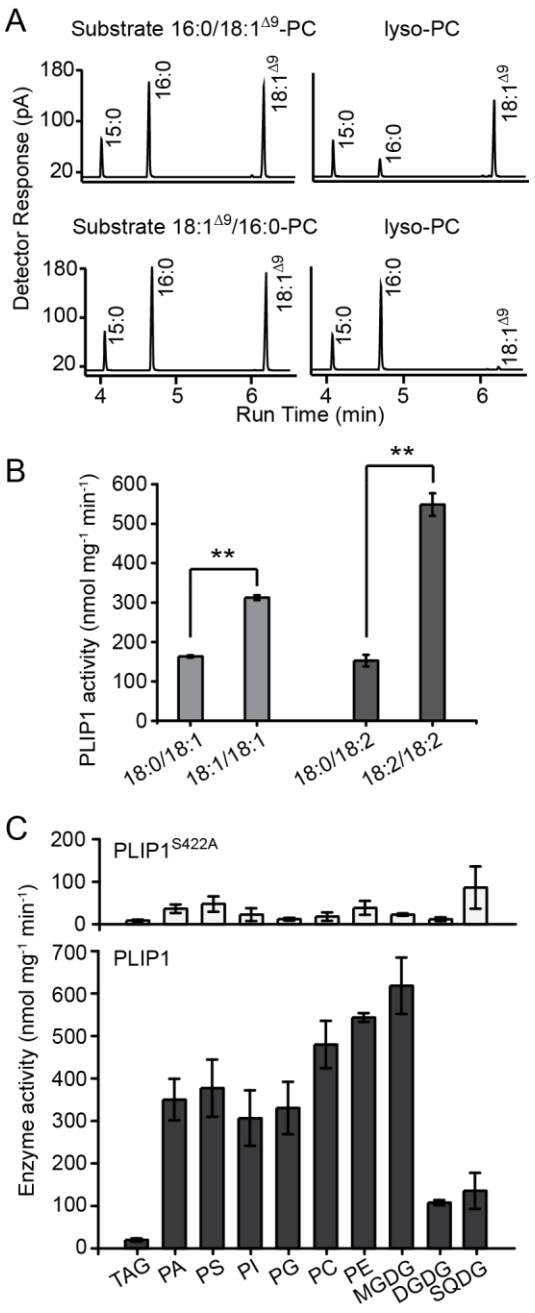

Figure 3. 5. Specificity of PLIP1 in vitro activity.

(A) Gas-liquid chromatograms of methyl esters derived from commercial PC substrates or lyso-PC fractions from PLIP1 lipase reactions with different PC substrates. 15:0 was used as an internal standard.

(B) PLIP1 lipase activity on commercial PC substrates (carbon number: double bond number; *sn-1/sn-2*) with different degrees of saturation of the *sn-1* acyl groups. PC containing 18:0/18:1 and 18:1/18:1 and PC containing 18:0/18:2 and 18:2/18:2 were compared, respectively. n=4, ± SD. Student's *t*-test was applied (**indicates $p<0.01$).

(C) PLIP1 activity on different substrates. For each PLIP1 lipase reaction, 60 µg lipids and 0.5 µg protein were used. The reactions were incubated at ambient temperature (~22 °C) for 1.5 h, which

Figure 3. 5. (cont'd)

was still during the linear portion of the reaction time course for PC (Supplemental Figure 2). PLIP1^{S422A} was included as a negative control and is shown in the top panel. All lipids contained two oleic acids (18:1), except MGDG, DGDG, and SQDG, which were isolated from plants, and PI, which was isolated from bovine liver. n=3-4 for each substrate, ± SD. DGDG, digalactosyldiacylglycerol; MGDG, monogalactosyldiacylglycerol; PA, phosphatidic acid; PC, phosphatidylcholine; PE, phosphatidylethanolamine; PG, phosphatidylglycerol; PI, phosphatidylinositol; PS, phosphatidylserine; SQDG, sulfoquinovosyldiacylglycerol; TAG, triacylglycerol.

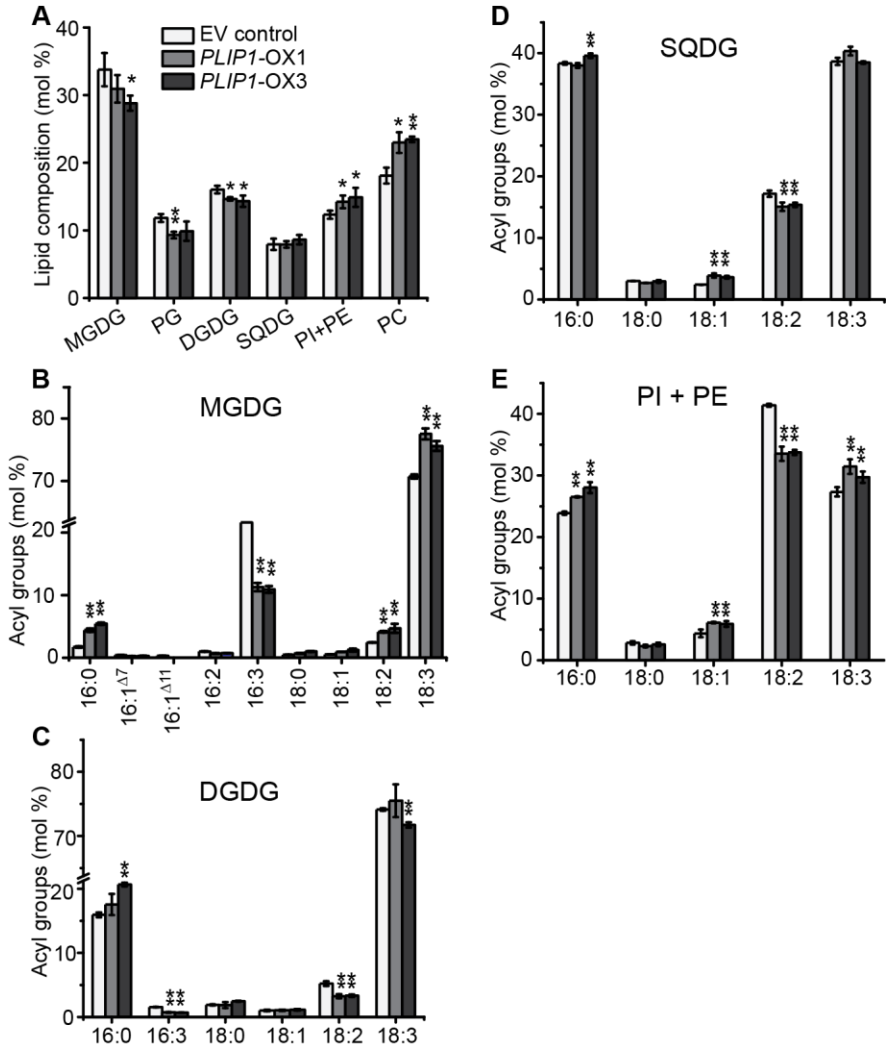

Figure 3. 6. Analysis of polar lipids in the leaves of 4-week-old, soil-grown *PLIP1*-OX and empty vector (EV) control plants.

(A) Relative abundance of major polar lipid classes in *PLIP1*-OX and EV control lines.

(B-E) Relative acyl group composition of MGDG, DGDG, SQDG, PI and PE supplemental to data shown in Figure 4B and C. Leaf samples harvested from one plant were analyzed as one biological repeat; n=3, ± SD. Student's *t*-test was applied comparing the EV control with each *PLIP1*-OX line (* indicates $p<0.05$; ** $p<0.01$). DGDG, digalactosyldiacylglycerol; MGDG, monogalactosyldiacylglycerol; PC, phosphatidylcholine; PE, phosphatidylethanolamine; PG, phosphatidylglycerol; PI, phosphatidylinositol; SQDG, sulfoquinovosyldiacylglycerol. Acyl groups with a molar percentage less than 0.5% were omitted.

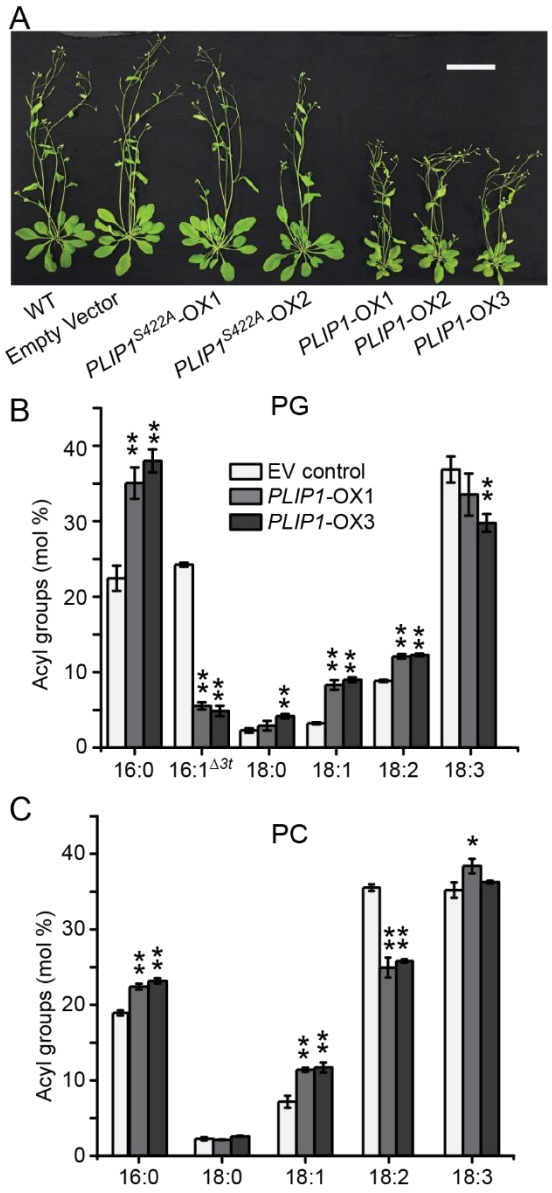

Figure 3. 7. Growth and lipid phenotypes of *PLIP1*-overexpression plants.
(A) Growth of 4-week-old soil-grown plants. Arabidopsis wild-type plant (WT), one empty vector control line, two *PLIP1*^{S422A}-OX and three *PLIP1*-OX overexpression lines are shown. Scale bar: 5 cm.
(B) and **(C)** Relative acyl composition of phosphatidylglycerol (PG) and phosphatidylcholine (PC) in *PLIP1*-OX and empty vector (EV) control lines. Mature leaf lipids were extracted and analyzed from the plants shown in **(A)**. Leaf samples harvested from one plant were taken as one biological repeat; n=4, ± SD. Student's *t*-test was applied to compare the EV control with each *PLIP1*-OX line, respectively (* indicates $p<0.05$; ** indicates $p<0.01$).

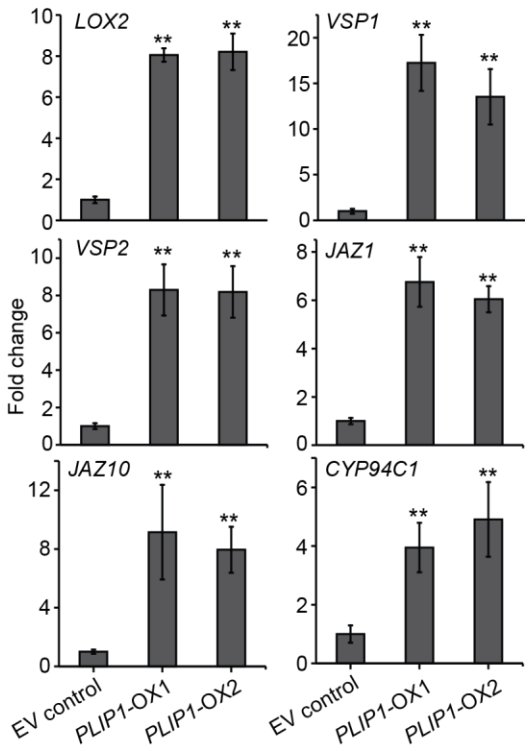

Figure 3. 8. Expression of jasmonic acid-responsive genes.
The expression levels of the indicated genes were determined by quantitative RT-PCR and expressed relative to *UBQ10* gene expression. Analysis of *JAZ10* includes *JAZ10.1, 10.2* and *10.3*, but not the *10.4* splicing isoform. RNA was extracted from the leaves of 3-week-old soil-grown plants. Leaves harvested from one plant were analyzed as one biological repeat; n=3, ± SD. Student's *t*-test was applied comparing the EV control with each *PLIP1*-OX line (** indicates $p<0.01$).

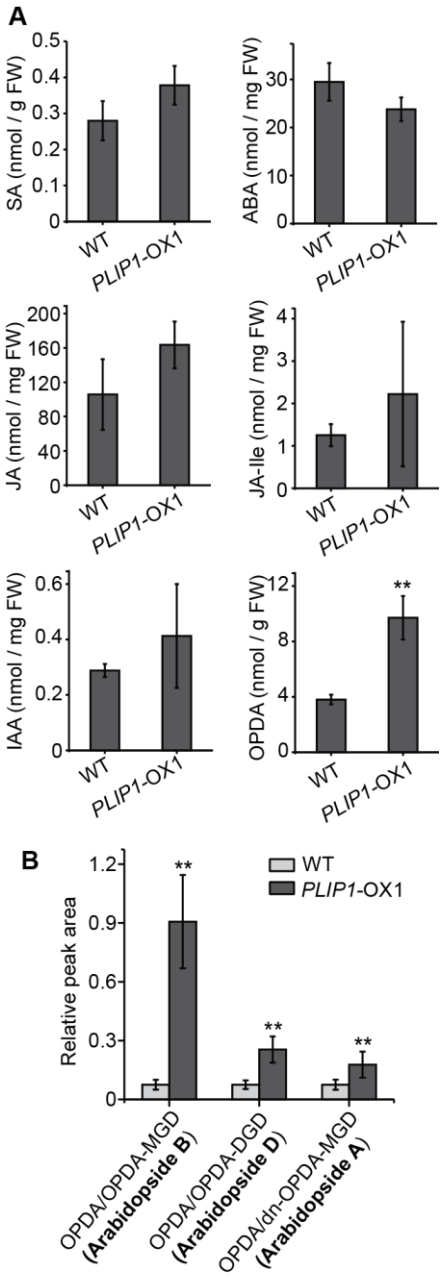

Figure 3. 9. Quantification of plant hormones and Arabidopsides in leaves of the wild type (WT) and *PLIP*-OX1.

(A) Plants were grown on soil for three weeks before the leaves were harvested for hormone extraction and quantification by LC-MS/MS. Leaves harvested from one plant were analyzed as one biological repeat; n=3, ± SD. Student's *t*-test was applied (**indicates $p<0.01$).

(B) Relative amounts of the major Arabidopsides in wild-type (WT) and *PLIP*-OX plant leaves. The indicated Arabidopside level was normalized to the level of 18:3/18:3-digalactosyldiacylglycerol, which did not change in WT or *PLIP*-OX1 plants. Leaves harvested from one plant were analyzed as one biological repeat; n=3-4, ± SD. Student's *t*-test was applied (**indicates $p<0.01$).

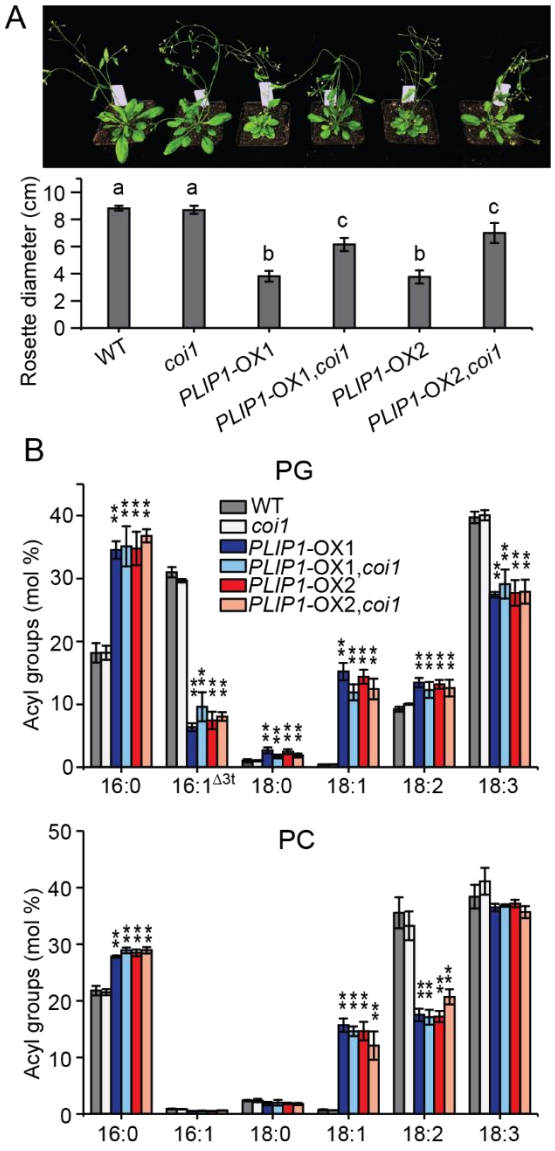

Figure 3. 10. Phenotypes of *PLIP1*-OX and *coi1* plants.
(A) Image of the 4-week-old plants grown on soil and the rosette diameter of the indicated plants. n=6, ± SD, one-way ANOVA with post-hoc Turkey HSD test was applied. Rosette diameters indicated by different letters (a, b and c) are significantly different ($p<0.01$).
(B) Relative acyl group compositions of leaf phosphatidylglycerol (PG) and phosphatidylcholine (PC) in the indicated plants in **(A)**. Leaf samples harvested from one plant were treated as one biological repeat; n=3, ± SD. Student's *t*-test was applied to compare WT with each of the remaining genotypes (** indicates $p<0.01$).

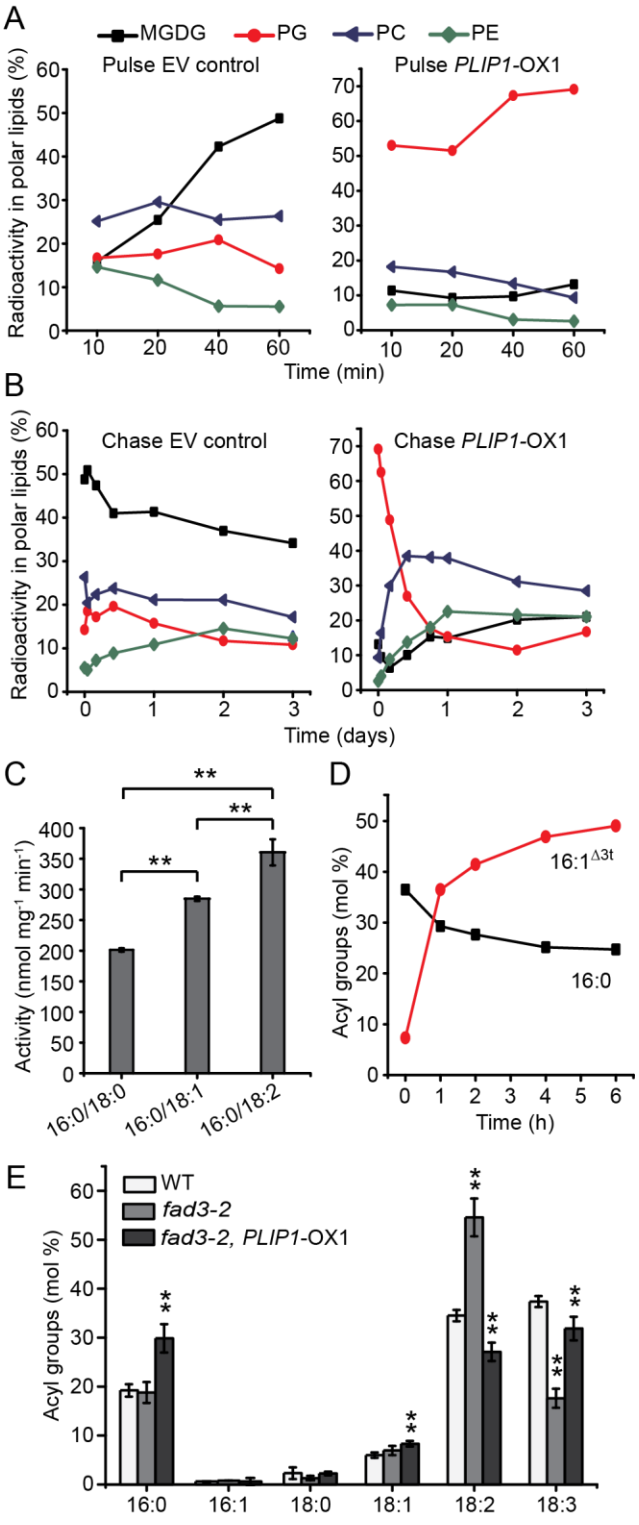

Figure 3. 11. PLIP1 precursor–product relationships in *PLIP1*-overexpression plants.
(A) and **(B)** In vivo pulse-chase acetate labeling of lipids in wild-type and *PLIP1*-OX1 plants. The length of the [^{14}C]-acetate labeling pulse was 60 min **(A)**, after which medium was replaced with non-labeled free acetate to initiate the chase with a duration of three days **(B)**. The fractions of label in all polar lipids are given as percentages of total incorporation of label in polar lipids.

Figure 3. 11. (cont'd)

Experiments were repeated three times with similar results, and one representative result is shown. MGDG, monogalactosyldiacylglycerol; PC, phosphatidylcholine; PE, phosphatidylethanolamine; PG, phosphatidylglycerol.

(C) Activity of purified recombinant PLIP1 on PC with different *sn-2* acyl groups. PC containing 16:0/18:0, 16:0/18:1, and 16:0/18:2 were used as substrates. n=4, ± SD. Student's *t*-test was applied (** indicates $p<0.01$).

(D) PLIP1 enzyme activity preference for molecular species of phosphatidylglycerol isolated from tobacco leaves. Acyl groups of lyso-phosphatidylglycerol are shown as molar percentages of total acyl groups at any given time point. Experiments were repeated three times with similar results and data from one representative experiment are shown.

(E) Relative acyl composition of PC in wild-type (WT), *fad3-2* and *fad3-2*, *PLIP1*-OX1 plants. Leaf lipids were extracted and isolated by TLC and fatty acid methyl esters derived from the lipids were analyzed by GC. Mature leaf samples harvested from one plant were taken as one biological repeat; n=4, ± SD. Student's *t*-test was applied (** indicates $p<0.01$).

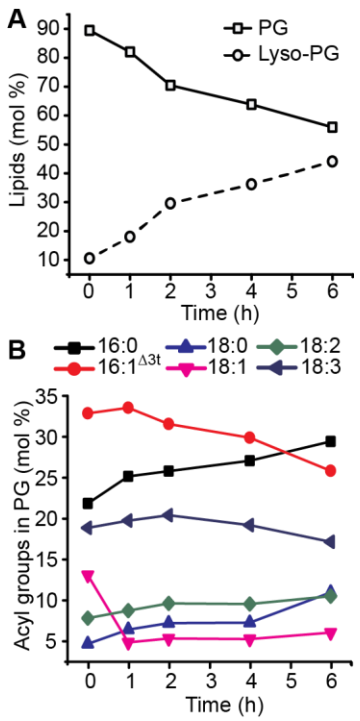

Figure 3. 12. Effect of *sn-2* acyl 16:1$^{\Delta 3t}$ on PLIP1 function.
(A) Change in the molar percentage of native phosphatidylglycerol (PG) isolated from 4-week-old tobacco leaves and lyso-PG in a time course of in vitro PLIP1 lipase reaction.
(B) PLIP1 enzyme activity preference for molecular species of PG isolated from tobacco leaves. Acyl groups of PG are shown as molar percentages of total acyl groups at any given time point. These data are supplemental to the acyl group analysis of lyso-PG shown in Figure 6D. Experiments were repeated three times with similar results, and data from one representative experiment are shown.

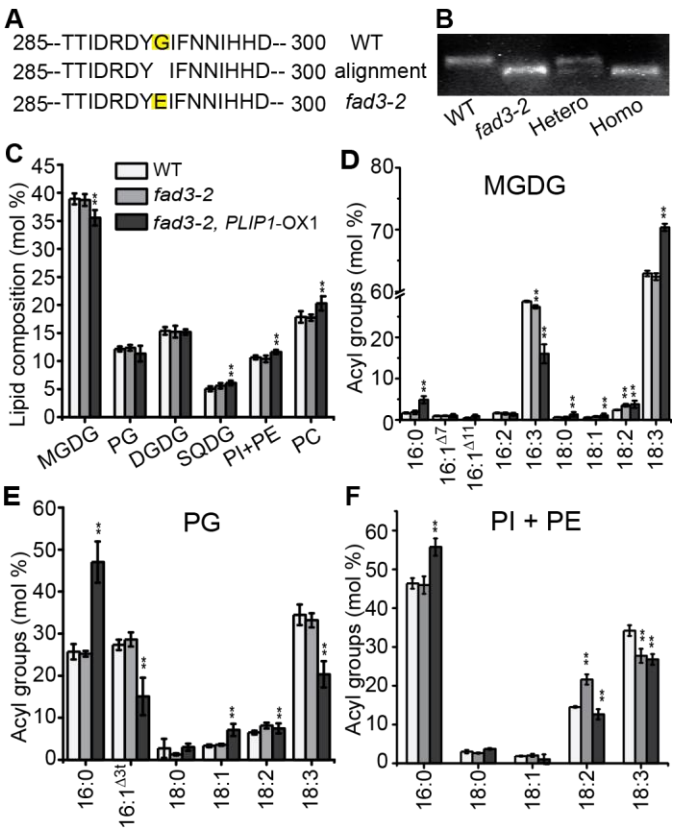

Figure 3. 13. Lipid analysis of offspring from a cross between *fad3-2* and *PLIP1*-OX1.
(A) Sequencing of the *FAD3* locus from the *fad3-2* mutant plant revealed a point mutation of G875A, which leads to a G292E mutation in the FAD3 protein.
(B) Genotyping of *fad3-2* and *PLIP1*-OX1 plants. PCR products amplified from plant genomic DNA were subjected to EcoRI digestion. The mutated *fad3-2* fragment was susceptible to digestion. Hetero, heterozygous; Homo, homozygous plants.
(C-F) Relative abundance of major polar lipid classes and relative acyl composition of other individual glycerolipids supplemental to Figure 6E. n=3-4 for each substrate, ± SD. Student's *t*-test was applied (** indicates $p<0.01$). For lipid abbreviations, refer to the legend of Figure 3.6. Acyl groups with a molar percentage less than 0.5% were omitted.

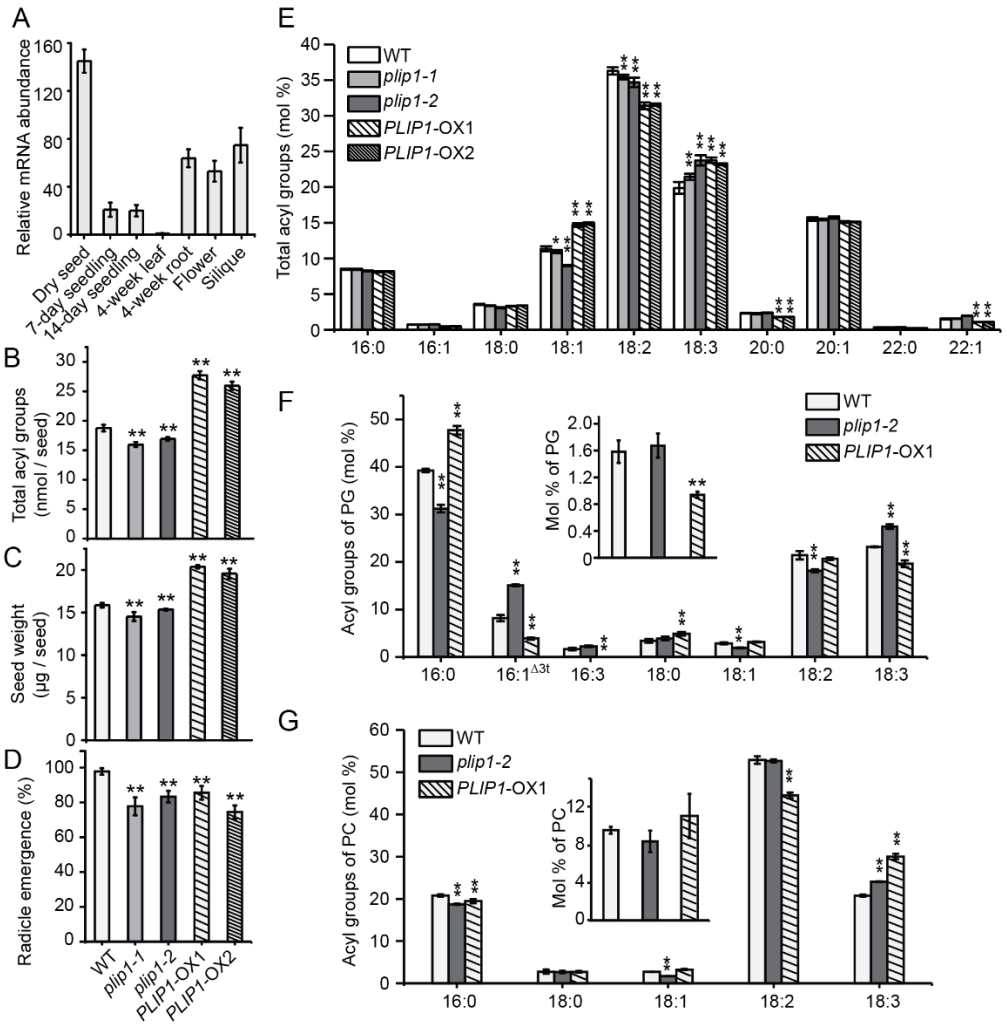

Figure 3. 14. Effect of PLIP1 on seed oil biosynthesis and germination.

(A) *PLIP1* transcript levels in different tissues or developmental stages determined by quantitative PCR. Expression levels were normalized to those lowest in 4-week-old leaf tissues and shown as relative fold changes. n=3 for each tissue, ± SD.

(B) Total acyl group content in dry seeds of wild type (WT), *plip1-1*, *plip1-2*, *PLIP1*-OX1 and *PLIP1*-OX2. 30 seeds were analyzed in bulk for each repeat; n=5, ± SD.

(C) Weight of the seeds shown in **(B)**. 200 seeds were analyzed for each repeat; n=4-7, ± SD.

(D) Germination of WT, *plip1-1*, *plip1-2*, *PLIP1*-OX1 and *PLIP1*-OX2 seeds. The fraction of seeds showing radical emergence was determined 40 h after stratified seeds were sown on MS medium. 100 seeds were used for each repeat, n=3, ± SD.

(E) Relative acyl group composition of dry seeds shown in **(B)**. Acyl groups with a molar percentage less than 0.5% were omitted. 30 seeds were analyzed in bulk for each repeat; n=5, ± SD.

(F) and **(G)** content and compositional analysis of phosphatidylglycerol (PG) and phosphatidylcholine (PC) in developing seeds isolated from WT, *plip1-1* and *PLIP1*-OX1 siliques harvested seven days after flowering. Molar percentages of PG and PC in lipids are shown in the inserted figures. 100 µL equivalent volume of developing seeds was used for each repeat. n=3, ± SD. Where appropriate, Student's *t*-test was applied to compare WT values with those each other line, respectively (* indicates $p<0.05$; ** indicates $p<0.01$).

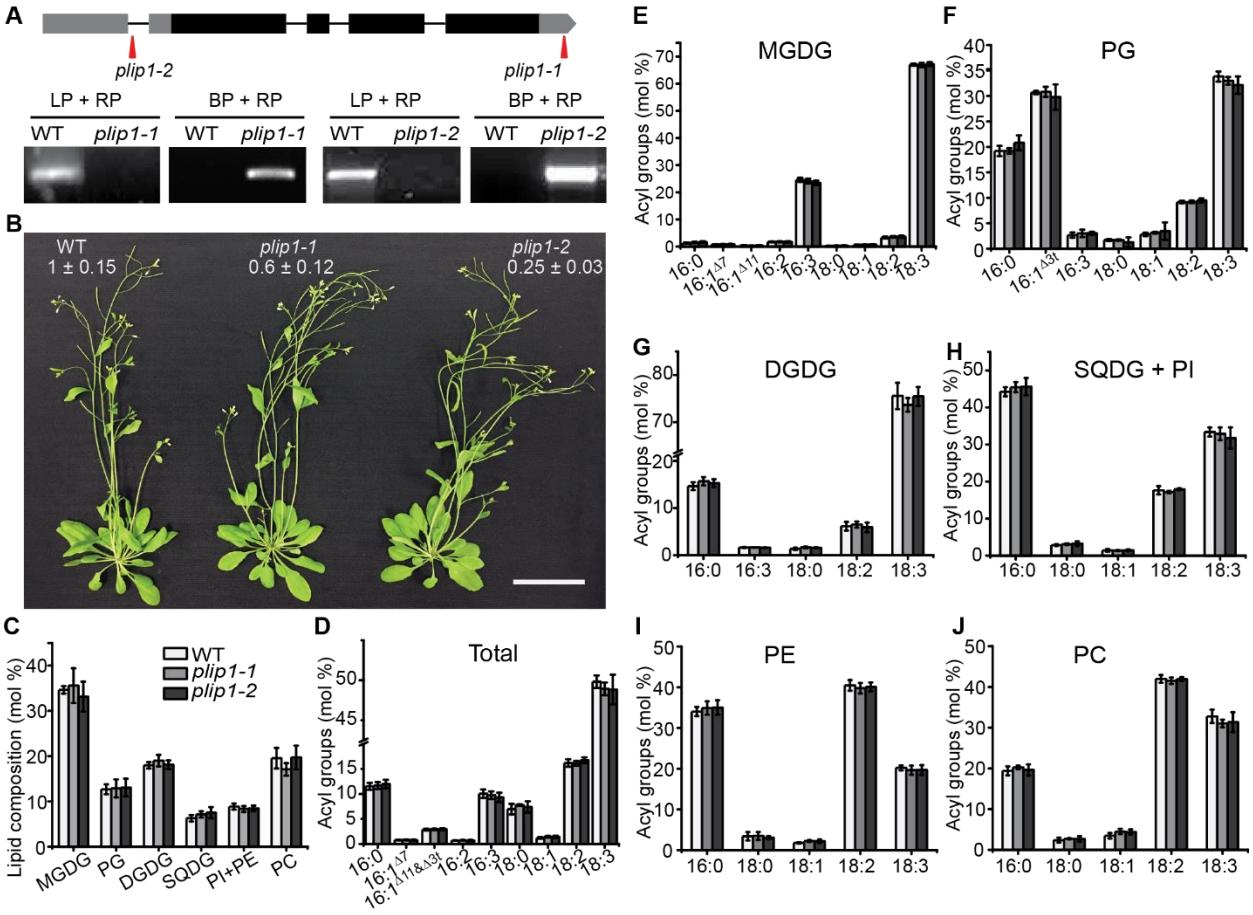

Figure 3. 15. Genotyping, phenotypic and lipid analysis of the *plip1* mutants.
(A) Genotyping of the *plip1* mutants. Top panel, positions of T-DNA insertions of *plip1-1* and *plip1-2* in the *PLIP1* gene. Gray box, untranslated regions; black box, exons; black lines, introns. Bottom panel, genotyping of the homozygous *plip1* alleles.
(B) Growth phenotypes of 4-week-old wild-type (WT) plants and two *plip1* mutants grown on soil (scale bar: 5 cm). Numbers indicate the relative *PLIP1* transcript levels in 2-week-old seedlings of wild-type (WT), *plip1-1* and *plip1-2* plants grown on MS medium. Leaves harvested from one plant were analyzed as one biological repeat; n=3-4, ± SD.
(C-J) Relative abundance of major polar lipid classes and relative acyl group composition of the major glycerolipids from leaves of 4-week-old soil-grown wild-type (WT), *plip1-1* and *plip1-2* plants**.** Leaves harvested from one plant were analyzed as one biological repeat; n=3-4, ± SD. DGDG, digalactosyldiacylglycerol; MGDG, monogalactosyldiacylglycerol; PC, phosphatidylcholine; PE, phosphatidylethanolamine; PG, phosphatidylglycerol; PS, phosphatidylserine; SQDG, sulfoquinovosyldiacylglycerol; TAG, triacylglycerol.

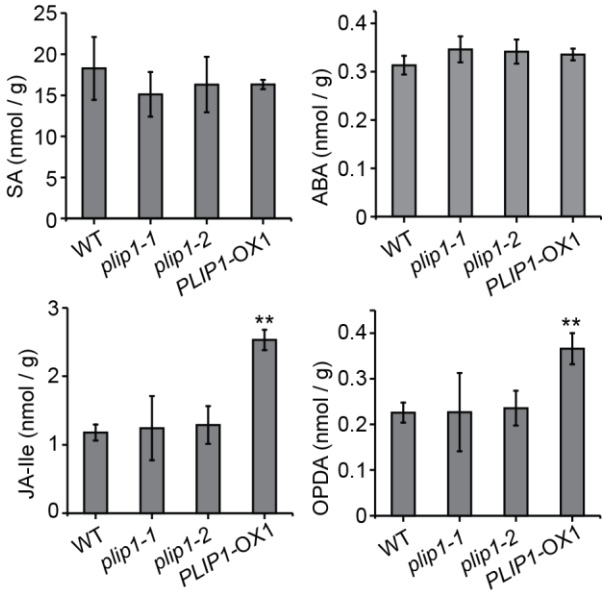

Figure 3. 16. Hormone quantification in *plip1* and *PLIP1*-OX1 dry seeds.
100 mg dry seeds of each genotype were used for hormone extraction as one biological repeat; n=4, ± SD. Student's *t*-test was applied to compare the WT with every other genotype (** indicates $p<0.01$).

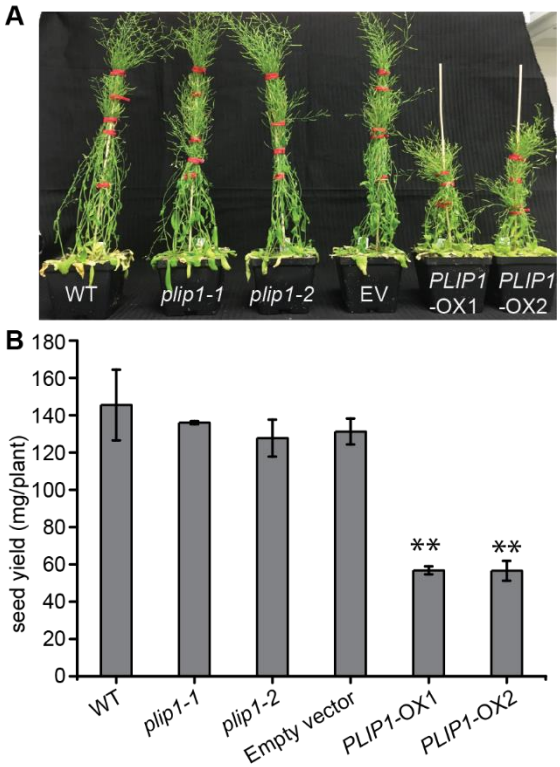

Figure 3. 17. Growth phenotypes of mature *plip1* mutant and *PLIP1*-OX plants.
(A) Growth phenotypes of 8-week-old wild type (WT), two *plip1* mutants, empty vector control (EV), and two *PLIP1*-OX plants.
(B) Seed yield measurement from plants in **(A)**. Seeds harvested from four plants grown in the same pot were used in each repeat; n=3, ± SD. Student's *t*-test was applied to compare the WT with every other genotype (** indicates $p<0.01$).

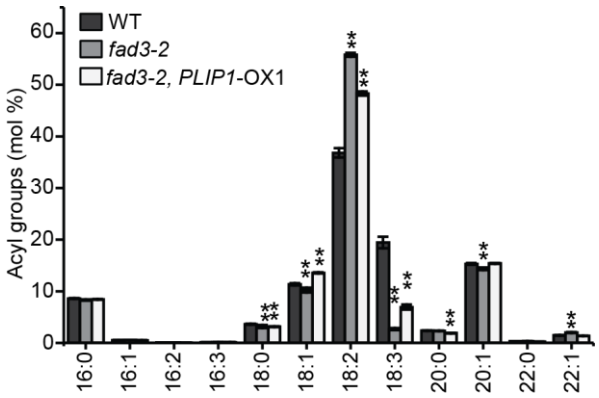

Figure 3. 18. Relative composition of total acyl groups in the wild type (WT), *fad3*-2, and *fad3-2, PLIP1*-OX1 dry seeds.

30 seeds per replicate, n=6 ± SD. Student's *t*-test was applied to compare the WT with every other genotype (** indicates $p<0.01$).

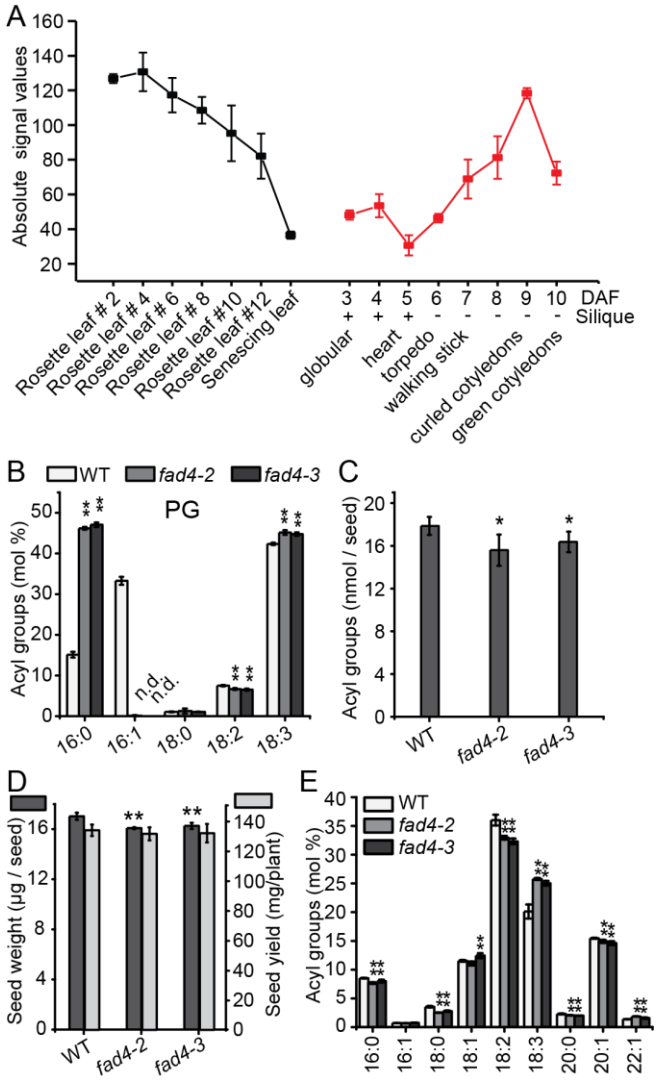

Figure 3.19. Analysis of *fad4-2* and *fad4-3* plants.

(A) Absolute expression levels of *FAD4* in leaves and developing seeds at different stages. Data were extracted from the Arabidopsis eFB browser. Average values from triplicates are shown, and the error bars represent SD.

(B) Leaf phosphatidylglycerol (PG) acyl group composition of 3-week-old MS medium-grown wild type (WT), *fad4-2* and *fad4-3* plants. Leaves harvested from one plant were pooled as one biological repeat; n=3-4, ± SD. n.d., not detected.

(C) Total acyl group content in dry seeds of WT, *fad4-2* and *fad4-3*. 30 seeds were used for each repeat; n=5, ± SD.

(D) Seed weight and yield measurements of WT, *fad4-2* and *fad4-3* plants. For seed weight measurement, 200 seeds were used for each repeat, n=3, ± SD. For seed yield measurement, seeds harvested from 4 plants grown in the same pot were used as one repeat, n=3, ± SD.

(E) Relative acyl group composition of seed lipid extracts from of WT, *fad4-2* and *fad4-3*. 30 seeds were used for each repeat, n=5, ± SD. Acyl groups with a molar percentage less than 0.5% were omitted. Where appropriate, Student's *t*-test was to compare the WT and each *fad4* mutant (* indicates $p<0.05$; ** $p<0.01$).

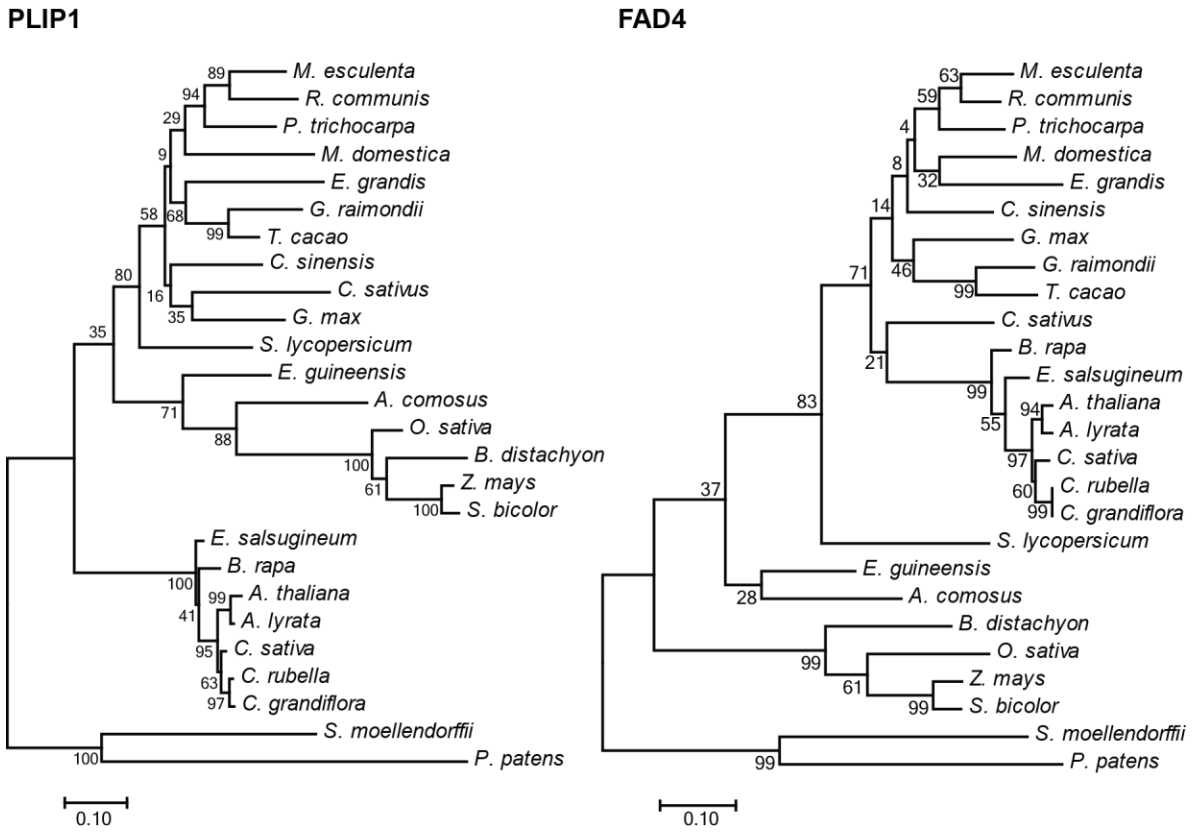

Figure 3. 20. Phylogenetic trees of PLIP1 and FAD4 in land plants.
The phylogenetic trees were built using the Maximum Likelihood method with PLIP1 or FAD4 homologous sequences from 26 land plant species with sequenced genomes. All sequence accession numbers are shown in Supplemental Table 2. Bootstrap values (based on 1000 replicates) are indicated at the tree nodes. The scale measures evolutionary distances in substitutions per amino acid.

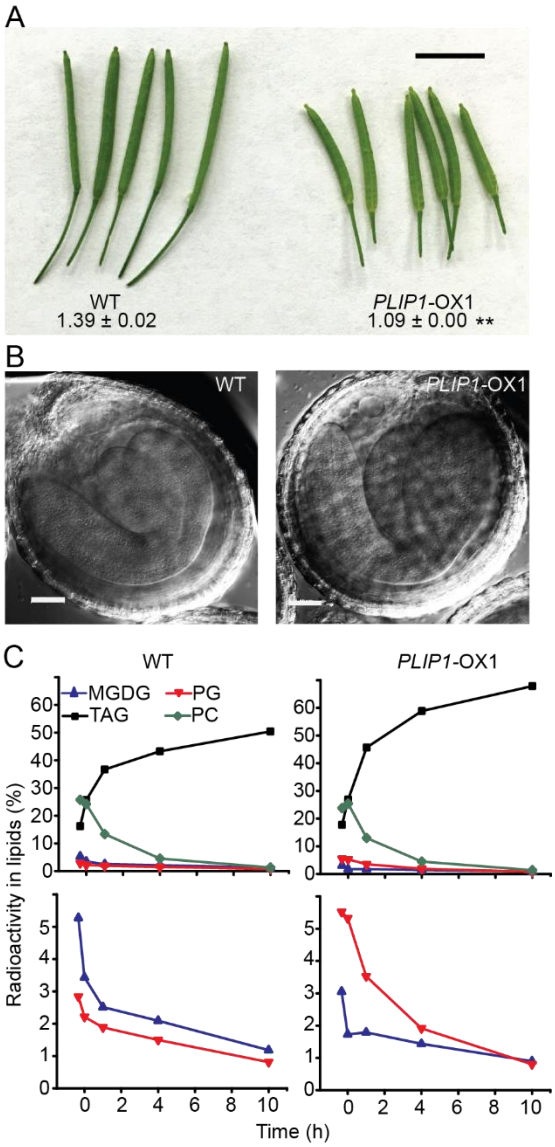

Figure 3. 21. Phenotypic analysis of *PLIP1*-OX1 embryos.
(A) Morphology of the wild-type (WT) and *PLIP1*-OX1 siliques nine days after flowering. Scale bar: 0.5 cm. The numbers indicate the length of siliques. n=9-12, ± SD. Student's *t*-test was applied (** indicates $p<0.01$).
(B) Differential interference contrast images of embryos isolated from siliques of WT and *PLIP1*-OX1 plants. Scale bars: 50 µm. Representative images are shown.
(C) Pulse-chase labeling of developing embryos isolated from siliques of wild-type (WT) and *PLIP1*-OX1 plants. 100 µL equivalent volume of developing seeds were used for each time point. The first two time points represent the labeling pulse. Embryos were transferred to unlabeled medium after one hour. Values represent the fraction of label in select individual lipids compared to label in total lipids. The top panels show four lipids, as indicated. The lower panels show PG and MGDG again, but on an expanded scale. Experiments were repeated three times on *PLIP1*-OX1 seeds and one time on *PLIP1*-OX2 seeds, with similar results. One representative result is shown. MGDG, monogalactosyldiacylglycerol; PC, phosphatidylcholine; PG, phosphatidylglycerol; TAG, triacylglycerol.

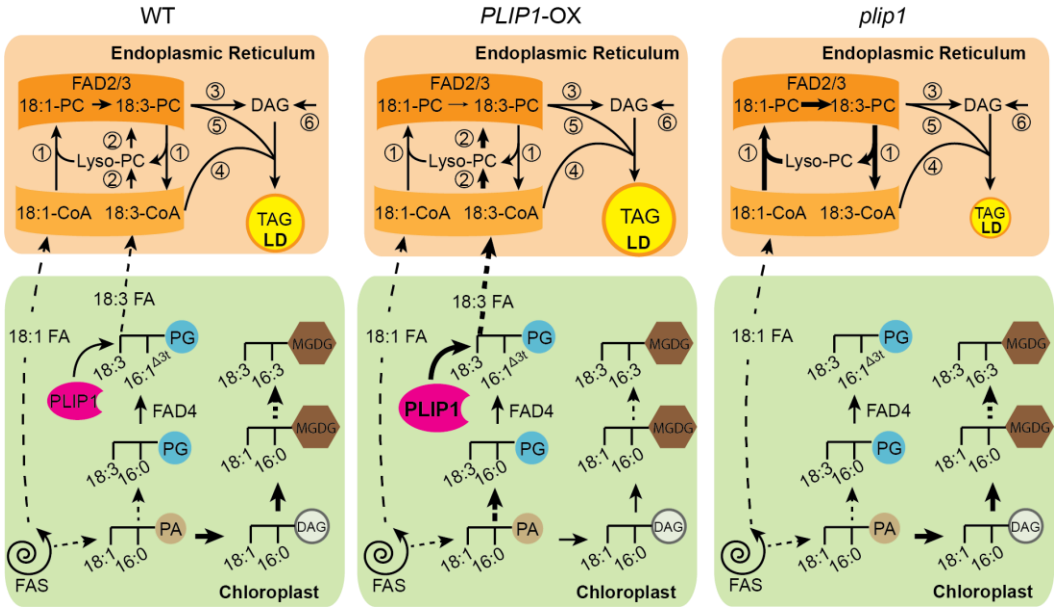

Figure 3. 22. Hypothesis for the role of PLIP1 in triacylglycerol biosynthesis.
The left panel depicts the wild type (WT), the middle panel the *PLIP1*-overexpression lines, and the right panel the *plip1* mutant. The thickness of the arrows indicates the relative fluxes in the three different lines. Reactions or sets of reactions are numbered as follows: 1. In WT (left panel) acyl exchange on phosphatidylcholine (PC) involving desaturation of acyl groups by FAD2/3 provides one mechanism to introduce polyunsaturated fatty acids (FAs) into phosphatidylcholine (PC). 2. A parallel mechanism to introduce PUFAs into PC involves PLIP1. In the chloroplast, PLIP1 hydrolyzes 18:3/16:1$^{\Delta 3t}$-phosphatidylglycerol (PG) and other 16:1$^{\Delta 3t}$-phosphatidylglycerol species (not shown here) at the *sn-1* glyceryl position and releases 18:3 (carbon: double bonds) or other acyl groups at the *sn-1* position. The released acyl group is exported to the Endoplasmic Reticulum and incorporated into the acyl-CoA pool and PC. 3. A head group exchange mechanism leads to diacylglycerol (DAG) formation from PC containing PUFAs. 4. Triacylglycerol (TAG), which accumulates in lipid droplets (LDs), is formed by the action of DAG-acyltransferases, which can introduce additional acyl groups into DAG from the acyl-CoA pool. 5. Phospholipid-DAG acyltransferase provides an additional route for the incorporation of PUFAs from PC into TAG. 6. DAG can also be formed by de novo assembly through the Kennedy pathway, which, however, is thought to play a minor role in the synthesis of TAGs in seeds. In the chloroplast, biosynthesis of PG and monogalactosyldiacylglycerol (MGDG) share the precursor phosphatidic acid (PA), with more PA being shuttled to MGDG biosynthesis in the wild type. In *PLIP1*-OX lines (middle panel), both PG biosynthesis and degradation are accelerated, resulting in increased export of 18:3 and other acyl groups and their direct incorporation into PC (reactions 2). Direct incorporation of 18:3 competes with polyunsaturated FA formation by the acyl-editing pathway of PC involving FAD2/3 (reactions 1), but leads to increased flux of 18:3 into the end product TAG. As a result of increased PG turnover in chloroplasts of *PLIP1*-OX lines, PA is preferably shuttled into PG biosynthesis, which subsequently reduces its availability for MGDG assembly in the plastid visible in changes in the MGDG acyl composition. In the *plip1* mutant (right panel), the PLIP1-dependent pathway is deficient, resulting in decreased TAG biosynthesis. Without the competing effect of PLIP1 on the acyl exchange reactions and FAD2/3, more 18:1 is converted to 18:3, explaining the altered acyl composition of TAG and other extraplastidic lipids.

REFERENCES

REFERENCES

Ajjawi, I., Lu, Y., Savage, L.J., Bell, S.M., and Last, R.L. (2010). Large-scale reverse genetics in Arabidopsis: case studies from the Chloroplast 2010 Project. Plant Physiol **152,** 529-540.

Alonso, J.M., Stepanova, A.N., Leisse, T.J., Kim, C.J., Chen, H., Shinn, P., Stevenson, D.K., Zimmerman, J., Barajas, P., Cheuk, R., Gadrinab, C., Heller, C., Jeske, A., Koesema, E., Meyers, C.C., Parker, H., Prednis, L., Ansari, Y., Choy, N., Deen, H., Geralt, M., Hazari, N., Hom, E., Karnes, M., Mulholland, C., Ndubaku, R., Schmidt, I., Guzman, P., Aguilar-Henonin, L., Schmid, M., Weigel, D., Carter, D.E., Marchand, T., Risseeuw, E., Brogden, D., Zeko, A., Crosby, W.L., Berry, C.C., and Ecker, J.R. (2003). Genome-wide insertional mutagenesis of *Arabidopsis thaliana*. Science **301,** 653-657.

Andersson, M.X., and Dörmann, P. (2009). Chloroplast Membrane Lipid Biosynthesis and Transport. In The Chloroplast, A.S. Sandelius and H. Aronsson, eds (Berlin, Heidelberg: Springer Berlin Heidelberg), pp. 125-158.

Aronsson, H., and Jarvis, P. (2002). A simple method for isolating import-competent Arabidopsis chloroplasts. FEBS Lett **529,** 215-220.

Bates, P.D., Ohlrogge, J.B., and Pollard, M. (2007). Incorporation of newly synthesized fatty acids into cytosolic glycerolipids in pea leaves occurs via acyl editing. J Biol Chem **282,** 31206-31216.

Bates, P.D., Fatihi, A., Snapp, A.R., Carlsson, A.S., Browse, J., and Lu, C. (2012). Acyl editing and headgroup exchange are the major mechanisms that direct polyunsaturated fatty acid flux into triacylglycerols. Plant Physiol **160,** 1530-1539.

Benning, C. (2009). Mechanisms of lipid transport involved in organelle biogenesis in plant cells. Annu Rev Cell Dev Biol **25,** 71-91.

Benning, C. (2010). The Anionic Chloroplast Membrane Lipids: Phosphatidylglycerol and Sulfoquinovosyldiacylglycerol. In The Chloroplast: Biochemistry, Molecular Biology and Bioengineering., C.A. Rebeiz, C. Benning, H. Bohnert, H. Daniell, B. Green, K. Hoober, H. Lichtenthaler, A. Portis, and B. Tripathy, eds (Netherlands: Springer), pp. 171-184.

Boudière, L., Michaud, M., Petroutsos, D., Rébeillé, F., Falconet, D., Bastien, O., Roy, S., Finazzi, G., Rolland, N., Jouhet, J., Block, M.A., and Maréchal, E. (2014). Glycerolipids in photosynthesis: Composition, synthesis and trafficking. Biochim Biophys Acta, Bioenerg **1837,** 470-480.

Brady, L., Brzozowski, A.M., Derewenda, Z.S., Dodson, E., Dodson, G., Tolley, S., Turkenburg, J.P., Christiansen, L., Huge-Jensen, B., Norskov, L., Thim, L., and Menge, U. (1990). A serine protease triad forms the catalytic centre of a triacylglycerol lipase. Nature **343,** 767-770.

Browse, J., McCourt, P., and Somerville, C.R. (1985). A mutant of Arabidopsis lacking a chloroplast-specific lipid. Science **227,** 763-765.

Browse, J., McConn, M., James, D., Jr., and Miquel, M. (1993). Mutants of Arabidopsis deficient in the synthesis of alpha-linolenate. Biochemical and genetic characterization of the endoplasmic reticulum linoleoyl desaturase. J Biol Chem **268,** 16345-16351.

Campos, M.L., Yoshida, Y., Major, I.T., de Oliveira Ferreira, D., Weraduwage, S.M., Froehlich, J.E., Johnson, B.F., Kramer, D.M., Jander, G., Sharkey, T.D., and Howe, G.A. (2016). Rewiring of jasmonate and phytochrome B signalling uncouples plant growth-defense tradeoffs. Nat Commun **7,** 12570.

Clough, S.J., and Bent, a.F. (1998). Floral dip: a simplified method for Agrobacterium-mediated transformation of *Arabidopsis thaliana*. Plant J **16,** 735-743.

Dahlqvist, A., Stahl, U., Lenman, M., Banas, A., Lee, M., Sandager, L., Ronne, H., and Stymne, S. (2000). Phospholipid:diacylglycerol acyltransferase: an enzyme that catalyzes the acyl-CoA-independent formation of triacylglycerol in yeast and plants. Proc Natl Acad Sci U S A **97,** 6487-6492.

Dave, A., and Graham, I.A. (2012). Oxylipin Signaling: A Distinct Role for the Jasmonic Acid Precursor cis-(+)-12-Oxo-Phytodienoic Acid (cis-OPDA). Front Plant Sci **3,** 42.

Dave, A., Hernandez, M.L., He, Z., Andriotis, V.M., Vaistij, F.E., Larson, T.R., and Graham, I.A. (2011). 12-oxo-phytodienoic acid accumulation during seed development represses seed germination in Arabidopsis. Plant Cell **23,** 583-599.

Earley, K.W., Haag, J.R., Pontes, O., Opper, K., Juehne, T., Song, K., and Pikaard, C.S. (2006). Gateway-compatible vectors for plant functional genomics and proteomics. Plant J **45,** 616-629.

Gao, J., Ajjawi, I., Manoli, A., Sawin, A., Xu, C., Froehlich, J.E., Last, R.L., and Benning, C. (2009). FATTY ACID DESATURASE4 of Arabidopsis encodes a protein distinct from characterized fatty acid desaturases. Plant J **60,** 832-839.

Goosens, V.J., and van Dijl, J.M. (2016). Twin-Arginine Protein Translocation. Curr Top Microbiol Immunol **404,** 69-94.

Herr Jr, J. (1993). Clearing techniques for the study of vascular plant tissues in whole structures and thick sections. In Tested Studies for Laboratory Teaching, C.A. Goldman, P.L. Hauta, M.A. O'Donnell, S.E. Andrews, and R. van der Heiden, eds (Toronto, Canada: Association for Biology Laboratory Education), pp. 63–84.

Hurlock, A.K., Roston, R.L., Wang, K., and Benning, C. (2014). Lipid trafficking in plant cells. Traffic **15,** 915-932.

Ishiguro, S., Kawai-Oda, A., Ueda, J., Nishida, I., and Okada, K. (2001). The DEFECTIVE IN ANTHER DEHISCIENCE gene encodes a novel phospholipase A1 catalyzing the initial step of jasmonic acid biosynthesis, which synchronizes pollen maturation, anther dehiscence, and flower opening in Arabidopsis. Plant Cell **13,** 2191-2209.

Katavic, V., Reed, D.W., Taylor, D.C., Giblin, E.M., Barton, D.L., Zou, J., Mackenzie, S.L., Covello, P.S., and Kunst, L. (1995). Alteration of seed fatty acid composition by an ethyl methanesulfonate-induced mutation in Arabidopsis thaliana affecting diacylglycerol acyltransferase activity. Plant physiology **108,** 399-409.

Keegstra, K., and Yousif, A.E. (1986). Isolation and Characterization of Chloroplast Envelope Membranes. Method Enzymol **118,** 316-325.

Kelly, A.A., and Feussner, I. (2016). Oil is on the agenda: Lipid turnover in higher plants. Biochim Biophys Acta **1861**, 1253–1268.

Kobayashi, K., Endo, K., and Wada, H. (2016). Roles of lipids in photosynthesis. Subcell Biochem **86,** 21-49.

Le, B.H., Cheng, C., Bui, A.Q., Wagmaister, J.A., Henry, K.F., Pelletier, J., Kwong, L., Belmonte, M., Kirkbride, R., Horvath, S., Drews, G.N., Fischer, R.L., Okamuro, J.K., Harada, J.J., and Goldberg, R.B. (2010). Global analysis of gene activity during Arabidopsis seed development and identification of seed-specific transcription factors. Proc Natl Acad Sci U S A **107,** 8063-8070.

Li-Beisson, Y., Shorrosh, B., Beisson, F., Andersson, M.X., Arondel, V., Bates, P.D., Baud, S., Bird, D., Debono, A., Durrett, T.P., Franke, R.B., Graham, I.A., Katayama, K., Kelly, A.A., Larson, T., Markham, J.E., Miquel, M., Molina, I., Nishida, I., Rowland, O., Samuels, L., Schmid, K.M., Wada, H., Welti, R., Xu, C., Zallot, R., and Ohlrogge, J. (2013). Acyl-lipid metabolism. Arabidopsis Book **11,** e0161.

Li, N., Gugel, I.L., Giavalisco, P., Zeisler, V., Schreiber, L., Soll, J., and Philippar, K. (2015). FAX1, a novel membrane protein mediating plastid fatty acid export. PLoS Biol **13,** e1002053.

Li, X., Moellering, E.R., Liu, B., Johnny, C., Fedewa, M., Sears, B.B., Kuo, M.H., and Benning, C. (2012). A Galactoglycerolipid Lipase Is Required for Triacylglycerol Accumulation and Survival Following Nitrogen Deprivation in Chlamydomonas reinhardtii. Plant Cell **24**, 4670–4686.

Li, Y., Beisson, F., Pollard, M., and Ohlrogge, J. (2006). Oil content of Arabidopsis seeds: the influence of seed anatomy, light and plant-to-plant variation. Phytochemistry **67,** 904-915.

Lu, B., and Benning, C. (2009). A 25-amino acid sequence of the Arabidopsis TGD2 protein is sufficient for specific binding of phosphatidic acid. J Biol Chem **284,** 17420-17427.

Lu, Y., Savage, L.J., Ajjawi, I., Imre, K.M., Yoder, D.W., Benning, C., DellaPenna, D., Ohlrogge, J.B., Osteryoung, K.W., Weber, A.P., Wilkerson, C.G., and Last, R.L. (2008). New connections across pathways and cellular processes: industrialized mutant screening reveals novel associations between diverse phenotypes in Arabidopsis. Plant Physiol **146,** 1482-1500.

Marchler-Bauer, A., Derbyshire, M.K., Gonzales, N.R., Lu, S., Chitsaz, F., Geer, L.Y., Geer, R.C., He, J., Gwadz, M., Hurwitz, D.I., Lanczycki, C.J., Lu, F., Marchler, G.H., Song, J.S., Thanki, N., Wang, Z., Yamashita, R.A., Zhang, D., Zheng, C., and Bryant, S.H. (2015). CDD: NCBI's conserved domain database. Nucleic Acids Res **43,** D222-226.

McCourt, P., Browse, J., Watson, J., Arntzen, C.J., and Somerville, C.R. (1985). Analysis of photosynthetic antenna function in a mutant of *Arabidopsis thaliana* (L.) lacking trans-hexadecenoic acid. Plant Physiol **78,** 853-858.

Mhaske, V., Beldjilali, K., Ohlrogge, J., and Pollard, M. (2005). Isolation and characterization of an Arabidopsis thaliana knockout line for phospholipid: diacylglycerol transacylase gene (At5g13640). Plant Physiol Biochem **43,** 413-417.

Moellering, E.R., Muthan, B., and Benning, C. (2010). Freezing tolerance in plants requires lipid remodeling at the outer chloroplast membrane. Science **330,** 226-228.

Murashige, T., and Skoog, F. (1962). A revised medium for rapid growth and bio assays with tobacco tissue cultures. Physiol Plant **15,** 473-497.

Ngaki, M.N., Louie, G.V., Philippe, R.N., Manning, G., Pojer, F., Bowman, M.E., Li, L., Larsen, E., Wurtele, E.S., and Noel, J.P. (2012). Evolution of the chalcone-isomerase fold from fatty-acid binding to stereospecific catalysis. Nature **485,** 530-533.

Pazos, F., Ranea, J.A., Juan, D., and Sternberg, M.J. (2005). Assessing protein co-evolution in the context of the tree of life assists in the prediction of the interactome. J Mol Biol **352,** 1002-1015.

Quast, C., Pruesse, E., Yilmaz, P., Gerken, J., Schweer, T., Yarza, P., Peplies, J., and Glockner, F.O. (2013). The SILVA ribosomal RNA gene database project: improved data processing and web-based tools. Nucleic Acids Res **41,** D590-596.

Ribot, C., Zimmerli, C., Farmer, E.E., Reymond, P., and Poirier, Y. (2008). Induction of the Arabidopsis PHO1;H10 gene by 12-oxo-phytodienoic acid but not jasmonic acid via a CORONATINE INSENSITIVE1-dependent pathway. Plant Physiol **147,** 696-706.

Richmond, G.S., and Smith, T.K. (2011). Phospholipases A_1. Int J Mol Sci **12,** 588-612.

Robinson, C., and Bolhuis, A. (2001). Protein targeting by the twin-arginine translocation pathway. Nat Rev Mol Cell Biol **2,** 350-356.

Rodrigues, R.A., Silva-Filho, M.C., and Cline, K. (2011). FtsH2 and FtsH5: two homologous subunits use different integration mechanisms leading to the same thylakoid multimeric complex. Plant J **65,** 600-609.

Roston, R., Gao, J., Xu, C., and Benning, C. (2011). Arabidopsis chloroplast lipid transport protein TGD2 disrupts membranes and is part of a large complex. Plant J **66,** 759-769.

Roston, R.L., Gao, J., Murcha, M.W., Whelan, J., and Benning, C. (2012). TGD1, -2, and -3 proteins involved in lipid trafficking form ATP-binding cassette (ABC) transporter with multiple substrate-binding proteins. J Biol Chem **287,** 21406-21415.

Routaboul, J.M., Benning, C., Bechtold, N., Caboche, M., and Lepiniec, L. (1999). The TAG1 locus of Arabidopsis encodes for a diacylglycerol acyltransferase. Plant Physiol Biochem **37,** 831-840.

Scherer, G.F., Ryu, S.B., Wang, X., Matos, A.R., and Heitz, T. (2010). Patatin-related phospholipase A: nomenclature, subfamilies and functions in plants. Trends Plant Sci **15,** 693-700.

Schwacke, R., Schneider, A., van der Graaff, E., Fischer, K., Catoni, E., Desimone, M., Frommer, W.B., Flugge, U.I., and Kunze, R. (2003). ARAMEMNON, a novel database for Arabidopsis integral membrane proteins. Plant Physiol **131,** 16-26.

Tanoue, R., Kobayashi, M., Katayama, K., Nagata, N., and Wada, H. (2014). Phosphatidylglycerol biosynthesis is required for the development of embryos and normal membrane structures of chloroplasts and mitochondria in Arabidopsis. Febs Lett **588,** 1680-1685.

Troncoso-Ponce, M.A., Cao, X., Yang, Z., and Ohlrogge, J.B. (2013). Lipid turnover during senescence. Plant Sci **205-206,** 13-19.

Wang, G., Ryu, S., and Wang, X. (2012). Plant phospholipases: an overview. Methods Mol Biol **861,** 123-137.

Wang, K., Hersh, H.L., and Benning, C. (2016). SENSITIVE TO FREEZING2 Aids in Resilience to Salt and Drought in Freezing-Sensitive Tomato. Plant Physiol **172,** 1432-1442.

Wang, X. (2004). Lipid signaling. Curr Opin Plant Biol **7,** 329-336.

Wang, Z., and Benning, C. (2011). Arabidopsis thaliana polar glycerolipid profiling by thin layer chromatography (TLC) coupled with gas-liquid chromatography (GLC). J Vis Exp **49**, 2518

Winkler, F.K., D'Arcy, A., and Hunziker, W. (1990). Structure of human pancreatic lipase. Nature **343,** 771-774.

Winter, D., Vinegar, B., Nahal, H., Ammar, R., Wilson, G.V., and Provart, N.J. (2007). An "Electronic Fluorescent Pictograph" browser for exploring and analyzing large-scale biological data sets. PloS One **2,** e718.

Xie, D.X., Feys, B.F., James, S., Nieto-Rostro, M., and Turner, J.G. (1998). COI1: an Arabidopsis gene required for jasmonate-regulated defense and fertility. Science **280,** 1091-1094.

Xu, C., Fan, J., Cornish, A.J., and Benning, C. (2008). Lipid trafficking between the endoplasmic reticulum and the plastid in Arabidopsis requires the extraplastidic TGD4 protein. Plant Cell **20,** 2190-2204.

Xu, C., Fan, J., Froehlich, J.E., Awai, K., and Benning, C. (2005). Mutation of the TGD1 chloroplast envelope protein affects phosphatidate metabolism in Arabidopsis. Plant Cell **17,** 3094-3110.

Yan, Y., Stolz, S., Chetelat, A., Reymond, P., Pagni, M., Dubugnon, L., and Farmer, E.E. (2007). A downstream mediator in the growth repression limb of the jasmonate pathway. Plant Cell **19,** 2470-2483.

Zeng, W., Brutus, A., Kremer, J.M., Withers, J.C., Gao, X., Jones, A.D., and He, S.Y. (2011). A genetic screen reveals Arabidopsis stomatal and/or apoplastic defenses against Pseudomonas syringae pv. tomato DC3000. PLoS Pathog **7,** e1002291.

Zhang, Y., and Turner, J.G. (2008). Wound-induced endogenous jasmonates stunt plant growth by inhibiting mitosis. PloS One **3,** e3699.

CHAPTER 4

Two Abscisic Acid Responsive Plastid Lipase Genes Involved in Jasmonic Acid Biosynthesis in *Arabidopsis thaliana*

ABSTRACT

Chloroplast membranes with their unique lipid composition are crucial for photosynthesis. Maintenance of the chloroplast membranes requires a finely tuned lipid anabolic and catabolic machinery. Despite the presence of a large number of predicted lipid-degrading enzymes in the chloroplasts, their biological functions remain largely unknown. Recently, we described PLASTID LIPASE 1 (PLIP1) as a plastid phospholipase A_1 that contributes to seed oil biosynthesis. The Arabidopsis genome encodes two putative PLIP1 paralogs which we designated PLIP2 and PLIP3. PLIP2 and PLIP3 are also located in the chloroplasts, but likely with different locations in the plastid. PLIP2 possesses similar biochemical properties in vitro to PLIP1, but in vivo studies suggest that PLIP2 prefers monogalactosyldiacylglycerol as substrate, while PLIP3 prefers phosphatidylglycerol. Overexpression of *PLIP2* or *PLIP3* severely reduces plant growth and leads to accumulation of oxylipins. Genetically blocking jasmonate perception restored the growth of the overexpression plants. The expression of *PLIP2* and *PLIP3*, but not *PLIP1* is induced by abscisic acid (ABA), and *plip1,2,3* triple mutants exhibit compromised oxylipin biosynthesis in response to ABA. We propose that PLIP2 and PLIP3 provide a mechanistic link between ABA mediated abiotic stress responses and oxylipin signaling.

INTRODUCTION

Chloroplasts in plants and algae are organelles that carry out a number of crucial biological functions including photosynthesis. They also participate in plant immune responses through the production of defense signaling compounds such as oxylipins and ultimately jasmonic acid (JA). Membranes with a unique lipid composition are required for the proper functioning of the chloroplasts. Chloroplast membranes contain predominately galactolipids, monogalactosyldiacylglycerol (MGDG) and digalactosyldiacylglycerol (DGDG), as well as two anionic lipids phosphatidylglycerol (PG), and sulfoquinovosyldiacylglycerol (SQDG) (Andersson and Dörmann, 2009; Benning, 2010; Boudière et al., 2014). In seed plants, lipid assembly begins in the plastids where fatty acid (FA) synthesis occurs. In Arabidopsis, two pathways are responsible for plant lipid assembly (Benning, 2009; Hurlock et al., 2014). De novo synthesized FAs can either directly enter the plastid (prokaryotic) pathway or are exported to the endoplasmic reticulum (ER) and assembled in to lipids there (eukaryotic pathway). Lipid precursors synthesized in the ER can also return to the plastid and contribute to chloroplast lipid biosynthesis (Wang and Benning, 2012; Hurlock et al., 2014). Lipids synthesized by the two pathways can be distinguished by their glyceryl *sn-2*-bound acyl groups due to the specificity of the respective acyltransferases (Frentzen et al., 1983; Frentzen, 1986). Plastid pathway-derived galactolipids contain 16-carbon acyl groups at the *sn-2* glyceryl position, while ER-derived lipids contain 18-carbon acyl groups in this position.

To date, many of the genes and enzymes responsible for chloroplast lipid biosynthesis have been identified, yet still little is known about the role of enzymes involved in chloroplast lipid degradation. Turnover of glycolipids requires lipases to release the acyl or the head groups from the three different positions of the glyceryl backbone (Troncoso-Ponce et al., 2013; Kelly and

Feussner, 2016). Based on their preferred hydrolysis position, phospholipases are classified into three groups (Wang et al., 2012): Phospholipase C (PLC) and phospholipase D (PLD) cleave the phosphodiester bonds adjacent and distal to the *sn-3* glyceryl position, respectively. Phospholipases A (PLA) release FAs from glyceryl *sn-1* or *sn-2* positions; PLA_1 hydrolyses at the *sn-1* position while PLA_2 at *sn-2*. Free FAs released by PLAs from the membrane lipids can be subsequently oxygenated by either enzymatic reactions or chemical oxidation (Blee, 1998; Mueller, 2004; Mosblech et al., 2009). In plants, enzyme-mediated FA oxidation predominantly works on polyunsaturated FAs, e.g., linolenic acids (18:3; number of carbons : number of double bonds in the acyl chain) through the lipoxygenase pathway (Porta and Rocha-Sosa, 2002). Lipoxygenases initiate the synthesis of FA hydroperoxides. Their subsequent conversion occurs through an array of alternative pathways (Porta and Rocha-Sosa, 2002; Mosblech et al., 2009). Structurally and functionally diverse oxylipins are produced during different developmental stages, in different tissues as well as in response to different environmental cues (Gobel et al., 2002; Porta and Rocha-Sosa, 2002; Andersson et al., 2006). The best characterized lipid oxidation pathway is the allene oxide synthase pathway which leads to the synthesis of oxylipins, including 12-oxo phytodienoic acid (OPDA), JA and the conjugates between JA and amino acids, *e.g.*, the bioactive JA-isoleucine (JA-Ile) (Turner et al., 2002; Wasternack and Hause, 2013). JA production and signaling are primarily induced by wounding damage caused by herbivore insects or necrotrophic microbes (Creelman et al., 1992; Trusov et al., 2006). Developmentally, JA is essential for stamen development, size of petioles and petals, as well as lignin biosynthesis (Feys et al., 1994; McConn and Browse, 1996; Ellis et al., 2002; Buseman et al., 2006; Denness et al., 2011). DEFECTIVE IN ANTHER DEHISCENCE1 (DAD1) is a PLA_1 that is primarily present in the reproductive tissues, where it initiates JA biosynthesis critical for pollen maturation, anther

dehiscence and flower opening in Arabidopsis (Ishiguro et al., 2001). In leaf tissues, *DONGLE* encodes a DAD1-homologous lipase contributing to wounding-induced JA production (Hyun et al., 2008). In addition, synergetic or antagonistic interactions between JA and other phytohormones including salicylic acid, ethylene and ABA have emerged (Thomma et al., 1998; Song et al., 2014; Suzuki, 2016), suggesting that the interaction between different hormones is an important strategy for plants to fine-tune their responses to environmental cues.

It is known that JA biosynthesis is stimulated by applied ABA or during ABA-inducing abiotic stress conditions (Creelman and Mullet, 1995; Adie et al., 2007; Avramova, 2017), but the underlying mechanisms are not well understood. During abiotic stress, rising ABA levels induce JA synthesis, which synergistically optimizes plant abiotic defenses by altering the plant transcriptome, facilitating the closure of stomata, inhibiting cell division, as well as epigenetically modifying defense genes during dehydration responses (Murata et al., 2015; Riemann et al., 2015; Liu et al., 2016; Valenzuela et al., 2016). A basic-helix-loop-helix transcription factor MYC2 plays roles in JA perception and ABA signaling, and has been proposed as one of the factors linking ABA and JA signaling (Kazan and Manners, 2013).

In Arabidopsis, over 50 lipases are predicted to be localized in the chloroplasts with unverified enzymatic activities and unknown biological functions (Ajjawi et al., 2010). Recently, we discovered a thylakoid associated lipase named PLIP1, which is a PLA_1 that releases polyunsaturated FAs from chloroplast PG and exports the FAs to the ER for seed oil biosynthesis (Wang et al., 2017). BLAST searches and phylogenetic analyses identified two putative PLIP1 paralogs in the Arabidopsis genome, which we designated PLIP2 and PLIP3. Both PLIP2 and PLIP3 are located in the chloroplasts. Their characterization and possible role in JA biosynthesis in response to increased ABA levels following abiotic stress is explored below.

MATERIALS AND METHODS

Plant Material and Growth Conditions

All experiments were performed in the *Arabidopsis thaliana* Col-0 ecotype. The T-DNA insertion lines SALK_1234548 (*plip2-1*), SALK_134525 (*plip2-2*), SALK_006633 (*plip3-1*) and SALK_115539 (*plip3-2*) were obtained from the Arabidopsis Biological Resource Center, Ohio State University. For the overexpression lines, the coding sequences of *PLIP2* or *PLIP3* were inserted into the pENTR™/TEV/D-TOPO® vector (Life Sciences; Catalog number: K240020) before recombining them into the pEarleyGate 101 vector (YFP at the C-terminus) (Earley et al., 2006) with the Gateway LR Clonase Kit (Thermo Fisher Scientific; Catalog number: 11791-020). The final constructs were introduced into Col-0 wild-type plants by *Agobacterium tumefaciens*-mediated floral dip (Clough and Bent, 1998). Transformed seeds were initially screened for resistance to Basta, followed by confirmation by RT-PCR. Primers used for genotyping of T-DNA insertion lines or for RT-PCR analysis of overexpression lines are given in Table 4.1. The growth condition for the Murashige and Skoog (MS) medium grown and the soil-grown Arabidopsis plants are the same as previously reported (Wang et al., 2017).

Phylogenetic Analysis

The top 20 PLIP1 putative paralog amino acid sequences were obtained by comparing the AtPLIP1 protein sequence against the Arabidopsis proteome using the BLASTp program in TAIR BLAST 2.2.8 (http://www.arabidopsis.org/Blast/index.jsp) with the default parameters. The amino acid alignment was created using the MUSCLE program with default settings employing MEGA (version 7.0.21) software. The Maximum Likelihood phylogenetic trees were built using MEGA (version 7.0.21) and the bootstrap percentages were based on 1000 replicates.

Confocal Laser Scanning Microscopy

The confocal images were taken with an Nikon A1Rsi confocal microscope on leaves of 3-week-old Arabidopsis grown on MS agar plates. YFP fusion proteins were detected with the configuration A1CYFR using a 514 nm laser for excitation and a 530-600 nm band pass filter for fluorescence emission. For the chlorophyll autofluorescence, a 647 nm laser was used for excitation and a 660 nm long pass filter for emission detection. Images were merged and pseudcolored using the NIS-Elements AR software (version 4.30.01 64-bit).

Chloroplast Import Assay

Isolation of pea chloroplasts, import assays and post-import trypsin treatment were done essentially as previously described (Xu et al., 2005). The constructs used for production of labeled proteins were pET41a-*PLIP2* and pET41a-*PLIP2*. N-terminal 6×His tag and TEV cleavage sites were removed using a Q5 Site-Directed Mutagenesis Kit (New England Biolabs).

Recombinant Protein Production

The *PLIP2* coding sequence was amplified from the Arabidopsis wild-type cDNA and inserted into the pGEM-T-Easy plasmid (Promega). It was then inserted into the pET41a plasmid at the BamHI and XhoI restriction sites. The PLIP2^{S428A} point mutation construct was generated with a Q5 Site-Directed Mutagenesis Kit (New England Biolabs). Final pET41a-*PLIP2* and pET41a-*PLIP2*^{S428A} constructs were introduced into BL21 (DE3) *E. coli* strains for protein production. Cultures grown in LB medium (containing 0.1% glucose) were inoculated with fresh *E. coli* colonies and grown to log phase (OD_{600} 0.8) at 37 °C. Protein production was then induced by adding isopropyl-β-D-thiogalactopyranoside (IPTG) to the final concentration of 0.2 mM, and

the culture was transferred to 14 °C. Cells were harvested after 1.5 h of induction. Cultures were harvested and sonicated to lyse cells. Supernatant was collected after centrifugation at 10,000 × *g* for 30 min, and subjected to another 1-h centrifugation at 100,000 × *g* to remove the supernatants. The pellet fraction was then resuspended with PBS buffer to give rise to microsomes. Microsomes harvested from the cultures expressing *PLIP2*, *PLIP2*^{S428A} or the empty vector were used for the following lipase assays.

PLIP2 Lipase Assay

The lipase assay was performed essentially according to Wang et al. 2017. Briefly, microsomes harvested from 1 L induced cultures producing PLIP2 were resuspended in 1 mL PBS buffer. For each lipase assay, 100 µg dried lipids were first resuspended in 300 µL reaction buffer (0.1 M PBS, pH 7.4; 4.2 mM Anzergent 3-12 (Anatrace)) and dispersed by sonication. Then, 50 µL microsomes were added to each reaction followed by another 10 s sonication to mix. The reaction was incubated at ambient temperature (~22 °C) for 1 h or as indicated for time courses (Figure 4.1). The reaction was stopped by lipid extraction, followed by lipid separation by TLC and quantification by gas chromatography as described below.

Lipid Analysis

Lipid extraction, TLC of polar and neutral lipids, transesterification, and gas chromatography were done as described in Wang and Benning 2011. For polar lipids, activated ammonium sulfate-impregnated silica gel TLC plates (TLC Silica gel 60; EMD Chemical, Germany) were used for lipid separation with a solvent consisting of acetone, toluene and water (91:30:7.5 by volume). Lipids were visualized by brief exposure to iodine vapor on TLC plates.

Acyl groups of the isolated lipids were then converted to methyl esters, which were subsequently quantified by a gas chromatography.

Pulse-Chase Labeling

The pulse-chase labeling experiments on 4-week-old soil-grown plant leaves were performed essentially according to Wang et al. 2017.

Hormone Measurements and Oxylipin Profiling

Hormone extraction and measurements were done based on Wang et al., 2017. 12OH-JA and 12OH-JA-Ile were added as standards. Their transitions from deprotonated molecules to characteristic product ions were monitored (12OH-JA, m/z 225.09 > 58.90; 12OH-JA-Ile, m/z 338.23 > 130.09), and the collision energies and source cone potentials were optimized for each compound with the QuanOptimize software before integration into the LC-MS/MS method.

For oxylipin profiling, oxidized lipids were extracted and analyzed using a Waters Xevo G2-XS Q-TOF mass spectrometer according to Wang et al. 2017. The metabolite chromatograms from the WT and the *PLIP*-OX leaves samples were normalized and aligned using the Progenesis QI software (version 2.2) to identify peaks accumulated in the *PLIP*-OX, but not the WT samples. Identification of the Arabidopside metabolites was based on their accurate masses and the signature OPDA or dn-OPDA fragment ions (m/z values are 291.19 and 263.16, respectively). The peak areas of the Arabidopsides were normalized to that of the 18:3/18:3-DGDG ([M-H]-, m/z 981.61).

Accession Numbers

Sequence data from this article can be found in the Arabidopsis TAIR database (https://www.arabidopsis.org/) under the following accession numbers: At3g61680 for *PLIP1*, At1g02660 for *PLIP2*, At3g62590 for *PLIP3*, At5g24780 for *VSP1*, At3g45140 for *LOX2*, At1g32640 for *MYC2*, At1g19180 for *JAZ1*, At5g13220 for *JAZ10*, AT2G27690 for *CYP94C1*.

RESULTS

PLIP2 and PLIP3 are Putative Paralogs of PLIP1 in Arabidopsis

PLIP1 was included in the Chloroplast 2010 project studying chloroplast targeted proteins (Ajjawi et al., 2010) and later characterized as a phospholipase A_1 enzyme leading to acyl export from the chloroplasts and contributing to seed oil biosynthesis (Wang et al., 2017). Comparing the PLIP1 protein sequence against the Arabidopsis proteome using BLASTp with default settings in TAIR (http://www.arabidopsis.org) identified two putative paralogs of PLIP1 in Arabidopsis encoded by AT1G02660 and AT3G62590, which were designated PLIP2 and PLIP3, respectively. Phylogenetic analysis of the top 20 Arabidopsis proteins similar to PLIP1 (Figure 4.2) showed that PLIP2 and 3 closely clustered with PLIP1, but were distinct from other predicted α / β hydrolases. However, PLIP2 and 3 peptide sequences only share 41% and 37% identity with the PLIP1 peptide, respectively (57% and 51% similarity, respectively). PLIP2 and 3 are more closely related to each other sharing 51% identity and 65% similarity.

PLIP2 and 3 are Located in the Chloroplast

PLIP1 is imported into the chloroplast with an N-terminal transit peptide (Wang et al., 2017). PLIP2 and 3 were also predicted to be located in the chloroplast using different subcellular location prediction programs, e.g., TargetP (Emanuelsson et al., 2000) or PredSL (Petsalaki et al., 2006). To experimentally verify this prediction, the coding sequences for PLIP2 or 3 derived from an Arabidopsis wild-type (Col-0) cDNA were spliced to the open reading frame of YFP at its 5'-end (creating a C-terminal fusion of YFP to the PLIPs). When the *PLIP-YFP* constructs were stably expressed in wild type under the control of the CaMV 35S promoter, the YFP signals were observed specifically overlapping with the chlorophyll signals using confocal microscopy (Figure

4.3 A). Interestingly, the chloroplast sizes were smaller in plants overexpressing either *PLIP2* or *3* than those expressing the empty vector (EV) control. This phenotype is probably corresponding to the reduced plant size when overexpressing *PLIP* cDNAs described below.

The *PLIP2* and *3* genes are predicted to encode 78,346 D and 73, 044 D proteins, respectively. Based on the ARAMEMNON database (Schwacke et al., 2003), PLIP2 and 3 have similar predicted topologies, both containing four transmembrane domains with a very short transit peptide at the N-terminus. A chloroplast import assay was performed to confirm the plastid location of PLIP2 and 3. *PLIP2* and *3* cDNAs were translated in vitro in the presence of labeled methionine. The translation products were then tested for import into isolated pea (*Pisum sativum*) chloroplasts. As shown in Figure 4.3 B, both PLIP2 and 3 were imported into chloroplasts. During the import, the precursor protein of PLIP2 was processed to a smaller protein, while PLIP3 did not show detectable processing possibly due to the small size of the transit peptide. The PLIP2 signal was present in both the pellet and supernatant fractions. Trypsin is a protease capable of penetrating the chloroplast outer, but not the inner envelope membrane, respectively. With trypsin treatment, only the mature PLIP2 protein was retained in the smaller pellet fraction, while the soluble fraction was not affected (Figure 4.3 B). This suggests that PLIP2 is probably ubiquitously present in the chloroplast envelope membranes, stroma and thylakoids. For PLIP3, the signal was predominantly associated with the membrane fractions in the pellet and the signal intensity partially faded with trypsin treatment, indicating that PLIP3 is a membrane protein embedded in the chloroplast envelope membranes and thylakoids. Taken together, PLIP2 and 3 are likely chloroplast located proteins, but have distinct subplastid locations.

PLIP2 is a Phospholipase A_1 with Ser^{428} as the Catalytic Site

Both PLIP2 and 3 are annotated as triacylglycerol lipases in TAIR and contain conserved Lipase 3 domains similar to PLIP1. Lipases are characterized by a signature catalytic triad comprised of Ser-Asp-His, and reduced occasionally to a dyad (Ser-Asp). Sequence alignment of PLIP2 and 3 with classic lipases using NCBI's conserved domain database (Marchler-Bauer et al., 2015) identified a conserved triad in PLIP2, while only a dyad was identified in PLIP3 (Figure 4.4). To verify whether PLIP2 and 3 possess any lipase activity, recombinant *PLIP2* or *3* constructs were introduced into *E. coli* or *Saccharomyces cerevisiae* and protein production was investigated by immunoblotting against the 6 × His tag included in the N-terminus. Using different variations of the protocol, we were unable to observe production of the recombinant PLIP3 protein neither in *E. coli* nor in yeast. However, production of the recombinant PLIP2 protein and a mutant protein in which the putative catalytic residue Ser^{428} was changed to Ala ($PLIP2^{S422A}$) were successful in *E. coli* using a protocol with a brief induction period and growth under low temperature (Figure 4.5 A). Phosphatidylcholine (PC) was then provided to the microsome fractions isolated from *E. coli* cultures expressing *PLIP2* or $PLIP2^{S422A}$. At the end of the reaction, lipids were extracted and analyzed on a thin layer chromatography (TLC) plate (Figure 4.5 B). Degradation of PC and production of lyso-PC were only observed with PLIP2, but not with $PLIP2^{S422A}$, suggesting that PLIP2 is a lipase with a conserved Ser^{428} as its catalytic residue.

Detection of lyso-lipids in the lipase assay implied that PLIP2 can only hydrolyze one of the two acyl-glyceryl ester bonds in PC. To determine the positional specificity of PLIP2, two defined molecular species of PC molecules with inverted acyl compositions were offered to PLIP2. At the end of the reaction, lyso-PC was isolated by TLC, and FA methyl esters derived from the lyso-lipid were analyzed by gas-chromatography (Figure 4.6 A). For PC with acyl groups

composed of 18:1$^{\Delta 9}$/16:0 (*sn-1*/ *sn-2*) as substrates, 18:1$^{\Delta 9}$ was selectively released while 16:0 was retained. The opposite pattern was observed for lyso-PC produced from 16:0/18:1$^{\Delta 9}$-PC. These data suggested that PLIP2 preferentially hydrolyzes the *sn-1* position and, therefore, is a phospholipase A_1. To further investigate a possible acyl group preference of PLIP2 at the *sn-1* glyceryl position, PLIP2 was offered different combinations of defined PC molecules carrying the same acyl groups at the *sn-2* but acyl groups with different degrees of saturation at the *sn-1* position (Figure 4.6 B). Comparing 18:0/18:1 with 18:1/18:1 PC, PLIP2 showed slightly higher activity with 18:1/18:1 PC, while no statistically significant difference was detected between18:0/18:2 and 18:2/18:2. This result implied that, at least in vitro, PLIP2 does not have a strong preference for the degree of saturation of acyl groups and is capable of releasing both saturated and unsaturated acyl groups from the *sn-1* position.

PLIP2 Uses MGDG as Primary Substrate, While PLIP3 Uses PG

Plant glycerolipid lipases such as PLIP1 tend to be promiscuous with regard to the glycerolipid head groups in vitro, and a facile approach to investigate their substrate specificity and to identify their native substrates is to overproduce them in the plant, thereby providing them with a native lipid environment (Wang et al., 2017). Accordingly, we then took advantage of the *PLIP2* and 3 overexpressing plants that were used for the localization study above. We generated over 20 independent overexpression lines for each of *PLIP2* and *PLIP3* constructs. Three lines for each construct were chosen for further studies based on the presence of the recombinant protein as detected by confocal microscopy. It should be noted that despite the use of the strong constitutive promoters, location of PLIP2-YFP and PLIP3-YFP were strictly limited to the chloroplasts in the overexpression lines. We performed lipidomic analysis on the relative abundance of polar lipids

and the acyl composition of individual polar lipids in one empty vector (EV) control line and two *PLIP2* overexpression (*PLIP2*-OX) lines (Figure 4.7 A and Figure 4.8), as well as two *PLIP3*-OX lines (Figure 4.9). The lipid phenotype of *PLIP2*-OX and *PLIP3*-OX plants was very similar to that of the previously reported *PLIP1*-OX plants (Wang et al., 2017). Specifically, two chloroplast lipids (MGDG and PG) and ER lipids (PI, PE and PC) showed statistically significant changes in their acyl compositions. MGDG exhibited primarily decreased 16:3 to 18:3 ratios, and PG showed decreased 16:1 to 16:0 ratios in all *PLIP2*-OX and *PLIP3*-OX plants. 16:3 acyl groups are predominantly present at the *sn-2* glyceryl position of plastid pathway-derived MGDG. These changes in acyl ratios suggest that PLIP2 and 3 might have a substrate preference for plastid pathway-derived MGDG and 16:1-PG.

The steady-state compositional changes observed for the chloroplast lipids MGDG and PG led us to investigate their synthesis and turnover in vivo with pulse-chase lipid labeling analysis in both the *PLIP2*-OX and *PLIP3*-OX plants. For this purpose, [^{14}C]-acetate was used to label the *de novo* synthesized FAs in detached leaves. In the *PLIP2*-OX leaves, MGDG was labeled approximately 20% higher during the pulse phase (Figure 4.7 B), suggesting that FA incorporation into MGDG is accelerated. During the chase phase (Figure 4.7 C), the label in MGDG was lost within the first 10 hours and labeled MGDG eventually reached a level comparable to that in the EV control plants. The accelerated turnover of the MGDG pool in the *PLIP2*-OX leaves suggested that MGDG is likely the favored native substrate of PLIP2 in vivo. In contrast, for the *PLIP3*-OX plants (Figure 4.10), pulse-chase labeling data showed that the labeling of the MGDG pool was not altered. Instead, PG was labeled almost twice as high during the pulse phase in the *PLIP3*-OX plants, and the label in PG was rapidly lost during the chase phase, a pattern that resembled that

previously observed for the *PLIP1*-OX plants (Wang et al., 2017). These data suggested that PLIP3 likely uses PG as its preferred substrate as was also concluded for PLIP1 (Wang et al., 2017).

The Growth and Lipid Phenotypes are Not Correlated in *PLIP*-OX Plants

One of the striking phenotypes of the *PLIP2* and *3* overexpression plants was that their vegetative growth was severely repressed under normal growth condition (Figure 4.11 A). This growth phenotype was similar to, but more severe than that observed for the *PLIP1*-OX plants (Figure 4.11 A). Despite the fact that overexpression of *PLIPs* significantly altered plant lipid composition, it seemed unlikely that these structural lipid changes were the underlying primary cause for the growth phenotype, because the lipid phenotypes were not correlated with the growth phenotype. To illustrate this fact, acyl group ratios of the presumed PLIP-preferred substrates MGDG (18:3/16:3) and PG (16:0/16:1) were chosen as representative indicators (Figure 4.11 A bottom panel). Based on these indicators, *PLIP1*-OX plants exhibited the most severe lipid changes, but showed the mildest growth reduction among all the *PLIP*-OX plants. On the contrary, the *PLIP2*-OX plants exhibited severely reduced vegetative growth, but only showed mild lipid changes for both MGDG and PG. This inconsistency between the lipid and growth phenotypes was also visible in the pulse-chase labeling data (Figure 4.7 and 4.10). This result implied that PLIP2 and 3 might be involved in physiological functions different from PLIP1.

The reduced vegetative growth of *PLIP2*-OX and *PLIP3*-OX plants was evident even when they grew on nutrient rich agar plates, and the *PLIP2*-OX plants are shown in Figure 6B as an example. Besides the reduced rosette sizes, these plants had shorter leaf petioles than the wild-type control plants. Also, a red pigment, likely anthocyanin, accumulated the center of the plants under normal growth conditions (Figure 4.11 B). The elevated level of the presumed anthocyanin was

particularly apparent during lipid extraction and phase partitioning as the red pigment stained the upper aqueous phase (Figure 4.11 C). Shortened petioles and accumulation of anthocyanin are typical phenotypes of plants with activated JA signaling or plants that overproduce JA, e.g., the *jazQ* (Campos et al., 2016) and the *dgl-D* mutants (Hyun et al., 2008), respectively. JA is an 18:3-FA derived phytohormone, which upon accumulation poises the plant transcriptome from growth to defense leading, among others, to reduced vegetative growth (Acosta and Farmer, 2010; Huot et al., 2014). In vitro characterization of PLIP2 determined its PLA_1 activity and capability of releasing polyunsaturated FAs (Figure 4.6). Also, PLIP2's presumed native substrate MGDG and PLIP3's presumed native substrate PG contain predominately 18:3 at the *sn-1* position. Therefore, we hypothesized that the stunted vegetative growth might be caused by the overproduction of JA and activation of the JA signaling pathway in the *PLIP*-OX lines.

To test whether JA signaling is relevant to the observed growth inhibition, the expression of JA-responsive marker genes was examined by quantitative PCR (Figure 4.11 D). As a result, all the analyzed JA maker genes were constitutively induced in the *PLIP*-OX plants, including genes involved in JA biosynthesis (*LOX2*), JA signal transduction (*MYC2*), downstream responses (*VSP1*), negative regulators of JA signaling (*JAZ1*, *JAZ10.1-3*), as well as JA catabolism (*CYP94C1*). In addition, the relative gene expression levels appeared correlated with the level of growth reduction. For example, the smallest *PLIP2*-OX plants showed the highest induction of the JA responsive genes, while *PLIP1*-OX plants only exhibited a mild induction consistent with its mild growth reduction (Figure 4.11 D). These data indicated that the JA mediated defense response is fully activated in the *PLIP*-OX plants.

Oxylipin Production and Signaling in *PLIP2*- and *3*-OX Plants

We hypothesized that the constitutively activated defense response in the *PLIP2*-OX and *PLIP3*-OX plants might be a consequence of increased levels of oxylipins, which could be produced from the FAs released by PLIP2 and 3. To investigate whether the levels of oxylipins were changed in the *PLIP2*-OX and *PLIP3*-OX plants, a targeted metabolite analysis was conducted to quantify the major phytohormone levels in leaf tissues (Figure 4.12 A). Most of the oxylipins were maintained at very low basal levels in the WT plants under the chosen growth condition (Figure 4.12 A). However, the *PLIP2*-OX plants showed increased levels of JA, OPDA, Methyl-JA, and JA-Ile. Also, two JA catabolites, 12OH-JA and 12OH- JA-Ile, accumulated to levels that were even higher than their active forms, JA and JA-Ile, respectively (Figure 4.12 A). This was consistent with the constitutive induction of JA catabolism genes in the *PLIP2*-OX plants (Figure 4.11 D), e.g., *CYP94C1* which encodes a hydroxylase involved in JA-Ile turnover (Heitz et al., 2012). Similar results were also observed in the *PLIP3*-OX plants (Figure 4.13 A).

We also tested whether other forms of oxylipins than those mentioned above accumulate in the overexpression lines. Oxylipins include classes of highly diverse and complicated lipid molecules, in which a typical fatty acid is replaced with an oxidized fatty acid (Gobel and Feussner, 2009; Mosblech et al., 2009). Oxylipins other than JA start to be recognized as important signaling molecules contributing to various aspects of plant physiology (Porta and Rocha-Sosa, 2002). To more comprehensively observe changes in oxylipin metabolism in the *PLIP2*-OX and *PLIP3*-OX plants, a non-targeted metabolite profiling was focused on extracted oxidized complex lipids using liquid chromatography-QTOF-MS. Through comparative metabolic profiling, a few metabolites were highly accumulated in the *PLIP2*-OX plants but not in the WT (Figure 4.12 B). By investigation of their accurate mass and their molecular fragmentation patterns, these metabolites

were tentatively identified as Arabidopsides (Figure 4.12 C). Arabidopsides are structurally very similar to galactolipids except they contain OPDA or dinor-OPDA instead of acyl groups at the *sn-1* and *sn-2* glyceryl positions. Arabidopsides do not usually accumulate in plants grown under normal condition unless plants are wounded. However, in the *PLIP2*-OX plants, the levels of Arabidopsides A, B and D were highly elevated. Arabidopsides have been proposed as storage pools for OPDA, and this is possibly a compensatory mechanism for fine-tuning free OPDA levels in the cells. Similarly, accumulation of these compounds was also detected in the *PLIP3*-OX plants (Figure 4.13 B).

The targeted phytohormone measurement and the non-targeted metabolite profiling strongly indicated that JA metabolism and consequently signaling were affected in the *PLIP2*-OX and *PLIP3*-OX plants. To directly test whether activated JA signaling specifically caused the reduced vegetative growth, one each of the *PLIP2*-OX and *PLIP3*-OX lines was crossed with a mutant defective in CORONATINE INSENSITIVE1 (*coi1*), carrying an knock-out mutant of the JA receptor. As a result, the growth inhibition of the *PLIP*-OX plants was completely reversed in *PLIP*-OX *coi1* homozygous offspring (Figure 4.14 A and Figure 4.15 A), while the lipid phenotypes remained the same as in the *PLIP*-OX plants (Figure 4.14 B and Figure 4.15 B). Thus, using this genetic approach, we were able to fully separate the primary lipid phenotype from the growth phenotype, confirming that the stunted growth phenotypes were caused by constitutive JA signaling due to oxylipin accumulation in the *PLIP2*-OX and *PLIP3*-OX plants.

PLIP2 and *PLIP3* Contribute to Oxylipin Production in response to ABA

The data presented thus far have only indirectly provided clues towards the biological functions of PLIP2 and 3. Taking into consideration the severely reduced vegetative growth of the

PLIP2-OX and *PLIP3*-OX plants it seemed plausible that *PLIP2* and *3* are possibly only induced under certain conditions or in specific tissues requiring increases in oxylipin levels. Based on data available at the Arabidopsis eFP browser (http://bar.utoronto.ca/efp/cgi-bin/efpWeb.cgi) (Winter et al., 2007), an online Arabidopsis transcriptomic database, *PLIP2* and *3* were specifically induced by ABA treatment as well as under ABA-mediated abiotic stress conditions (Figure 4.16). Interestingly, *PLIP2* and *3* are responsive to different abiotic stressors. Expression of *PLIP2* seems to be specifically induced by cold, while *PLIP3* is induced by osmotic and drought stress (Figure 4.16 B and D). To experimental verify ABA induction of *PLIP2* and *3*, two-week-old WT seedlings were transferred to MS agar plates containing ABA or the equivalent ethanol solvent as the Mock treatment (Figure 4.17 A). The expression of *PLIP2* and *3*, but not of *PLIP1*, was elevated within the first two-hours of exposure to ABA, and the response gradually attenuated during the following 48 hours, confirming that *PLIP2* and *3* are transcriptionally induced by ABA supplementation.

Characterization of the *PLIP2*-OX and *PLIP3*-OX plants suggested that the activity the two proteins gives rise to increased oxylipins levels and signaling. Under natural biological conditions, the expression of these genes is induced by ABA. In fact, a body of evidence shows that JA-responsive genes are also induced by ABA or conditions that lead to increased ABA levels, although mechanistic details of this relationship remain elusive (Adie et al., 2007; Valenzuela et al., 2016). To test the hypothesis that ABA induction of JA responsive genes is mediated by *PLIP* gene activation, we constructed *plip* triple mutant lines that are deficient in all three PLIP lipases. The triple mutant allowed us to address their potential functional redundancy. Two independent T-DNA insertion lines were first obtained for both PLIP2 and 3 (Alonso et al., 2003). These T-DNA insertion lines were physiologically indistinguishable from WT under normal growth

conditions (Figure 4.18 A), and their leaf lipid profile was indistinguishable from wild type as well. We further constructed the double mutant between *plip2-2* and *plip3-1* without showing any physiological phenotype under normal growth conditions. Since the *PLIP3* and *PLIP1* genes are closely linked on the same chromosome, we obtained the *PLIP* triple mutant using two different approaches, either with artificial microRNA to reduce the *PLIP1* expression, or with the CRISPR-Cas9 technology to knock out *PLIP1* in the *plip2-2/3-1* double mutant background. We obtained 14 independent microRNA knock-down lines in total, and the final two representative lines, *plip-tri1* and *plip-tri2* had no expression of *PLIP2* and *3*, but ~60% reduced expression of *PLIP1* (Figure 4.18 B). These plants were also physically nearly identical to the WT plants under normal growth conditions, and did not exhibit any lipid phenotype (Figure 4.18 C to I). For the CRISPR-Cas9 approach, we only obtained one homozygous line (*plip*-CRP) so far. Sequencing results showed that the *plip*-CRP plants have a single nucleotide insertion after the 223rd nucleotide in the *PLIP1* coding sequence, causing a frameshift (Figure 4.19).

To test the hypothesis whether PLIPs contribute to oxylipin production in response to ABA, plants were first grown on filter papers placed on top of the normal MS medium plates for two weeks. Following transfer to MS agar plates containing 10 μM ABA, quantification by LC-MS showed that oxylipins including OPDA, JA and JA-Ile were significantly elevated after 24 hours treatment (Figure 4.17 B to D) in the wild type, but their accumulation was abolished in the two *plip-tri* lines and one *plip*-CRP line (Figure 4.17 B to D), confirming that PLIPs are involved in ABA induced JA production.

PLIP 1,2,3 Triple Mutants are Hypersensitive to ABA

Aside from their inability to produce oxylipins in response to ABA application, *plip-tri* mutant germination and seedling establishment were hypersensitive to ABA. With ABA in the medium, the germination of the *plip-tri* seeds was severely reduced, although the seeds were able to germinate within two days without exogenous ABA (Figure 4.20 A). ABA hypersensitivity was also observed during seedling establishment for the *plip-tri* plants as they showed reduced growth and paler rosettes compared with the wild-type seedlings when grown on ABA-containing MS medium for two weeks (Figure 4.20 B). As established above, PLIP2 and 3 hydrolyze chloroplast membrane lipids providing 18:3 FA precursors for JA production when induced by ABA. Furthermore, decreased endogenous ABA levels were observed in the *PLIP2*-OX and *PLIP3*-OX plants which have elevated levels of oxylipins (Figure 4.12 A). To explain these observations, we hypothesize that JA antagonizes ABA anabolism or signaling, providing a feedback regulatory loop for the cooperative action of ABA and JA under certain conditions. To investigate how JA might affect ABA metabolism in WT and *PLIP*-compromised plants, we grew the plants on regular MS agar plates for two weeks, and subsequently transferred the plants to Methyl-JA containing plates. In a time-course assay from 1 to 48 h, endogenous ABA contents in different genotypes were quantified (Figure 4.12 C). ABA levels generally decreased in all the genotypes, suggesting JA might repress ABA metabolism. Furthermore, endogenous ABA levels were also found to be slightly lower in the *PLIP* compromised plants compared to the WT plants.

DISCUSSION

PLIP2 and PLIP3 Share Biochemical Properties with PLIP1

PLIP2 and PLIP3 were discovered based on their sequence similarity to PLIP1. They are more closely related to PLIP1 compared to other α / β hydrolases in the Arabidopsis genome (Figure 4.2). All three contain a conserved Lipase 3 domain. Even though we were unable to produce PLIP3 in in *E. coli* nor yeast, the PLIP2 recombinant protein was obtained (Figure 4.5). Further biochemical characterization of PLIP2 showed that it is also a Phospholipase A_1 (Figure 4.6). Lipases tend to be promiscuous with regard to offered lipid substrates *in vitro.* By ectopically overexpressing the respective lipase cDNAs in the plant, the recombinant lipases under investigation gain access to their native lipid substrates in a quasi-native environment causing changes in the lipid composition indicative of their respective substrate preference in vivo. Lipidomic analysis of the *PLIP2*-OX and *PLIP3*-OX plants showed very similar steady-state lipid changes (Figure 4.7 A, 4.8 and 4.9) compared to that of the previously reported *PLIP1*-OX plants (Wang et al., 2017), corroborating their similarity in their enzymatic activities. Especially, the correlative changes for chloroplast lipids (MGDG and PG) with ER lipids (PI, PE and PC) suggest that all three PLIPs can efficiently release polyunsaturated FAs that are subsequently exported from chloroplasts to the ER.

Further Pulse-Chase labeling analysis suggested that different *PLIP*-OX plants affect different lipid pools in vivo (Figure 4.7 and 4.10). In the *PLIP2*-OX plants, labeling and turnover of the MGDG pool was accelerated. On the other hand, the PG pool was labeled and turned over at an accelerated rate in the *PLIP3*-OX plants. These data imply that PLIP2 and PLIP3 preferentially access different substrates in vivo, PLIP2 the galactolipid MGDG and PLIP3 the phospholipid PG. Biosynthesis of both the plastid assembled MGDG and PG uses phosphatidic

acid (PA) as the common precursor. Accelerated degradation of either PG or MGDG pools requires that more plastid-derived PA, the precursor for both lipids, is diverted to other lipid pools, eventually indirectly leading to a similar ER lipid phenotype during steady state. Acyl compositional analysis of MGDG showed reduced 16:3, a signature FA of the plastid-assembled MGDG in the *PLIP2*-OX plants, corroborating the hypothesis that prokaryotic MGDG is likely the native substrate of *PLIP2*. Although PLIP2 and likely PLIP3 can act on MGDG and PG based on the available in vitro data for PLIP 1 and 2, their distinct subchloroplastid location might give s them preferential access to one or the other lipid explaining the observed apparent lipid preferences in vivo.

PLIP2 and PLIP3 are Involved in JA Biosynthesis

Overexpressing anyone of the three *PLIP* cDNAs causes a growth defect (Figure 6). This growth phenotype, however, does not correlate with the steady changes in lipid composition and hence, simply degradation of the membrane lipid composition due to increased lipase activity cannot explain this phenotype. Morphologically, the *PLIP2*-OX and *PLIP3*-OX plants resemble plants with activated defense responses (Figure 4.11). Indeed, JA-responsive marker genes were constitutively induced in the *PLIP*-OX plants, and their induction levels matched the severity of the growth reduction (Figure 4.11). Oxylipins including Arabidopsides accumulated in the *PLIP2*-OX and *PLIP3*-OX plants, (Figure 4.12). Arabidopsides were previously observed at very high levels in vegetative tissues after wounding or during the pathogen-induced hypersensitive response (Andersson et al., 2006; Buseman et al., 2006). Even though some of the Arabidopside species have been shown to directly participate in plant defense (Kourtchenko et al., 2007), they are generally thought to provide a temporary, inert storage pool for OPDA (Mosblech et al., 2009).

The biosynthesis of Arabidopsides is still a matter of debate, but in the *PLIP2*-OX and *PLIP3*-OX plants, Arabidopsides possibly serve to sequester the levels of free OPDA as a result of increased 18;3 release by the PLIPs. After PLIP2 or PLIP3 release the polyunsaturated FAs, free OPDA readily accumulates in the plastids possibly by oxidation of 18:3. OPDA is structurally a fatty acid, and may be detrimental to the cell in high quantities simply due its detergent properties. Presumably, a fraction of the free OPDA is converted to OPDA-Acyl Carrier Protein (ACP), which serves as substrate for the plastid acyl transferases that either assemble membrane lipids de novo or catalyze acyl exchange on existing membrane lipids giving rise to the observed Arabidopsides. This mechanism can also likely provide feedback regulation for the fine tuning of JA biosynthesis and signaling along with JAZ repressors and JA catabolism (Figure 4.11 and 4.12).

Finally, to examine whether the growth repression phenotype was specifically caused by JA metabolism and signaling, and no other factors, the *PLIP2*-OX and *PLIP3*-OX plants were crossed with a *coi1* mutant allele, which abolishes JA perception in plants (Figure 4.14). Homozygous *coi1* offspring in the PLIP-OX backgrounds reversed their stunted growth without affecting the lipid phenotype. Taken together, these data led to our hypothesis that PLIP2 and PLIP3 might be involved in initiating JA metabolism under conditions when they are overproduced, for example, following activation of their respective genes in response to environmental cues.

PLIP2 and PLIP3 Link ABA Signaling with JA Biosynthesis

As the three PLIPs possess similar biochemically characteristics, the question arises how they exert their distinct physiological roles. One possible explanation is their different subplastidic locations. PLIP1 is specifically associated with the thylakoid membranes (Wang et al., 2017).

Based on our current analysis, PLIP3 is a membrane protein associated with both the envelope and thylakoid membranes, while PLIP2 is found in the soluble and membrane fractions, and seems to be ubiquitously present in envelope membranes, stroma and thylakoids (Figure 4.3). Possibly, PLIP2 and PLIP3 are enriched in microenvironments that are in close proximity to other enzymes required for oxylipin synthesis, like lipoxygenase, Allene Oxide Synthase and Allene Oxide Cyclase to readily convert free FAs to oxylipins.

Another possible factor that could lead to distinct physiological functions might be the differing transcriptional regulation of their respective genes. *PLIP1* is specifically expressed during seed developmental stages, and has much lower basal expression levels in the leaf tissues compared to *PLIP2* and *PLIP3.* In addition, the expression of *PLIP2* and *PLIP3* in leaf tissues is ABA responsive, but that of *PLIP1* is not (Figure 4.16 and 4.17). Moreover, despite the fact that both *PLIP2* and *3* can be induced by applied ABA, public transcriptomic data show that they are induced by different abiotic stresses in vivo (Figure 4.16), implying that each of the two genes contain their own unique cis-elements in their promoters that can be recognized by different transcription factors sensing different stressors.

Having roles in both ABA responses and JA biosynthesis, PLIP2 and PLIP3 we hypothesize that they can mediate ABA induction of JA biosynthesis. Given the relatedness of their biochemical properties and subtle phenotypes of the individual mutants, triple PLIP1, 2, 3 mutants were generated. Two approaches, artificial microRNA and CRISPR-Cas9, were successful in overcoming the the close genetic linkage between *PLIP2* and *PLIP3* (Figure 4.18 and 4.19). All *plip* triple mutant lines exhibited compromised oxylipin biosynthesis in response to applied ABA (Figure 4.17), corroborating their roles in mediating ABA responsiveness of JA biosynthesis. JA production is most commonly induced by wounding damage due to herbivore

insects or necrotrophic microbes (Creelman et al., 1992; Trusov et al., 2006). Furthermore, a growing body of evidence suggests that JA biosynthesis is also stimulated by applying ABA to plants or during abiotic stress conditions that lead to ABA accumulation (Creelman and Mullet, 1995; Adie et al., 2007; Avramova, 2017). The transcription factor MYC2 has been proposed as a potential component in linking ABA and JA mediated physiological responses given its involvement in both JA perception and ABA signaling (Kazan and Manners, 2013). So far, it is still unknown how or even whether MYC2 contributes to ABA induced JA production. In the future, it would be interesting to investigate whether MYC2 is directly involved in the transcriptional induction of *PLIP2* or *PLIP3*, to determine whether MYC2 and PLIPs work in the same pathway. It is also important to study each PLIP gene's unique timing and its range of responsiveness to different environmental cues. In nature, plants continually encounter different adverse environmental conditions. Possibly, the PLIP genes evolved allowing plants to cope with different abiotic / biotic stresses and integrate their protective responses for example during coinciding drought conditions and insect outbreaks (Suzuki, 2016).

Aside of their inability to induce JA biosynthesis in response to ABA application, the *plip* triple mutants were also hypersensitive to ABA during germination and early seedling development (Figure 4.20). Application of JA treatment to the WT and the *plip* triple mutant seedlings led to a trend of gradually decreasing ABA levels in all the genotypes overtime (Figure 4.20). Decreased ABA content was also observed in the *PLIP2*-OX plants (Figure 4.12). Therefore, one possible explanation for the ABA hypersensitivity phenotype might be that JA negatively regulates ABA biosynthesis. However, other possibilities cannot be precluded at this point. For example, besides ABA metabolism, it is important to investigate whether PLIP2 and PLIP3 are directly or indirectly involved in ABA signaling. It is possible that other oxylipin

products as a result of PLIP2 and PLIP3 activation serve as negative regulators of ABA signaling, a possibility that still needs to be further explored.

ACKNOWLEDGEMENTS

This work was done in collaboration with several collaborators. John E. Froehlich conducted the chloroplast import assay in Figure 4.3. Hope L. Hersh generated the *plip*-CRISPR lines in Figure 4.19. I would also like to thank Dr. Ronghui Pan and Dr. Jianping Hu, Michigan State University for providing the artificial microRNA constructs; Dr. Sheng Yang He, Michigan State University and Dr. Jian-Kang Zhu, Purdue University for providing the CRISPR-Cas9 constructs and instructions; Dr. Anthony Schilmiller, Michigan State University for assisting with the plant hormone measurement and oxylipin profiling assays. We would also like to thank Dr. Koichi Sugimoto, Michigan State University for generally sharing the standards of JA-Ile, 12OH-JA and 12OH-JA-Ile; Dr. Jian Yao in Sheng Yang He lab for providing the *coi1-30* mutant seeds, Michigan State University for helpful discussions and suggestions.

APPENDIX

Primer	Sequence 5' – 3'	Purpose
PEG_PLIP2 F	CACCATGGACAGTTTGTGTTTGAA T	For pEarlyGate 101
PEG_PLIP2 R	TCAACGGAAACTAAAGACGTTGA	For pEarlyGate 101
PEG_PLIP3 F	CACCATGGAGGGTGTTTTCTTAAAA AT	For pEarlyGate 101
PEG_PLIP3 R	TCACTTGAAGAAACTAAAATGTGCT TG	For pEarlyGate 101
BamHI_PLIP2 F	TCGGATCCATGGACAGTTTGTGTTT GAATAG	For the pET41a to produce PLIP2 in *E. coli*
PLIP2_XhoI R	GACTCGAGTCAACGGAAACTAAAG ACGTT	
BamHI_PLIP3 F	TCGGATCCATGGACAGTTTGTGTTT GAATAG	For the pET41a to produce PLIP3 in *E. coli*
PLIP3_SalI R	GAGTCGACTCACTTGAAGAAACTA AAATGTGC	
PLIP2_pYes2.1 F	GCCATGGACAGTTTGTGTTTGAATA G	For the pYes2.1 to produce PLIP2 in yeast
PLIP2_pYes2.1 R	ACGGAAACTAAAGACGTTGAAAGC	
PLIP3_pYes2.1 F	GCCATGGAGGGTGTTTTCTTAAAAA T	For the pYes2.1 to produce PLIP3 in yeast
PLIP3_pYes2.1 R	CTTGAAGAAACTAAAATGTGCTTGT GA	
pET41a_His del F	ATGTATATCTCCTTCTAAAGTAAAC AAA	pET41a construct for chloroplast import
pET41a_His del R	ATGGCGTTTAATACGGCTATG	
PLIP2_S428A F	ACCGGTCATGCATTAGGTGGA	S428A point mutation
PLIP2_S428A R	GAAACGGAATTTAGCGCTGGT	
PLIP2_qPCR F	AGCGACAGATCGGCTTATGG	For qPCR analysis of *PLIP2* expression
PLIP2_qPCR R	GCGATGCTCCCTTTTTGCTC	
PLIP3_qPCR F	CAGATGTTTGCCAAATTGTCGT	For qPCR analysis of *PLIP3* expression
PLIP3_qPCR R	TCCTCGCCATTGTTGTTCTC	
TIP-41_like F	GTGAAAACTGTTGGAGAGAAGCAA	qPCR reference gene
TIP-41_like R	TCAACTGGATACCCTTTCGCA	
UBQ10 qPCR F	TCCGGATCAGCAGAGGCTTA	qPCR reference gene
UBQ10 qPCR R	TCAGAACTCTCCACCTCAAG	
LBb1.3	ATTTTGCCGATTTCGGAAC	For genotyping of *plip2* and 3 mutants
plip2-1 LP	CACAATCCACTTCGTCTCCTC	For genotyping of *plip2-1*
plip2-1 RP	CAACAGTAGAAGACAAGGCGC	
plip2-2 LP	AAATCGCTAGCTATGCTGCAG	For genotyping of *plip2-2*
plip2-2 RP	TCCAATAACGGTTAAGCAACG	

Table 4. 1. Primer sequences used in this study.

Table 4. 1. (cont'ed)

	AAAGGAAGATTTGATCGGACG	For genotyping of *plip3-1*
plip3-1 LP		
plip3-1 RP	CAACAGTAGAAGACAAGGCGC	
plip3-2 LP	TTACCAGAAGTTCATGCCCAC	For genotyping of *plip3-2*
plip3-2 RP	AAATCTCTTGCATTTCCTCGC	
PLIP1-miRNA I	gaTCTTAAAACGTCATTTGCCGGctctc ttttgtattcca	
PLIP1-miRNA II	agCCGGCAAATGACGTTTTAAGAtcaa agagaatcaatga	For knocking down *PLIP1* with artificial microRNA
PLIP1-miRNA III	agCCAGCAAATGACGATTTAAGTtcac aggtcgtgatatg	
PLIP1-miRNA IV	gaACTTAAATCGTCATTTGCTGGctaca tatatattccta	
VSP1 F	AGAGCTGGAGCTGGTGTTGTTAAG	For qPCR analysis of *VSP1* (At5g24780) expression
VSP1 R	GAACACCCATTCCGGTAACACCAT	
LOX2 F	GGGCGTACTGGTCGTGGTTA	For qPCR analysis of *LOX2* (At3g45140) expression
LOX2 R	TCCCGAGTTCCAAGAGGTTTT	
MYC2 F	AGAAACTCCAAATCAAGAACCAGC TC	For qPCR analysis of *MYC2* (At1g32640) expression
MYC2 R	CCGGTTTAATCGAAGAACACGAAG AC	
JAZ1 F	GCACCGCTAATAGCTTAGCCAAGA	For qPCR analysis of *JAZ1* (At1g19180) expression
JAZ1 R	TCTGTCAATGGTGTTGGGGAGGAT	
JAZ10.1-3 F	AGAGCTGGAGCTGGTGTTGTTAAG	For qPCR analysis of *JAZ10.1*, *10.2* and *10.3* (At5g13220) expression
JAZ10.1-3 R	GAACACCCATTCCGGTAACACCAT	
CYP94C1 F	TCTCACTCTTTCACTTACTCTTCC	For qPCR analysis of *CYP94C1* (AT2G27690) expression
CYP94C1 R	CGTTTGATGGATTCGCTGTG	
coi1-30 F	atggaggatcctgatatcaag	For genotyping the *coi1-30* locus
coi1-30 R	AGTCACTGACAATCATCCGTCG	
pROK2-LB3	TTGGGTGATGGTTCACGTAG	
PLIP1 CPR F	gattGATGAAAACGAGTCGATCTG	For knock out PLIP1 with CRISPR-Cas9
PLIP1 CPR R	aaacCAGATCGACTCGTTTTCATC	
PLIP1 CPR_geo F	ATCGAGTTCCGACAATCACTTGT	For genotyping of the CRISPR-Cas9 lines
PLIP1 CPR_geo R	GACGTGTCCGTTTCAAATAGCAAC	

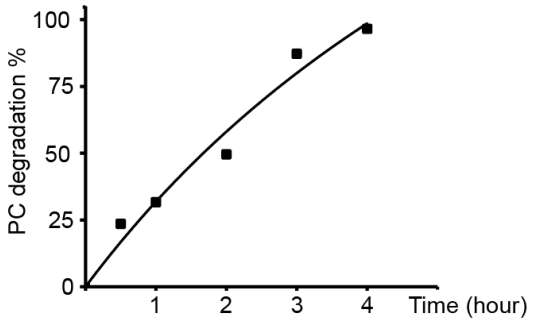

Figure 4. 1. Time course of PLIP2 lipase activity with phosphatidylcholine (PC) as substrate. As substrate, 120 µg 18:1/18:1-PC was provided to microsomal recombinant PLIP2 and the lipase assay was stopped at times indicated. Lipids were subsequently extracted and analyzed by TLC. Remaining PC and produced lyso-PC were isolated and their acyl contents were quantified as methyl esters by liquid gas chromatography. Fractions of PC degradation at different times is calculated as 2 (molarity of lyso-PC acyl groups) / (2 (molarity of lyso-PC acyl groups) + (molarity of PC acyl groups)) *100.

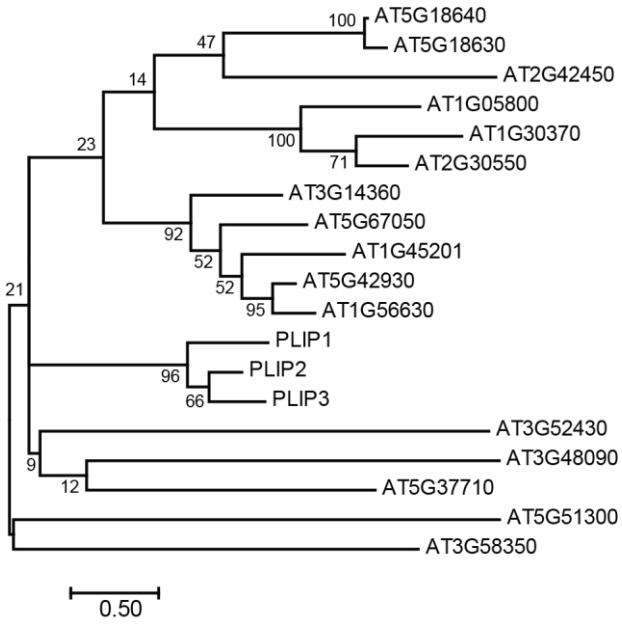

Figure 4. 2. Phylogenetic analysis of the top 20 PLIP1 similar sequences in Arabidopsis. The phylogenetic tree was built using the Maximum Likelihood method with PLIP1and the top 20 Arabidopsis similar protein sequences identified from the BLASTp search. Sequences alignments are shown in Supplemental File 1. Bootstrap values (based on 1000 replicates) are indicated at the tree nodes. The scale measures evolutionary distances in substitution per amino acid.

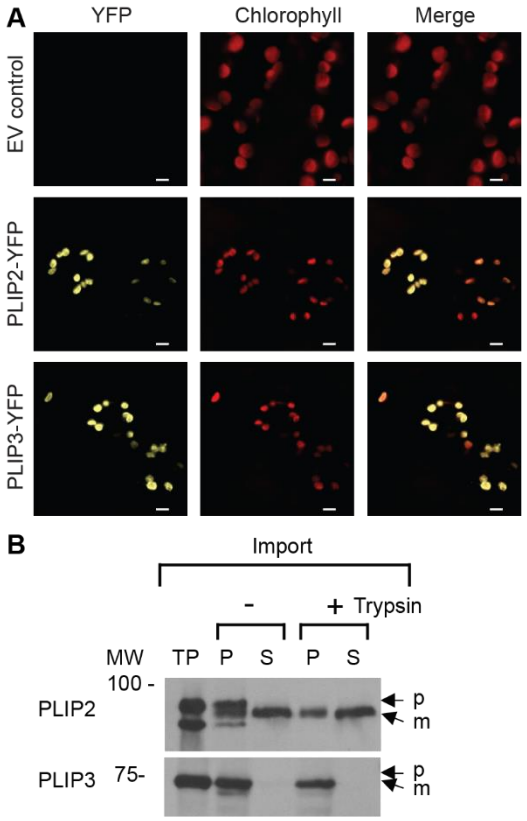

Figure 4. 3. Subcellular localization of PLIP2 and PLIP3 in Arabidopsis.
(A) Subcellular localization of YFP tagged PLIP2 and PLIP3 in leaf mesophyll cells of 3-week-old Arabidopsis Col-0 transformed with *PLIP2-YFP* or *PLIP2-YFP* driven by the 35S promoter, or empty vector (EV) control using confocal laser scanning microscopy. Chlorophyll autofluorescence is shown in red, and YFP fluorescence is shown in yellow. Overlay of chlorophyll and YFP are shown as well (Merge). Representative images from one experiment are presented. Scale bars: 5 µm.
(B) Chloroplast import experiments with radiolabeled PLIP2 and PLIP3. Chloroplasts were treated with (+) or without (-) trypsin. Total chloroplast membranes (P) or soluble (S) fractions were analyzed by SDS-PAGE followed by fluorography. TP, translation products; p, precursor; m, mature form; MW, molecular weight markers.

Figure 4. 4. Alignment of PLIP2 (A) and PLIP3 (B) with class 3 lipase protein sequences available in the NCBI conserved domain database (CDD).

The alignment result was produced by blasting the PLIP2 or PLIP3 protein sequence against the CDD database using CD-search (https://www.ncbi.nlm.nih.gov/Structure/cdd/wrpsb.cgi) with default settings. Reference protein names are represented as either Protein Data Bank ID (e.g., 1TIA and 3TGL) or as NCBI GI number. The conserved catalytic triads are highlighted in yellow, and the non-conserved in grey.

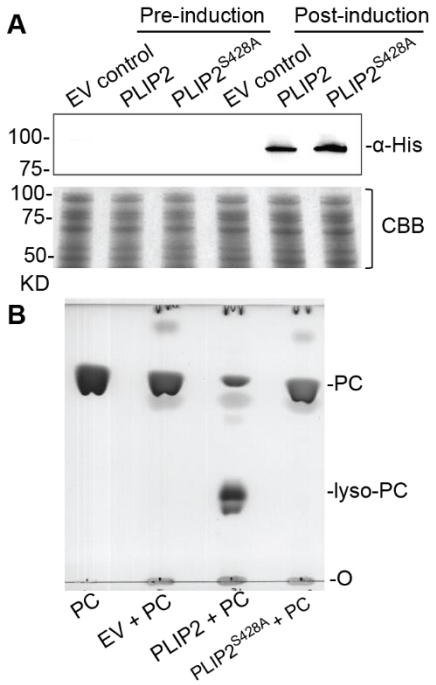

Figure 4. 5. Production of the recombinant PLIP2 proteins and its lipase activity in vitro.
(A) Detection of PLIP2 and PLIP2^{S428A} protein by immunoblotting against the N-terminus 6 × His tag (top panel) and Coomassie Brilliant Blue (CBB) staining (bottom panel) in the lysed *E. coli* cultures with or without isopropyl β-D-1-thiogalactopyranoside induction. The *E. coli* strain carrying the empty vector (EV) was included as a negative control.
(B) Thin-layer chromatogram of products of a representative in vitro lipase reaction using PC with *E. coli* microsomes carrying the wild-type (PLIP2 + PC), or the mutant enzyme (PLIP2^{S428A} + PC). Substrate without enzyme (PC) or with *E. coli* microsome carrying the EV control (EV + PC) were included as controls. PC, phosphatidylcholine. O, origin of sample loading. Lipids were visualized by iodine vapor staining.

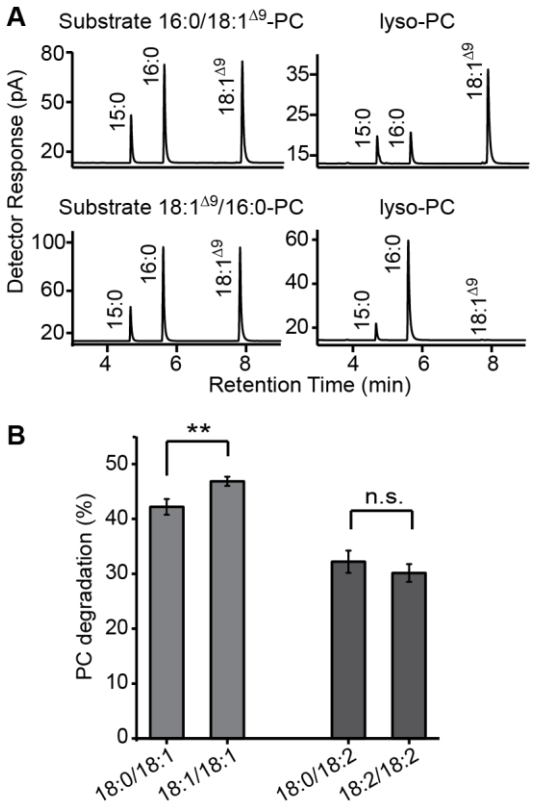

Figure 4. 6. In vitro lipase activity of PLIP2.
(A) Gas-liquid chromatograms of methyl esters derived from defined PC substrates or lyso-PC fractions from PLIP2 lipase reactions with different PC substrates. 15:0 was used as an internal standard.
(B) PLIP2 lipase activity on defined PC substrates (carbon number : double bond number; *sn-1/sn-2*) with different degree of saturation of the *sn-1* acyl groups. PC containing 18:0/18:1 and 18:1/18:1 and PC containing 18:0/18:2 and 18:2/18:2 were compared, respectively. $n = 4$, ± SD. Student's *t*-test was applied (**indicates $p<0.01$; n.s., not significant).

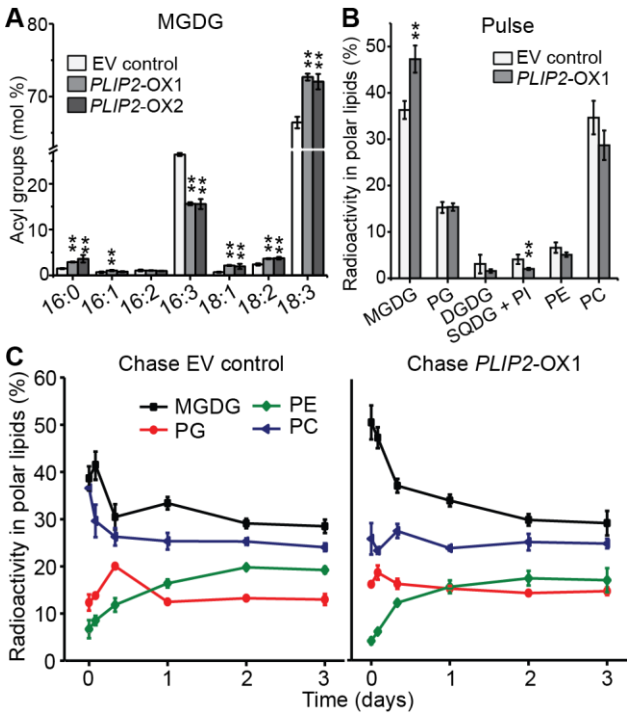

Figure 4. 7. The steady-state and dynamic lipid phenotypes of the *PLIP2*-OX plants.
(A) Relative acyl composition of monogalactosyldiacylglycerol (MGDG) in *PLIP2*-OX and empty vector (EV) control lines. Leaf samples harvested from one plant were pooled as one biological repeat; $n = 4$, ± SD. Student's *t*-test was applied to compare the empty control (EV) control plants with each of the two *PLIP2*-OX plants (**indicates $p<0.01$).
(B) and **(C)** In vivo pulse-chase acetate labeling of lipids in the EV control and the *PLIP2*-OX1 plants. The [^{14}C]-acetate labeling pulse lasted for 60 min. The fractions of label in all polar lipids were calculated as percentages of total incorporation of label in polar lipids **(B)**. After the pulse, [^{14}C]-acetate medium was replaced with non-labeled free acetate to initiate the chase with a duration of three days **(C)**. The fractions of label in all polar lipids is given during time course. Experiments were repeated three times with similar results and one representative result is shown. $n = 3$, ± SD. MGDG, monogalactosyldiacylglycerol; PC, phosphatidylcholine; PE, phosphatidylethanolamine; PG, phosphatidylglycerol.

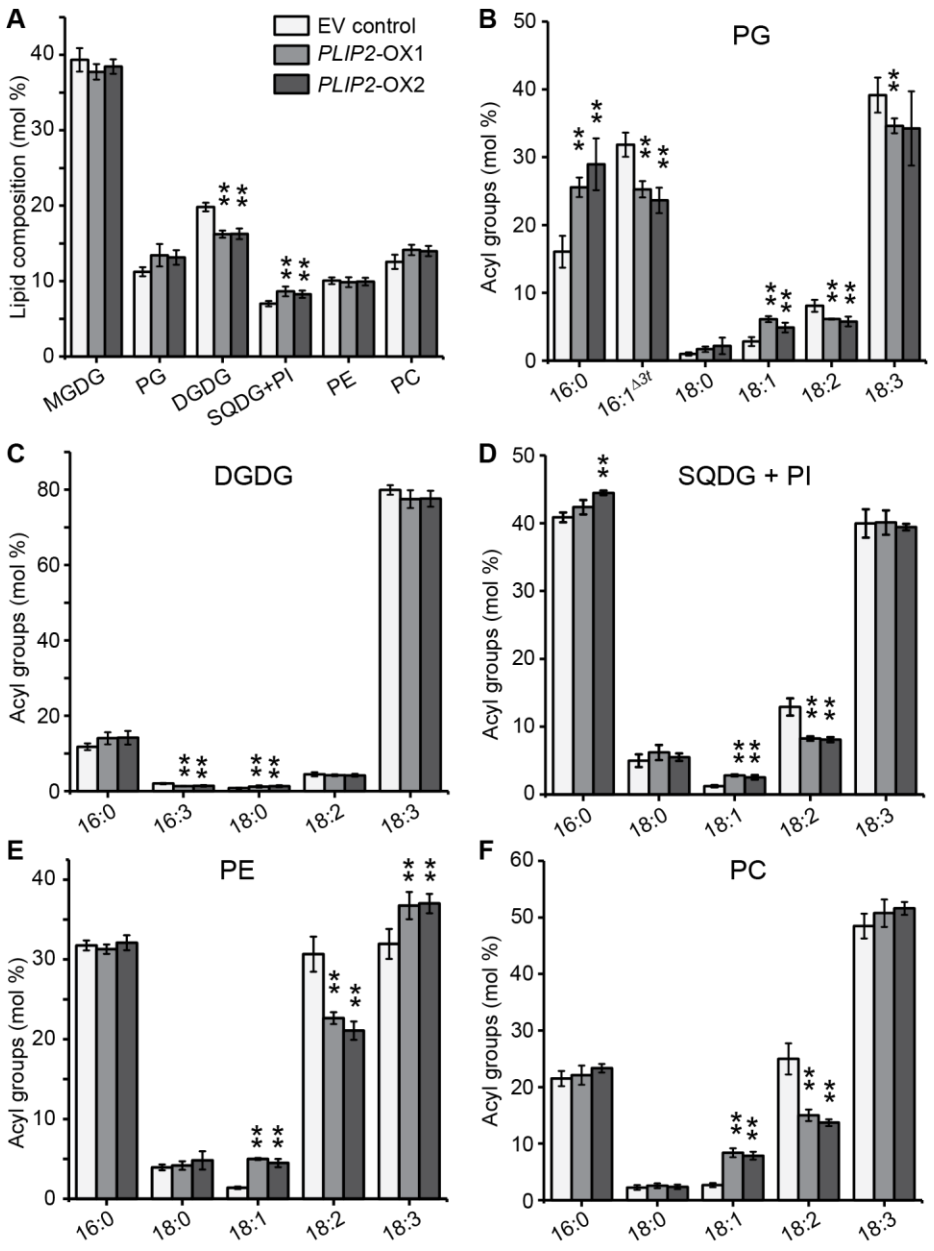

Figure 4. 8. Analysis of polar lipids from the 4-week-old soil-grown *PLIP2*-OX and empty vector (EV) control plant leaves.

(A) Relative abundance of major polar lipid classes in *PLIP2*-OX and EV control lines.

(B-F) Relative acyl group composition of PG, DGDG, SQDG, PI, PE and PC supplemental to data shown in Figure 5A. $n = 4$, ± SD. Student's *t*-test was applied (** indicates $p<0.01$). DGDG, digalactosyldiacylglycerol; PC, phosphatidylcholine; PE, phosphatidylethanolamine; PG, phosphatidylglycerol; PI, phosphatidylinositol; SQDG, sulfoquinovosyldiacylglycerol. Acyl groups with a molar percentage less than 0.5% were omitted.

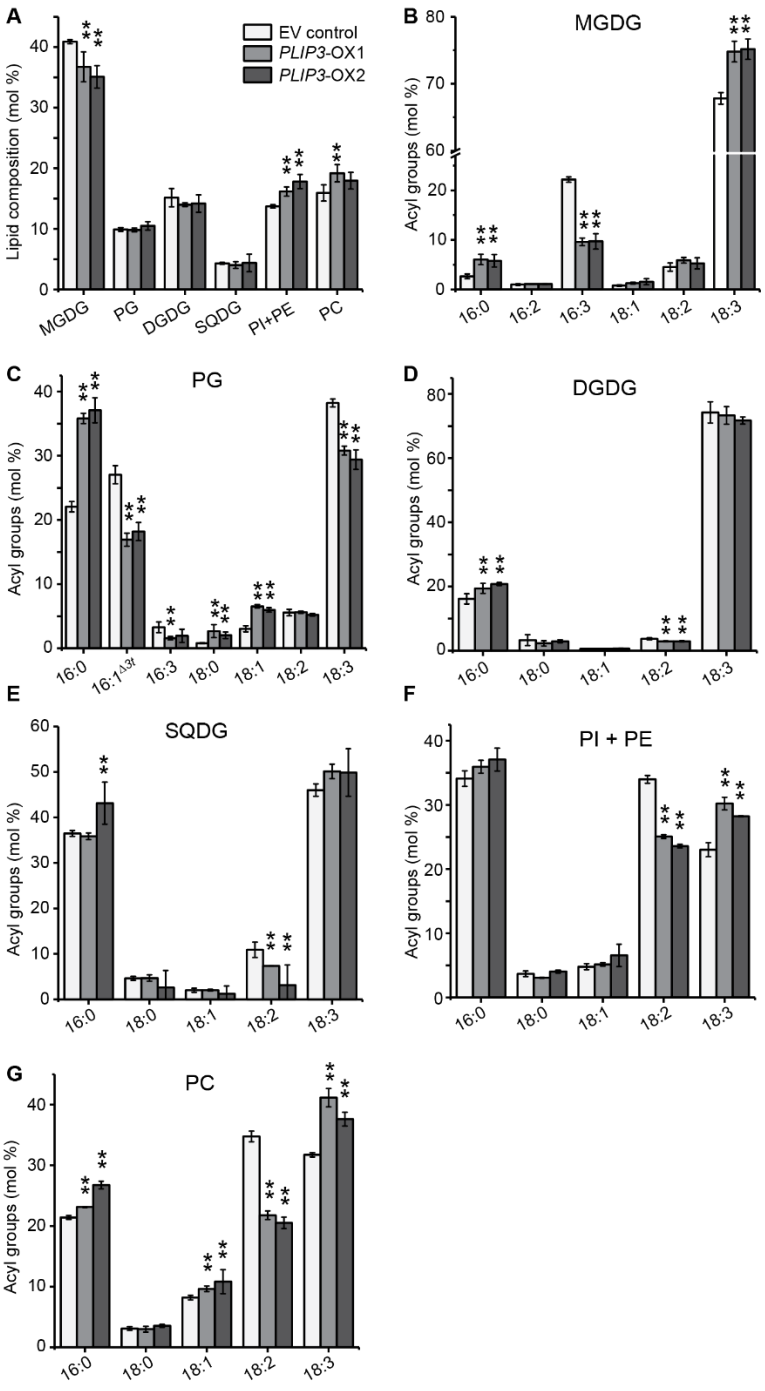

Figure 4. 9. Analysis of polar lipids from 4-week-old soil-grown *PLIP3*-OX and empty vector (EV) control plant leaves.

(A) Relative abundance of major polar lipid classes in *PLIP3*-OX and EV control lines.

(B-G) Relative acyl group composition of MGDG, PG, DGDG, SQDG, PI, PE and PC. $n = 4$, ± SD. Student's *t*-test was applied (** indicates $p<0.01$). DGDG, digalactosyldiacylglycerol; MGDG, monogalactosyldiacylglycerol; PC, phosphatidylcholine; PE, phosphatidylethanolamine; PG, phosphatidylglycerol; PI, phosphatidylinositol; SQDG, sulfoquinovosyldiacylglycerol. Acyl groups with a molar percentage less than 0.5% were omitted.

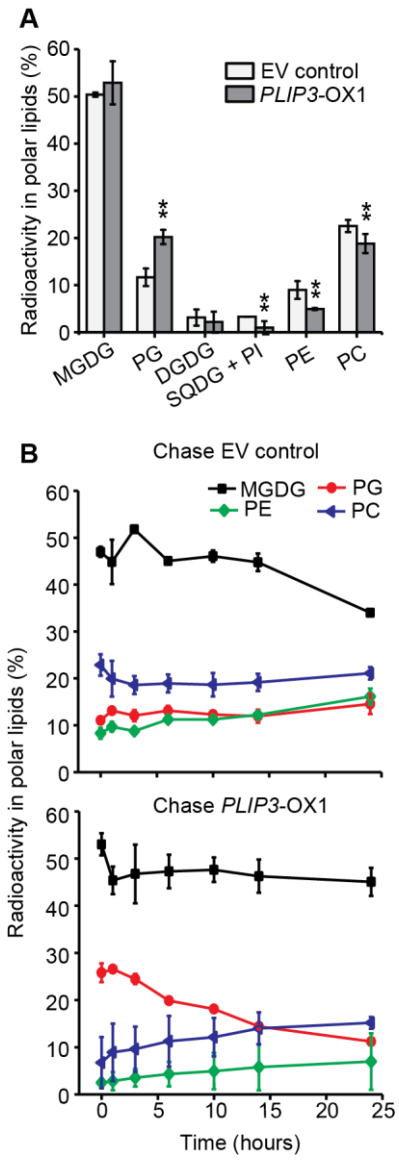

Figure 4. 10. In vivo pulse-chase acetate labeling of polar lipids in the empty vector (EV) control and the *PLIP3*-OX plants.

(A) Radioactivity in the lipids at 40 min of the pulse phase. The [^{14}C]-acetate labeling pulse lasted for 60 min. Detached leaves of 4-week-old plants were used. The fractions of label in individual polar lipid were calculated as percentages of total incorporation of label in polar lipids.

(B) Chase of the polar lipids in the EV control and the *PLIP3*-OX plants. After the pulse, [^{14}C]-acetate medium was replaced with non-labeled free acetate to initiate the chase with a duration of 24 hours. The fractions of label in all polar lipids were determined during a time course. Experiments were repeated three times with similar results and one representative result is shown. *n* = 3, ± SD. MGDG, monogalactosyldiacylglycerol; PC, phosphatidylcholine; PE, phosphatidylethanolamine; PG, phosphatidylglycerol.

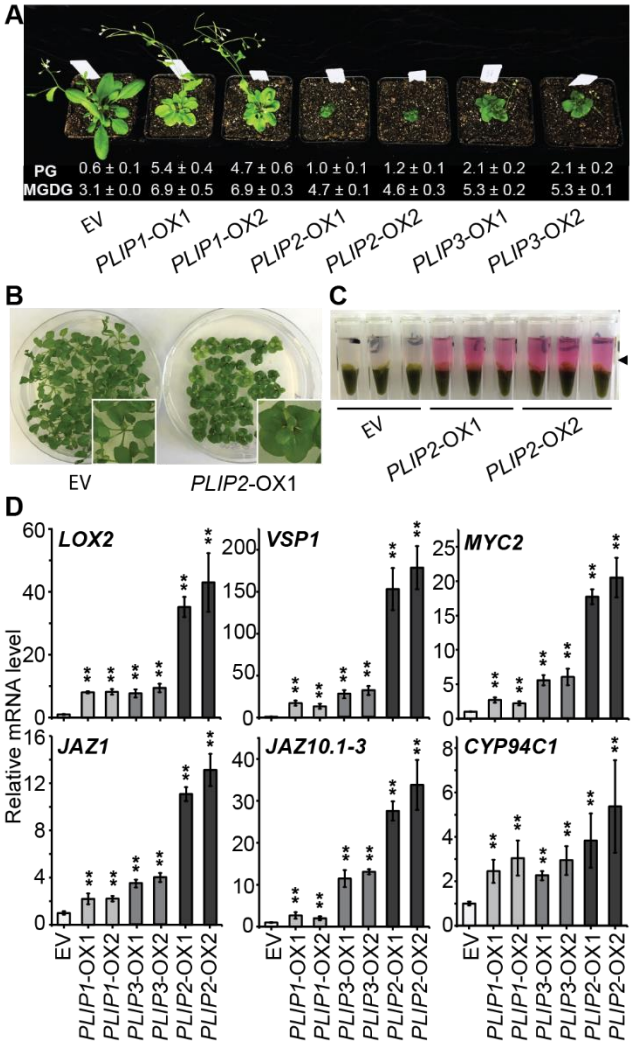

Figure 4. 11. Morphology of the *PLIP*-OX plants.

(A) Growth of 4-week-old soil-grown plants. One empty vector (EV) control line, two lines of *PLIP1*-OX, *PLIP2*-OX and *PLIP3*-OX plants are shown. The relative mol % fraction of PG and MGDG in each line are indicated. $n = 4$, ± SD.

(B) Morphology of the 24-day-old EV and *PLIP2*-OX1 plants grown on MS agar medium. Inserts show representative individual plant for details.

(C) Phase separation of the lipid extracts from the EV and *PLIP2*-OX plants in **(B)**. Three independent extracts are shown for each genotype. The upper aqueous phases accumulating anthocyanin are indicated by an arrow. The image was taken with the plastic reaction tubes inserted into transparent glass tubes on a rack.

(D) Expression of JA responsive genes in the EV and the *PLIP*-OX plants. Expression levels of indicated genes were determined by quantitative RT-PCR and normalized to the levels in the EV plants as fold changes. Analysis of *JAZ10* includes *JAZ10.1, 10.2* and 10.3, but not *10.4* splicing forms; $n = 3$, ± SD. Student's *t*-test was applied to compare the level in the EV plants and every other genotype (**indicates $p<0.01$).

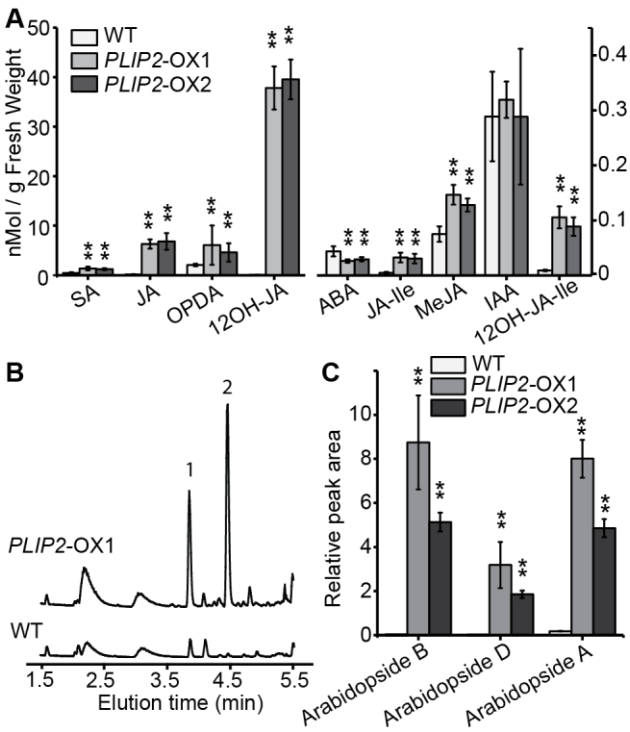

Figure 4. 12. Phytohormone quantification and comparative oxylipin profiling in the WT and the *PLIP2*-OX plants.

(A) Plants were grown on soil for three weeks before the leaves were harvested for hormone extraction and quantification by LC-MS/MS. The two y-axes apply to compounds with different order of magnitudes in quantity on the left and right panels, respectively. $n = 4$, ± SD. Student's *t*-test was applied to compare the level in the EV plants and to each other *PLIP2*-OX line (**indicates $p<0.01$).

(B) Partial metabolite profiling chromatographs from three-week-old wild-type (WT) and *PLIP2*-OX1 plant leaves. Numbers indicate the two representative metabolite peaks that are elevated in the *PLIP2*-OX1 plants compared to WT. 1 represents Arabidopside A, 2 Arabidopside B.

(C) Relative amount of the three major oxylipins accumulating in the *PLIP2*-OX1 plant identified by comparative metabolite profiling in **(B)**. The indicated compound levels were normalized to the 18:3/18:3 digalactosyldiacuylglycerol which remains unchanged in WT or the *PLIP2*-OX plants. $n = 4$, ± SD. Student's *t*-test was applied (**indicates $p<0.01$).

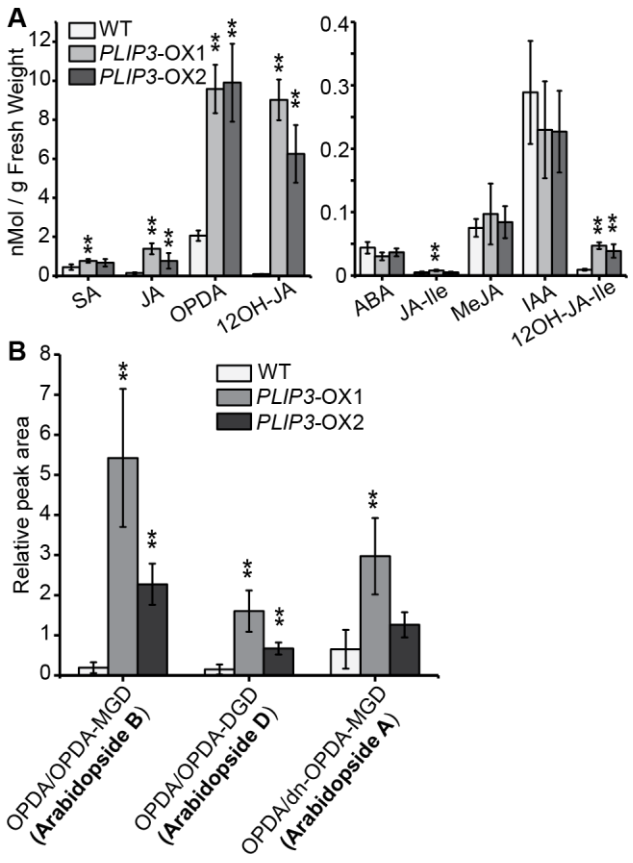

Figure 4. 13. Phytohormone quantification and oxylipin profiling in the wild-type (WT) and the *PLIP3*-OX plants.

(A) Plants were grown on soil for three weeks before the leaves were harvested for compound extraction and quantification by LC-MS/MS. $n = 4$, ± SD. Student's *t*-test was applied to compare the levels in the EV plants and each of the *PLIP3*-OX lines (**indicates $p<0.01$).

(B) Relative amounts of the three major classes of Arabidopsides in the WT and the *PLIP2*-OX1 plant leaves identified by comparative metabolite profiling. The indicated compound levels were normalized to the 18:3/18:3 digalactosyldiacuylglycerol which remains unchanged in WT or the *PLIP3*-OX plants. $n = 4$, ± SD. Student's *t*-test was applied (**indicates $p<0.01$).

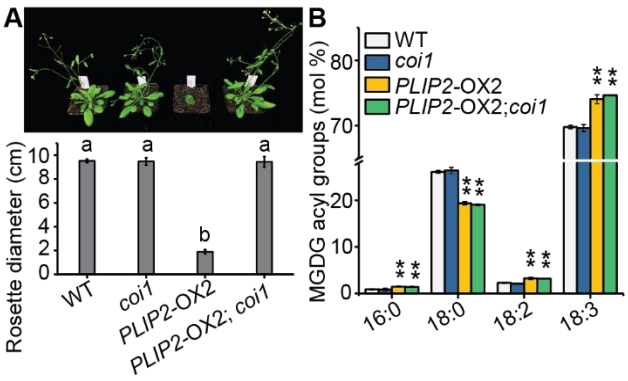

Figure 4. 14. Rescue of growth in *PLIP2*-OX *coi1* homozygous plants.
(A) Image of 4-week-old plants grown on soil and the rosette diameter of the indicated plants below the corresponding images. n = 6, ± SD. one-way ANOVA with post-hoc Turkey HSD test was applied. Rosette diameters indicated by different letters are significantly different ($p<0.01$).
(B) Relative acyl group compositions of leaf monogalactosyldiacylglycerol in the indicated plants in **(A)**. Leaves harvested from one plant were pooled as one biological repeat. n = 3, ± SD. Student's *t*-test was applied to compare the wild type (WT) with each of the remaining genotypes (**indicates $p<0.01$).

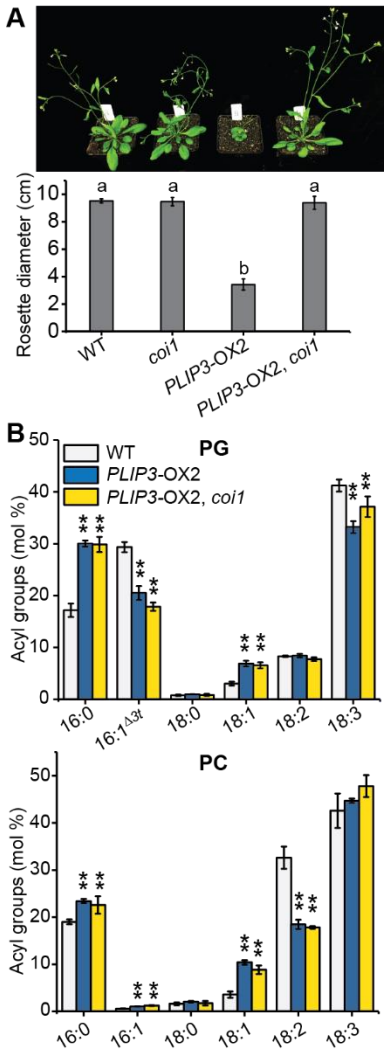

Figure 4. 15. Phenotypes of *PLIP3*-OX *coi1* plants.
(A) Image of the 4-week-old plants grown on soil and the rosette diameter of the indicated plants. n = 6, ± SD. one-way ANOVA with post-hoc Turkey HSD test was applied. Rosette diameters indicated by different letters are significantly different ($p<0.01$).
(B) Relative acyl group compositions of leaf phosphatidylglycerol (PG) and phosphatidylcholine (PC) in the indicated plants in **(A)**. Leaves harvested from one plant were pooled as one biological repeat. n = 3, ± SD. Student's t-test was applied to compare the wild type (WT) with each of the remaining genotypes (**indicates $p<0.01$).

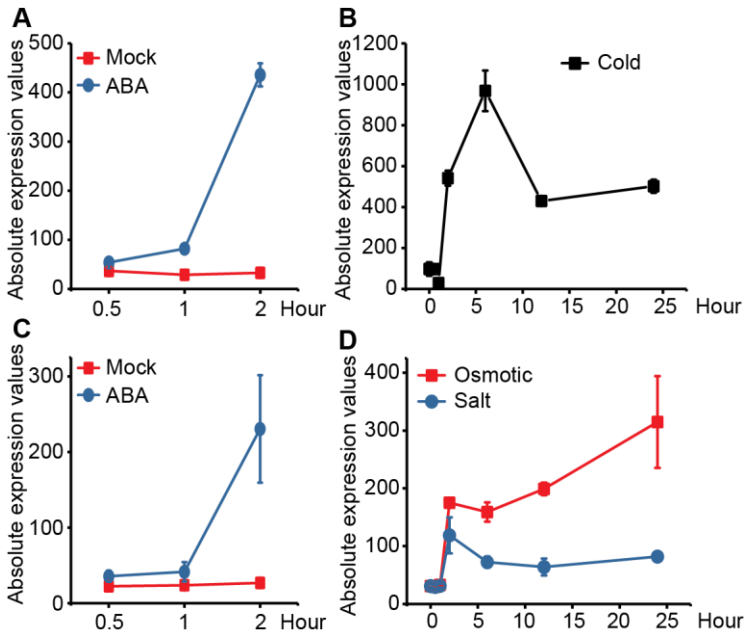

Figure 4. 16. Transcriptional induction of *PLIP2* and *PLIP3* as shown in the eFP database.
(A) and **(B)** Absolute expression values of *PLIP2* in response to ABA treatment **(A)** or under cold stresses **(B)**.
(C) and **(D)** Absolute expression values of *PLIP3* in response to ABA treatment **(C)** or under salt and osmotic stresses **(B)**. Data were extracted from the Arabidopsis eFB browser (http://bar.utoronto.ca/efp/cgi-bin/efpWeb.cgi).

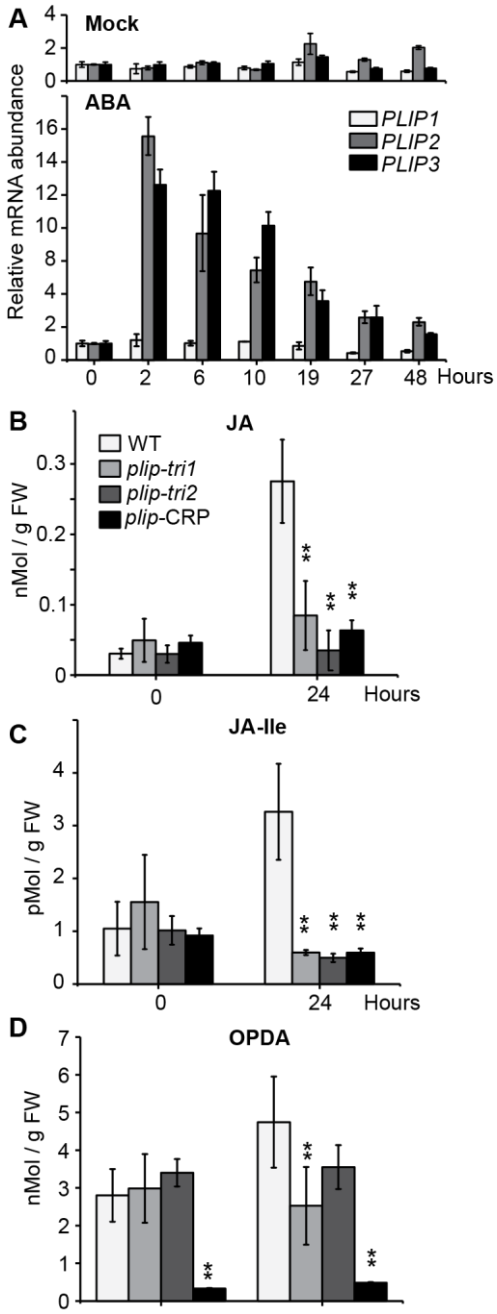

Figure 4. 17. Induction of *PLIP* transcription by ABA.
(A) Expression of *PLIP* genes in response to 7µM ABA or equivalent ethanol solution (Mock) treatment in 2-week-old seedlings determined by quantitative RT-PCR during a time course as indicated.
(B) to **(D)** Oxylipin contents in the wild-type (WT), two *plip-tri* lines and one *plip*-CRP line before and after 24-hour 7µM ABA additon. $n = 3$, ± SD. Student's *t*-test was applied to compare (WT) with each of the remaining genotypes (**indicates $p<0.01$).

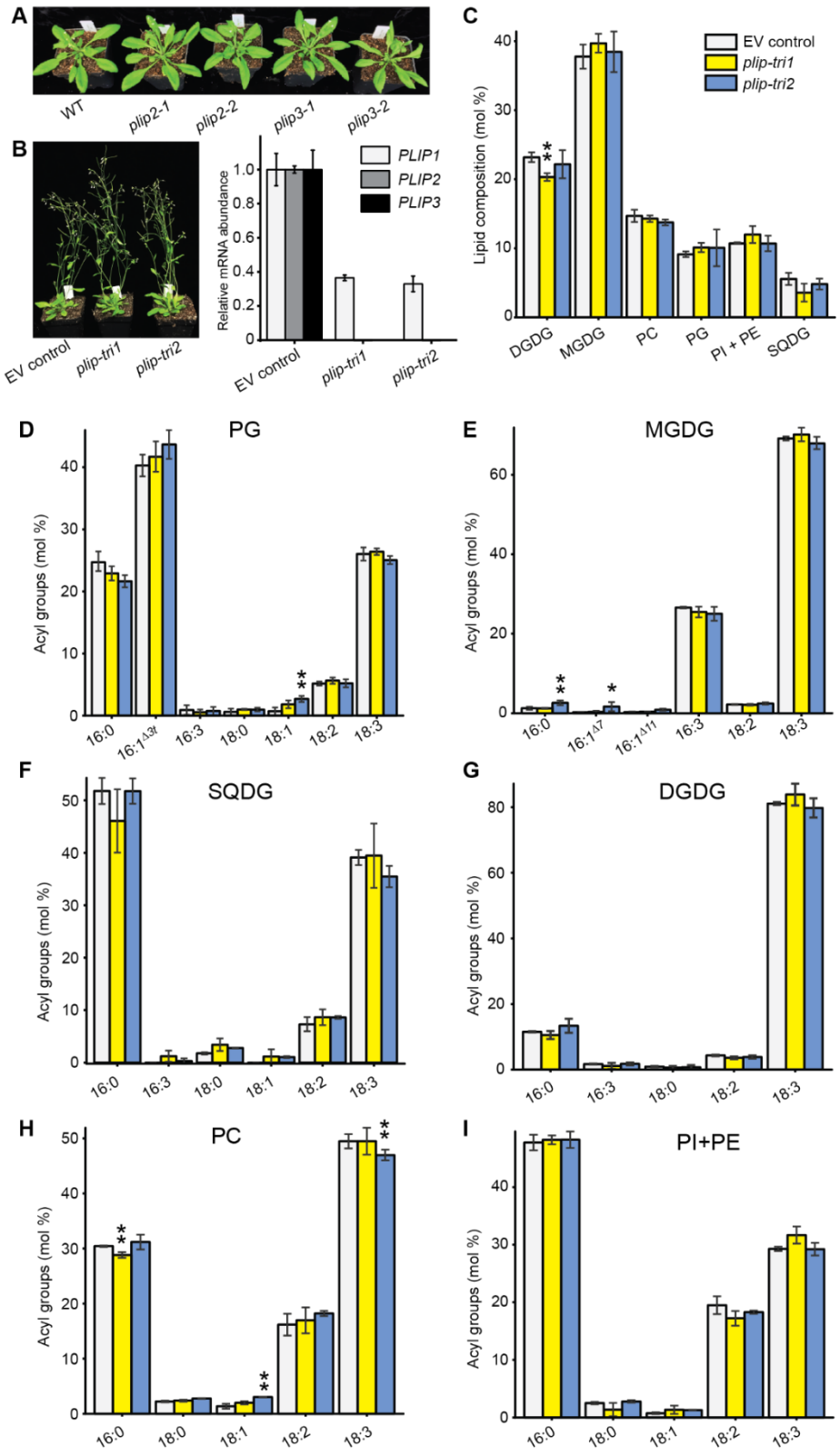

Figure 4. 18. Growth and the lipid phenotype of the *plip* single and triple mutants.

Figure 4. 18. (cont'd)

(A) Morphology of the 4-week-old soil-grown wild type (WT) and two T-DNA insertional alleles of *plip2* and *plip3*, respectively. The T-DNA insertional line SALK123458 was designated as *plip2-1*, SALK134251C as *plip2-2*, SALK006633 as *plip3-1*, SALK 006633 as *plip3-2*.
(B) Morphology of the 5-week-old soil-grown empty vector (EV) control and two independent *plip-tri* mutant lines and the expression of *PLIP*s in these plants. The *plip-tri* lines were created by reducing *PLIP1* expression by artificial microRNA approach in the *plip2 plip3* double mutant. The expression levels of *PLIPs* were normalized to those in the EV control (set to 1).
(C) Relative abundance of major polar lipid classes in EV control and the *plip-tri* lines.
(D-I) Relative acyl group composition of PG, MGDG, SQDG, DGDG, PC, PI and PE. $n = 3$, ± SD. Student's *t*-test was applied (** indicates $p<0.01$). For lipid abbreviations, refer to the legend of Figure 4.9.

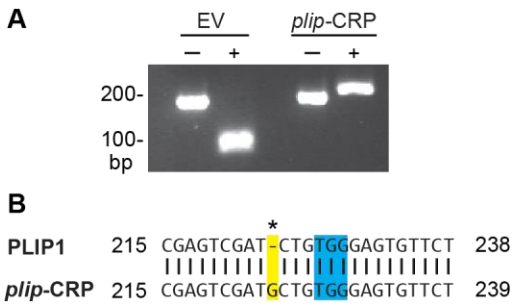

Figure 4. 19. Genotyping of the *plip*-CRISPR line.
(A) Digestion patterns of the PLIP1 amplicon from the empty vector (EV) control and the *plip*-CRP genomic DNAs. The PLIP1 amplicon was digested (+) with Dpn II or not (-). The wild type PLIP1 amplicon (178 bp) is expected to be cut into two fragments (93bp and 85bp).
(B) Sequencing of the PLIP1 locus from the *plip*-CRP plants revealed a single nucleotide insertion between the 223rd and 224th nucleotide of the coding sequence, leading to frameshift of the *PLIP1* sequence. The inserted nucleotide is highlighted in yellow, and the PAM motif is highlighted in blue.

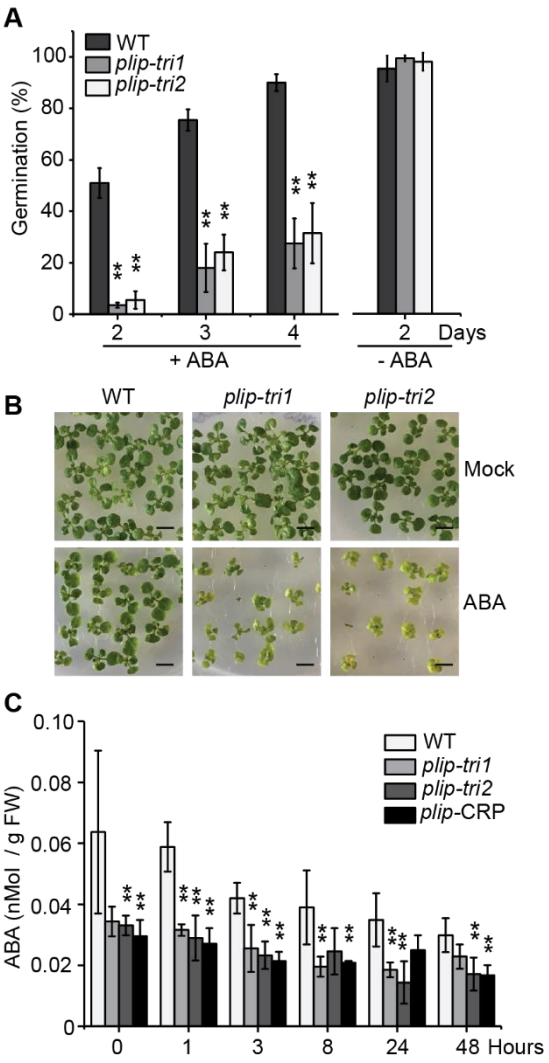

Figure 4. 20. The *plip-tri* plants are hypersensitive to ABA.
(A) Germination rates of the wild-type and *plip-tri* seeds with or without 2 µM ABA addition on phytoagar plates. Observation of 100 seeds in one plate was treated as one biological repeat. *n* = 4, ± SD. Student's *t*-test was applied to compare (WT) with each of the remaining genotypes (**indicates p<0.01).
(B) Morphology of the 2-week-old WT and *plip-tri* seedlings grown on MS agar plates with 0.5µM ABA or the equivalent ethanol solvent (Mock). Scale bars: 0.5 cm.
(C) ABA content in the 2-week-old WT, *plip-tri* and *plip*-CRP seedlings during a 48-h time course follwoing the addition of 10 µM Methyl-JA to the MS agar medium. 3-5 seedlings were pooled as one biological repeat. *n* = 3, ± SD. Student's *t*-test was applied to compare (WT) with each of the remaining genotypes (**indicates p<0.01).

REFERENCES

REFERENCES

Acosta, I.F., and Farmer, E.E. (2010). Jasmonates. Arabidopsis book **8,** e0129-e0129.

Adie, B.A., Perez-Perez, J., Perez-Perez, M.M., Godoy, M., Sanchez-Serrano, J.J., Schmelz, E.A., and Solano, R. (2007). ABA is an essential signal for plant resistance to pathogens affecting JA biosynthesis and the activation of defenses in Arabidopsis. Plant Cell **19,** 1665-1681.

Ajjawi, I., Lu, Y., Savage, L.J., Bell, S.M., and Last, R.L. (2010). Large-scale reverse genetics in Arabidopsis: case studies from the Chloroplast 2010 Project. Plant Physiol **152,** 529-540.

Alonso, J.M., Stepanova, A.N., Leisse, T.J., Kim, C.J., Chen, H., Shinn, P., Stevenson, D.K., Zimmerman, J., Barajas, P., Cheuk, R., Gadrinab, C., Heller, C., Jeske, A., Koesema, E., Meyers, C.C., Parker, H., Prednis, L., Ansari, Y., Choy, N., Deen, H., Geralt, M., Hazari, N., Hom, E., Karnes, M., Mulholland, C., Ndubaku, R., Schmidt, I., Guzman, P., Aguilar-Henonin, L., Schmid, M., Weigel, D., Carter, D.E., Marchand, T., Risseeuw, E., Brogden, D., Zeko, A., Crosby, W.L., Berry, C.C., and Ecker, J.R. (2003). Genome-wide insertional mutagenesis of *Arabidopsis thaliana*. Science **301,** 653-657.

Andersson, M.X., and Dörmann, P. (2009). Chloroplast Membrane Lipid Biosynthesis and Transport. In *The Chloroplast*, A.S. Sandelius and H. Aronsson, eds (Berlin, Heidelberg: Springer Berlin Heidelberg), pp. 125-158.

Andersson, M.X., Hamberg, M., Kourtchenko, O., Brunnstrom, A., McPhail, K.L., Gerwick, W.H., Gobel, C., Feussner, I., and Ellerstrom, M. (2006). Oxylipin profiling of the hypersensitive response in *Arabidopsis thaliana*. Formation of a novel oxo-phytodienoic acid-containing galactolipid, arabidopside E. J Biol Chem **281,** 31528-31537.

Avramova, Z. (2017). The jasmonic acid-signalling and abscisic acid-signalling pathways cross talk during one, but not repeated, dehydration stress: a non-specific 'panicky' or a meaningful response? Plant Cell Environ **40,** 1704-1710.

Benning, C. (2009). Mechanisms of lipid transport involved in organelle biogenesis in plant cells. Annu Rev Cell Dev Biol **25,** 71-91.

Benning, C. (2010). The Anionic Chloroplast Membrane Lipids: Phosphatidylglycerol and Sulfoquinovosyldiacylglycerol. In The Chloroplast: Biochemistry, Molecular Biology and Bioengineering., C.A. Rebeiz, C. Benning, H. Bohnert, H. Daniell, B. Green, K. Hoober, H. Lichtenthaler, A. Portis, and B. Tripathy, eds (Netherlands: Springer), pp. 171-184.

Blee, E. (1998). Phytooxylipins and plant defense reactions. Prog Lipid Res **37,** 33-72.

Boudière, L., Michaud, M., Petroutsos, D., Rébeillé, F., Falconet, D., Bastien, O., Roy, S., Finazzi, G., Rolland, N., Jouhet, J., Block, M.A., and Maréchal, E. (2014). Glycerolipids in photosynthesis: Composition, synthesis and trafficking. Biochim Biophys Acta **1837,** 470-480.

Buseman, C.M., Tamura, P., Sparks, A.A., Baughman, E.J., Maatta, S., Zhao, J., Roth, M.R., Esch, S.W., Shah, J., Williams, T.D., and Welti, R. (2006). Wounding stimulates the accumulation of glycerolipids containing oxophytodienoic acid and dinor-oxophytodienoic acid in Arabidopsis leaves. Plant Physiol **142,** 28-39.

Campos, M.L., Yoshida, Y., Major, I.T., de Oliveira Ferreira, D., Weraduwage, S.M., Froehlich, J.E., Johnson, B.F., Kramer, D.M., Jander, G., Sharkey, T.D., and Howe, G.A. (2016). Rewiring of jasmonate and phytochrome B signalling uncouples plant growth-defense tradeoffs. Nat Commun **7,** 12570.

Clough, S.J., and Bent, a.F. (1998). Floral dip: a simplified method for Agrobacterium-mediated transformation of Arabidopsis thaliana. Plant J **16,** 735-743.

Creelman, R.A., and Mullet, J.E. (1995). Jasmonic acid distribution and action in plants: regulation during development and response to biotic and abiotic stress. Proc Natl Acad Sci U S A **92,** 4114-4119.

Creelman, R.A., Tierney, M.L., and Mullet, J.E. (1992). Jasmonic acid/methyl jasmonate accumulate in wounded soybean hypocotyls and modulate wound gene expression. Proc Natl Acad Sci U S A **89,** 4938-4941.

Denness, L., McKenna, J.F., Segonzac, C., Wormit, A., Madhou, P., Bennett, M., Mansfield, J., Zipfel, C., and Hamann, T. (2011). Cell wall damage-induced lignin biosynthesis is regulated by a reactive oxygen species- and jasmonic acid-dependent process in Arabidopsis. Plant Physiol **156,** 1364-1374.

Earley, K.W., Haag, J.R., Pontes, O., Opper, K., Juehne, T., Song, K., and Pikaard, C.S. (2006). Gateway-compatible vectors for plant functional genomics and proteomics. Plant J **45,** 616-629.

Ellis, C., Karafyllidis, I., Wasternack, C., and Turner, J.G. (2002). The Arabidopsis mutant *cev1* links cell wall signaling to jasmonate and ethylene responses. Plant Cell **14,** 1557-1566.

Emanuelsson, O., Nielsen, H., Brunak, S., and von Heijne, G. (2000). Predicting subcellular localization of proteins based on their N-terminal amino acid sequence. J Mol Biol **300,** 1005-1016.

Feys, B., Benedetti, C.E., Penfold, C.N., and Turner, J.G. (1994). Arabidopsis mutants selected for resistance to the phytotoxin coronatine are male sterile, insensitive to methyl jasmonate, and resistant to a bacterial pathogen. Plant Cell **6,** 751-759.

Frentzen, M. (1986). Biosynthesis and Desaturation of the Different Diacylglycerol Moieties in Higher Plants. J Plant Physiol **124,** 193-209.

Frentzen, M., Heinz, E., McKeon, T.A., and Stumpf, P.K. (1983). Specificities and selectivities of glycerol-3-phosphate acyltransferase and monoacylglycerol-3-phosphate acyltransferase from pea and spinach chloroplasts. Eur J Biochem **129,** 629-636.

Gobel, C., and Feussner, I. (2009). Methods for the analysis of oxylipins in plants. Phytochemistry **70,** 1485-1503.

Gobel, C., Feussner, I., Hamberg, M., and Rosahl, S. (2002). Oxylipin profiling in pathogen-infected potato leaves. Biochim Biophys Acta **1584,** 55-64.

Heitz, T., Widemann, E., Lugan, R., Miesch, L., Ullmann, P., Desaubry, L., Holder, E., Grausem, B., Kandel, S., Miesch, M., Werck-Reichhart, D., and Pinot, F. (2012). Cytochromes P450 CYP94C1 and CYP94B3 catalyze two successive oxidation steps of plant hormone Jasmonoyl-isoleucine for catabolic turnover. J Biol Chem **287,** 6296-6306.

Huot, B., Yao, J., Montgomery, B.L., and He, S.Y. (2014). Growth-defense tradeoffs in plants: a balancing act to optimize fitness. Mol Plant **7,** 1267-1287.

Hurlock, A.K., Roston, R.L., Wang, K., and Benning, C. (2014). Lipid trafficking in plant cells. Traffic **15,** 915-932.

Hyun, Y., Choi, S., Hwang, H.J., Yu, J., Nam, S.J., Ko, J., Park, J.Y., Seo, Y.S., Kim, E.Y., Ryu, S.B., Kim, W.T., Lee, Y.H., Kang, H., and Lee, I. (2008). Cooperation and functional diversification of two closely related galactolipase genes for jasmonate biosynthesis. Dev Cell **14,** 183-192.

Ishiguro, S., Kawai-Oda, A., Ueda, J., Nishida, I., and Okada, K. (2001). The DEFECTIVE IN ANTHER DEHISCIENCE gene encodes a novel phospholipase A1 catalyzing the initial step of jasmonic acid biosynthesis, which synchronizes pollen maturation, anther dehiscence, and flower opening in Arabidopsis. Plant Cell **13,** 2191-2209.

Kazan, K., and Manners, J.M. (2013). MYC2: the master in action. Mol Plant **6,** 686-703.

Kelly, A.A., and Feussner, I. (2016). Oil is on the agenda: Lipid turnover in higher plants. Biochim Biophys Acta **1861,** 1253-1268.

Kourtchenko, O., Andersson, M.X., Hamberg, M., Brunnstrom, A., Gobel, C., McPhail, K.L., Gerwick, W.H., Feussner, I., and Ellerstrom, M. (2007). Oxo-phytodienoic acid-

containing galactolipids in Arabidopsis: jasmonate signaling dependence. Plant Physiol **145,** 1658-1669.

Liu, N., Staswick, P.E., and Avramova, Z. (2016). Memory responses of jasmonic acid-associated Arabidopsis genes to a repeated dehydration stress. Plant Cell Environ **39,** 2515-2529.

Marchler-Bauer, A., Derbyshire, M.K., Gonzales, N.R., Lu, S., Chitsaz, F., Geer, L.Y., Geer, R.C., He, J., Gwadz, M., Hurwitz, D.I., Lanczycki, C.J., Lu, F., Marchler, G.H., Song, J.S., Thanki, N., Wang, Z., Yamashita, R.A., Zhang, D., Zheng, C., and Bryant, S.H. (2015). CDD: NCBI's conserved domain database. Nucleic Acids Res **43,** D222-226.

McConn, M., and Browse, J. (1996). The critical requirement for linolenic acid is pollen development, not photosynthesis, in an arabidopsis mutant. Plant Cell **8,** 403-416.

Mosblech, A., Feussner, I., and Heilmann, I. (2009). Oxylipins: structurally diverse metabolites from fatty acid oxidation. Plant Physiol Biochem **47,** 511-517.

Mueller, M.J. (2004). Archetype signals in plants: the phytoprostanes. Curr Opin Plant Biol **7,** 441-448.

Murata, Y., Mori, I.C., and Munemasa, S. (2015). Diverse stomatal signaling and the signal integration mechanism. Annu Rev Plant Biol **66,** 369-392.

Petsalaki, E.I., Bagos, P.G., Litou, Z.I., and Hamodrakas, S.J. (2006). PredSL: a tool for the N-terminal sequence-based prediction of protein subcellular localization. Genomics Proteomics Bioinformatics **4,** 48-55.

Porta, H., and Rocha-Sosa, M. (2002). Plant lipoxygenases. Physiological and molecular features. Plant Physiol **130,** 15-21.

Riemann, M., Dhakarey, R., Hazman, M., Miro, B., Kohli, A., and Nick, P. (2015). Exploring jasmonates in the hormonal network of drought and salinity responses. Front Plant Sci **6,** 1077.

Schwacke, R., Schneider, A., van der Graaff, E., Fischer, K., Catoni, E., Desimone, M., Frommer, W.B., Flugge, U.I., and Kunze, R. (2003). ARAMEMNON, a novel database for Arabidopsis integral membrane proteins. Plant Physiol **131,** 16-26.

Song, S., Huang, H., Gao, H., Wang, J., Wu, D., Liu, X., Yang, S., Zhai, Q., Li, C., Qi, T., and Xie, D. (2014). Interaction between MYC2 and ETHYLENE INSENSITIVE3 modulates antagonism between jasmonate and ethylene signaling in Arabidopsis. Plant Cell **26,** 263-279.

Suzuki, N. (2016). Hormone signaling pathways under stress combinations. Plant Signal Behav **11,** e1247139-e1247143.

Thomma, B.P., Eggermont, K., Penninckx, I.A., Mauch-Mani, B., Vogelsang, R., Cammue, B.P., and Broekaert, W.F. (1998). Separate jasmonate-dependent and salicylate-dependent defense-response pathways in Arabidopsis are essential for resistance to distinct microbial pathogens. Proc Natl Acad Sci U S A **95,** 15107-15111.

Troncoso-Ponce, M.A., Cao, X., Yang, Z., and Ohlrogge, J.B. (2013). Lipid turnover during senescence. Plant Sci **205-206,** 13-19.

Trusov, Y., Rookes, J.E., Chakravorty, D., Armour, D., Schenk, P.M., and Botella, J.R. (2006). Heterotrimeric G proteins facilitate Arabidopsis resistance to necrotrophic pathogens and are involved in jasmonate signaling. Plant Physiol **140,** 210-220.

Turner, J.G., Ellis, C., and Devoto, A. (2002). The jasmonate signal pathway. Plant Cell **14 Suppl,** S153-164.

Valenzuela, C.E., Acevedo-Acevedo, O., Miranda, G.S., Vergara-Barros, P., Holuigue, L., Figueroa, C.R., and Figueroa, P.M. (2016). Salt stress response triggers activation of the jasmonate signaling pathway leading to inhibition of cell elongation in Arabidopsis primary root. J Exp Bot **67,** 4209-4220.

Wang, G., Ryu, S., and Wang, X. (2012). Plant phospholipases: an overview. Methods Mol Biol **861,** 123-137.

Wang, K., Froehlich, J.E., Zienkiewicz, A., Hersh, H.L., and Benning, C. (2017). A plastid phosphatidylglycerol lipase contributes to the export of acyl groups from plastids for seed oil biosynthesis. Plant Cell **29,** 1678-1696.

Wang, Z., and Benning, C. (2011). Arabidopsis thaliana polar glycerolipid profiling by thin layer chromatography (TLC) coupled with gas-liquid chromatography (GLC). J Vis Exp **49**, 2518.

Wang, Z., and Benning, C. (2012). Chloroplast lipid synthesis and lipid trafficking through ER-plastid membrane contact sites. Biochem Soc Trans **40,** 457-463.

Wasternack, C., and Hause, B. (2013). Jasmonates: biosynthesis, perception, signal transduction and action in plant stress response, growth and development. An update to the 2007 review in Annals of Botany. Ann Bot **111,** 1021-1058.

Winter, D., Vinegar, B., Nahal, H., Ammar, R., Wilson, G.V., and Provart, N.J. (2007). An "Electronic Fluorescent Pictograph" browser for exploring and analyzing large-scale biological data sets. PloS One **2,** e718.

Xu, C., Fan, J., Froehlich, J.E., Awai, K., and Benning, C. (2005). Mutation of the TGD1 chloroplast envelope protein affects phosphatidate metabolism in Arabidopsis. Plant Cell **17,** 3094-3110.

CHAPTER 5

Future perspectives

Cell membranes in biological systems primarily serve as barriers for cells and the internal organelles, providing compartments to make cells work at high efficiency. The membrane composition with regard to the lipids and membrane associated proteins dynamically changes in a process referred to as membrane remodeling. In sessile plants, membrane remodeling is not only important for multiple stages of growth, but also a vital strategy to adapt to the changing environment including freezing, nutrient scarcity, etc. Chloroplast membranes are essential for chloroplast functions including photosynthesis. Functional and mechanistic understanding of chloroplast membrane homeostasis under different conditions is crucial for elucidating basic chloroplast functions and engineering of more resilient and productive crops.

SFR2 in Engineering Stress Tolerant Plants

SFR2 mediated lipid remodeling was originally discovered as a freezing tolerance mechanism in *Arabidopsis thaliana* (Warren et al., 1996; Thorlby et al., 2004; Moellering et al., 2010). Conservation of SFR2 among all land plants, regardless of their freezing sensitivity, led to the discovery of its function in salt and drought tolerance in *Solanum lycopersicum* (Wang et al., 2016). Thus, functional comparison of the homologous SFR2s from different plants provides a valuable approach for the molecular investigation and engineering of SFR2.

*Sl*SFR2 and *At*SFR2 share high sequence identity (59%) and similarity (72%), but the in vitro studies suggest that *Sl*SFR2 activity is about twice that of *At*SFR2 under similarly optimized conditions (Wang et al., 2016). This implies that the divergent regions of these two sequences likely affect the SFR2's catalytic activity. A domain swap experiment can possibly be performed between these two proteins to systematically understand the functions of the divergent regions. For example, a similar approach was conducted between the Arabidopsis and Brachypodium

TRIGALACTOSYLDIACYLGLYCEROL1 (TGD1) proteins for identification of a specific divergent loop that is responsible for the oligogalactolipid production in the *tgd* mutants in Arabidopsis (Yang et al., 2017). Even though the crystal structure of SFR2 is not available yet, structure homology modeling of *At*SFR2 identifies three regions that distinguish SFR2 from glycosyl hydrolases (Roston et al., 2014). Comparison between the sequence fragments identified from these two approaches might further narrow down the effective regions. Alternatively, more SFR2 homologous sequences can be included to study the correlation between the SFR2 enzyme activities and their corresponding organisms' native tolerance to environmental stresses. For example, *Eutrema salsugineum* is a member of the Brassicaceae family and phylogenetically closely related to Arabidopsis (Bressan et al., 2001; Inan et al., 2004). As an extremophile plant with a wider range of salinity and drought tolerance than Arabidopsis, Eutrema could provide a facile tool to explore how the unique sequence regions of *Es*SFR2 might contribute to its superb tolerance. With more SFR2s from different organisms being characterized in vitro, specific regions or residues could be uncovered and engineered to achieve higher efficiency and sensitivity. The activation mechanism of SFR2 in response to abiotic stresses is not fully understood yet thus far. Possibly, this approach can also help elucidate regions that are involved in SFR2 activation.

Arabidopsis *sfr2* mutant have damaged chloroplast membranes but possesses intact plasma membranes during freezing, which suggests that chloroplasts are more susceptible to freezing-induced membrane damage and that SFR2 serves as the primary line of defense protecting membranes against these stresses, or that other mechanisms act on plasma membranes not involving SFR2. SFR2 is located on the chloroplast outer-envelope membrane facing the cytosol. Presumably, the outer envelope membrane lipids will be remodeled providing protection during dehydration. To increase stress tolerance, provide additional insights into the activation of the

enzyme, and to further explore the protective function of oligogalactolipids, one potential approach might be to ectopically relocate SFR2 to other subplastid membranes, e.g., the inner envelope and thylakoid membranes.

Activation of SFR2 is based on a post-translational mechanism by directly sensing Mg^{2+} and low pH (Roston et al., 2014; Barnes et al., 2016). In vitro, Mg^{2+} alone is able to activate SFR2 (Roston et al., 2014; Wang et al., 2016). In vivo, the majority of Mg^{2+} is sequestered in the vacuole and the cytosol Mg^{2+} level is determined by a class of Mg^{2+} / H^{+} antiporters on the vacuole membrane (Shaul, 2002). To expand the impact of SFR2 on plant physiology, genes for certain vacuolar Mg^{2+} / H^{+} exchangers, e.g., AtMHX (Shaul et al., 1999) could be engineered to express under the control of an ABA responsive promoter. Following drought or salt stresses, more Mg^{2+} will be pumped into the cytosol to activate SFR2 providing the chloroplasts with a more sensitive protection mechanism.

Taken together, these approaches and ideas discussed above can potentially be combined in order to generate a crop plant more tolerant of abiotic stresses.

PLIP1 in Seed Oil Biosynthesis

The PLIP1 and FAD4 pathway contributes to seed oil biosynthesis by releasing fatty acids (FAs) from plastid PG, and exporting FAs to the ER phosphatidylcholine (PC) pool before finally entering seed oil biosynthesis. The underlying mechanism of how the acyl groups enter TAG via PC is not clear. Multiple pathways are in principle available to channel the FAs from PC to TAG. One pathway is to be the head group exchange mechanism to convert PC to diacylglycerol (DAG) (Lu et al., 2009). DAG is then acylated to TAG by the action of DAG-acyltransferases (DGAT) with additional acyl groups from the acyl-CoA pool (Lung and Weselake, 2006). Another pathway

is direct incorporation of polyunsaturated FAs from PC into TAG through the phospholipid: DAG acyltransferases (PDAT) (Dahlqvist et al., 2000). To determine which pathway might work along with the PLIP1-FAD4 mediated export of FAs from plastids, double mutant lines between *plip1* and mutants of key enzymes in different pathways, e.g., *rod1, dgat1* and *pdat1* can be constructed by crossing and the seed oil contents can be examined for understanding how PLIP1 fits with the previously elucidated seed oil biosynthesis pathways. DGAT1 and PDAT1 pathways work redundantly during seed development and oil biosynthesis, and remarkably, the *dgd1 pdat1* double mutant deficient for the main DGAT1 and PDAT is not viable (Zhang et al., 2009). Conceivably, because the PLP1 pathway only contributes approximately 10% to seed TAG biosynthesis, the seeds from the progenies of *plip1* crossed with the individual pathway mutants should be viable. Labeling experiments of seeds with different genotypes can also be conducted for further anlaysis of the contribution of the different mechanisms to TAG biosynthesis in seeds.

Another interesting question that arises from the study of PLIP1 is how the hydrolyzed acyls groups are exported. As discussed in Chapter 3, FA exporter 1 (FAX1) and fatty acid-binding proteins (FAPs) are possible components in FA export in the *PLIP1* overexpression plants (Ngaki et al., 2012; Li et al., 2015). Combining mutants deficient in FAX1 or FAPs with the *PLIP1*-OX plants should be a straightforward approach for analyzing the relationship between PLIP1 and other components. Alternatively, the unique growth reduction phenotype of the *PLIP1*-OX plants can be taken advantage of in a forward genetics screening experiment. Ectopical overexpression of *PLIP1* leads to overaccumulation of oxylipins and activation of JA signaling, which causes the stunted growth in the *PLIP1*-OX plants (Wang et al., 2017). Screening of repressor mutants that reverse the growth reduction can conceivably identify novel players in fatty acid and oxylipin transport, as well as the missing components of JA signaling and its cellular transport.

PLIP2 and 3 in the Interaction Between ABA and JA

PLIP2 and 3 have been identified as putative paralogs of PLIP1. They exhibit similar biochemical activities as PLIP1, but likely play different physiological roles in Arabidopsis. PLIP1 contributes to seed oil biosynthesis, while the *plip2* and *plip3* seeds show no detectable effects on either the seed oil content or acyl compositions. The seeds of the *plip* triple mutant are indistinguishable from those of the *plip1* seeds. Furthermore, the expression of *PLIP2* and *3*, but not *PLIP1* is induced by ABA. Interestingly, based on the public transcriptomic database, *PLIP2* and *PLIP3* are induced by different abiotic conditions. Therefore, it is possible that they are involved in mitigating different abiotic stresses in vivo. It might be important to evaluate the physiological responses of the individual *plip* mutants under different conditions to gain a more comprehensive understanding of their physiological functions. The phenomics platform built by the Kramer lab can be of help in detecting subtle physiological phenotypes of the mutant plants in response to dynamic conditions in a more sensitive manner (Davis et al., 2016). This can also help understanding the real functions of the PLIP-mediated interaction between ABA and JA signaling.

Another interesting observation for the *plip* triple mutants is their hypersensitivity to applied ABA. The original hypothesis was that JA signaling antagonizes ABA biosynthesis. Decreased levels of ABA were indeed observed in both wild-type and *plip* triple mutant seedings with JA treatment. However, this is unlikely to be the only reason causing the hypersensitive phenotype, because the ABA reduction caused by JA treatment is only minor and requires a long-time scale. Therefore, it seems likely that inactivation of *PLIPs* also affects ABA signaling and that PLIPs are negative regulators for ABA signaling. To further investigate this issue, it would be interesting to create higher order mutants that are also deficient in key components in ABA signaling, e.g., the protein kinases and ABA INSENSITIVE (ABI) transcription factors, in the

background of the *plip* triple mutant (Finkelstein, 2013). This would help understand which ABA signaling step(s) PLIP takes part in.

To sum up, plant membrane lipid remodeling is a highly regulated dynamic process. This is still comparatively underexplored topic in plant lipid field. Further studies promise to uncover more novel mechanisms of lipid remodeling and their relationships with other biological processes, e.g., lipid signaling in abiotic stress tolerance, etc.

REFERENCES

REFERENCES

Barnes, A.C., Benning, C., and Roston, R. (2016). Chloroplast membrane remodeling during freezing stress is accompanied by cytoplasmic acidification activating SENSITIVE TO FREEZING 2. Plant Physiol **171,** 2140-2149.

Bressan, R.A., Zhang, C., Zhang, H., Hasegawa, P.M., Bohnert, H.J., and Zhu, J.-k. (2001). Learning from the Arabidopsis Experience . The Next Gene Search Paradigm **127**, 1354-1360.

Dahlqvist, A., Stahl, U., Lenman, M., Banas, A., Lee, M., Sandager, L., Ronne, H., and Stymne, S. (2000). Phospholipid:diacylglycerol acyltransferase: an enzyme that catalyzes the acyl-CoA-independent formation of triacylglycerol in yeast and plants. Proc Natl Acad Sci U S A **97**, 6487-6492.

Davis, G.A., Kanazawa, A., Schottler, M.A., Kohzuma, K., Froehlich, J.E., Rutherford, A.W., Satoh-Cruz, M., Minhas, D., Tietz, S., Dhingra, A., and Kramer, D.M. (2016). Limitations to photosynthesis by proton motive force-induced photosystem II photodamage. Elife **5**.

Finkelstein, R. (2013). Abscisic Acid synthesis and response. Arabidopsis Book **11**, e0166.

Inan, G., Zhang, Q., Li, P., and Wang, Z. (2004). Salt cress. A halophyte and cryophyte Arabidopsis relative model system and its applicability to molecular genetic analyses of growth and development of extremophiles. Plant Physiol **135**, 1718-1737.

Li, N., Gugel, I.L., Giavalisco, P., Zeisler, V., Schreiber, L., Soll, J., and Philippar, K. (2015). FAX1, a novel membrane protein mediating plastid fatty acid export. PLoS Biol **13**, e1002053.

Lu, C., Xin, Z., Ren, Z., Miquel, M., and Browse, J. (2009). An enzyme regulating triacylglycerol composition is encoded by the ROD1 gene of Arabidopsis. Proc Natl Acad Sci U S A **106**, 18837-18842.

Lung, S.C., and Weselake, R.J. (2006). Diacylglycerol acyltransferase: a key mediator of plant triacylglycerol synthesis. Lipids **41**, 1073-1088.

Moellering, E.R., Muthan, B., and Benning, C. (2010). Freezing tolerance in plants requires lipid remodeling at the outer chloroplast membrane. Science **330**, 226-228.

Ngaki, M.N., Louie, G.V., Philippe, R.N., Manning, G., Pojer, F., Bowman, M.E., Li, L., Larsen, E., Wurtele, E.S., and Noel, J.P. (2012). Evolution of the chalcone-isomerase fold from fatty-acid binding to stereospecific catalysis. Nature **485**, 530-533.

Roston, R.L., Wang, K., Kuhn, L.A., and Benning, C. (2014). Structural determinants allowing transferase activity in SENSITIVE TO FREEZING 2, classified as a family I glycosyl hydrolase. J Biol Chem **289,** 26089-26106.

Shaul, O. (2002). Magnesium transport and function in plants: the tip of the iceberg. Biometals **15**, 309-323.

Shaul, O., Hilgemann, D.W., de-Almeida-Engler, J., Van Montagu, M., Inze, D., and Galili, G. (1999). Cloning and characterization of a novel $Mg2^{+}/H^{+}$ exchanger. EMBO J **18**, 3973-3980.

Thorlby, G., Fourrier, N., and Warren, G. (2004). The SENSITIVE TO FREEZING2 gene , required for freezing tolerance in *Arabidopsis thaliana* , Encodes a beta-glucosidase **16**, 2192-2203.

Wang, K., Hersh, H.L., and Benning, C. (2016). SENSITIVE TO FREEZING2 Aids in Resilience to Salt and Drought in Freezing-Sensitive Tomato. Plant Physiol **172**, 1432-1442.

Wang, K., Froehlich, J.E., Zienkiewicz, A., Hersh, H.L., and Benning, C. (2017). A plastid phosphatidylglycerol lipase contributes to the export of acyl groups from plastids for seed oil biosynthesis. Plant Cell **29**, 1678-1696.

Warren, G., McKown, R., Marin, a.L., and Teutonico, R. (1996). Isolation of mutations affecting the development of freezing tolerance in *Arabidopsis thaliana* (L.) Heynh. Plant Physiol **111**, 1011-1019.

Yang, Y., Zienkiewicz, A., Lavell, A., and Benning, C. (2017). Coevolution of domain interactions in the chloroplast tgd1, 2, 3 lipid transfer complex specific to Brassicaceae and Poaceae plants. Plant Cell **29**, 1500-1515.

Zhang, M., Fan, J., Taylor, D.C., and Ohlrogge, J.B. (2009). DGAT1 and PDAT1 acyltransferases have overlapping functions in Arabidopsis triacylglycerol biosynthesis and are essential for normal pollen and seed development. Plant Cell **21**, 3885-3901.